FLOW PATTERNS AND PERFORMANCE OF DISTILLATION TRAYS

A THESIS SUBMITTED

BY

BAFRED AUDU ENJUGU

A candidate for the degree of

DOCTOR OF PHILOSOPHY

The Department of Chemical Engineering

Aston University in Birmingham

May 1986

Dedicated to

my

Parents

CERTIFICATE

I hereby certify that the work presented has been done by the candidate except where otherwise acknowledged, and that this thesis has not been submitted for a higher degree at any other University.

B.A.Enjugu

".....And so we see that the poetry fades out of the problem, and by the time the serious application of exact science begins we are left with only pointer readings."

Eddington

ABSTRACT

It is known that distillation tray efficiency depends on the liquid flow pattern, particularly for large diameter trays. Scale-up failures due to liquid channelling have occurred, and it is known that fitting flow control devices to trays sometimes improves tray efficiency. Several theoretical models which explain these observations have been published.

Further progress in understanding is at present blocked by lack of experimental measurements of the pattern of liquid concentration over the tray. Flow pattern effects are expected to be significant only on commercial size trays of a large diameter and the lack of data is a result of the costs, risks and difficulty of making these measurements on full scale production columns.

This work presents a new experiment which simulates distillation by water cooling, and provides a means of testing commercial size trays in the laboratory. Hot water is fed on to the tray and cooled by air forced through the perforations. The analogy between heat and mass transfer shows that the water temperature at any point is analogous to liquid concentration and the enthalpy of the air is analogous to vapour concentration. The effect of the liquid flow pattern on mass transfer is revealed by the temperature field on the tray.

The experiment was implemented and evaluated in a column of 1.2 m. dia. The water temperatures were measured by thermocouples interfaced to an electronic computerised data logging system.

The "best surface" through the experimental temperature measurements was obtained by the mathematical technique of B. splines, and presented in terms of lines of constant temperature. The results revealed that in general liquid channelling is more important in the bubbly "mixed" regime than in the spray regime. However, it was observed that severe channelling also occurred for intense spray at incipient flood conditions. This is an unexpected result.

A computer program was written to calculate point efficiency as well as tray efficiency, and the results were compared with distillation efficiencies for similar loadings.

The theoretical model of Porter and Lockett for predicting distillation was modified to predict water cooling and the theoretical predictions were shown to be similar to the experimental temperature profiles. A comparison of the repeatability of the experiments with an errors analysis revealed that accurate tray efficiency measurements require temperature measurements to better than $\pm 0.1^{o}C$ which is achievable with conventional techniques. This was not achieved in this work, and resulted in considerable scatter in the efficiency results. Nevertheless it is concluded that the new experiment is a valuable tool for investigating the effect of the liquid flow pattern on tray mass transfer.

ACKNOWLEDGEMENTS

The author would like to:

Thank the Nigerian Governments for the financial support provided throughout the duration of this project.

Acknowlege his debt to Professor K E Porter for his enthusiastic supervision of this project and support at all and particularly difficult times.

Express his thanks to the staff of the Department for their advice in the design and careful construction of equipment.

Finally, the author would like to thank all the above, the Nigerian students contemporaneous at the University, his friends, his relatives, and especially all members of his family, without whose encouragement and faith in him, this thesis would never have been written.

CONTENTS

A LIST OF FIGURES

LIST OF TABLES

1. INTRODUCTION

Distillation is the most widely used method of separation. Distillation processes account for between 2-3% of world energy consumption. Currently much effort is directed towards developing less energy consuming methods such as membranes adsorption. However, advantages of energy integration involving the use of waste heat means that distillation methods are still the most widely used and are expected to remain so. The current world recession plus demands for energy savings also means that most capital investment now goes into revamping existing equipment. Taken all together, the need arises for tighter design and in the words of Frank Rush [100] "... perhaps the greatest energy reduction we can accomplish in the immediate future is to operate our existing distillation systems more efficiently. We need to run our distillation systems "leaner and harder"". All this amounts to a need for better understanding of the distillation phenomena.

Devices abound for effecting good contact between vapour and liquid and thus separating the phases. Of these, the most common ones are cross-flow trays consisting of bubblecaps, valve and sieve trays fitted to columns. Column packings are less frequently used than trays. Designers always prefer to use tested devices, an attitude that kept bubblecap trays in use long after they were known to be more expensive than sieve trays [4,52,73]. Nowadays the sieve tray is preferred because of its cheapness and design reliability [18,31].

Small diameter trays (0.5m and below) might reasonably be designed on the assumption of completely mixed liquid, that is, the liquid concentration is the same all over the tray. It has been known for many years that liquid concentration changes as the liquid crosses the tray. The early models used to describe the flow mechanism were:

a) the existence of several well mixed pools, Kirschbaum [58,59,60],

b) Plug flow of liquid especially for very large trays, Lewis [65], and

c) Liquid backmixing for sizes in between completely mixed and plug flow, Diener [27]. However, all these are based on the assumption that the tray flow path may be represented by a rectangular shape.

More recently, theoretical models of tray efficiency have attempted to take into account the shape of real trays, that is; circular columns, straight downcomers and flow paths of changing width. In some cases, particularly with large diameter trays, the nature of liquid flow through the flow paths of changing width are shown to have very significant effectson the overall tray efficiency. In a series of experimental work carried out by Union Carbide Ltd [130,131] it was revealed that substantial discrepancies exist between the predicted and obtained tray efficiencies of large trays.

Theoretical work on relating the changes in liquid concentration accross the tray to the tray efficiency has gone as far as it is

reasonable to go. By contrast, experimental information about the concentration changes on large diameter distillation trays are rare. The problems involved in obtaining such information are enormous. First, it is difficult to gain access to operating columns in order to take samples of liquid on an operating tray without interfering with the process. This exercise could prove very expensive and involves high risks. It is also not feasible to simultaneously take a required number of samples, terminate further seperation taking place and analyse the samples without high losses of accurracy.

The starting point for this work is the suggestion that large diameter trays might be investigated in the laboratory by the technique of water cooling which involves feeding hot water on to a tray and cooling it by air forced through the tray perforations. The water temperature is measured at different predetermined positions on the tray. As shown in the following Section an analogy exists between water cooling processes and distillation. The process of water cooling is dependent on air enthalpy and water temperature in much the same way as distillation or mass transfer in general is dependent on vapour concentration (or vapour pressure) and liquid concentration of the component of interest. Thus this experiment holds the promise to break through the experimental barrier impeding further understanding of flow mechanism on trays. If it is possible to measure water temperatures at many points and draw temperature profiles (lines of constant temperature) analogous to liquid concentration profiles,

the existing theories may be checked and if they are found inadequate new and improved theories of tray efficiency may be developed.

This work presents the first detailed study of this technique using a tray of 1.22m (4ft) in diameter, that is, of commercial size. This is in fact the size of column used to generate practical distillation data by FRI, and in part of this work an attempt has been made to reproduce, using air-water, the flow behaviour expected for some of the FRI test systems [102,103].

An advantage of the water cooling technique is that the measurement of water temperature may be made by thermocouples or platinum resistance thermometers and the signals generated may besent to electronic/computer interfaces and data logging apparatus.

This work describes the construction and use of the 1.22m (4ft) diameter test rig, the development of interfaces and data logging, the development of a statistical test fit technique for computing the "best fit" for the temperature field on the tray and a method of calculating point and tray efficiency.

It is shown that the water coling technique provides a method of investigating liquid flow pattern effects on the temperature (concentration field). Experiments show the effect of maldistributed flow due to poor installation of tray and the effect of flow control devices.

The determination of tray efficiency was unsatisfactory in this work and thus led to a detailed study of the errors involved and their effect on the calculation of tray eficiency by the water cooling procedure.

A comparison between the experimental temperature profiles and temperature profiles theoretically predicted profiles are much more straight and symetrical than those experimentally detrmined.

The background to the work which was briefly outlined above is discussed in more detail in the literature survey which follows.

2. LITERATURE SURVEY

2.1 Introduction

Many more factors are now known to influence the performance of distillation columns than previously thought. Initial research into distillation columns was confined to exploring stable operating limits [29,30,52] and the description of the appropriate mixing models on a distillation tray [37,82]. The concepts of the models were derived from experiments carried out on small laboratory size trays. The flow behaviour of vapour/liquid mixtures on small trays is such that there is no loss of purpose by representing their flow paths as simple rectangles. The discrepancies arising from the use of the resultant models to design large size trays led to the discovery of the effects that tray hydraulics and liquid flow patterns have on the performance of trays. The structure of bubbles which define the interfacial contact area between the separating phases forms what is now described as the flow regime of the mixture on the tray. It seems that the flow patterns of different flow regimes differ and thus have dissimilar effects on the tray performance. The main point of these studies is that shape and size of tray can influence the flow pattern and efficiency on a tray. Consequently, some effort has been made to employ flow control devices on trays. The effects of these are also discussed in this section. The analogy between the water cooling theory and distillation theory which enables the development of this project is discussed in some detail.

2.2 Definitions of Efficiency Terms

The Murphree [79] concept of efficiency is a measure of the approach of the separating phases in contact with each other to a state where no further separation takes place or to the equilibrium state. This is the most used concept and as such is adopted in this work.

2.2.1 Point Efficiency

The Murphree vapour point efficiency E_{OG}, measures the approach as a ratio of the actual concentration change to the maximum possible change at a point on a tray.

It is expressed as:

$$E_{OG} = \frac{y_1 - y_2}{y_1 - y^*} \qquad 2.1$$

where y_2 and y_1 are the compositions of vapour leaving and entering the point on a tray, respectively. y^* is the composition of the vapour in equilibrium with the liquid x_n, which is assumed to be perfectly mixed vertically along a vapour stream. Similarly, the liquid point efficiency is expressed as:

$$E_{OG} = \frac{y_1 - y_2}{y^* - y_2} \qquad 2.2$$

where x_2 and x_1 are the inlet and outlet liquid compositions respectively while x^* is the liquid concentration in equilibrium with y which is assumed to be constant along a horizontal plane through the mixture. While it is possible to imagine a constant liquid concentration along a short flow path of a vapour stream that of a vapour concentration remaining constant along a liquid stream is less obvious. Consequently, the concept of a liquid point efficiency is not often used.

2.2.2 Murphree Tray Efficiency

The Murphree vapour tray efficiency [79] is the measure of the ratio of the actual to maximum possible concentration change for a whole tray.

This is expressed as :

$$E_{MV} = \frac{y_1 - \bar{y}_2}{y_1 - y^*} \qquad 2.3$$

where $y^* = mx_o + c$ i:e, in equilibrium with liquid leaving the tray.

The less frequently used liquid tray efficiency, E_{ML} is written as

$$E_{ML} = \frac{\bar{x}_o - \bar{x}_1}{x^*_o - \bar{x}_1} \qquad 2.4$$

Tray efficiency is the integral effect of individual point efficiencies over the whole active area of the tray. When concentration gradients occur on trays (which is common) tray efficiencies in excess of 100% may be found.

2.2.3 Overall Column Efficiency

The state of the art definition ofthe overall column efficiency is the ratio of the number of theoretical trays N_T to the number of actual trays N required for a given seperation in a column. That is:

$$E_O = \frac{N_T}{N} \qquad 2.5$$

The overall column efficiency is developed in the following way;

I) The use of mass transfer characteristics including the determination of overall transfer inefficients together with interfacial area to calculate the point efficiency, E_{OG}.

II) The calculation of Murphree Tray Efficiency, E_{MV} from E_{OG} taking into account the general tray design and a knowledge of the liquid flow mechanisms on the tray.

iii) The calculation of the overall column efficiency, E_O from the trays efficiencies and a knowledge of the ratios of the slopes of the equilibrium line to the operating line.

The procedure can be set out as:

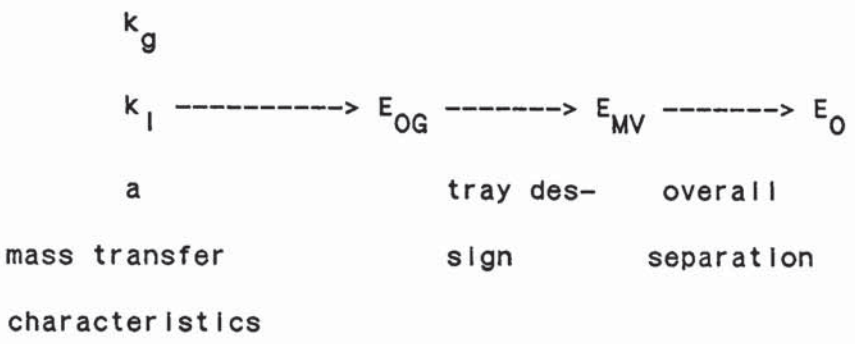

The early models of flow patterns on trays all considered the liquid flow along a path or channel of uniform width (i:e, they were assumed to be ractangular in shape). The later models which accomodated the circular shape of real trays with straight downcomers are of more relevance to this work. Thus in the following section a review of early (rectangular) models is given followed by a more detailed description of the later models.

2.3 Early Models of Tray Efficiency

The early models of tray efficiency are based on two related factors. The concepts were derived from descriptions of small diameter trays flow mechanisms and these were simply combined with the mixing characteristics of the same to arrive at the tray efficiency. A summary of these models is given in Table 2.1 below.

2.3.2 Discussion and Conclusion on Early Models

Murphree [79] proposed complete mixing of liquid on the tray. For the more widely known Lewis, Case I the liquid flow pattern was assumed to be in ideal plug flow. For each of these Cases the relationship between point efficiency and tray efficiency is different. However, by substituting the conditions of completely mixed or ideal plug flow into the models described above the final equations arrived at are similar. It is thus implicit in these models that the completely mixed and the ideal plug flow are the limiting extremes. The models above have shown a progression of mixing concepts developed to fully describe liquid flow behaviour on a typical tray. Of these the Eddy diffusion (or Simple Backmixing) model remains the most widely accepted and forms the basis for the design of current trays in practice.

2.3.1 Table 2.1 A List of Early Models of Tray Efficiency

Author[ref]	Description	Model Equations
Lewis [65]	Lewis,Case I (Plug flow)	$E_{mv} = \frac{1}{\lambda}(\exp(\lambda E_{OG}) - 1)$
	Lewis,Case II (Parallel flow)	$E_{MV} = \frac{\alpha - 1}{\ln \alpha (\frac{1}{E_{OG}} + \frac{1}{\alpha - 1}) - 1}$ where $\alpha = \frac{Y_n - (Y_n)_o}{Y_{n-1} - (Y_{n-1})}$ and $E_{MV} = \frac{\alpha - 1}{\lambda - 1}$
	Lewis,Case III (Counterflow)	a.For $\alpha < 1$; $= SQRT(\frac{\alpha^2 - (1-E_{OG})^2}{E_{OG}^2(1 - \alpha^2)}) * \cos^{-1}(1 - \frac{(\alpha - 1)(\alpha - 1) + \lambda E_{OG}}{\alpha(2 - E_{OG})})$ where α and E_{MV} remain same as Case II In the special case that $\lambda = 1$ solutions to Cases II and III are obtained by a Taylor series expansion

Gautreaux and O'Connell [37]	Mixed pools in series	$\frac{E_{MV}}{E_{OG}} = \frac{1}{\lambda E_{OG}}\left((1 + \frac{\lambda E_{OG}}{n})^{n} - 1 \right)$ where n is the number of arbitrary pool stages, with n = 1 being the nearest to the liquid inlet while n = n is the final pool at outlet. For n = 1 or the completely Mixed pool tray; $\frac{E_{MV}}{E_{OG}} = 1$ For n ---> ∞ ideal plug flow $\frac{E_{MV}}{E_{OG}} = \frac{1}{\lambda E_{OG}}(\exp(\lambda E_{OG}) - 1)$ c.f. Lewis, Case I
Oliver and Watson [82]		$\frac{E_{MV}}{E_{OG}} = \frac{(1 - F)}{E_{OG}\ln(1 + \lambda(1 - F)E_{MV})}$ where $F = \frac{X_n - X_{eq}}{X_n - X_{n+1}}$ X_{eq} is the equilibrium composition of liquid

Warzell [127]	Recycle stream	$\frac{E_{MV}}{E_{OG}} = \frac{C}{\lambda E_{OG}}(\exp(\lambda E_{OG}/C) - 1)$ where the function C is defined as : $C = \frac{X_{1n+1} - X_n}{X_{e,n+1} - X_n}$
Johnson and Marangozis [54]	Splashing of liquid	$\frac{E_{MV}}{E_{OG}} = \frac{1}{2\alpha + (1/B)} \frac{\alpha + \frac{1}{B}}{\alpha}.\exp(\alpha)$ $- \frac{\alpha}{\alpha + (1/B)}\exp(-\alpha - \frac{1}{B})$ $- \frac{(1/B)}{\alpha.(\alpha + (1/B)}$ where B is the mixing parameter and α is a parameter of the 2^o as $\alpha = \frac{1}{2B} - \text{SQRT}\ (\frac{1}{4B^2} + \frac{E_{OG}}{B})$
Gerster et al. [39]	Eddy Diffusion or Simple Backmixing	$\frac{E_{MV}}{E_{OG}} = \frac{1 - \exp(-(n + Pe))}{(n + Pe)(1 + (n+Pe)/n)}$ where $n = \frac{Pe}{2}(\text{SQRT}(1+4\frac{\lambda E_{OG}}{Pe}) - 1$ $Pe = \frac{UZ}{D_e}$, Z is liquid flow path length and D_e/U is the mixing length

Foss et al [36]	Residence time	$\frac{E_{MV}}{E_{OG}} = \frac{1 - \int_0^\infty \exp(-\lambda E_{OG} \cdot t/t_L) \cdot \frac{F(t)\,dt}{F(t)\,dt}}{\int_0^\infty \exp(-\lambda E_{OG} \cdot t/t_L) \cdot \frac{F(t)\,dt}{F(t)\,dt}}$

where F(t) dt is the fraction of liquid which remains for a time between t and tdt and t_L is the mean residence time of liquid on the tray. The model equation can also be represented by the Laplace Transform of F(t),

$$L(F(t)) = \int_0^\infty e^{-P \cdot t} F(t)\,dt$$

where $P = \lambda E_{OG} / t_L$

Diener	Diener's Equations	Defn. of terms:
[27]	a. Modified Lewis, Case I (plug flow)	$B = 4(1 - \alpha)\, E_{OG}/(\alpha + E_{OG} - \lambda).Pe$

$$Pe = \frac{UZ}{D_e} \text{ and } b = -\frac{Pe}{2}$$

i. For $B < 1$: $c = -\frac{Pe}{2}\sqrt{1-B}$

$$\frac{E_{MV}}{E_{OG}} = \frac{(1 - \alpha).\Theta}{c(\alpha + E_{OG} - 1)(b^2 - c^2)+}$$

where

$$\Theta = e^{b}((b^2 + c^2)\sinh c - 2c\cosh c) + 2cb \cdot \Theta . E_{OG}$$

ii. For $B > 1$: $\alpha = -(\frac{Pe}{2})\sqrt{B-1}$

$$\frac{E_{MV}}{E_{OG}} = \frac{(1 - \alpha).\psi}{a(\alpha + E_{OG} - 1)(a^2 + b^2) + \psi E_{OG}}$$

where $\psi = e^{b}((b^2 - c^2)\sin a - 2ab\cos a) + 2ab$

For the special case, $\lambda = 1; \lambda - 1$ is expressed in powers of $a - 1$ by the Taylor series to yield:

$$\frac{E_{MV}}{E_{OG}} = \frac{2.Pe^2}{((2.E_{OG}(\exp(-Pe) + Pe - 1) + Pe^2(2 - E_{OG}))}$$

Modified, Lewis

$$\frac{E_{MV}}{E_{OG}} = \frac{1}{E_{OG}} \int_{-\frac{1}{2}}^{\frac{1}{2}} \frac{q_n + (Z_n)_u - 1/(aE_{OG}) Z_{n-u}}{q_n / E_{OG} + ((E_{OG} - 1) / E_{OG})} du$$

where $q_n = (y_n)_0 - (y_{n-1})_1$

$$Z_n = y_n - (y_n)_0$$

$$Z_{n-1} = y_{n-1} - (y_{n-1})_1$$

note: a shift to centre-line as origin.

The overprediction of tray efficiency found in industrial columns that are based on this design method, is an outcome of the rectangular configuration adopted by this and indeed by other early models. Other factors also hitherto omitted in design include tray size and shape, liquid entrainment, by-passing, liquid residence time and weeping.

All-together the failure of the design methods discussed above led to new thinking in tray design. It was recognised that shape and size play an important part in the design of large scale columns and further, that different models may be required to describe systems operating in different "flow regimes" in which either the vapour or liquid momentum determines the structure of the froth.

Models proposed for large columns are reviewed in the following subsection.

2.4 Design Methods for Large Trays

A detailed review of the Retrograde models by Bell [9,10,11,112,113], the Channelling and Spray Diffusion models by Porter and Lockett [67,68,70,71,89,91,101] and the Developing Flow Patterns model by Sohlo et al. [61,62,63,109,110,111] is made. These models predict similar flow patterns and the deleterious effects that the patterns have on tray efficiency. Applied to large trays the models show the influence of size on nonuniform flow of liquid across an operating tray. It is pointed out that experimental data is required to substantiate these models.

2.4.1 Retrograde Flow Model (Bell)

Velocity distributions on a sieve tray were determined from residence time measurements. The measurements were carried out by the fibre optic technique. Interpretation ofthe velocity measurements identifies two possible phenomena for liquid nonuniformities in tray columns. These are described as i) the simple nonuniform velocity flow distribution and ii) the nonuniform velocity flow distribution upon which a retrograde flow is superimposed. Retrograde flow is the term used when flow on the tray is in the direction opposite to the general direction of flow of liquid. The presence of either phenomenon can substantially reduce tray efficiency. Experimental results obtained and hence the predicted flow patterns conformed with observations presented in the film by Keller and Yanagi [57]. The initial retrograde model assumed the absence of transverse mixing. Later models were an extension of

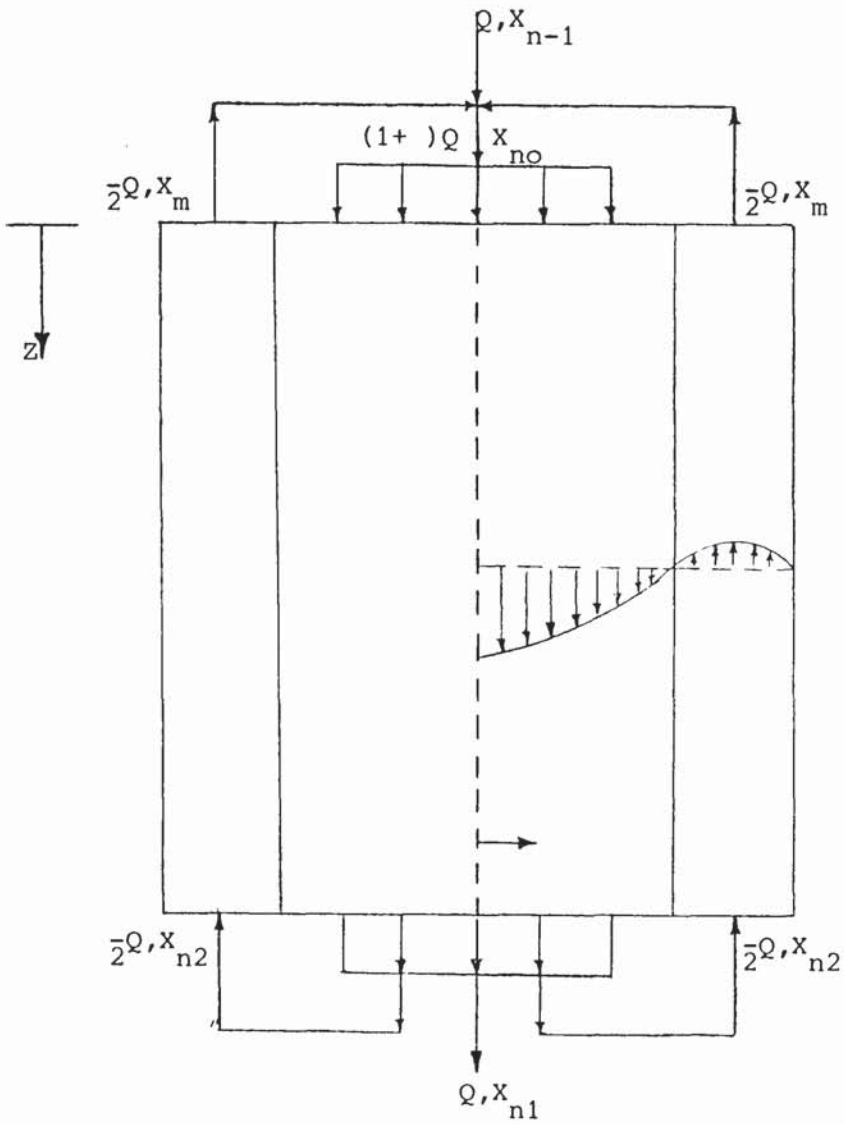

FIG:2.1 Schema for the Nonuniform Retrograde Flow Model

It is further assumed that mass transfer takes place in both the forward and retrograde flow paths. A material balance over an element of froth is derived as:

$$\frac{1}{Pe_{\xi}}.\frac{\partial^2 x_n}{\partial \xi^2} + \frac{1}{Pe_z}.\frac{\partial^2 x_n}{\partial z^2} - q(\xi).\frac{\partial x_n}{\partial z}.+ \lambda E_{OG}(x^*_{n+1} - x_n) = 0 \qquad 2.7$$

where the Peclet numbers are defined as:

$$Pe_z = \frac{W\bar{v}}{E_z} \qquad 2.8$$

$$Pe_{\xi} = \frac{W\bar{v}}{E_{\xi}}(\frac{D}{2W})^2 \qquad 2.9$$

E_z and E_{ξ} are the mixing coefficientsin the flow and transverse directions respectively.

However, the axial Peclet numbers for commercial scale trays being between 30 to 50 have been shown to have no significant effect on tray efficiency and thus Pe_z is ignored.

Assumptions for equation 2.7 are

a) No vertical liquid concentration gradient

b) Linear equilibrium over the concentration range on the tray

c) Constant vapour and liquid rates

d) Constant point efficiency E_{OG} across the tray

e) Constant concentration of entering vapour

f) Constant froth density on the tray

g) Unidirectional (bulk) liquid flow in the axial direction

Introducing these assumptions into equation 2.7 reduces it to

$$\frac{1}{Pe_{\xi_l}} \cdot \frac{\partial^2 x_n}{\partial \xi_l^2} - q(\xi_l)\frac{\partial x_n}{\partial z} + \lambda E_{OG}(x^*_{n+1} - x_n) = 0 \qquad 2.10$$

A normalized liquid concentration X_n is defined as:

$$X_n(z,\xi_l) = \frac{x_n(z,\xi_l) - x^*_{n+1}}{x_{n-1} - x^*_{n+1}} \qquad 2.11$$

The equations for mass transfer both the forward and retrograde flow paths become:

$$\frac{1}{Pe_{\xi_1}} \frac{\partial^2 X_n}{\partial \xi_1^2} - q(\xi_1)\frac{\partial X_n}{\partial z} + \lambda E_{OG} X_n = 0 \quad \xi_1 < \beta \qquad 2.12$$

$$\frac{1}{Pe_{\xi_1}} \cdot \frac{\partial^2 X_n}{\partial \xi_1^2} - q(\xi_1)\frac{\partial X_n}{\partial z} - \lambda E_{OG} X_n = 0 \quad \xi_1 < \beta \qquad 2.13$$

The Boundary Conditions are specified as:

At the tray inlet z = 0:

$$X_n(0,\xi_1) = X_{n0} \quad \xi_1 < \beta \qquad 2.14$$

By symmetry at = 0

$$\frac{\partial X_n}{\partial \xi_1}\Big|_{=0} = 0 \qquad \xi_1 < \beta \qquad 2.15$$

At the impermeable column wall $\xi_1 = 1$:

$$\frac{\partial X_n}{\partial \xi_1}\Big|_{=1} = 0 \qquad \xi_1 = 1 \qquad 2.16$$

At the interface between the two flow paths E = B, the continuity equation is:

$$\frac{\partial X_n}{\partial \xi_1}\Big|_{\beta} = \frac{\partial X_n}{\partial \xi_1}\Big|_{\beta} \qquad \xi_1 = \beta \qquad 2.17$$

This condition assumes that the Peclet numbers in the two flow paths are the same.

At the tray outlet z = 1

$$X_{n2}(1,\xi_1) = X_{n1}(1, B - \delta(\xi_1 - \beta)) \qquad 2.18$$

This unusual condition provides for flow rotation taking place at the outlet weir such that a flow path near the centre of the tray rotates to a position near the wall. The scale factor δ is defined as the ratio of the fraction of forward flow area involved in recirculation to the retrograde flow area.

$$\delta = \frac{\beta - \alpha}{1 - \beta} \qquad 2.19$$

Fluid mixing at the tray inlet is between the fluid ensuing from the tray above and that from the retrograde flow stream. The resulting mass balance equation gives

$$X_{n0} = \frac{1 + \alpha X_{m0}}{1 + \alpha} \qquad 2.20$$

X_{m0} is the normalized mixing cup average composition of the fluid leaving the retrograde flow path.

2.4.2.2 Solutions of the Equations

A normalized gas phase composition is defined as

$$Y_n(z,\xi_l) = \frac{y_n(z,\xi_l) - y_{n+1}}{y^*_{n-1} - y_{n+1}} \qquad 2.21$$

where y^*_{n-1} is the vapour composition in equilibrium with the incoming liquid.

The definitions of the tray and point efficiencies are written in the form:

$$E_{MV} = \frac{\bar{Y}_n}{Y^*_{n1}} = \frac{\bar{y} - y_{n+1}}{\bar{y}^*_{n+1} - y_{n+1}} \qquad 2.22$$

and from $$E_{OG} = \frac{y_n(z,\xi_l) - y_{n+1}}{m(x_n(z,\xi_l) - x^*_{n+1}} \qquad 2.23$$

one gets $$Y_n(z,\xi_l) = E_{OG}.X_n(z,\xi_l) \qquad 2.24$$

To obtain the average composition of the vapour leaving the tray $\bar{y}_n$, equation 2.24 is averaged over the entire tray.

$$\bar{\bar{Y}}_n = \int_0^{\bar{\xi}_l}\int_0^{\xi_l} Y_n(z,\xi_l).dzd\xi_l = E_{OG}\int_0^{\bar{\xi}_l}\int_0^{\xi_l} X_n(z,\xi_l).dzd\xi_l \qquad 2.25$$

By the definition of the normalised liquid and vapour compositions:

$$Y^{*}_{n1}(\xi_1) = X_n(1,\xi_1) \qquad 2.26$$

To evaluate this requires knowledge of the average composition of the liquid leaving the tray. The actual liquid leaving the tray is that flowing between $\xi_1 = 0$ and $\xi_1 = \xi_{1_o}$. The average vapour composition in equilibrium with this outlet liquid stream is given by the expression;

$$\bar{Y}^{*}_{n1} = \frac{\int_o^{\xi_1} q(\xi_1).X_n(1,\xi_1)d\xi_1}{\int_o^{\xi_1} q(\xi_1)d\xi_1} \qquad 2.27$$

Dividing equation 2.25 by equation 2.27 taking into account $\int_o^{\xi_1} q(\xi_1)d\xi_1 = 1$ gives the tray to point efficiencies ratio as:

$$\frac{E_{MV}}{E_{OG}} = \frac{\int_o^{1}\int_o^{1} X_n(z,\xi_1).dzd\xi_1}{\int_o^{\xi_1} q(\xi_1)X_n(1,\xi_1)d\xi_1} \qquad 2.28$$

This equation 2.28 is solved by numerical computation

2.4.2.3 RTD by the Fibre Optic Technique

Multiple fibre probes are used to detect such flourescent tracers as uranine and Rhodamine - B which have a very rapid activation and decay time. A schema for the method is shown in figure 1 of reference [9]. The probes are divided into two seperate bundles to form a bifurcation. One limb is used to conduct light from a mercury lamp light source in to the liquid. The light excites any tracer passing through the fibre tip and causes it to flouresce. A portion of the flourescent light is conducted up the second set of fibres in the other limb to a photomultiplier tube, it is amplified, multiplexed and recorded as digital signals. In clear liquid, the probes have a range of jurisdiction of roughly 1 cm radius and height, 4cm. The tracers also show linear characteristics with concentration. The peak height of the output signals is computed as a function of tracer concentration.

A typical layout of the probes on one half of the tray is indicated by the numbers in figure 9 of reference [2] . It shows the probes arranged on a rectangular grid. The tray is assumed to be symmetrical over the centre line. To determine the residence time distribution (RTD) a pulse of tracer was injected into the downcomer leading to the tray. The pulse response was simultaneously detected at each of the probes at short intervals (1 second) and stored seperately. The RTD was worked out from the concentration - live data for individual probes. To determine the average velocity distribution a pulse of tracer was rapidly injected into one of the first row of probes. Only the pulse

responses from the four probes in line with the injection points were monitored at specified sampling rates. The average velocity of the fluid was calculated by dividing the distance between two consecutive probes located in the same longitudinal (that is parallel to the flow axis) row by the difference in mean residence time between the two probes.

2.4.2.4 Discussion of the RTD Results

It is customary to consider the results in two forms. First, a qualitative representation of the flow patterns which illustrates areas of nonuniformities on the tray is made. And second, from a suitable model that approximates the flow patterns solutions of the efficiency equations are treated in terms of the mixing parameters Pe and the flow characteristics λE_{OG}. A comparison of the efficiency values is made with those obtained by the 'simple backmixing model' outlined in the AIChE Bubble tray Design Manual.

The predicted flow patterns on a half tray of rectangular geometry is given in figure 4 of reference [9]. The complete effects of varying the forward flow fraction (α), the fraction of retrograde flow (β), Pe and the velocity distribution are given in some detail elsewhere in reference [11]. In experimental practice, it becomes difficult to affect all the variables that are in a model. Distillation runs carried out in a 8ft (2.4m) diameter column - The results of RTD measurements are given in figure 10 of reference [9]. Although U-shaped profiles were observed the presence of retrograde flow patterns were not obvious. Further

experiments were carried out in a 5-tray capacity 4 ft (1.22m) diameter air/water simulator column using a sieve tray [11]. The results indicate flow nonuniformities on the tray. Here again zones of high residence times near the wall are found thus suggesting a tendency for stagnation but not necessarily retrograde flow. There is evidence that inadequate mixing within the inlet downcover can influence the tray flow patterns. There is also conclusive evidence that high vapour loads destroy the "pools" or the stagnant areas formed near the wall.

Calculations for the tray efficiency were based on equation 2.28 taking into account the observations for total forward flow $\beta = 1$ and no retrograde flow $\alpha = 0$. The Peclet numbers calculated were in excess of 30 and could therefore be regarded as having the same influence as if they were infinity. Figure 2.2 below is a plot of the ratio of Murphree tray efficiency for a tray on which a linear velocity distribution to the idealized efficiency E_{MVO} obtained by assuming uniform velocity distribution with fractional wall slip velocity as the parameter.

From the analytical solutions of the limiting case in reference [10] it is clear that the dual influence of liquid mixing and velocity distribution though interrelated are distinguishable. This may not also have a practical interpretation.

Assuming isotropic mixing, that is $E_z = E_\xi$, it is clear that axial and transverse dispersions differ by the 'geometry' factor

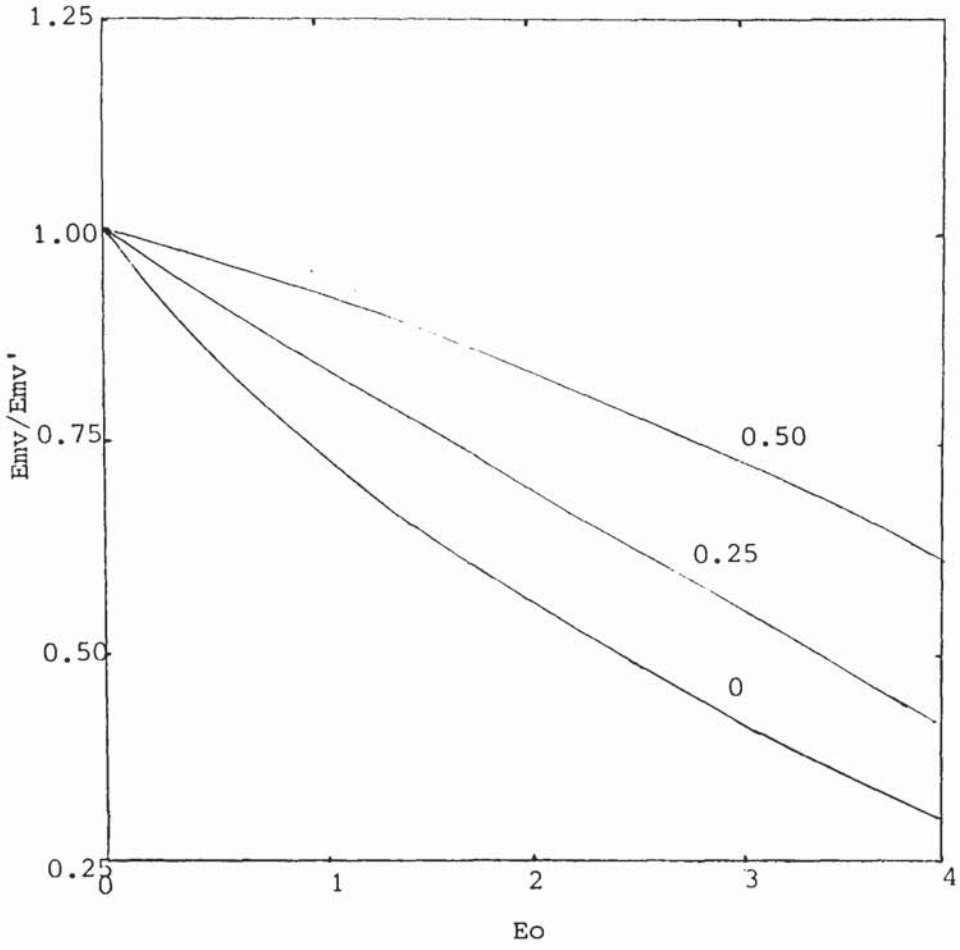

- Emv:using the retrograde model for which linear velocity distribution exists
- Emv':assuming an ideal uniform velocity distribution
- Parameter is the slip velocity at the wall

FIF:2.2 The predicted effect of velocity distribution on Tray Efficiency

$(D/2W)^2$. This means that in single pass trays transverse dispersion will always be more than axial dispersion, or $Pe_{E_1} < Pe_z$, although both may be sufficiently high to have negligible effect on tray efficiency.

Crsss flow effects yield higher values of E_{MV}/E_{OG} for high values of λE_{OG}, typical of absorption systems than it does for distillation systems where the value of λE_{OG} is about unity.

2.4.3 Channnelling Model (Porter and Lockett)

The derivation ofthe flow model was based on observations taken from two simple experiments carried out on both single - and two-pass trays. The 'trays' used were 4 ft (1.22m) and 8 ft (2.44m) in diameter. The first set of experiments involved air and water in cross-flow in a single-pass 4 ft diameter sieve tray column. Cine photographs of the movements of a dye tracer was recorded. These are shown in figure 2 of reference [89]. Two separate liquid flow patterns were apparent in distinct regions of the tray. These consist of a central region between the downcomers where the dye movement and disappearance was rapid and to both sides of this region near the walls were areas where the dye persisted for relatively long times. These observations were repeated over several different conditions.

In order to separate the effects of liquid mixing by vapour the second set of experiments were carried out without any passage of vapour. To do this a 7 ft (2.13m) diameter wooden model was constructed to the shape of a distillation tray. The patterns of liquid movements were determined by floating table-tennis balls on the liquid surface. Their movements was recorded by cine photography. The balls in the region between the downcomers flowed straight across the tray with seemingly uniform velocity while those in the regions outside the downcomers either remained stagnant or underwent gentle closed-recirculation patterns.
From these simple set of experiments the following conclusions were drawn:

i. Tray geometry influences liquid flow patterns.

ii. Liquid channelling occurs in the section of the tray between the downcomers and increases with decreasing downcomer area.

iii.Liquid channelling is also dependent on liquid rate and the ratio of weir length to plate diameter.

iv. Channelling occurs in two-pass trays. The flow patterns however differ depending on whether the flow of liquid is from side downcomers to central downcomers or vice-versa.

In what follows the derivation of the theoretical model based on the above observations is given. The model gives concentrations at different points on a tray and when combined with the definition equations of efficiencies, can be used to predict the Murphree tray efficiency.

The model is sometimes referred to as the 'stagnant zones' model a fitting description since the deleterious effects on tray efficiency are mainly attributed to the presence of the stagnant regions of the tray. For clarity a schema of the regions is shown in Figure 2.3a. The active region describes that section of the tray between the downcomers. The stagnant regions are those regions to both sides of the active region up to the column walls. The only interchange of liquid between the two regions is by gas agitation.

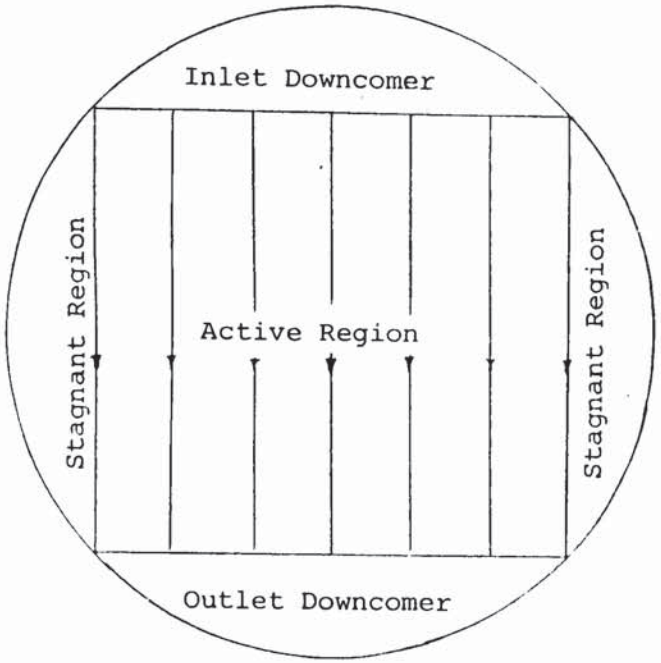

a. A schema of the liquid flow pattern

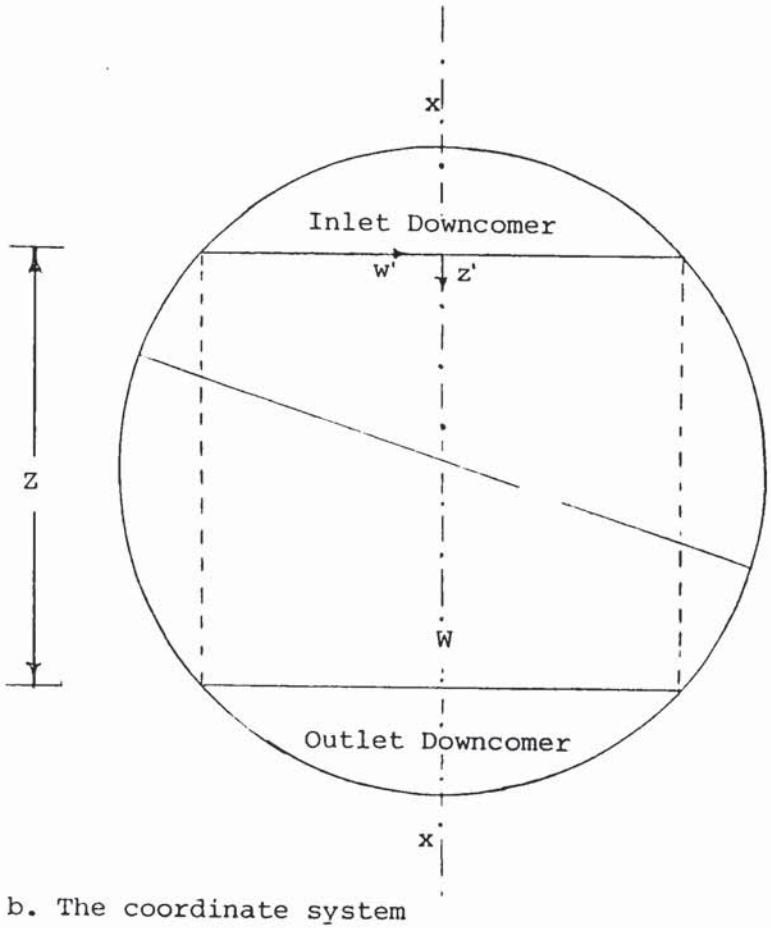

b. The coordinate system

FIG:2.3 A description of the formulation of the Channelling Model

2.4.3.1 Mathematical Development of the Theory

The Theory is developed for a binary mixture.

Assumptions made are in two categories.

I. General Assumptions

a) The vapour and liquid entering the tray are each well mixed. This is clearly an oversimplification since in practice vapour entering large trays is not completely mixed and liquid entering the tray is incompletely mixed inside the downcomers.

b) Straight equilibrium line over the concentration change on the tray.

c) Constant point efficiency E_{OG} over the tray.

II. Assumptions Specific to the Model

a) The flow per unit width of weir is uniform at all points in the active region.

b) Bulk flow of liquid in the stagnant region is zero.

c) Liquid mixing is described by Eddy diffusion.

d) The Eddy diffusion coefficient is equal in both the flow and transverse directions.

The coordinate system used in the analysis is shown in figure 2.3b.

Material balance on an element of froth shown schematically in figure 2.4 yields.

For the Active Region

$$D_e\left(\frac{\partial^2 x}{\partial w'^2} + \frac{\partial^2 x}{\partial z'^2}\right) - \frac{L'}{h_f \rho_L \rho_f}\cdot\frac{\partial x}{\partial z'} + (y_1 - y_2)\frac{G'}{h_f \rho_L \rho_f} = 0 \qquad 2.29$$

I II III

Where term I, the eddy diffusion term, describes the transfer of material through liquid mixing by the vapour;

term II, the bulk flow term, describes the transfer of material by liquid flow through the froth.

term III, describes the transfer of material through the passage of vapour.

For the Stagnant Regions

$$D_e\left(\frac{\partial^2 x}{\partial w'^2} + \frac{\partial^2 x}{\partial z'^2}\right) + (y_1 - y_2)\frac{G'}{h_f \rho_L \rho_f} = 0 \qquad 2.30$$

In the Stagnant regions terms II and III of equation 2.29 above are the same in equation 2.30. However, the bulk flow term II does not apply in view of the assumption IIb made above.

A dimensionless concentration term X is defined as:

$$X = \frac{x - x_e^*}{x_1 - x_e^*} \qquad 2.31$$

$$z = z' / D \qquad 2.32$$

$$w = w' / D \qquad 2.33$$

$$z_1 = Z / D \qquad 2.34$$

$$w_1 = W / 2D \qquad 2.35$$

$$L' = L / D \qquad 2.36$$

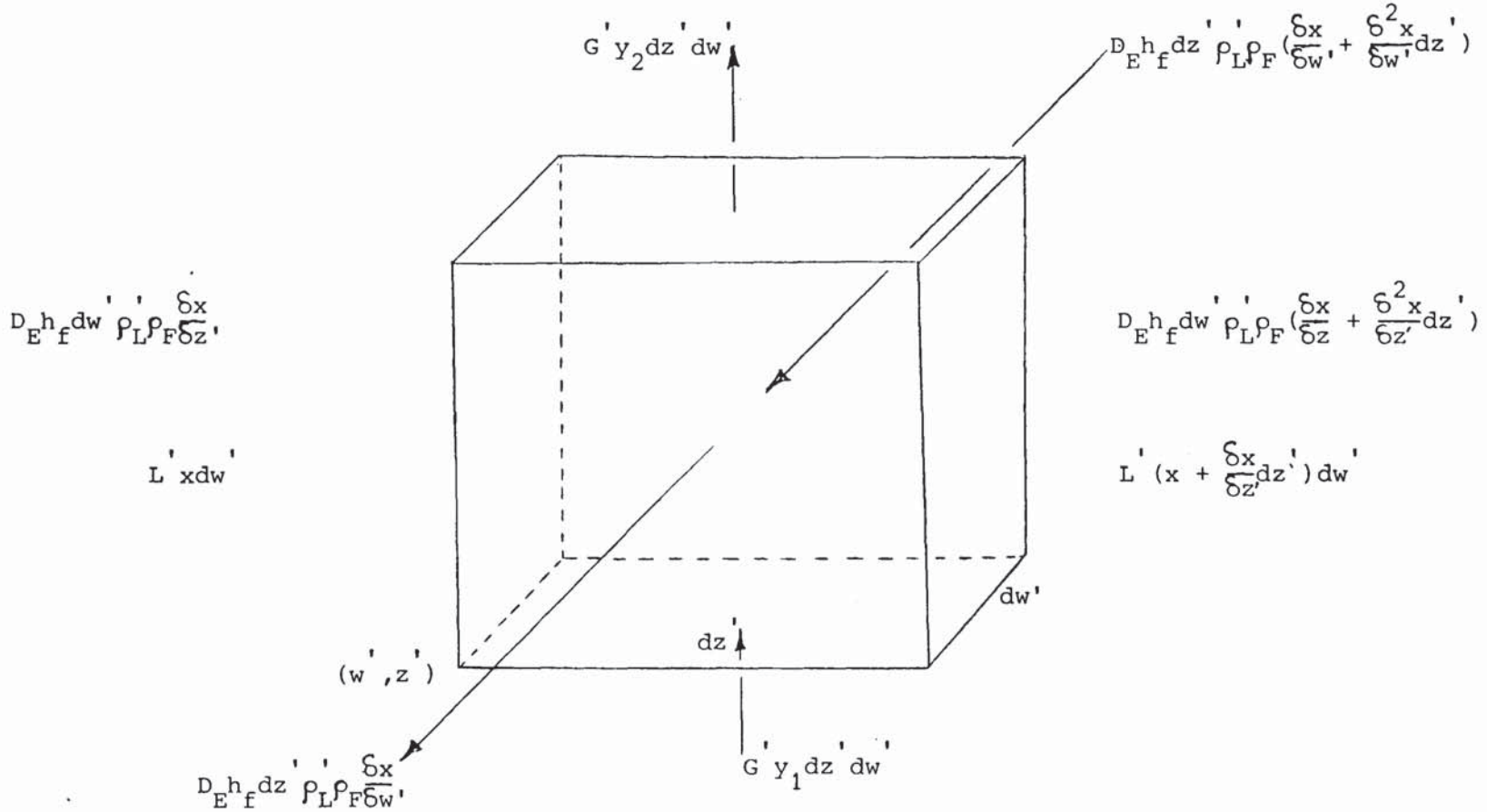

FIG:2.4 Material Balance over an Element of Froth

$$G' = G / A \qquad 2.37$$

$$Pe = LD / (W.h_f \rho'_L \rho_f D_e) \qquad 2.38$$

$$\lambda = mG / L \qquad 2.39$$

Substituting the dimensionless terms into the balance equations and rearranging gives:

For the Active Region

$$\frac{1}{Pe}\left(\frac{\partial^2 X}{\partial W^2} + \frac{\partial^2 X}{\partial z^2}\right) - \frac{\partial X}{\partial z} - \lambda E_{OG}\left(\frac{WD}{A}\right)X = 0 \qquad 2.40$$

and

For the Stagnant Regions

$$\frac{1}{Pe}\left(\frac{\partial^2 X}{\partial W^2} + \frac{\partial^2 X}{\partial Z^2}\right) - \lambda E_{OG}\left(\frac{WD}{A}\right)X = 0 \qquad 2.41$$

Boundary Conditions

The boundary conditions are shown in figure 2.5 below.

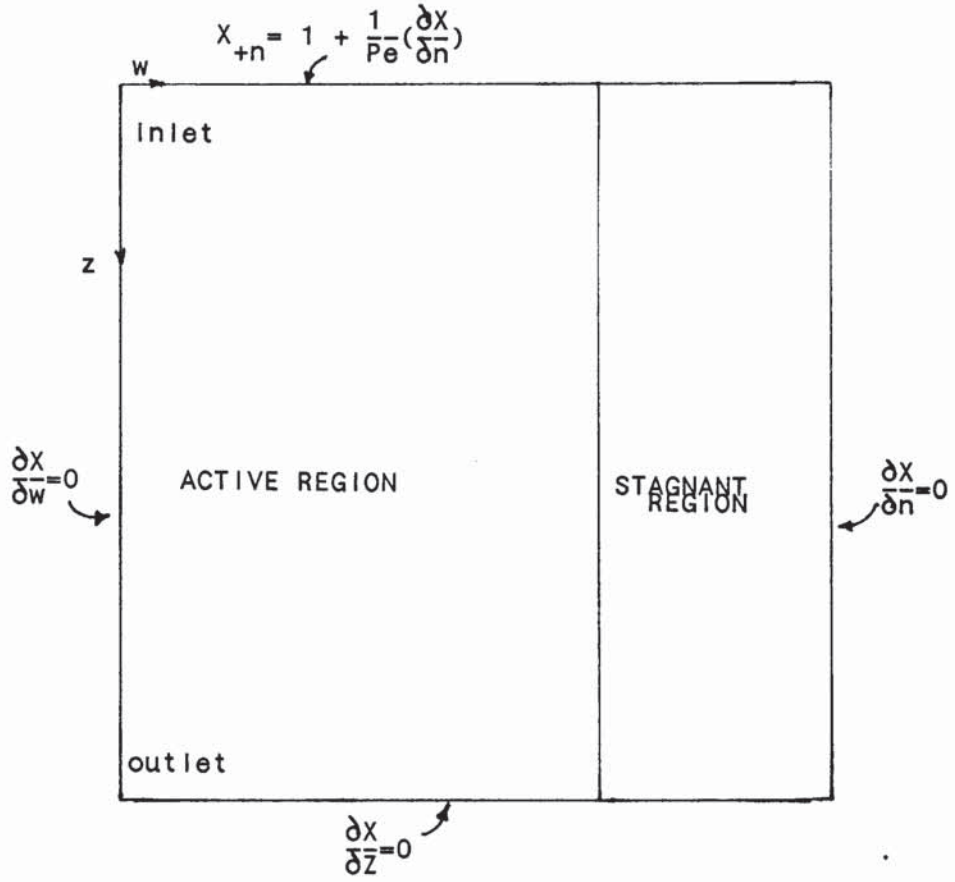

FIG: 2.5 Boundary Conditions on a rectangular plate

a) At the liquid inlet; the Danckwerts' boundary conditions is invoked [24,25],

$$z = 0 \quad X_{+n} = 1 + \frac{1}{Pe}.\frac{\partial X}{\partial z} \qquad 2.42$$

b) At the impermeable column wall:

$$\frac{\partial X}{\partial n} = 0 \qquad 2.43$$

c) At the liquid outlet:

$$\frac{\partial X}{\partial z} = 0 \qquad 2.44$$

2.4.3.2 Relationship between the Flow Patterns, Point and Tray Efficiency

The flow pattern equations 2.40 and 2.41 can be solved numerically, and by taking into account the boundary conditions they yield the concentrations on the tray, the point and tray efficiencies.

Since there is incomplete mixing, liquid concentration X is expected to vary across the tray and with it the vapour concentration corresponding to the point for X. The average change in vapour concentration leaving the tray can be obtained by integrating;

$$\bar{y}_2 - y_1 = \frac{mE_{OG}}{A} \int_A (x - x_e^*).dA \qquad 2.45$$

where dA stands for the integral over the whole bubbling area of the tray.

The Murphree vapour tray efficiency is given as:

$$E_{MV} = (\bar{y}_2 - y_1) / (y_2^* - y_1) \qquad 2.46$$

where y_2^* is the concentration of the vapour leaving in equilibrium with the mean concentration of the liquid leaving, ie.

$$y_2^* = m\bar{x}_2 + b \qquad 2.47$$

Now $\bar{x}_2$, the leaving liquid concentration may vary across the width of the outlet weir, therefore the mean value of y_2^* is given by

$$y_2^* = \frac{1}{W}\int_{-W/2}^{W/2} (m.x_2 + b).dw' \qquad 2.48$$

Since y, x, x_e, m, and b are all assumed to be constant the following relationship can be derived.

$$\frac{E_{MV}}{E_{OG}} = \frac{1}{A}\int_A X.dA \; / \; (\frac{1}{W}\int_{-W/2}^{W/2} X_2.dw') \qquad 2.49$$

Since $A \propto D^2$ no generality is sacrificed by reducing the dimensionless group DW/A to the form W/D. The relationship given in equations 2.40 and 2.41 express the tray concentration in terms of the dimensionless groups λE_{OG}, Pe, and W/D. The ratio W/D which gives a measure of the relative size of the stagnant zones to that of the active region does not appear in the simple backmixing theory. Typical concentration profiles are given in reference [89]. The effect of decreasing the weir length and hence the ratio W/D is increased stagnant regions on the tray. Also increasing E_{OG}, creates concentration gradients in both the flow and transverse directions of the tray.

2.4.3.3 Predictions of the Model

Scale-up effects are demonstrated in this model. On the large diameter columns in commercial use there is a tendency for channelling of the liquid to take place which causes drastic reductions in tray efficiency.

For a fixed ratio of weir length to column diameter in a given system there is a maximum diameter (relating directly to the Pe number) beyond which cross-flow effects show no further influence on tray efficiency. At the maximum column diameter the contribution to tray efficiency due to crossflow effects is counteracted by the influence of the stagnant zones. A plot of efficiencies ratio against column diameter predicted by this model is shown in figure 2.6 below.

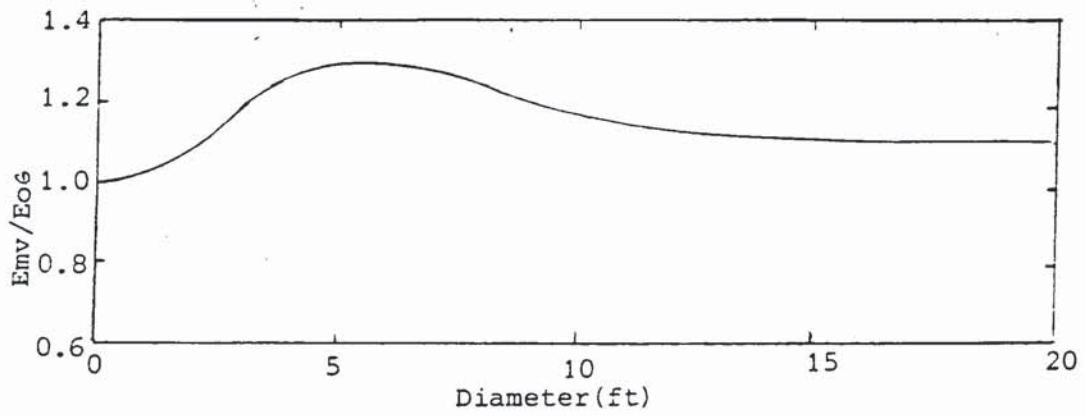

W/D = 0.6; Eo = 0.75

FIG:2.6 Predicted change in Plate Efficiency with Column Diameter

The maximum tray efficiency occurs at relatively low values of Pe (directly related to low D) at low values of λE_{OG}. The maximum tray efficiency can also be obtained for large trays when λE_{OG} is increased.

Above a certain column diameter the tray efficiency could become significantly less than the point efficiency.

2.4.3.4 The Concept of the Width of The Mixing Zone

The width of the mixing zone is a measure of the distance covered by diffusional mixing between the stagnant zones and the active zone [89]. It is assumed that the liquid in the stagnant zones is not replenished by liquid in the bulk flow. The liquid in the stagnant zones tend to approach equilibrium. Vapour passing through the stagnant zones is not enriched in the more volatile component of the separating mixture. This is called vapour bypassing.

A hypothetic boundary is defined, distance S=0.0, at the interface between the stagnant zones and the active zone such that at

$$S = 0.0 \; ; \; X = X^{*}$$

also at a semi-infinite distance

$$S = \infty; \; X = 0.0$$

Assuming the diffusion term has no component in the flow direction, a relationship between the transport of the more volatile component and the distance S is found to be

$$\frac{X}{X^{*}} = \exp\left(-\mathrm{SQRT}\left(\frac{m.G'.E_{OG}}{D_e h_f \rho_L \rho_f}\right).S\right) \qquad 2.50$$

For a ten times reduction in concentration from the hypothetic boundary into the stagnant zone (a reasonable approach to equilibruim) the solution to the equation yield a distance of between 1.0ft (0.30m) and 2.0ft (0.60m). This is independent of tray diameter. A well mixed pool is estimated to have a length of roughly 1.0ft , Williams, Begley and Wu [132]. This clearly shows that for small trays where the stagnant zones occupy an insignificant fraction of the tray (<<1.0ft) the width of the mixing zone will have no influence on tray efficiency whereas on large trays trays large stagnant zones are expected and therefore some parts of the stagnant regions will be replenished with the more volatile component.

2.4.3.5 Further Observations of the Channelling Model

The assumption of complete vapour mixing is an oversimplification. A study of the effects of lateral vapour mixing on distillation tray efficiency is presented in reference [69]. Vapour mixing in the vertical direction is neglected. In reference [71] it is shown that the effect of vapour mixing is insignificant in small trays only. In large trays however, completely mixed vapour is predicted to give much higher tray efficiencies than unmixed vapour. The reason is derived from the concept of stagnant zones and how it relates to the fraction of vapour bypassing on the tray. If the stagnant zones occupy a reasonably large fraction of the tray area then clearly a significant fraction of vapour bypassing would occur on the tray. This phenomenon is more likely to occur on large trays. In a completely mixed case the lean vapour ensuing from the

stagnant zones is well mixed in the rich vapour thus resulting in less severe losses in overall efficiency on the next tray. A gradual reduction in tray efficiency due to the vapour will occur on subsequent trays particularly if (by conventional arrangement for single cross-flow trays) the stagnant zones lie one above the other. In dealing with conventional large commercial trays, the assumption of partial mixing of the vapour is a realistic one and is often invoked in the design equations [71].

2.4.4 Features of the Channelling and Retrograde Models

The good agreement between the concentration profiles predicted by the channelling model and those predicted by the retrograde model warrants a comparative examination of characteristic features of these models. The Table 2.2 below lists the features.

An important criticism of these models is that whether explicitly or implicitly no consideration is given to such tray design features as hole size and free area. It is now established that hole size and free area may determine if the froth structure is "Bubbly" ,"Intensely Mixed" or "Spray". It is expected that the flow pattern for bubbly is different from that of spray. Although a separate model for the spray regime has been proposed by Porter and Lockett [91], the conditions that favour the choice of the channelling model in preference to this model are not obvious from their model equations. The exclusive model for Spray Diffusion is discussed in the following section

Table 2.2

Comparative features of the Channelling and Retrograde flow models

Variable	Channelling Model	Retrograde Model
Tray Efficiency	Lower tray efficiency than the AIChE model	Lower tray efficiency than the AIChE
Mixing Group(Pe)	Assumed equal in all directions.	Slightly less in the transverse direction Predicts significant enhancement of tray over point efficiency where mixing is more in in transverse direction
Operating Variable λE_{OG}	Enhancement of tray efficiency over point efficiency is high for high λE_{og} Steeped concentration gradients are predicted for high λE_{OG}	The deleterious effect of retrograde flow is most severe for high values of λE_{OG} and vice-versa

Tray Shape and Geometry (W/D)	Stagnant zones to increase with low W/D hence lowered tray efficiency.	The worst cases of velocity distribution $q(\xi_1)$ for high values of the weir length and hence low (W/D)
Velocity Distri -bution	-	This parameter is determined by experiments only, but measures the extent to which tray efficiency maybe lowered
Width of the mixing zone	Plays an important part in tray efficiency depe ndent on the size of tray and hence stagnant zones.	-
Scale-up	Stagnant zones to increa se with increase in tray diameter.At a diameter a above 3m a change over to double-pass is recom- mended	-
Scope	Thought not applicable to Spray regime systems	-

*Note:"-" indicate no obvious correlation to be gleaned from in model.

2.4.5 The Spray Diffusion Model (Porter and Lockett)

Commercial trays operating under conditions of low weir loads and high vapour capacity often operate in the Spray regime. Since in this regime the gas momentum is dominant over liquid momentum and liquid droplets formed in this regime are dispersed in a gas continuous phase, it seems reasonable that the underlying flow pattern should be described by a separate model from ones that emphasize the bulk flow of liquid (with backmixing). A good understanding of the mechanism of liquid transport in this regime is imperative. Existing proposals give conflicting conclusions.

The mechanism proposed by Porter, Safekourdi and Lockett [91] report that "droplet concentration gradients" form on a typical operating tray. They form at the vicinity of the inlet weir which constitutes the source and diminish in concentration towards the exit weir or the sink. The movement of the liquid droplets is by random motion which is analogous to a diffusion process. By contrast, Raper et al. [94,95,96,97] claim that liquid is successively atomised in a series of backmixed zones along the tray. In the final zone which is close to the outlet weir the droplets effectively jump over the weir into the outlet downcomer. A similar observation pertaining to the droplets behaviour at the outlet weir was purported by Zuiderweg and coworkers [137,49]. Raper et al. also report a pool of liquid that develops close to the outlet weir causing retrograde (or backflow of liquid). This mechanism at the outlet weir seems to have some additional influence on the tray efficiency to the spray diffusion process

itself. The observations noted above throw up some further important questions.

In particular, is the gas momentum sufficient to move all the liquid across the tray and over the outlet weir?. Another puzzle is illustrated by the following analysis: it is possible to derive a concentration versus distance plot along the centreline of figure 3 of reference [91]. This is shown in figure 2.7. It is shown that the last 30% of the tray contributes only a relatively small amount to the mass transfer process compared to the rest of the tray. In the proposal of Raper et al. the region of backflow tails off from the exit weir where the mass transfer would infact be minimal compared to that upstream of the tray. The authors claim substantial influence on tray efficiency attributed to the mixing behaviour in this region. This is clearly inconsistent with the above analysis.

The gas momentum in itself is insufficient to transport all the liquid across the tray and over the weir. This fact is implicit in reference [91]. It is possible that in the vicinity of the outlet weir, a liquid layer is formed which is large and is thus forced across the weir in addition to droplets jumping from further upstream.

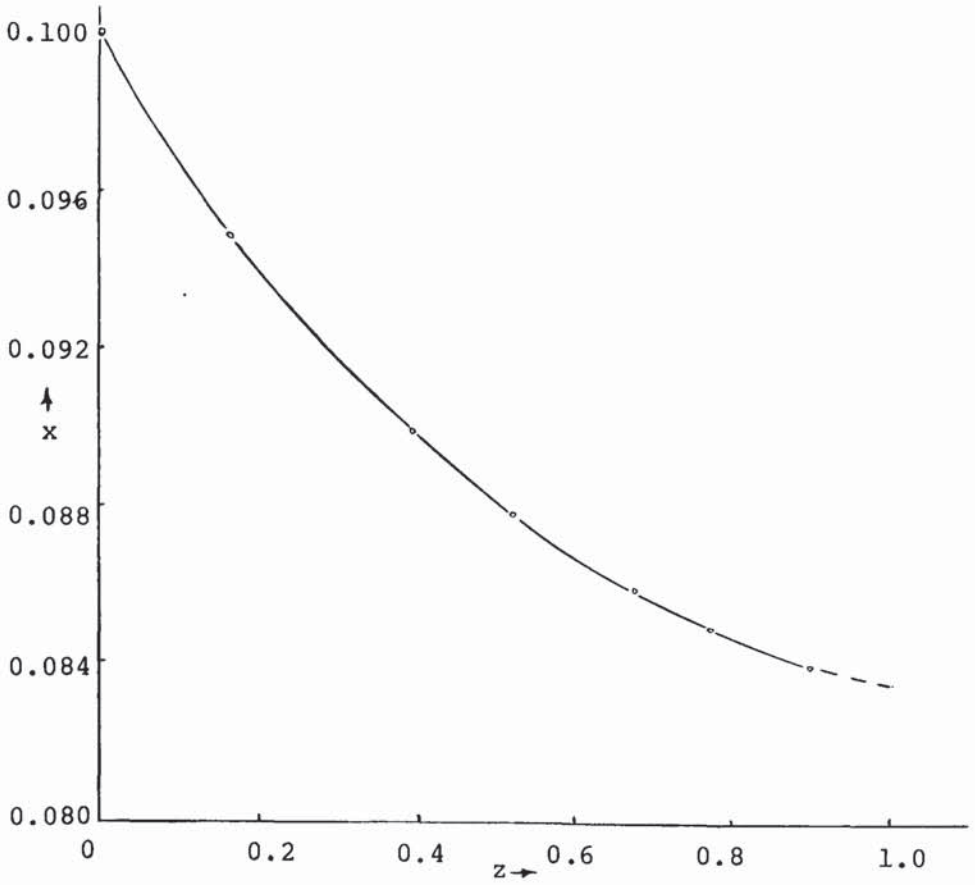

Fig.2.7 Calculated liquid concentration profile (x) along the centre-line for the spray regime $\lambda E_{OG}=0.5$, $W/D=0.6$, $Pe_s=1.07$
(derived from fig.3 of reference 91)

In view of these unanswered questions the model proposed by Porter et al. would seem to give the reasonable guide to the nature of flow patterns on in the Spray regime. The theoretical development of the model is described below.

2.4.5.1 Derivation of the Spray Diffusion Model

An ideal spray in which separate (that is no coalescence of) liquid droplets are entrained upwards and move through various trajectories at random is assumed. This is to simplify the model. Diffusion equations are described according to the theory of Chandrasekhar [17]. The driving force to cause the liquid to flow across the tray is the droplet concentration gradient.

A material balance over a differential element in a spray bed, figure 2.8 is made as follows;

the diffusion flux in the Z' direction is

$$N_z' = -D_{es}\rho_L dw' \frac{\partial h'}{\partial z'} \qquad 2.51$$

A similar expression can be written for the w' direction.

The following dimensionless ratios are defined:

$$z = z' / Z \qquad 2.52$$

$$w = w' / Z \qquad 2.53$$

$$h = h' / h_l' \qquad 2.54$$

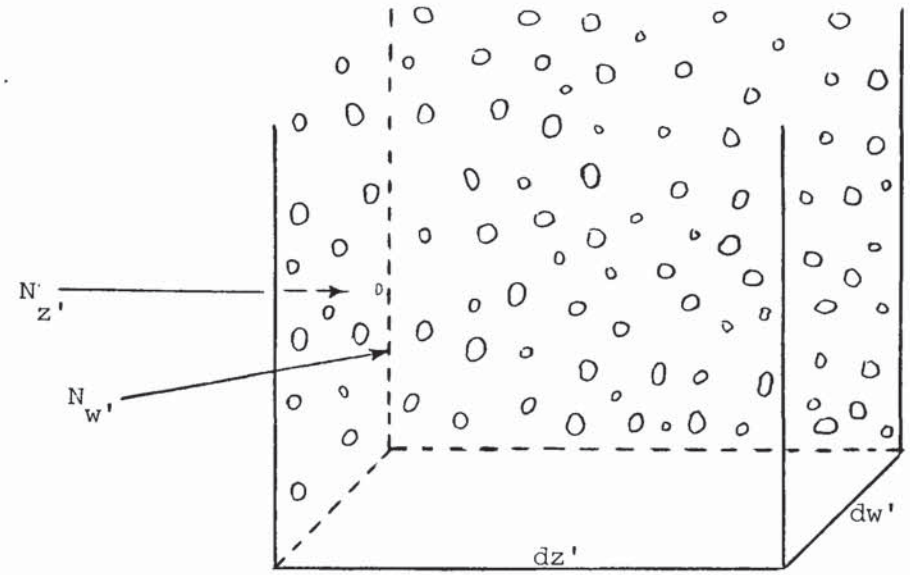

FIG:2.8 An element of froth(droplets) in a Spray bed

A material balance on the element using equation 2.51 and the dimensional ratios yields

$$\frac{\partial^2 h}{\partial z^2} + \frac{\partial^2 h}{\partial w^2} = 0 \qquad 2.55$$

Boundary Conditions

a) At the liquid inlet

$$h = 1.0 \qquad 2.56$$

b) At the liquid outlet

$$h = h_0 \quad ; \text{ an arbitrary droplet hold-up} \qquad 2.57$$

c) At the impermeable column

$$\frac{dh}{dn} = 0 \qquad 2.58$$

where n is the distance normal to the wall along which there is no further movement of drops. Normalised solutions of the balance equation give the drop concentration profile as shown in figure 2.9. The model predicts "plug flow" behaviour for the drop concentration change across the tray.

2.4.5.2 Predictions of Tray Efficiency in the Spray Regime

Assumptions of the model are:

a) constant point efficiency E_{OG} everywhere on the tray

b) linear equilibrium relationship

c) well mixed vapour and liquid streams entering the tray

d) no concentration change in the vertical direction

A material balance for the more volatile component (assuming a binary system) within the froth element in figure 2.8 would give:

$$D_{es}\rho_L\left(\frac{\partial^2(h'x)}{\partial z'^2} + \frac{\partial^2(h'x)}{\partial w'^2}\right) + G'(y_1 - y_2) = 0 \qquad 2.59$$

Recall the definition of point efficiency:

$$E_{OG} = \frac{y_2 - y_1}{y^* - y_1} = \frac{y_2 - y_1}{m(x - x^*_{e1})} \qquad 2.60$$

A Peclet number for Spray Diffusion is defined as:

$$Pe_s = \frac{Z.L}{WD_{es}\rho_L h_l}, \qquad 2.61$$

Substituting equation 2.60 and equation 2.61 into equation 2.59 yields

$$\frac{\partial^2(h.x)}{\partial z^2} + \frac{\partial^2(h.x)}{\partial w^2} - Pe_s\left(\frac{WZ}{A}\right)\lambda E_{OG}(x - x^*_{e1}) = 0 \qquad 2.62$$

Expanding :

$$h\left(\frac{\partial^2 X}{\partial z^2} + \frac{\partial^2 X}{\partial w^2}\right) + 2\left(\frac{\partial h}{\partial z}\frac{\partial X}{\partial z} + \frac{\partial h}{\partial w}\frac{\partial X}{\partial w}\right) - Pe_s\left(\frac{WZ}{A}\right)\lambda E_{OG}X = 0 \qquad 2.63$$

where $X = x - x^*_{e1}$ 2.64

Boundary Conditions

a) at the tray inlet:

$$X = X_I \text{ a constant} \qquad 2.65$$

b) at the tray outlet:

$$\frac{\partial X}{\partial z} = 0 \text{ Wehner and Wilhelm [129]} \qquad 2.66$$

a) at the impermeable column wall:

$$\frac{\partial X}{\partial n} = 0 \qquad 2.67$$

The diffusional flux at the liquid inlet may be written as

$$\frac{L}{W\rho_L} = D_{es}\left(\frac{\partial h'}{\partial z'}\right)_i \qquad 2.68$$

combining this equation with the definition equation for Pe_s, the following relationship is obtained:

$$Pe_s = \frac{-Z}{h_i}\left(\frac{\partial h'}{\partial z'}\right)_i \qquad 2.69$$

This Peclet number is meant to represent a random mixing mechanism that describes the transport of liquid and the changes in mass transfer due to liquid mixing. From equation 2.69 there is a maximum possible value for Pe_s which is found to be close to unity. Concentration profiles calculated from the model are of the form shown in figure 2.10. However, calculated Murphree tray efficiency and hence the enhancement of tray efficiency over point efficiency gives a pattern similar to that obtained by the AIChE. The small values of the maximum possible Pe_s suggest complete mixing of the liquid droplets while the predicted concentration profiles and the enhancement of tray efficiency over point efficiency are in agreement with those expected from plug flow behaviour.

This model, like the others before it, also requires substantial experimental data to clarify some of the conflicting observations made above.

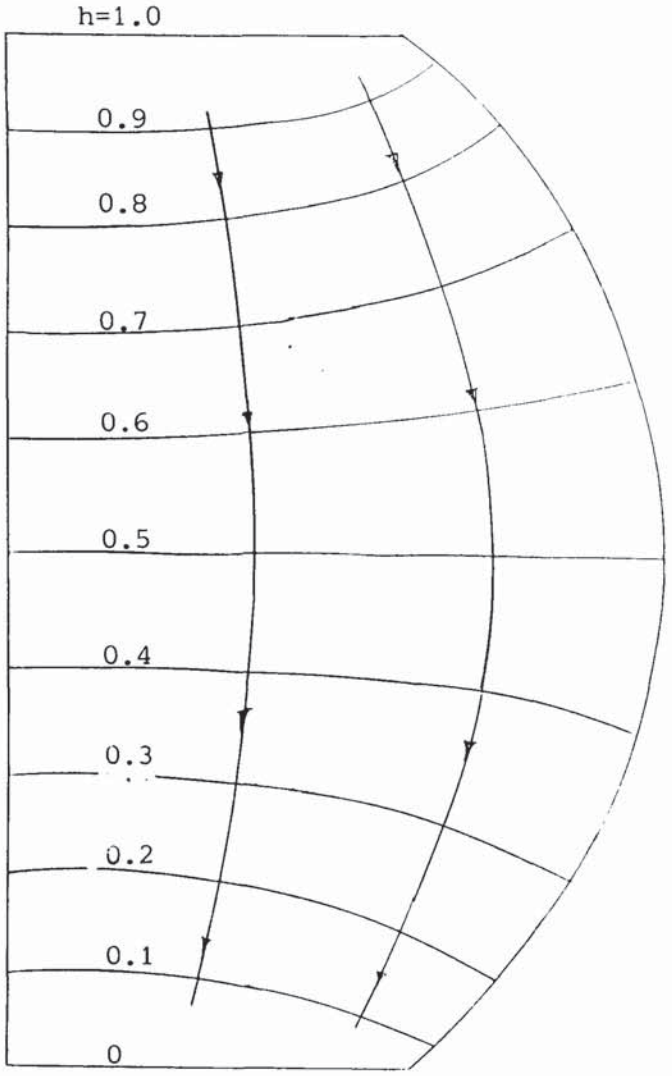

FIG:2.9 Calculated drop concentration profile

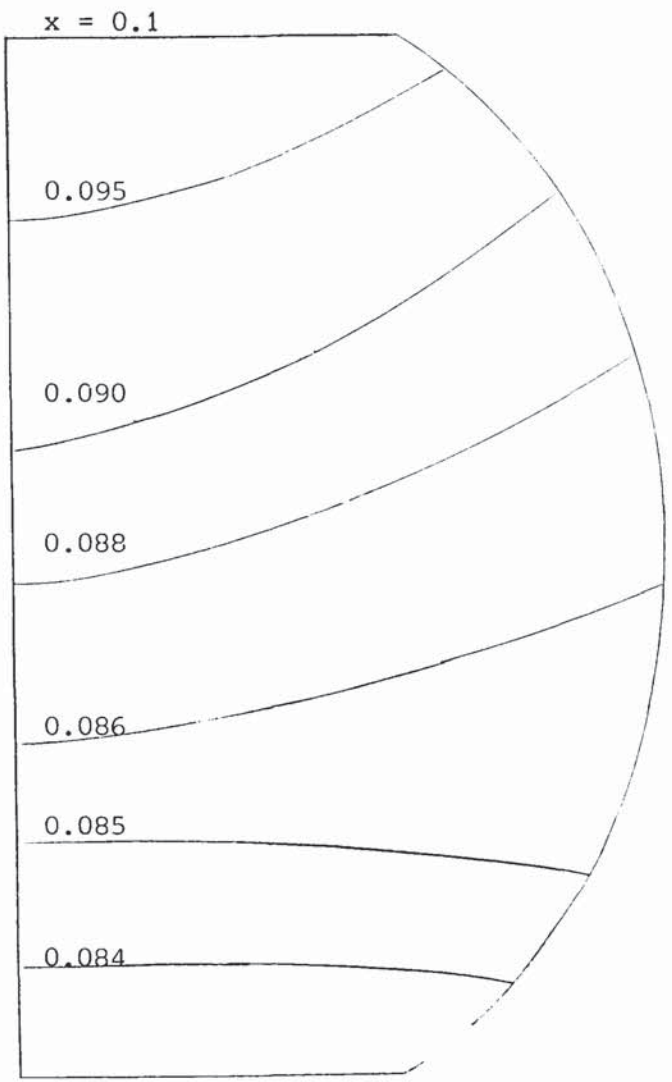

FIG:2.10 Calculated liquid concentration profile(x) for the Spray regime $\lambda Eo_c = 0.5, W/D=0.6, Pe_s = 1.07$.

2.4.5 Developing Flow Patterns (Sohlo)

It is expected that the positions on a tray where nonuniformities actually commence would influence tray efficiency in different ways [61,62,63,109,110,111]. This was considered to provide a possible explanation for existing discrepancies between some experimental findings and the predictions of the flow pattern models of Bell/Solari and Porter/ Lockett, where the flow patterns are generally assumed to develop early on, that is near the tray inlet weir. This observation adds yet another interesting dimension to the study of flow patterns on trays.

The derivation of the model equations is given below and is followed by an analysis of the implications of the model.

2.4.5.1 Derivation of the Mathematical Model

The general assumptions listed in subsection 2.4.3.1 are invoked along with that which states equal liquid mixing in both the flow and transverse directions. A rectangular tray geometry is employed for convenience.

The following dimensionless quantities are defined:

$$z = z' / Z \qquad 2.70$$

$$w = w' / W \qquad 2.71$$

$$X = \frac{x - x_{in}}{x^* - x_{in}} \qquad 2.72$$

$$v_z = v_z' / \bar{v}' \qquad 2.73$$

$$v_w = v_w' / \bar{v}' \qquad 2.74$$

$$\bar{Pe} = \bar{v}' z / D \qquad 2.75$$

$$\lambda = m.G / L \qquad 2.76$$

The material balance over an element of froth is given as

$$\frac{1}{\bar{Pe}}\left(\frac{\partial^2 X}{\partial z^2} + \left(\frac{z}{w}\right)^2 \frac{\partial^2 X}{\partial w^2}\right) - v_z \frac{\partial X}{\partial z} - v_w \frac{\partial X}{\partial w} - \lambda E_{OG} X = 0 \qquad 2.77$$

The continuity equation may be used to relate the dimensionless velocity component as

$$\frac{\partial V_z}{\partial z} + \frac{z}{w} \frac{\partial V_w}{\partial w} = 0 \qquad 2.78$$

Boundary Conditions

a) at the liquid inlet

$$z = 0 \quad 0 < w < 1 \quad X_+ = 1 + \frac{1}{V_z \overline{Pe}} \frac{\partial X}{\partial z} \qquad 2.79$$

b) at the liquid outlet

$$z = 1 \quad 0 < w < 1 \quad \frac{\partial X}{\partial z} = 0 \qquad 2.80$$

c) at the rectangular walls (an uncommon assumption)

$$0 < z < 1 \quad \frac{\partial X}{\partial w} = 0 \qquad 2.81$$

An axial velocity component normalised to the mean liquid velocity is defined as

$$V_z(z,w) = (1-V_s(z))f_v(w) + V_s(z) \qquad 2.82$$

where $f_v(w)$ is a function of the transverse liquid flow nonuniformities. A uniform velocity distribution corresponds to a value of the slip velocity at the column wall: $V_s = 1$. When $V_s = 0$ the distribution is independent of axial position and the distribution is said to be fully developed.

An equation for the transversed liquid channelling in the special circumstances of severe liquid channelling, is given as:

$$f_s(w) = 2.14 + 1.47w - 19.9w^2 + 29.83w^3 - 13.47w^4 \qquad 2.83$$

Various developing profiles were considered by the authors in their analysis. The results of the analyses are summarised in the next subsection.

2.4.5.2 Predictions of the Developing Flow Pattern Model

Large variations in plate efficiency are prdicted for various configurations of the slip velocity distribution particularly for large values of the Peclet number. It is noted that the Peclet number is defined such that $\overline{Pe} \propto D$ which implies that the large values of $\overline{Pe}$ correspond to large trays.

It is shown that even for linear development the model predicts high efficiencies even for large trays. Linear development is the nearest assumption to real operating trays.

By imposing various profiles of transverse mixing the model predicts that intense transverse mixing gives significant changes (improvements) in the enhancement of tray efficiency over point efficiency.

The result of assuming a rapid development of nonuniformities in the model is an exaggerated effect of liquid channelling and hence an underestimation of tray efficiency.

In small to medium size trays, late development of nonuniformity has little effect on tray efficiency. In large trays however, late development can have significant influence on tray efficiency.

2.4.5.3 Conclusion on Developing Flow Patterns

One observes that the basis for this model stems from the flow patterns where the experiments were conducted under the Spray regime for which an understanding of the shape of the flow patterns currently presents the greatest problems. Flow patterns reportedly develop quite early under conditions where the liquid loading is high and thus less likely to spray. It is clear that this approach will require experimental work covering a wide range of conditions in order to fully substantiate the claims of the model.

2.4.6 Conclusion on the Models For Large Trays

It is concluded that while all the models discussed above, with the exception of the Spray Diffusion model, reasonably account for both the existence and the deleterious effects of nonuniformities on tray efficiency, the equations representing them are not all the same. The choice of the individual critical parameters also differ.

The formulation of the Spray Diffusion model admits that it will always be misleading to isolate liquid flow pattern models from the flow regimes for which they may be applied. Since flow regimes describe the structure of the froth on a tray it seems reasonable to expect that the structure would be related in some way to the movement of the froth. Unfortunately research efforts into the two phenomena have not so far been properly coordinated. There is a meeting point between flow patterns on large trays and the flow regimes in which they operate. This fact is covered in some detail in the paper published by Porter and Jenkins [90].

In the subsection following, the concepts of the flow regimes are reviewed.

2.5 Flow Regimes

The basic distinction between the flow regimes is the structure of the froth (or gas-liquid mixture) on the tray. The distinction is often made between a predominantly liquid droplets structure and one that is not. Consequently, in the past, mention has only been made of the droplet dominated Spray regime and otherwise, often called the Bubbly or Emulsified regime.

The proposed froth structures of the flow regimes are given in the figure 2.11 below [137]. The Spray regime is depicted in figure 2.11a while figure 2.11b shows the Bubbly or Emulsified regime. The difference in bubbles size distribution as well as the way in which the bubbles cross the weir on the tray is illustrated in the figures.

The Bubbly regime is found in high pressure systems of low molecular weight compounds. The Spray regime is associated with low pressure systems (or vacuum) in which the compounds have high molecular weights. A new regime was identified by Hofhuis and Zuiderweg [49] which represents intermediate pressures, froth structure and froth flow, to those of the Spray and Bubbly regimes. This was called the Mixed regime and is representative of atmospheric pressure systems.

There are differences between the correlations (most are semi-empirical) derived by various authors for the transition from the

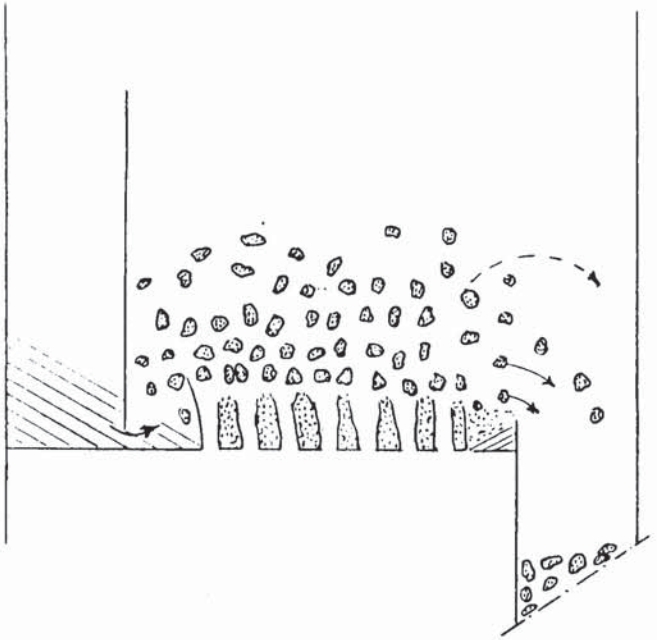

a.Supposed Froth Structure in Spray Regime
A gas continuous phase(comprises liquid droplets)

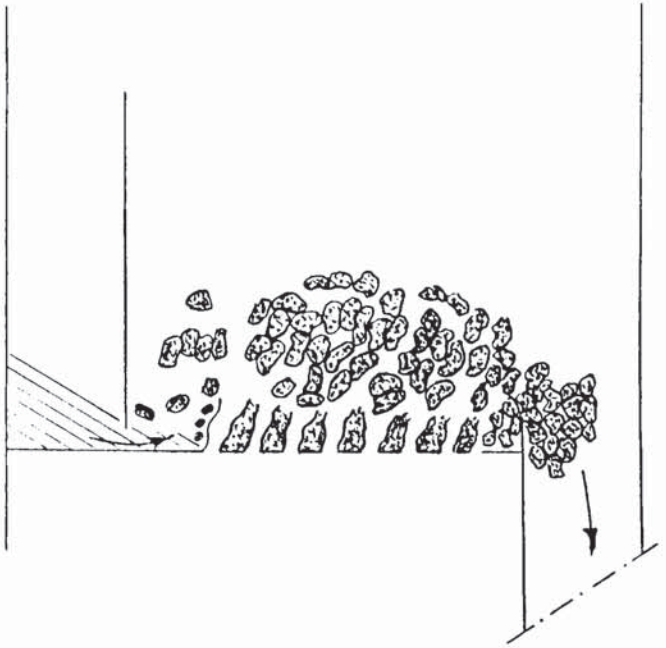

b.Supposed Froth Structure in Emulsified or Bubbly Regime
A liquid continuous phase

FIG:2.11 Supposed Froth Structure in Flow Regimes

Spray regime. This is thought to arise mainly because of the differences in the techniques employed to measure the transition and also due to differences in the ways that the regimes are described. The methods used to determine the transition and the correlations derived are listed in Table 2.3. Some of these are further discussed below.

Table 2.3

Reference	Method used	Equip.Size	Correlation
de Gooderen [41]	Surface tension change	4-in dia	-
Shakov et al [104]	Pressure drop & entrainment		
Porter and Wong [92]	Light transmission	18x18(in)	$\frac{z}{D_h} = \left(\frac{u_h - u}{u_h - u_s}\right)^{*6.7)+2.8}$
Burgess and Robinson [14]	Light transmission	4ft	-
Pinczewski and Fell [86]	Electrical probe	30·5cm x 61cm	$Z_{ct} = \frac{Kd\,(\rho_L-\rho_V)u_h^{1/3}}{\sigma}$ K 0.0067 for d=1.27cm.

Table 2.3 cont.

Reference	Method used	Equip.Size	Correlation
Payne and Price [84]	Light transmission	17x17.75(in)	$\frac{h_{LT}}{D} = 1.5u_h(\frac{\rho_g}{\rho_L} * \frac{}{gD})^{0.5}$
Barber and Wijn [6]	Photographic technique	4-ins flash vessel	$h_L/d_P = 1.35(\frac{p}{d_p})^{0.33} * (\frac{u_g(\rho_g/\rho_L)^{.5})^{.4}}{F(g.d_h)^{0.5}} - 0.59)$
Lockett [69]	-		$u_V(\frac{\rho_V^{0.5}}{\rho_L}) = 0.36\ \frac{h_L}{d_h}.F$
Hofhuis and Zuiderweg [49]	Light transmission	-	$u_V(\frac{\rho_V^{0.5}}{\rho_L}) = 0.85\frac{(gh_L)^{0.5}}{d_h}h_L.F$
Porter and Jenkins [90]	Entrainment data correlation	4ft	$\frac{q/b}{C_{sb}(\rho_V/(\rho_L - \rho_V)}0.5 = 0.07$

General Symbols used (symbols specific to the ref. not included)

d hole diameter (units as in reference)

h liquid hold-up (units as in reference)

u gas velocity

z,Z liquid hold-up

F F-factor

ρ density

Subscripts

T at transition

V,g gas phase

L liquid phase

d hole

2.5.1 Porter and Wong Correlation

The correlation [92], derived by the authors is probably best described as one which predicts the transition from the Spray regime. It is based on the changes observed by light transmitted through a bed of consisting of a gas/liquid mixture. The liquid droplets that make up the spray bed are distributed in various sizes in the space above the tray. Theoretically the droplets of similar size are expected to form a plane above the tray whose height is determined by their terminal velocity, U_t . Droplets with a terminal velocity below U_t will rise above the plane and then descend or get entrained in the gas stream. Drops of corresponding size and hence similar terminal velocity to U_t will form the hypothetic plane. These are designated as the "large drops". It was foound that for drops larger than 5.00mm diameter the terminal velocity becomes independent of size. Coalescence between rising and descending drops form even larger drops that concentrate below the plane. The formation of larger drops increases with increase in the liquid flow rate (and thus liquid hold-up) on the tray. At transition, multiple coalescence takes place transforming the plane into the surface of a "bubbly" dispersion.

From the experimental findings of the authors the following correlation was derived:

$$\frac{h_{c,t}}{D_h \rho_f} = 4.0 + 9\left(\frac{(1-A_f c_t (g(\rho_L/\rho_g).1/U_s)^{0.5})}{1 - A_f}\right) \qquad 2.84$$

or

$$\frac{h_{c,t}}{D_h \rho_f} = 4.0 + 9\left(\frac{U_h - U_t}{U_h - U_s}\right) \qquad 2.85$$

The general equation for the large drops terminal velocity is given as:

$$U_t = C_t . \left(g . \frac{\rho_L}{\rho_g}\right)^{0.5} \qquad 2.86$$

where C_t is a constant($ft^{1/2}$)

Under laboratory conditions the following correlation was derived

$$U_t = 1.04 . \left(\frac{\rho_L}{\rho_g}\right)^{0.5} \qquad 2.87$$

where,

U_h= gas velocity through the holes (ft/s)

A_f= fractional free area

$U_s = A_f U_h$(ft/s)

D_h= hole diameter (in)

ρ_f= froth density(or liquid volume fraction)

$h_{c,t}$= liquid holdup per unit area at transition(in)

The methods of visual observations and the light transmission technique gave reasonable good agreement. The experiments were conducted on a "static" column, that is where there was no cross-flow of liquid thus eliminating any effects that the liquid momentum may have at the transition point. Although this model was used to predict the transition from Spray to Bubbly there is no quarantee that it may similarly be used to predict the transition in the reverse direction, that is from Bubbly to Spray. This is because the processes of droplet formation and coalescence are not finely divided mirror images. The hysteresis effects noted by Shakov et el. provide the first real indications that these processes occur over a wide range of conditions.

However, the approach adopted in the formulation of this model and the findings therein were unique and provided useful experimental results against which subsequent models were correlated.

2.5.2 Prince Correlation

A simple approach based on pressure drop measurements was adopted to develop this correlation [84]. The theory stems from the analogy of the jetting processes at a single orifice [32,48,83,86,93].

For a fixed gas rate the variation of residual pressure drop with liquid hold-up was examined. The residual pressure drop was defined as

$$P_{res} = P_T - P_{dp} - h_{cl} \qquad 2.88$$

where P_T is the operating tray pressure drop

P_{dp} is the dry plate pressure drop

h_{cl} is the clear liquid height

The liquid holdup is defined as the dynamic head less the orifice momentum effects (also referred to as the gas momentum recovery [26]). The transition between bubbly and spray is said to take place at the maximum value of of the residual pressure drop. Two methods were used to determine the liquid holdup: a) the direct measurements of dynamic head using manometers and b) gamma ray absorption to determine dispersion density.

The theory of the model is based on the behaviour of a single orifice in which both bubbly and jetting take place. The bubbly and jetting processes are considered as froth and Spray respectively. At the transition a simple correlation is proposed which may be used to describe the bubbly/spray transition on an operating tray. This relation is given as:

$$h/d_h = 1.5.Fr^* \qquad 2.89$$

or $$h_T/d_h = 1.5.e.Fr^* \qquad 2.90$$

where the modified Froude number Fr^* is given as

$$Fr^* = \left(\frac{\rho_g}{e\rho_L}.\frac{U_h^2}{gd_h}\right)^{0.5} \qquad 2.91$$

and d_h is the hole diameter (m),

h_T is the liquid hold-up at the transition (m),

h is the dispersion height at transition (m),

e is the liquid volume fraction (equal to the dispersion density in the air/water system).

Reasonable agreement was found between this correlation and the transition results of Fane and Sawistowski [32] for the distillation of benzene-heptane and heptane-toluene. It is interesting to note that in their first set of results, Prince et al.[83] established a coefficient of 1.5 for the modified Froude number while in subsequent experiments a value of 1.7 was required to correlate the same. This change is indicative of a slight shift towards an incipient Bubbly regime. While the authors attribute this shift to errors inherent in the experimental measurements it may well be that at transition the liquid flow rates cover a range of values rather than occur at a single point. It is necessary to make a correct estimate of the clear liquid height in order to implement the model.

The possibility of the transition occuring over a range of conditions is considered in the next correlation.

2.5.3 Zuiderweg and Hofhuis Correlation

Four separate flow regimes were identified [49,137]. Perhaps the most significant implication of this finding is that for the first time it is suggested that the transition from Spray to Bubbly and vice-versa occurs over a range of liquid flow rates for a fixed gas rate. This implies that the Bubbly and Spray regimes may not be representative of most operating systems as hitherto understood.

The four regimes identified are as follows:

a) Spray: dominant in vacuum distillation systems

b) Mixed: dominant at atmospheric pressure distillation

c) Emulsified: dominant at high liquid/vapour ratios, that is pressure systems

d) Free bubbly: dominant in conditions close to the weeping limit

These are represented in figure 18 of reference [49]. It gives a plot of the load (or capacity) factor versus the flow parameter. The weeping limit was calculated from the widely used Fair correlation [29,30,117], while the flooding curve was derived from experiments by the authors using air-water. At the flow parameter value = 0.1 a change in the slope of the flooding curve was observed to coincide with the point of transition to the Emulsion regime. The newly identified flow regimes are the Free Bubbly and the Mixed regimes. In the Free Bubbly regime the bubble formation occurs at the tray orifice and since this is consistently observed only close to the weeping limit it thus has limited practical importance. By contrast the Mixed regime exhibits general characteristics associated with both the Spray as well as the Bubbly regimes. That is, both the formation of bubbles and droplets appear to coexist in the Mixed regime. This is representative of atmospheric sytems and most distillation systems are thought to operate in this regime.

The correlation equations are given as

1) transition into the Spray regime

$$U_g \cdot \left(\frac{\rho_g}{\rho_L}\right)^{0.5} = (CF) = \frac{0.85 \cdot g^{0.5} h_L^{1.5} A_f}{d_h} \qquad 2.92$$

2) transition into the Emulsion (Emulsified) regime

$$\frac{U_L}{U_g}\left(\frac{\rho_L}{\rho_g}\right)^{0.5} > 3.0 b h_L \qquad 2.93$$

The equation 2.93 for the transition into the Emulsion regime shows that by varying the weir height which influences h_L and by varying the weir length the transition can be moved over a range of conditions from atmospheric to pressure distillation.

The criticisms of this model was made by Lockett in reference [68] where the author found discrepancies between this and other models. It was thus pointed out that the relationship between h_L / d_h and U_g as proposed in this model is misleading particularly at high gas velocities. This is because at high gas velocities, tray oscillation occurs and becomes significant to tray orifice behaviour [13].

Nevertheless, the model has distinguished separate flow regimes which must henceforth be considered in the design of trays. In the next correlation the effects of tray performance variables was introduced and consideration given to the existence of the regimes identified in this subsection.

2.5.4 Porter and Jenkins Correlation

What is paramount to the designer is not so much the tray orifice mechanisms at transition but rather knowledge of whether a particular combination of gas and liquid flow rates would result in Spray, Mixed or Bubbly. Such a combination is proposed by the authors [90] by correlating the changes in certain variables at transition in terms of the flow ratio number:

$$\Psi = (q/b)/U_g\left(\frac{\rho_V}{\rho_L - \rho_V}\right)^{0.5} \qquad 2.94$$

This group which was defined by Hofhuis and Zulderweg [49] is seen to be proportional to the ratio of the overall horizontal momentum flux of the liquid to the average vertical momentum flux of the gas (this definition was first given by Fair and Mathews in reference [117]). Use was made of the entrainment data of Lockett, Spiller and Porter [72]. Interpretation of the data showed that the locus of the minima in the entrainment curves at fixed gas rates was identical with the liquid hold-up at the transition from Spray to Bubbly as measured by Porter and Wong [92]. The entrainment data published by Sakata and Yanagi [102] for the

distillation systems; cyclohexane-n-heptane at 165kPa (1.69bars) was plotted in terms of the capacity factor and weir load with entrainment rate as a parameter. It was shown that both the entrainment points and the maximum capacity points for the system may be correlated by a straight line passing through the origin, figure 2.12. At the lower end of the curve, lie the points for the air water data of Lockett, Spiller and Porter derived to suit the tray design of Sakata and Yanagi. The reciprocal of the slope or more appropriately the value of the flow ratio number is:

$$\Psi = (q/b)/(U_{sb}.(\frac{\rho_V}{\rho_L - \rho_V})^{0.5} = 0.07 \qquad 2.95$$

The curve represented by this slope was considered to be the transition from the Spray regime to the Mixed regime and vice-versa. The entrainment rates in the Mixed regime are, as expected, lower than those in the Spray regime. No entrainment was recorded in the Emulsion regime of reference [102]. However, the value of $\Psi = 0.20$, employed by Hofhuis and Zuiderweg was adopted for the transition from Emulsion to Mixed regime and vice-versa. It must be pointed out that the equations of the flow ratio group used by these authors differs somewhat in general from that used by Hofhuis and Zuiderweg. Hofhuis and Zuiderweg used the equation

$$\Psi = (q/b)/(U_{sb}(\frac{\rho_V}{\rho_L})^{0.5} \qquad 2.96$$

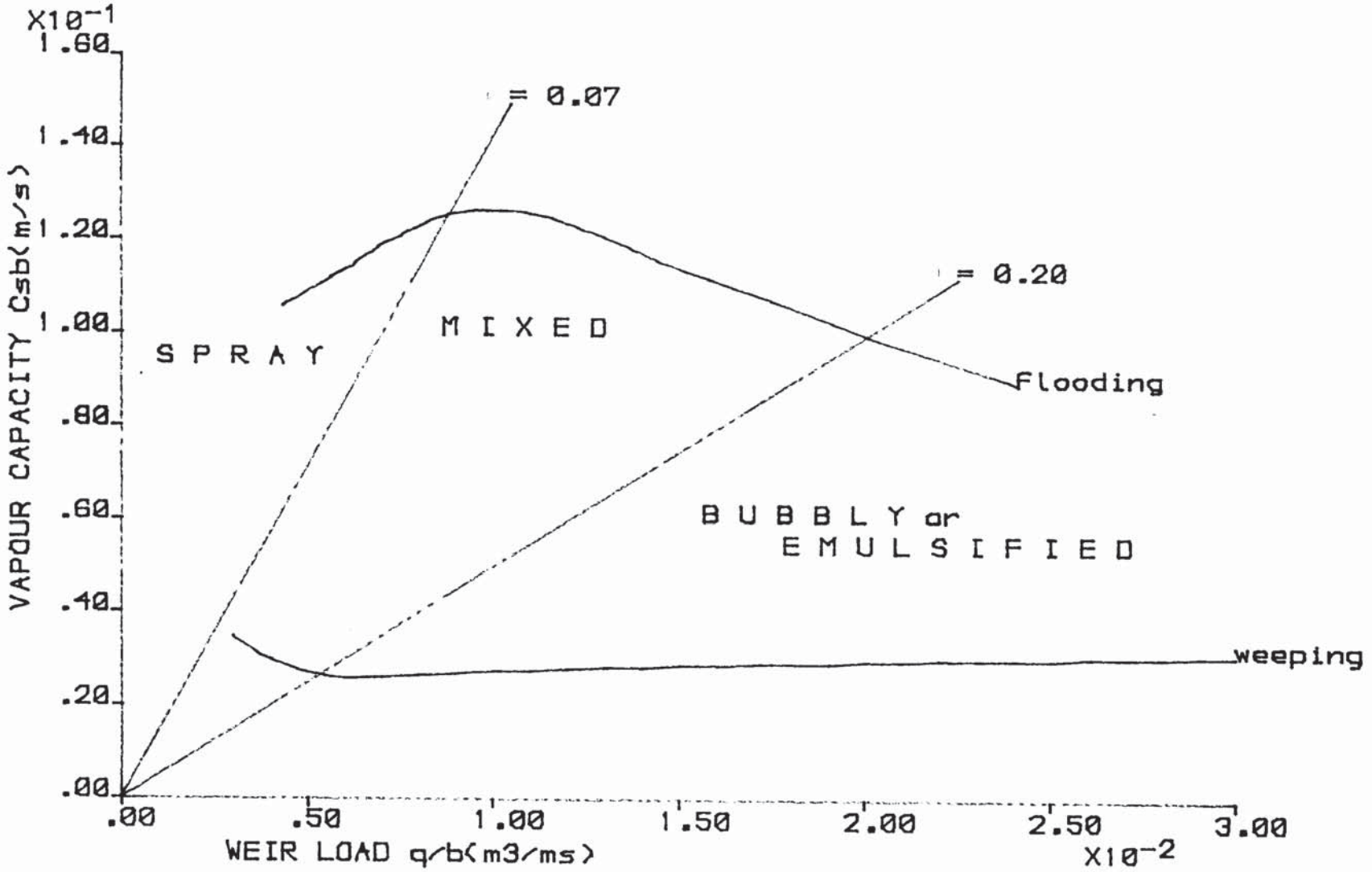

FIG2-12 FLOW REGIMES TRANSITION LINES
(PORTER/JENKINS)

In air-water systems this amounts to the same thing since,

$$\rho_L >> \rho_V \text{ or } \rho_L = \rho_L - \rho_V \qquad 2.97$$

In distillation systems this does not always apply.

The real merits of this correlation stems from the facts that:

a) At 80% flood there is good agreement between this correlation and that of Hofhuis and Zuiderweg. The correlation is developed along the entrainment results obtained from separate experiments by Porter and Wong at the transition from Spray to Bubbly and applied to data from a commercial sieve tray.

b) It represents the first direct correlation with maximum capacity

c) It is a simple relatinship and thus requires only the fundamental knowledge of the densities of the phases, the flow rates and tray design. Consequently, it is subject to quick and easy verification.

2.5.4.2 Application of the Correlation to Tray Design

This correlation is tailored to meet the designers needs in the following way. He can specify b and A(U_{sb}). The equation for the flow ratio group can be simplified to:

$$\Psi = X' \left(\frac{A}{b}\right) \qquad 2.98$$

where $$X' = q/\left(U_{col}\left(\frac{\rho_V}{\rho_L - \rho_V}\right)^{0.5}\right) \qquad 2.99$$

the bubbling area being:

$$A = C * D^2 \qquad 2.100$$

where C is a constant

Therefore, the flow ratio group becomes,

$$\Psi = X.D^2 / b \qquad 2.101$$

The ratio of weir length to tray diameter b/D has been used as a design parameter in the channelling models of Porter et al [68,70,89].

Put $b' = b / D$

then $$\Psi = X.b'.D \qquad 2.102$$

The system properties which may remain practically constant for a particular operation together with the operating variables q and U_{sb} belong in the parameter X . It follows from equation 2.102 that by varying b one can traverse a range of flow regimes. It also predicts that for a fixed weir length b, in a particular system, by increasing the tray diameter the regime can change from Spray to Mixed or even Emulsified. Lower values of the flow ratio group are associated with small diameter trays and from the equation 2.102 a tendency to spray may also be expected. These predictions prove to be consistent with the observations in normal distillation practice.

Where $\Psi > 0.20$, that is at high weir loads for large diameter trays the value of the flow ratio group may be reduced by increasing the number of passes on the tray, e.g, from single pass to double pass. This is illustrated by the total flows chart in figure 14and figure 15 of reference [90]. The figures confirm that the conclusions of Hofhuis and Zuiderweg that most trays operate in the Mixed regime and that the Spray regime is associated with low pressure distillation and small diameter trays is valid. Further, the total flows chart of reference [90] shows the diameters at which change over from single to two pass and four pass trays are recommended in order to lower the flow ratio group and thus improve capacity.

Comparisons between this correlation and the others shows little agreement. These are illustrated in figure 2.13. This desparity seems to be of a fundamental nature. It may well be that the hole

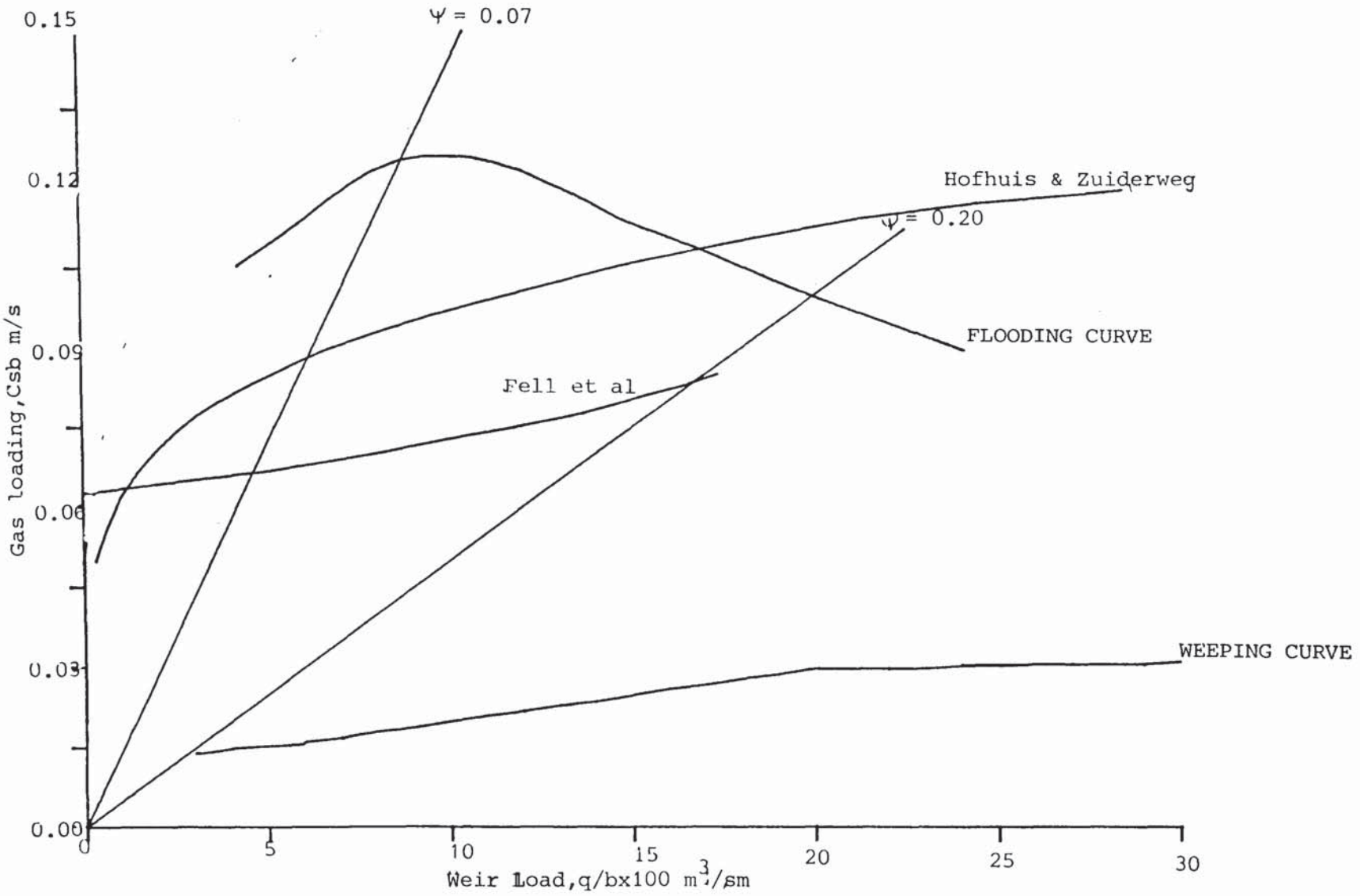

FIG: 2.13 Flow Regimes Transition Correlations on the Weir Load/Capacity Plot

diameter, strongly emphasized in other correlations but conspicuously missing in this one needs further consideration. However, it is noted that the transitions into the Spray regime proposed by other workers is closer to the flooding limit thus limiting its application in real practice.

2.5.5 Discussion and Conclusion on Flow Regimes

Use of the jet penetration theory to model the transition from Spray to non-Spray appears to be strongly favoured by researchers. Accordingly, the models are expressed in terms of the ratio of the clear liquid height to the hole diameter, froth density and/or physical properties of the system. This requires a precise prediction of the clear liquid height for which there is at present no accurate correlation. Both de Gooderen [40] and Zuiderweg and coworkers point out the possible effects of surface tension on the performance of trays operating outside the Spray regime. Surprisingly, this is not given any treatment in the models published in literature.

Although Hofhuis and Zuiderweg succesfully correlated the data of Pinckzewski and Fell [82] in certain conditions, it is apparent that at extreme values of weir loads and capacity factors, Spray is predicted at the flow ratio group values exceeding $\Psi > 0.20$, that is in the Emulsified regime.

The concept for representing the transition from Spray to Bubbly as a region between the two regimes is a new development in the study of flow regimes. This was first introduced by Hofhuis and Zuiderweg.

The analysis of Porter and Jenkins in which low weir loads are associated with vacuum distillation and tend to Spray while pressure systems Emulsify is consistent with the observations made in literature. This fact was also used to arrive at the transition lines by the authors.

The capacity of pressure systems is limited by downcomer area rather than entrainment as in low pressure systems. Downcomer flooding is sensitive in foaming systems, therefore the omission of surface tension as a parameter in the transition from the Mixed regime to the Bubbly regime is suspect.

It is expected that liquid mixing is high in the Spray regime. It may be deduced that the underlying flow pattern will be unique and with it the implications of flow regimes on mass transfer which is still unclear.

It is fair to say that research into flow regimes has yet to catch up with tray design methods.

In view of the limitations shown by the definitions and observations of the flow regimes it is clear that vast amounts of experimental work will be required to confirm or refute the diverse claims made in flow regimes studies.

At present the evidence for the effects of flow nonuniformities is so strong that much has been done to develop flow control devices on trays. Infact, the idea of flow control devices on trays is not entirely new since it formed the basis for some of the early models by Lewis [64]. Some of the devices experimented on in more recent times are discussed in the next Section.

2.6 Flow Control Devices

It was predicted by Porter and Lockett [68,70]) that for medium diameter trays (2-2.5m) it is not necessary to achieve an optimum liquid flow pattern. The sensitivity of efficiency to the liquid flow pattern only begins to show at diameters larger than 3.0m. It follows that for such size columns steps taken to improve the liquid flow pattern would reap economic benefits.

There are three different tray modifictions known from published literature which have been developed to eliminate flow nonuniformities at the sides of trays. These include:

1. The directional slotted sieve plate, developed and patented by Union Carbide [130,131]
2. The step flow downcomer, patented by Porter [88]
3. The FRI downcomer which consists of underflow gaps of varying heights (from the centre to the sides of the tray) [135].

2.6.1 The Slotted Sieve Plate

Directional slots were punched into a sieve plate so as to direct the passage of vapour across the plate. The nonuniformity of liquid is therefore removed entirely by the vapour momentum.

More slots were made in the converging section of the tray and towards the sides of the tray (column wall) than in the other parts. The results for such an arrangement are predictable. Improvements to flow were observed particularly in the converging section.

However, this begets two relevant questions. First,can the point efficiency rightly be considered to be the same in the slotted region as it is in the perforated region?. And, to what extent will the presence of the slots affect the lower (weeping) limit?

The primary objective was to minimise flow nonuniformities and the tests showed that this was achieved.

2.5.2 The Step Flow Dowmncomer

The device is a modification to the inlet downcomer. The top of the downcomer is, in general, of a conventional type since it is meant to fit the outlet downcomer of the tray immediately above. The bottom part is half a cylindrical tube with the circular part facing the active area of the tray. If, as is held by several authors,flow nonuniformities originate from the uneven momentum flux of the liquid issuing from a straight downcomer then liquid redistribution forced by the shape of the downcomer is expected to straighten the flow.

Dye studies were carried out by Safekourdi [101] using this device. The results reported were promising. The details of the

design, the application and results from this work are treated separately, later in Section 7.

2.5.3 FRI Downcomer

Fractionation Research Incorporated, FRI, employed a slotted downcomer with a small underflow gap at its centre and relatively larger underflow gaps at the sides. Details of the device are given elsewhere in reference [135]. Residence Times Distribution Experiments were carried out on the device. These showed that non-uniformities at the sides of the tray were largely eliminated. The size of trays used were 1.2m (4ft) and 2.4m (8ft) in diameter.

2.6.4 Conclusion on Flow Straightening Devices

The ultimate choice of a device is entirely an economic consideration since all the devices discussed have been shown to remove nonuniformities to a satisfactory extent. Based on this consideration it may be judged that the step flow downcomer is an attractive option since it is of a simple design and does not require additional devices to the tray.

Up to this point in the literature survey, the work discussed has been based on the experiments simulating mass transfer processes. It was earlier pointed out in Section 1, that difficulties inherent in mass transfer experiments are formidable and do infact limit the scope of such experiments. In the next subsection, the

water cooling theory which enables the analogy between mass trasfer and heat transfer to be made is discussed. This, as was earlier stated, is the basis of the water cooling technique used for the first time, in this work, to simulate mass transfer.

2.7 Water Cooling Theory

The water cooling theory considers the simultaneous heat and mass transfer that takes place from the surface of a film of water in contact with a flowing stream of air. It has wide industrial application and is often used in the design of cooling towers and refigerating systems. In this work it is sought to implement the analogy between a water cooling process and mass transfer processes such as distillation. The equations used to justify this are discussed.

2.7.1 Derivation of the Theory

The usual assumptions made in the development of the theory are [74,119]:

a) that water vapour follows the ideal gas laws(the deviations may be treated as insignificant),

b) that there is negligible loss of water through evaporation and,

c) that ALL heat losses are carried through the passing vapour and

d) the bulk-water state below the water-air interface is at substantially the same temperature as the interface, that means

that the rate of transfer of heat through the interface to the air phase is negligible compared to that from the water to the interface.

When a stream of air is passed through water, if evaporation occurs the water looses heat as a result of the difference between the vapour pressure of the water and that of air. It does so in the form of latent heat. Sensible heat loss (or gain) would also occur due to direct transfer by conduction between air and water.

An overall heat balance yields

$$L \Delta T = G \Delta H \qquad 2.103$$

Earlier works regarded the latent heat of evaporation and the sensible heat transfer as separate entities. Merkel [75,76] first proposed the concept of an overall enthalpy driving force by combining the effects of both mechanisms simultaneously.

If one considers an element with an area dA, figure 2.14 by denoting the interface by the subscript I, the bulk gas phase by G and the sensible and latent heat transfer by S and L respectively, the rate equations for the transfer of heat through the element can be expressed as:

a) For sensible heat transfer

$$dq_s = h_G(T_i - T_G).dA \qquad 2.104$$

where h_G is a surface or convective heat transfer coefficient.

b) For latent heat transfer

$$dq_L = K_G(D_i - D_G).\lambda_t.dA \qquad 2.105$$

where λ_t is the latent heat of vaporisation of water, D the humidity of the vapour and K_G the mass transfer coefficient between the interface and the gas bulk phase.

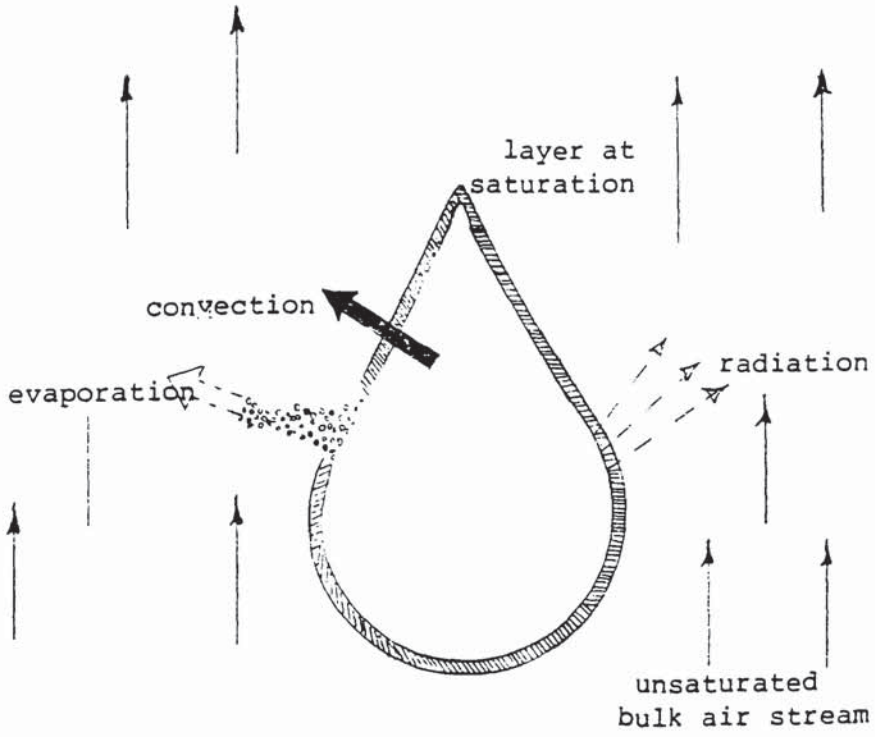

Figure 2.14 Mechanisms of heat loses from a water droplet (culled from reference 119)

Now, according to Merkel, the total heat transfer is given by adding equations 104 and 105 to yield:

$$dq_T = (h_G(T_l - T_G) + K_G(D_i - D_G)\lambda_t).dA \qquad 2.106$$

Assuming that the latent heat remains constant in the temperature range:

$$\Delta T = T_l - T_G, \qquad 2.107$$

the overall enthalpy change in the gas phase is given by,

$$H_l - H_G = c_w(T_l - T_G) + \lambda_t(D_l - D_G) \qquad 2.108$$

where c_w is the specific heat of water.

By substituting into equation 2.106 one obtains:

$$dq_T = K_G(H_l - H_G).dA = c_w L.dT_w \qquad 2.109$$

Separating like variables:

$$\frac{K_G dA}{L.c_w} = \frac{dT_l}{H_l - H_G} \qquad 2.110$$

Integrating;

$$\frac{K_G A}{Lc_w} = \int \frac{dT_l}{H_l - H_G} \qquad 2.111$$

It is clear from this basic equation of heat transfer which was first derived by Merkel that the it is not self-sufficient and therefore cannot be integrated analytically. Numerical methods are used. Usually the amount of water evaporated is negligible or neglected.

The theoretical similarities between water cooling and distillation have been made in literature, although there is no known publication of experimental evidence showing this [45,74,115]. For instance, the ratio $Lc_s / K_G a'$ is known as the "height of an equivalent theoretical plate",H.E.T.P or often as "the height of a transfer unit", in distillation terminology. In water cooling this represents the height required for the air to attain equilibrium with the water, that is, the theoretical height required for enough contact to have been made to saturate the air, leaving. In this case the number of transfer units, or the reciprocal of the H.E.T.P is given as,

$$c_w \int \frac{dT_l}{H_l - H_G} = \frac{K_G . a_m}{L} . Z = N.T.U \qquad 2.113$$

The treatment of water cooling tower as a distillation column is best illutrated by Hutchinson and Spivey [53]. They derived an overall heat balance equation over an entire N-trayed column which is of the form :

$$L.(T_{N-1} - T_N) = G.(H_N - H_{N+1})$$

or

$$T_{N-1} = \frac{H_N - H_{N+1}}{L / G} \qquad 2.114$$

Once the overall heat balance is used to compute the water temperature leaving the column (or it is given) it is possible to do a tray to tray calculations to determine the temperature gradient across the column. Unlike mass transfer operations the feed point for the water is always at the top of the column.

This analysis has only given a general similarity between the methods of calculations for the two processes. It seems quite reasonable to extend this to include the concept of efficiency.

2.8 The Analogy Between Heat and Mass Transfer Characteristics

It was shown in subsection 2.2 that the concepts of efficiency are derived from basic principles in mass transfer through the resistances to mass tranfer in the individual phases. This in turn is affected by the froth structure and bubble size distribution which are influenced by the rate of gas passing through the tray. The mechanism of gas passage through the froth is often approximated by one of two models:

a) complete mixing in the vertical direction, giving, the point efficiency as :

$$E_{OG} = N_{OG} / (1 + N_{OG}) \qquad 2.115$$

b) the plug flow case, which gives;

$$E_{OG} = 1 - e^{-N_{OG}} \qquad 2.116$$

The variable N_{OG} is the number of overall gas phase transfer units and is defined as:

$$N_{OG} = K_{OG}a\ h_f A_f (y^* - y) \qquad 2.117$$

The analoque to this appears quite frequently in water cooling theory. It is defined as:

$$N'_{OG} = K_G a\ h_f A_f (H^* - H) \qquad 2.118$$

It is noted that for air-water systems (humidification and dehumidification) the overall coefficient of mass transfer is defined in terms of the humidity of the gas, it thus has the units of $kg/sm^3(kg/kg)$.

Considering the individual phase mass transfer units the "two-film" theory may be invoked. The following relationship can be derived;

$$N_{OG} = k_G a\ h_f A_f (y_i - y) = k_L a\ h_f A_f (x - x_i)$$

$$= K_G a\ h_f A_f (y^* - y) \qquad 2.119$$

Mass transfer resistances can be derived by rearranging equation 2.119 to give:

$$\frac{1}{K_G a} = \frac{1}{k_G a}\cdot\left(\frac{y^* - y}{y_i - y}\right) = \frac{1}{k_G a} + \frac{1}{k_G a}\left(\frac{y^* - y_i}{y_i - y}\right)$$

$$= \frac{1}{k_G a} + \frac{1}{k_L a}\left(\frac{y^* - y_i}{x - x_i}\right)$$

$$= \frac{1}{k_G a} + \frac{m}{k_L a} \qquad 2.120$$

Now to determine a similar expression for heat transfer the assumption is made that the surface heat transfer coefficient within the liquid-air interface is numerically equal to the mass transfer film coefficient. This is the Lewis 'semi-empirical' relationship [66,115].

2.8.1 The Lewis Number

The Lewis number is a measure of the ratio of the diffusivity to the conductivity of the film of moist air at the interface. These quantities are represented individually by the Schmidt and Prandtl numbers, such that by definition ;

$$Le = \frac{Sc}{Pr} \qquad 2.121$$

or $$Le = \frac{u/(\rho . D_l)}{u . c_{pm}/k}$$

$$= \frac{k/c_{pm}}{\rho . D_l} \qquad 2.122$$

Since the film layer is difficult to establish and hence the corresponding variables, the relationship is often expressed in a more general form:

$$Le = \frac{k/(z_l c_{pm})}{\rho(D_l/z_l)}$$

or $$Le = \frac{h_l/c_{pm}}{\rho D_l/z_l}$$

or $$Le = \frac{h_l}{K' c_{pm}} \qquad 2.123$$

where h_l is the surface heat transfer coefficient at the interface and K' is the mass transfer coefficient from the interface to the bulk air stream. The physical meaning of these equations is that within the film surrounding the water surface the transfer of mass or material and that of heat occurs at equal rates. Both processes are not influenced by the exterior conditions of the surrounding bulk fluids .

The value of the Lewis number is between 0.9 and 1.0 but for most practical purposes, it suffices to use unity.

2.8.2 The Resistances in Heat Transfer

Similar expressions to those of mass transfer can be drawn for binary mixtures in which heat transfer takes place between the surfaces. The notations used are not universal, but rather are chosen in order to show the comparisons with the corresponding forms for mass transfer.

A heat flux through the surface may be represented thus:

$$Q' = K_T a\, h_f A_f (H^* - H) = h_w a.h_f A_f (T - T_I) = k_T a.h_f A_f (H_I - H) \qquad 2.124$$

The resistances follow;

$$\frac{1}{K_T a} = \frac{1}{k_T a}\left(\frac{H^* - H}{H_I - H}\right) = \frac{1}{k_T a}\left(\frac{(H^* - H_I) - (H - H_I)}{H_I - H}\right)$$

$$= \frac{1}{k_T a}.\left(1 + \frac{H^* - H_I}{H_I - H}\right)$$

$$= \frac{1}{k_T a} + \frac{1}{h_w a}\left(\frac{H^* - H_I}{T - T_I}\right)$$

$$= \frac{1}{k_T a} + \frac{m'}{h_w a} \qquad 2.125$$

The last two terms in the equation can be rearranged to give:

$$-\frac{h_w}{k_T} = \frac{H_I - H}{T - T_I} \qquad 2.126$$

The equation 2.126 is that of the slope of the lines from the "start-to-finish" points on the operating line up to the saturation line for a given process.

In practice the task of determining the transfer coefficients, $K_G a$ and $K_T a$ is a formidable one. Often it suffices to base the determination of the point efficiency on the general equations .

The liquid concentration term in mass transfer is analogous to the liquid temperature term in water cooling.

It seems that the basis is set for implementing the water cooling theory to simulate mass transfer in a trayed column.

2.9 Conclusion on Literature Survey

The review of literature in this work leads to certain conclusions about tray design methods.

It is now fully established that the early models failed to take into account the effects of such features as shape and flow nionuniformities on efficiencies. The resultant equations are an oversimplification that assumes a rectangular configuration for the liquid flow path on the tray and thus overpredicts tray efficienccies in large trays.

The models applicable to large trays were proposed by the authors: Porter and Lockett [68,70,71,89]; Bell [9,10,11,112,113,114]; Sohlo et al.[61,62,63,109,110,111]; Kafarov et al.[55] and others. They all seem to predict nonuniformities on tray sides and account for the effects of such nonuniformities on the tray efficiency. The parameters emphasized however, differ.

The Spray diffusion model of Porter and Lockett [91,101] suggests that under conditions where the froth structure may be described as Spray, this and not the channelling model must be used. The other models make no such distinction.

The specifications of points of transition between flow regimes in trays is still not well correlated. This problem is one of disagreement on what constitutes the transition as well as methods employed to identify it. Perhaps the answer to this is the broad band of conditions that make up the newly identified Mixed regime.

The experimental observations of Weiler et al.[130,131] were carried out under the prescribed Spray regime of Porter and Jenkins. The findings represent an interesting coincidence with the observations of Raper et al.[94,95,96,97] particularly in the shape of the RTD lines towards the tray outlet.

It is noted that the derivation of the developing flow patterns of Sohio et al. was partly guided by the experimental findings of Weiler et al..The authors, however, failed to acknowledge that the experiments were carried out under conditions that favour Spray. Flow patterns in the Spray regime cannot be generalised with those outside it.

The evidence of retrograde flow and stagnancy were scant on trays of 1.2m and 2.4m diameter. These findings confirm the observation that at intermediate diameters and below, flow nonuniformities do not show clearly.

There is discrepancy on the tray size above which it is recommended to switch over from single to double pass so as to minimise flow nouniformities. 3.0m is recommended by Porter and Lockett while Smith and Delnicki [118] found that flow nonuniformities do not show up in columns below 5.0m in diameter.
The latters experiments were carried out under vacuum. This author believes that the discrepancy arises from the separate flow regimes for which the different approaches are applicable.

The evidence presented in literature on flow straighteners are promising. However, since they represent a fundamental change to tray design they must be applied over a wider range of sizes and flow conditions before firm conclusions can be made on them. A proper assesment of their viability must be carried out along economic lines.

It has become clear from this literature survey that further insight into tray design methods would only be possible when the existing models can be substantiated with experimental data. The difficulties involved in extracting such data have already been stated in Section 1.

In the latter part of the review, the application of the water cooling theory to simulate distillation was investigated. The main thrust of this work is concerned with the evaluation of the water cooling technique to provide the much needed experimental data.

3. APPROACH TO THE PROBLEM

The literature survey has shown that further development of the tray efficiency models (and the authenticity of the existing ones) is somewhat inhibited by lack of experimental data to test the effects of liquid flow patterns on mass transfer. It has been shown that the technique of water cooling offers a promising alternative for obtaining such data. However, work is required to develop and evaluate the technique. This work is presented below. Most of what is described is concerned with the development of the technique and the calculation procedures. This is followed by a program of work and the use of the technique to determine temperature profiles on conventional trays and trays fitted with flow straightening devices.

3.1 Choice of column and Plate

A 1.22m (4ft) diameter column was considered large enough for piloting. It is of commercial scale and although at this size it is already predicted that channelling will not have much effect on tray efficiency, significant effects on concentration profiles may be expected.

The plate chosen is a Sieve Plate having 12.7mm (1/2in) holes, 8% Free Area, and 26% downcomer area, all meant to be the similar to the FRI tray used in reference [102], both because it is the most common tray in practice and for the added possibility of comparing results from reference [103]. Details of the Tray are given in the Table below.

Table 3.1 Tray Design Detail

Column Diameter (m)	1.22
Tray Spacing,(Test Tray to Top) (mm)	800
Perforated Tray,thickness (mm)	1.5
Edge of Hole facing Vapour flow (description)	sharp
Hole Diameter and Spacing, (mm x mm)	12.7x41.0
Outlet Weir:height x length, (mm x mm)	75 x 940
Downcomer Area, m^2	0.13
Effective bubbling area, (m^2)	0.8554
Hole Area, (m^2)	0.0715

3.2 Development of the Water Cooling Method of Testing Trays

The following procedure was adopted:

3.2.1 Development of water cooling theory and prediction of expected temperature profiles. Will the technique provide a method of evaluating existing theoretical models?.

3.2.2 Development of temperature measurements and data logging. There was the need to make as many measurements at as many parts of the tray as possible so as to establish a tray temperature field.

3.2.3 Data processing to determine the "best" lines or surface of temperature measurements.

3.2.4 Methods of calculating tray efficiency and point efficiency were developed.

All of the work described above was required to develop the simple idea of water cooling to the point where it may be used to test trays.

3.3 Experiments on Trays

These include :

3.3.1 Tests of the effects of flow patterns on temperature profiles

a) Maldistributed flow

b) uniform flow on a conventional tray and

c) the effects of flow control devices

3.3.2 Tests on a conventional tray

Flow rates were set to simulate the hydraulic conditions ofmsome FRI tests and to explore differences between different flow regimes as shown by the temperature profile.

3.3.3 Calculation of point efficiency and tray efficiencies

3.3.4 The Evaluation of Repeatability and the effects of measurement errors.

Finally;

3.4 A Comparison of Experimental Temperature Profiles with those Predicted from the Channelling Model of Porter and Lockett

The major experimental work and the implications of the findings are described below in the sequence given above.

4. DESCRIPTION OF THE APPARATUS

The water cooling experiments described in this section were carried out in two separate stages. In the preliminary stage, the results of temperature measurements led to the conclusion that serious improvements in the method of data collection as well as the distribution of air and water into the column, were required. Thus the column was completely revamped. First, a description of the column rig used for the preliminary experiments is given. This is followed by a detailed description of the main physical changes in the revamped column. Experimental evidence from the two arrangements are given separately. Other experiments relevant to the water cooling technique are discussed in this section.

All air-water experiments were carried out in a 1.22m (4ft) diameter column. The column was 4.0m high and had an average wall thickness of 6.3mm. The capacity was 4 trays at an average tray spacing of 0.61m. Steel rings, 51mm x 6.3mm were fitted along the internal wall of the column to serve as tray supports.

The column was made of polymethylmethacrylate, trade named Perspex, which was tansparent thus enabling visual observations into the column to be made. The trayed section of the column was covered at the top by an entrainment separator (also called the demister) and a built-in removable PVC (Polyvinyl-chloride) air duct. The bottom section of the column constituted the sump. The material of the sump was therefore made of strong glass reinforced

PVC and had an average wall thickness of 12.7mm. This was of relatively higher thermal resistance than perspex and thus suitable for the retention of hot water in circulation during the water cooling experiments. The sump had a capacity of about 1.00m^3. It was covered from the trayed section of the column to prevent air from coming into contact with the recycled water.

The main test rig is shown in figure 4.1. A flow sheet of the test rig is given in figure 4.2.

4.2 Peripheral Equipment

4.2.1. Air Fan

A centrifugal fan with the capacity of 2600kg/s was used to supply air to the column. Due to its high decibel level, the fan was placed some 20m away from the column in a separate room. The discharge of the fan was introduced to the column (tangentially) through a rectangular duct of cross-section, 46cm x 46cm.

4.2.2. Water Pump

A centrifugal pump lifted water from the sump to the top of the column. It was operated below full capacity at only 0.00-1.14x10^{-3} m^3/s. The maximum possible capacity of of 7.58x$10^{-3}$$m^3/s$ was unattainable because of the extra head required due to the height of the column. The discharge from the pump was passed through three

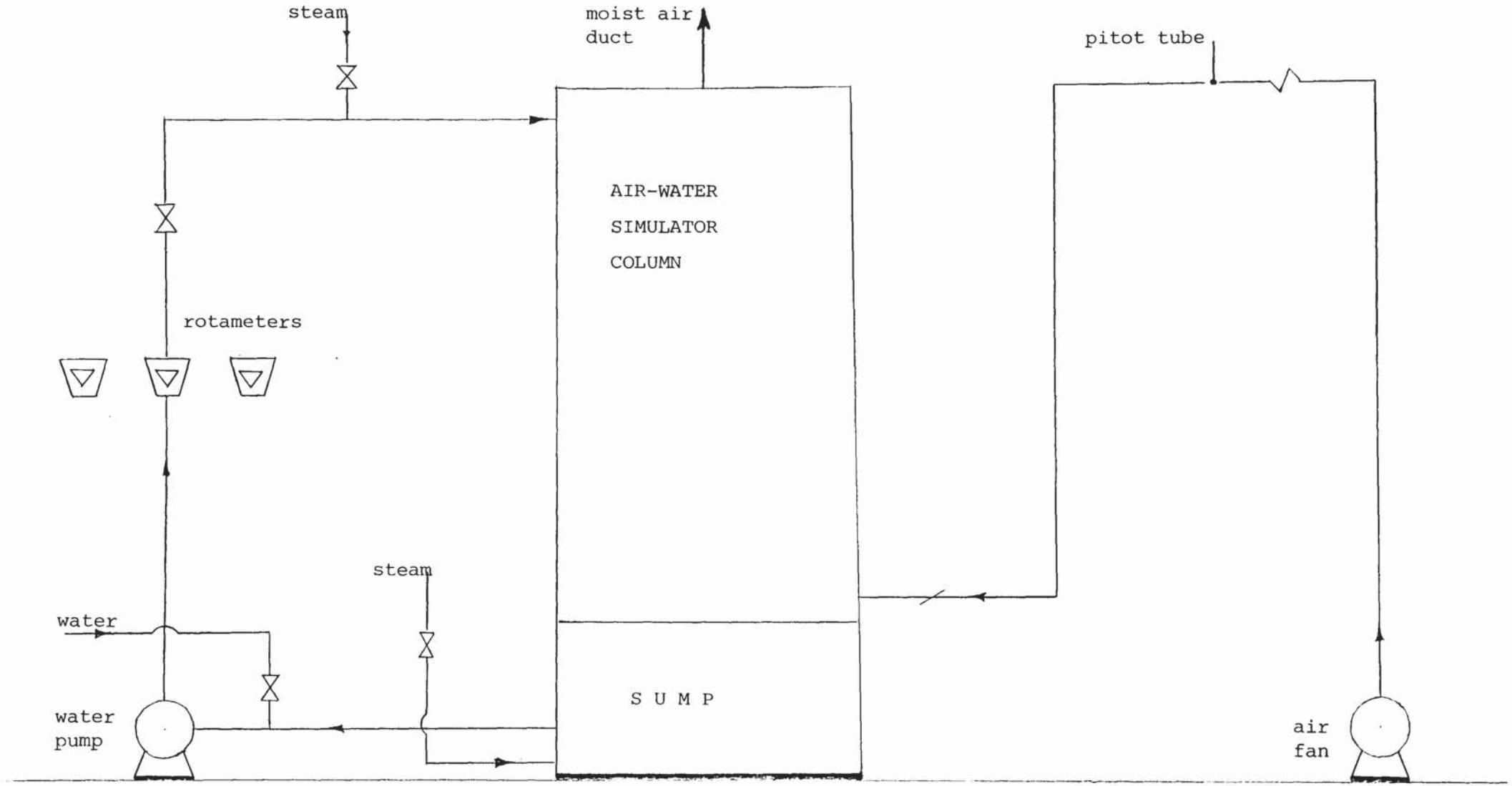

FIG:4.1 A Flowsheet of the Column Rig

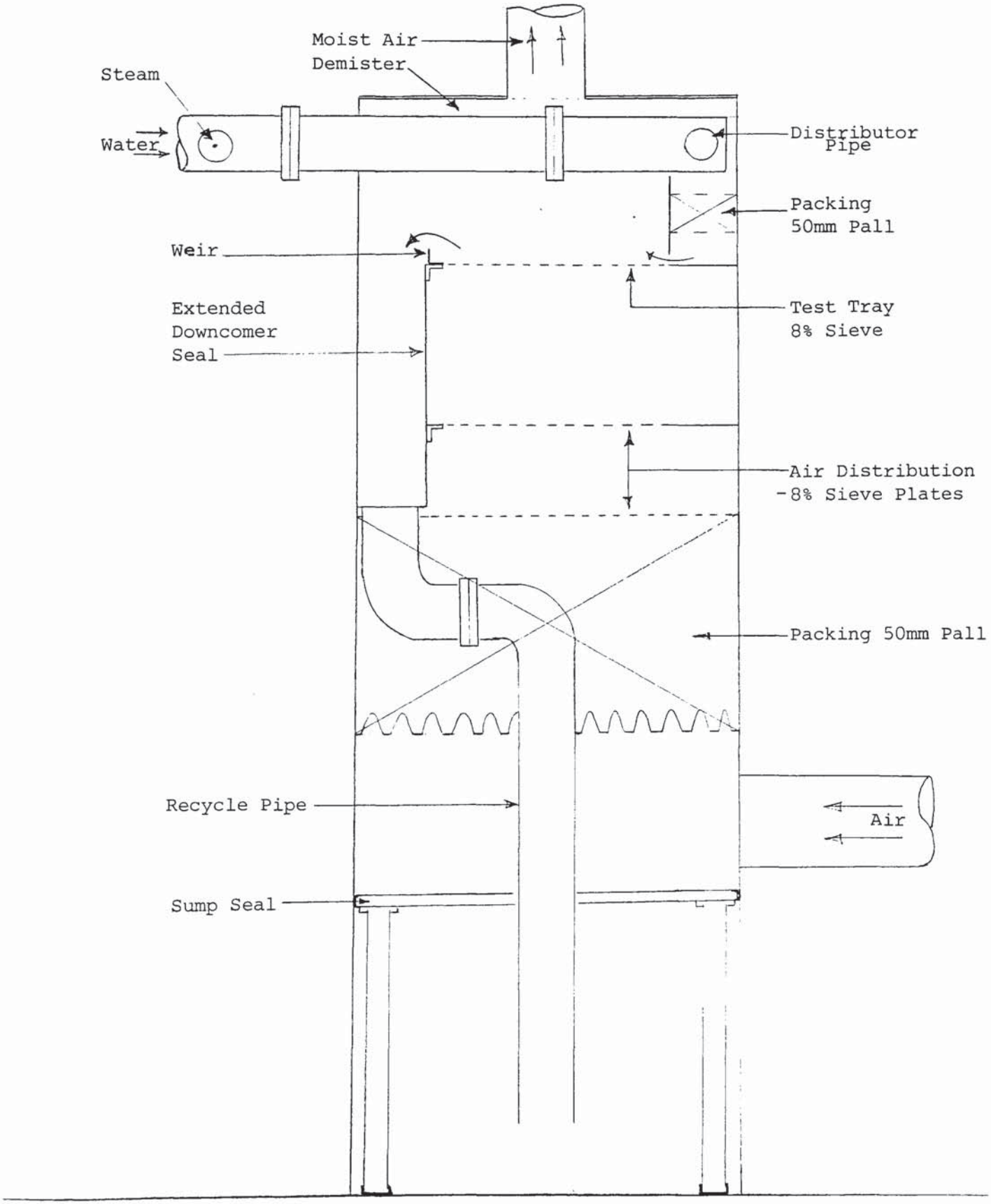

FIG:4.2 Revamped Column Showing Internals

separate pipes fitted with rotameters to monitor the rate of water going into the column.

4.2.3. Steam Generator

A steam generator with a capacity of 120psi was used to supply steam for general purpose use in the building. It was tapped from the main line at 80psi for use in the water cooling experiments.

4.3 Material Feed Lines into the Column

Since the development of this technique was intended to determine the liquid flow patterns on trays all necessary precautions had to be taken to ensure that material fed into the tray tested was well distributed at entry. The precautions taken are described for each material.

4.3.1 Air

The tangential introduction of air into the column resulted in the air streams swirling as they approached the test tray. These effects were minimised by fitting two sieve trays below the test tray.

The existence of rectangular elbows in the air duct from the fan to the column resulted in wavelike oscillations of the air stream as it approached the column. A perforated mild steel plate was

shoved into the duct both to regulate the flow of air as well as to dampen the oscillations.

To assist control at low flow rates, a wooden plank was used to cover a fraction of the fan suction area. This also acted as a safeguard against back pressure which could lead to permanent damage to the fan.
Close control of air flow was effected downstream by fitting a simple butterfly valve close to the column.

4.3.2. Water

The discharge from the pump could be passed through one of three pipes described below.

Pipe	Internal Dia.	Orifice Dia.	Flow Rate Range
1	76.2(3.0in)	38.1(1.5in)	$0 - 0.303 \times 10^{-3}$
2	76.2(3.0in)	50.8(2.0in)	$0.303 - 1.518 \times 10^{-3}$
3	203.2(8.0in)	152.4(4.0in)	$0.758 - 7.583 \times 10^{-3}$

The distribution of the water / steam mixture into the test tray was effected by passing it through an inlet downcomer packed with 51mm Pall rings to a height of 500mm. The packing was held at a clearance of 200mm from the tray floor.

4.2.3 Steam

Steam was tapped from the main steam line in the laboratory and sparged into the sump when filled with cold water. The final section of the steam line was made of a 0.7m long, 12.7mm diameter perforated copper tube. The tube was sealed at the end. This last section was fitted into the bottom of the sump with a clearance of 50mm from the sump floor. Effective mixing of steam in the sump was achieved due to the perforations in the tube as well as the turbulence created by the water recycled into the sump.

4.3 Measurements of Operating and Systems Variables

The essential variables required to implement the water cooling technique fall into two separate groups. The air water flow rates may be called the operating variables. Water temperature and air enthalpy are grouped as the systems variables. It is assumed that under all the conditions for the experiments in this work other physical properties of the system such as viscosity and density did not change significantly. The procedure for the measurements of these variables is described individually.

4.3.1 Measurements of Air Flow Rates

A pitot tube was located at the longest straight section of the air duct. The change in the liquid head h, due to the passing air was read from the manometers of the pitot tube. The air velocity U_s was calculated from the equation :

$$U_s = \sqrt{2.g.\Delta H} \qquad 4.1$$

where g is the acceleration due to gravity ($9.81 m/s^2$)

The correct equation for the superficial air velocity through the sieve tray is:

$$U_s = C_d \sqrt{2.g.\Delta H} \qquad 4.2$$

where C_d, the discharge coefficient for the sieve tray is $C_d = 0.66$, [26].

The pitot tube fitted to the air duct, was calibrated against another pitot tube by doing a traverse across the top of the column. In brief, 220 individual measurements of point velocity were taken, at points on a square mesh for each of 10 flow rates.

An example of such measurements is presented in Table A:B4. The resulting calibration curve is given in figure A:B1. From these measurements, the total air flow was calculated and this was used to calibrate the single pitot tube in the duct. The correct values of the load factor, C_{sb} are plotted against the calibrated pitot reading in the duct in figure A:B2.

4.3.2 Measurements of the Water Flow Rates

The water flow rates were measured by rotameters fitted to the discharge pipes. These rotameters were calibrated in an earlier work by Norton Company [80].

4.3.3 Measurements of Temperature

Since temperature was the main variable in the development of this work certain specific steps were taken to ensure that it was satisfactorily determined. The steps taken were:

i. to obtain an accurate measurements device

ii. to employ a simple device that would fit into the tray without undue interference to flow

iii. to obtain a sufficient number of measurements on the tray

iv. to make an adequate location of measurement points to represent a temperature field corresponding to the liquid in the bubbling (active) area of the tray and,

v. to ensure that the measured quantity was the temperature of the air-water mixture on the tray and not, for instance, that of the tray floor or of the air.

The thermocouple was used to measure temperatures. The thermocouples used were of the type "K", that is an alloy of Nickel-Chromium / Nickel-Aluminium (Ni-Cr/Ni-Al). These have fast response and are also relatively cheap. In the preliminary work they were handmade from 0.48mm thick wires and encased in plastic sheaths. Readings of the thermocouple voltages were recorded from a manually operated Potentiometer System [28].

The Potentiometer System was made up of a selector switch unit with a provision for 20 thermocouples, a thermocouple placed in an ice-bath to serve as the cold junction, and a medium grade portable DC Potentiometer equiped with a battery operated detector which served as the null deflector. The thermocouple voltages were registered by the Potentiometer and recorded manually. The voltages were converted to temperatures using standard calibration charts [128].

Figure 4.3 shows the locations of measurements points on the tray. The thermocouples were laid horizontally across the tray at a clearance of 100mm from the tray floor. They were supported by narrow steel rods. The tips of the thermocouples were held a mere 15mm from the tray floor by tying them to studs welded to the steel rods.

a. thermocouple location on the tray (units: mm)

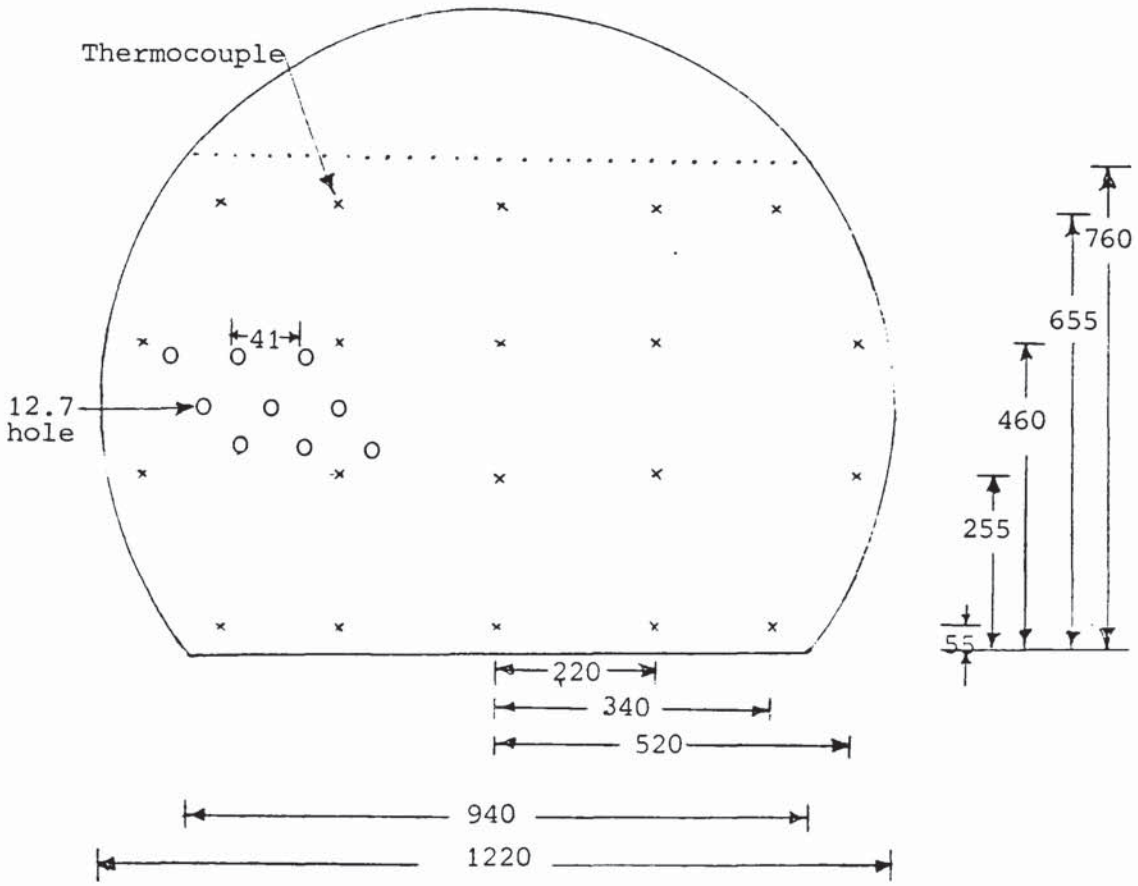

b. thermocouple layout in column

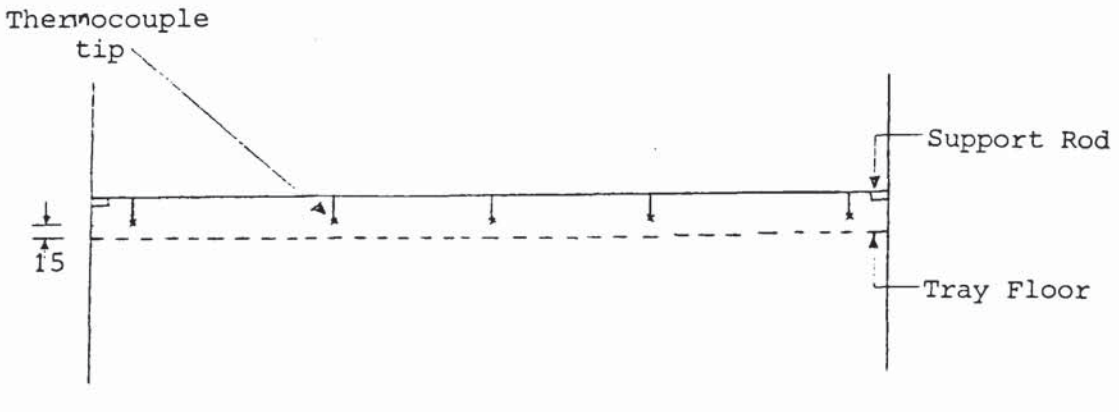

FIG:4.3 Thermocouples on Test Tray in preliminary experiments

4.4. Discussion of the Results of the Temperature Measurements.

Table 4.1 below, lists the voltages and corresponding temperatures in °C for a typical experiment carried out under the conditions specified. The temperatures are shown in their respective locations on the tray in figure 4.4a. The arrangement, a 4 x 5 array enables cross plots of temperatures against distance for each row to be made as shown in figure 4.4b. From these plots coordinates of constant temperatures were derived and joined together on a tray geometry to give the lines of constant temperatures or what henceforth became known as temperture profiles. An example is shown in figure 4.4c.

Table 4.1 Thermocouple Voltage and Corresponding Temperature Conversion based on reference [127]

C_{sb}=0.092 m/s; q/b = 0.960E-2 m^3/sm

Couple No.	Volts x 10^{-3}	T°C	Couple No.	Volts x 10^{-3}	T°C
1	1.472	36.80	11	1.354	33.85
2	1.705	42.63	12	1.285	32.13
3	1.684	42.10	13	1.280	32.00
4	1.564	39.10	14	1.343	33.58
5	1.369	34.23	15	1.422	35.55
6	1.407	35.18	16	1.442	36.05
7	1.370	34.25	17	1.341	33.53
8	1.451	36.28	18	1.341	33.53
9	1.521	38.03	19	1.437	35.93
10	1.520	38.00	20	1.425	35.63

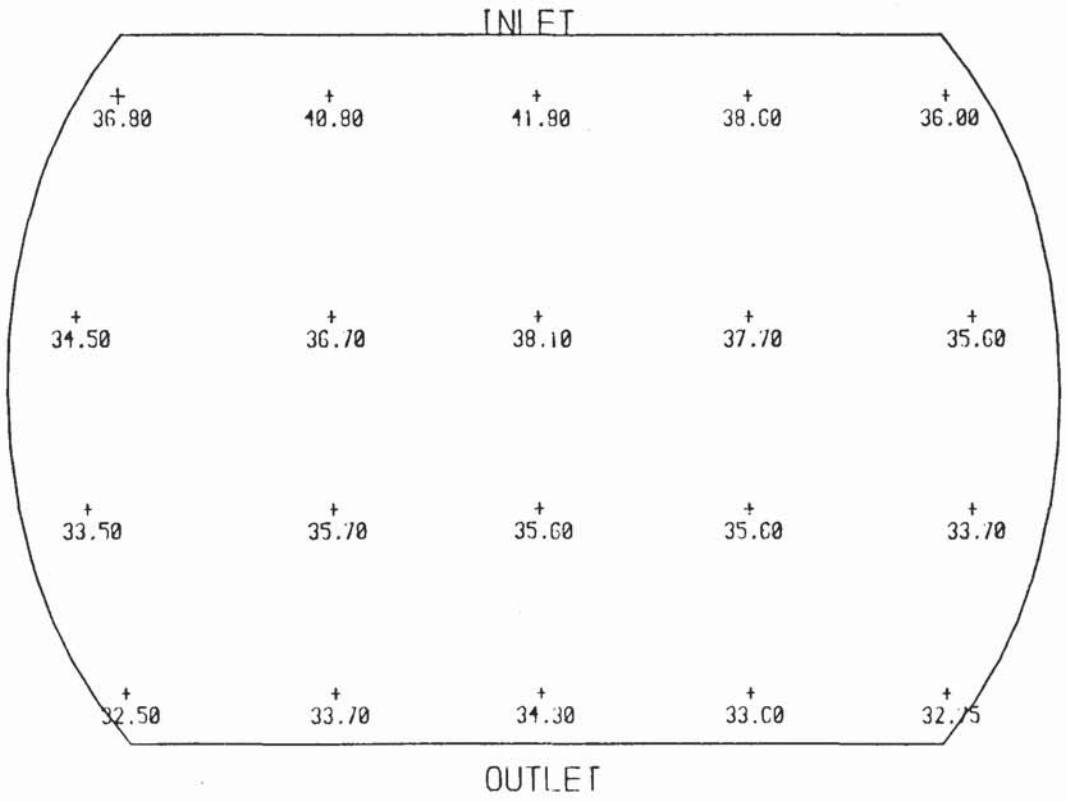

a: TEMPERATURES(°C) ON A TRAY

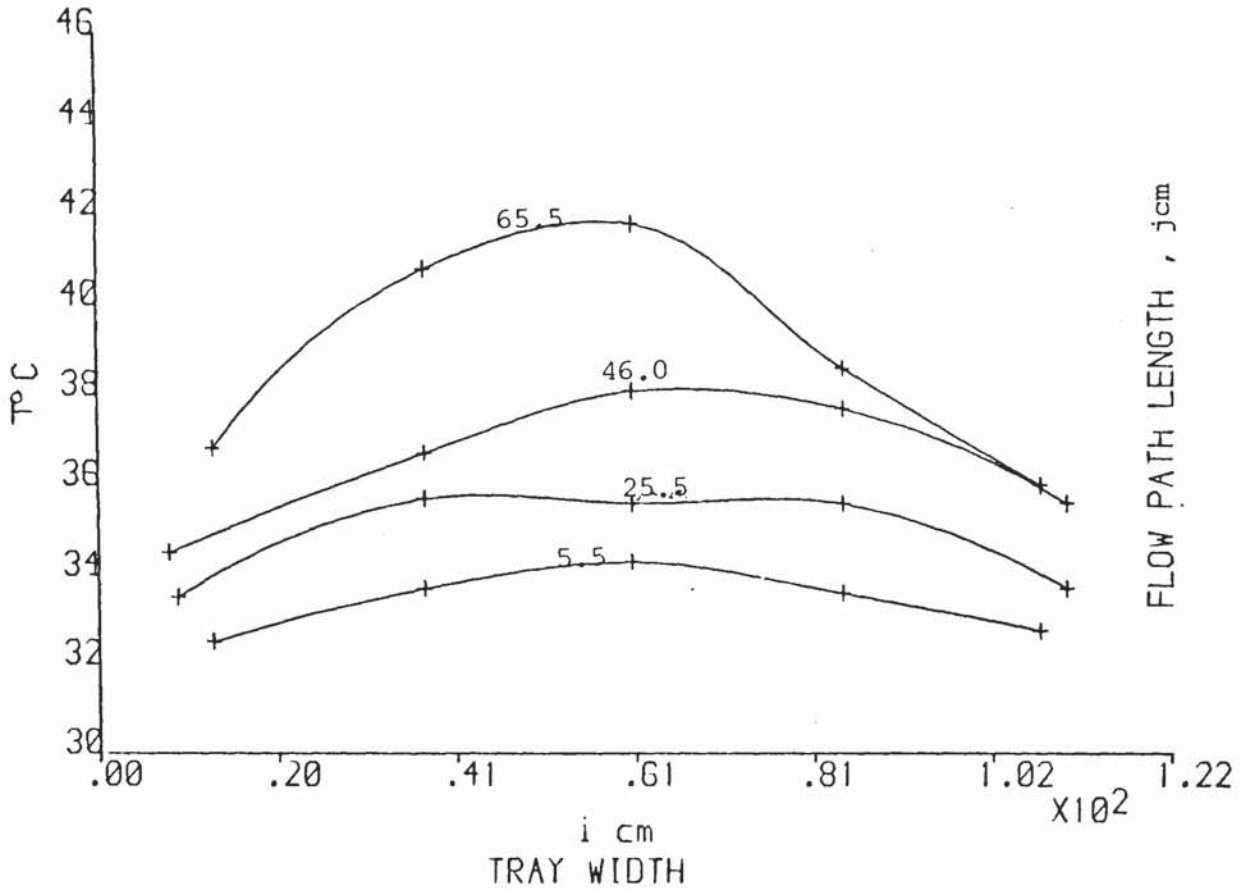

b. CROSS PLOTS

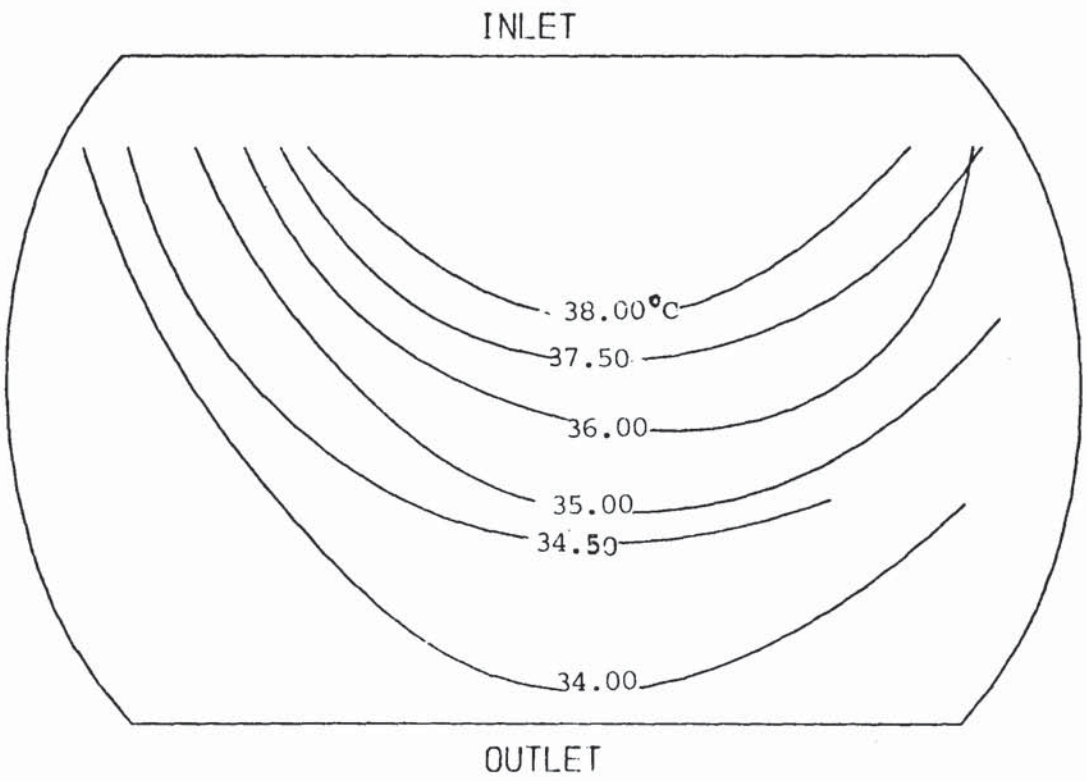

C:TEMPERATURE PROFILES

FIGURE 4.4 : TEMPERATURE PROFILES
(FROM CROSS-PLOTS)
Csb=0.092m/s ;q/b=0.960E-2m3/sm

The main advantage gained from using this measurement equipment was that it offered the prospects, at this initial stage of the work, of testing the technique by using very cheap and available equipment. The lessons learnt from the findings are best summarised in the following sub-section.

4.4.1. Inferences from the Temperature Measurements.

It could be inferred from the results that:

I. the temperature drop across the tray in the low liquid rates of the Spray regime could be as high as 12°C and as low as 3° C in the Mixed regime. The implications of this are discussed later.

II. the potentiometer pointer was unstable in the Spray regime. The pointer was oscillating rapidly over a wide range of readings and thus judgement had to be made to ascertain the mean reading.

III. Irregular patterns of temperature profiles were prevalent with this set up. Irregular profiles is used to describe profiles that either intersect or cross in places on the tray geometry.

IV. The method of data collection and recording was time consuming, tiresome and prone to errors of judgement. Although the voltage response of the device was fast the process of establishing a mean reading for a thermocouple and manually recording this was about 15 mins. for all 20 thermocouples particularly for the Spray regime.

v. Too much judgement was required to draw the temperature profiles. Since only the transverse direction was used to cross-plot the temperatures on the tray it was implicit in this that errors in the longitudinal (or flow) direction were assumed to be relatively small. There is no evidence to support this thus making this assumption another possible source of error in the analysis.

4.5 Conclusion on the Temperature Measurements

The conclusions drawn were that:

i. from the apparent instability of the temperatures in the Spray regime, the temperatures detected could be that of the passing air jets and intermittent bridges of liquid under the thermocouple tips.

ii. from the irregular patterns it can be concluded that poor distribution patterns emanated from the entering streams of air and water.

iii. the handmade thermocouples were inadequate (calibration is given in Appendix B, Table A:B2) to confidently determine the temperature profiles in the Mixed regime where the overall temperature drop across the tray was relatively low (3 C in places).

4.6 Reconstruction of the Column Rig

The conclusions drawn from the preliminary equipment led to a complete revamping of the whole column rig. The column was revamped specifically to meet the following requirements:

i. to remove uncertainties about poorly distributed air and water entering the tray.

ii. to further improve the positioning of the thermocouples so as to avoid direct contact between the gas jets issuing from the tray holes and the thermocouple tips

iii. to use more thermocouples on the tray with better thermocouple accuracy.

iv. to develop a method of measurements of the inlet wet-bulb temperature inside the column.

v. to develop data logging to give time averaged, and if required, time dependent measurements of temperatures on the tray.

vi. relocation of the steam entry point at the top of the column thus bringing it closer to the test tray than from its previous location inside the sump.

vii. to make other relevant changes to the rig

The physical changes made to the column to achieve these requirements are discussed in turn below.

4.6.1 Improvement on the Distribution of Air and Water

I. Air distribution

51mm Pall rings were packed to a total height of 910mm directly above the air inlet point in the column above the sump. This was in addition to the two distribution trays preceding the test tray as shown in figure 4.2.

II. Water distribution

A PVC pipe, 76.2mm internal diameter was attached to each side of the main feed pipe inside the inlet downcomer. Two holes were made under each pipe and in the main pipe so as to enhance the distribution of the water entering the downcomer. This was in addition to the packing inside the downcomer described in subsection 4.3.2. This is shown in figure 4.5.

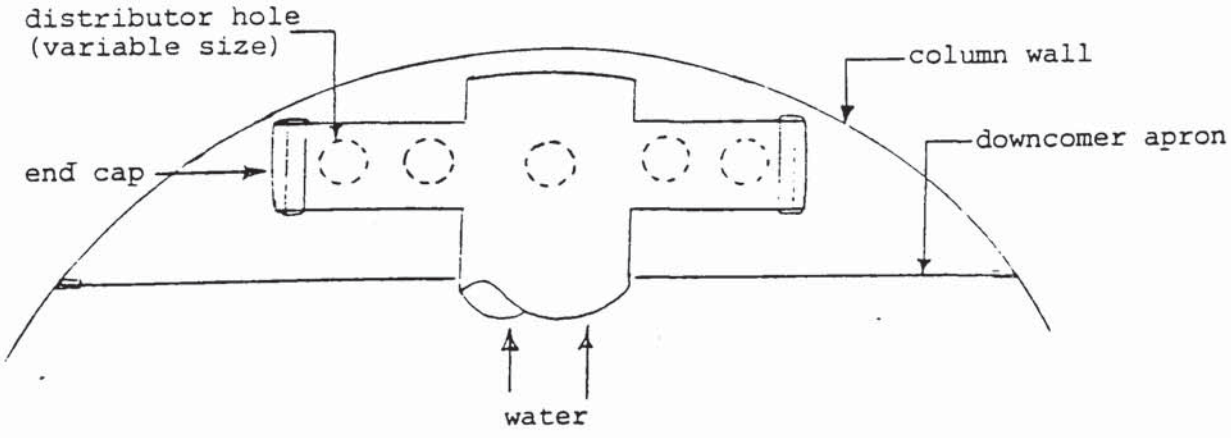

FIG:4.5 Water Distributor Pipe

4.6.2 Development of Positioning of Thermocouples.

In the preliminary tests carried out the results were in agreement with the conclusion made in reference [120], that whenever the thermocouple tip was immersed in the froth (usually at below 15mm), the temperature gradient in the vertical direction within the froth remained negligible.

The thermocouple stem was placed on the tray floor at the point where the measurement was required. Then, the last 5mm to the tip was bent and held upwards. As much as possible this was carefully situated at the centre of the triangle of holes on the tray, that being the furthest location from the direct gas jets, as shown in figure 4.6 below.

Figure 4.6 also shows the new locations on the whole tray. In all, 24 were placed in the bubbling area of the tray. At 0.19mm thickness these were thinner than the handmade ones. A 25th and 26th thermocouple was placed in the inlet downcomer and on the outlet weir respectively. The whole set of thermocouples were supplied by commercial manufacterers [20].

4.6.3 Development of the Wet-Bulb Temperature Measurement

It was required to measure the wet-bulb temperature inside the column in order to determine the enthalpy of the air in the column. A special device had to be used for this, to avoid entrainment, weeping and leakage which often occur inside working

a. thermocouple location on tray (units: mm)

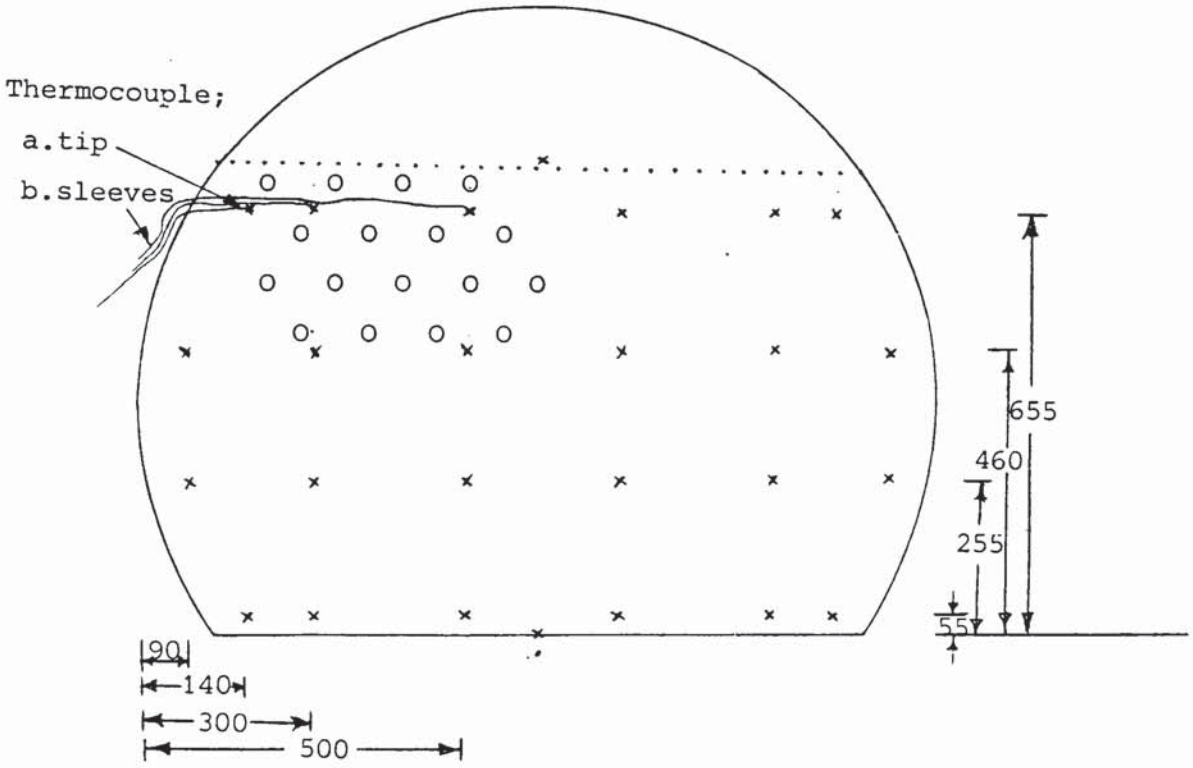

b. thermocouple tip clearance from tray floor

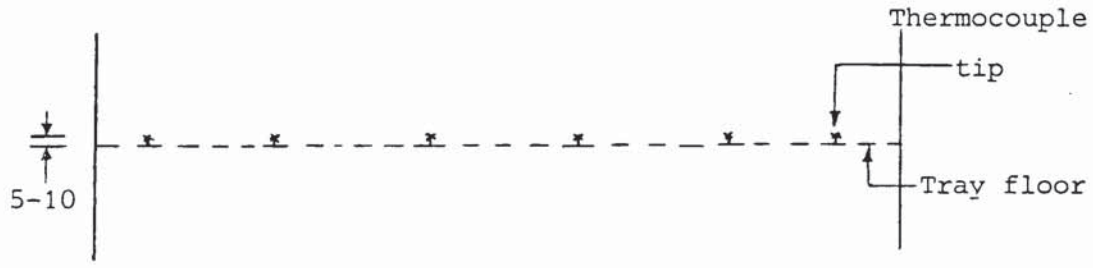

FIG:4.6 Thermocouples Placement on test Tray in Final Experiments

columns. First, preliminary work was carried out to determine if, following the basic concepts of wet-bulb thermometry, there is a minimum air velocity below which radiation effects would give misleading results [15,16].

4.6.3.1 Determination of the minimum velocity to measure the Wet-bulb temperature.

A simple bench scale experiment was carried out in the laboratory. Air was supplied from a vacuum pump into an air channel made of PVC tubing. The air flow was controlled by adjusting a T-tube fitted to the air channel. A thermocouple with its tip wrapped inside a wick was used to measure the wet-bulb temperature inside the channel. Two dry-bulb thermocouples were located before and after the wet-bulb.

The results obtained at different laboratory conditions (different days and times of day) are plotted against a range of air velocities in figure 4.7. The air velocities were those within the expected range of the water cooling experiments.

When there is no air flow across the wick, U_s = 0.0m/s the recorded temperature is that of the moist wick and practically equal to the water temperature. The plots show that the wet-bulb temperatures were below this temperature and also well below the dry bulb temperatures. At velocities above 1.0m/s no further changes in the wet-bulb temperatures occured.

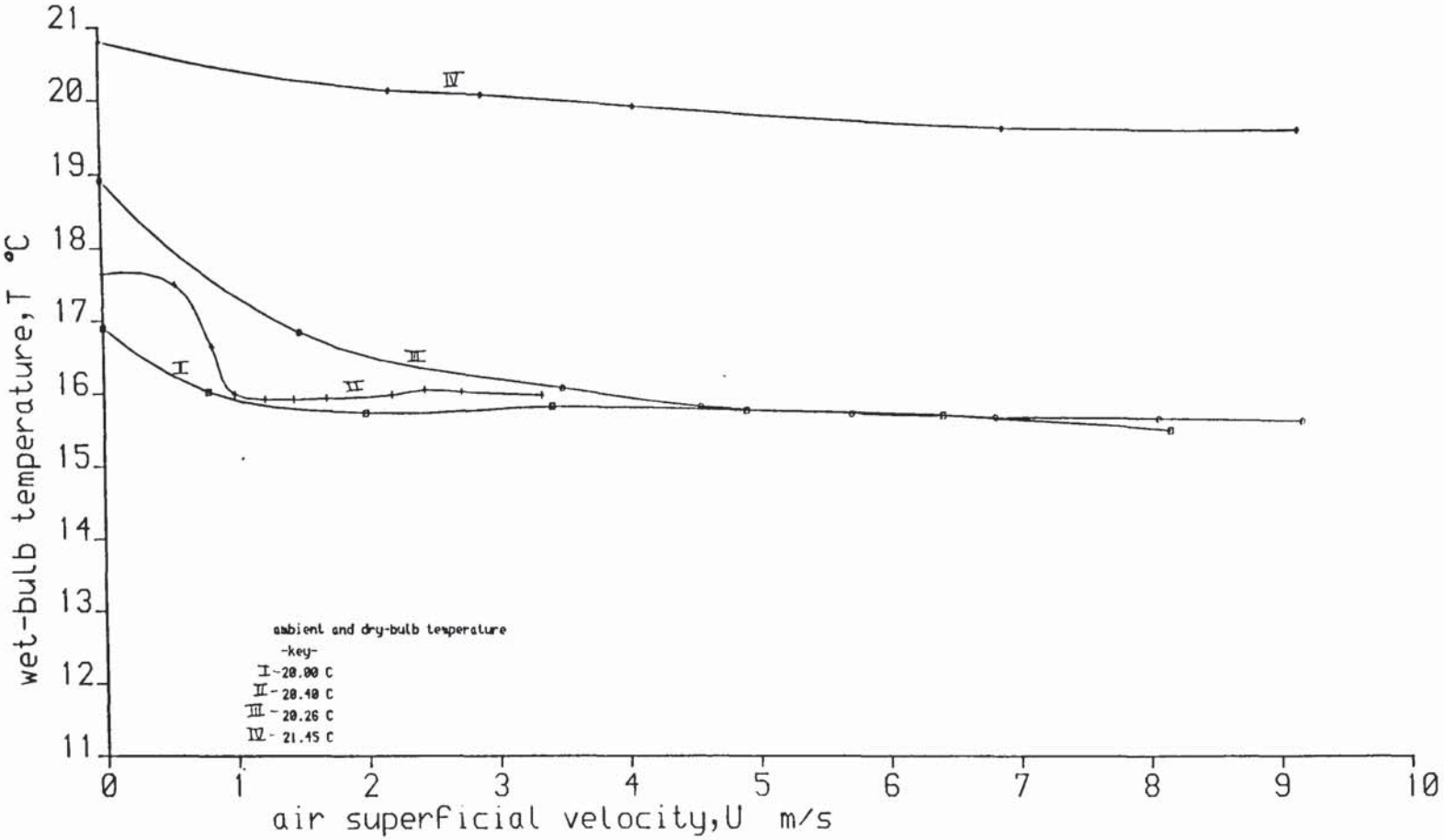

FIG:4.7 A Plot of Air Wet-Bulb Temperature against superficial velocity

All the water cooling experiments were carried out at column superficial air rates above 1.0m/s.

4.6.3.2 Wet-bulb Measurements inside an Operating Column.

A Vapour Sampler was first developed and satisfactorily employed by Kastenek and Standart [56], to eliminate entrained liquid in vapour samples taken from operating distillation columns. In this work, the vapour sampler was slightly modified and converted for use as a wet-bulb measurement device.The working of the thermocouple vapour sampler is described below.

Additional enthalpy is picked up by an air stream in which water droplets are entrained. The measured wet-bulb temperatures would be those that approach the saturated air temperatures. The function of the vapour sampler is to eliminate all but the minutest of the droplets. A diagram of the sampler is given in figure 4.8.

It consists of two horizontal concentric cylinders. A large outer cylinder is made of PTFE (trade name for polytetrafluoroethylene) and has an opening, a third of its circumference, across the whole of its length. It serves as the moist air inlet. The air streams spiral through the cylinder and emerge via a narrow slit into the inner cylinder. A deflector plate is attached to the far side of the slit in the inner cylinder. This helps to divert the air streams into the slit. When large droplets impinge on the PTFE wall, they coalesce and fall and are drained out of the sampler by gravity.

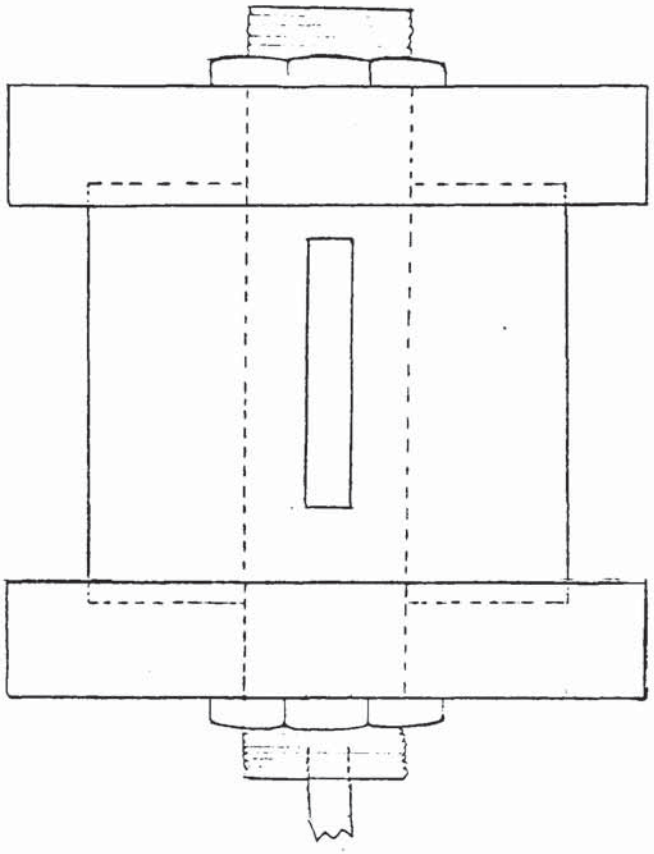

a.Plan

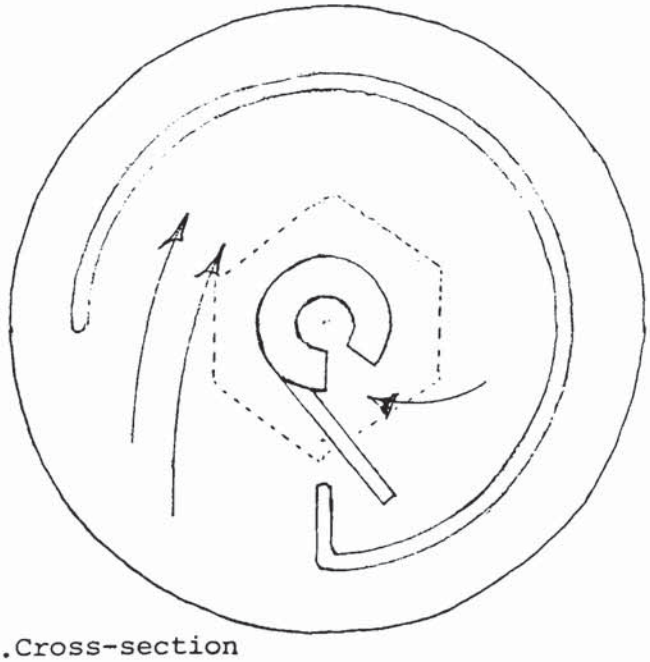

b.Cross-section

FIG:4.8 Modified Vapour Sampler for Wet-bulb Temperature Measurements

A pool of water into which part of the wick is immersed is held in one end of the inner cylinder. The wick's thermocouple is placed downstream of the slit. The dry bulb is placed at the sampler inlet. The other end of the inner cylinder is fitted with a long PVC tubing extended out of the column.
The outer cylinder is held by thick PTFE rings at both ends.

Both long exposure of the wick and high air velocities around it could result in the equilibrium conditions between the air and water required for the wet-bulb maesurement. To maintain high velocities the PVC tubing from the inner cylinder was connected to a fan outside the column. This arrangement resulted in the pool of water being dried up from the wick such that the temperatures recorded were approaching the dry-bulb. To overcome this problem a narrow copper tube was fitted to the pool to replenish the water at required intervals.

4.6.3.2 Other Wet-Bulb Measurements

Other measurements of the wet-bulb were made to cross check the measurements for the water cooling experiments. These include:

I. Measurements of the temperatures of a wetted tray by passing air for an infinite period

II. Measurements of the wet-bulb outside the column using a sling psychrometer

III. Measurements of the wet-bulb inside the column with air only.

4.7 Development of Electronic Interfacing for Data Logging

The Potentiometer System was replaced by an electronic interfacing system [122] which was connected directly to the rig. It was capable of speeding up the whole process of data collection, data treatment and storage. A peripheral device was used to convey the thermocouples signals to the interface unit. Another peripheral device was used for storage. The components that make up the electronic interfacing unit are described below.

4.7.1 Components of the Interfacing Unit.

The interfacing unit is made up of three main components that include i) the controller, ii) the IEEE-488 bus and iii) a Microlink internal bus. A comprehensive information flow sheet is presented in figure 4.9.

i. The controller used is a microcomputer, because it is compatible with the IEEE-488. In addition, as a computer, it can also be used to perform calculations, such as the conversion of voltage signals into temperature, and real timing for various purposes;

ii. The IEEE-488 bus has the facility to communicate (to and fro) information to the controller. It is equiped with 16 lines which handle data acquisition, information relay and control (e.g; timing);

iii. The microlink interface is an external module which is adaptable to the IEEE-488. It handles the Tc-16 (nomenclature) temperature monitor which selects the thermocouple, does multiplexing and voltage amplification to achieve high precision.

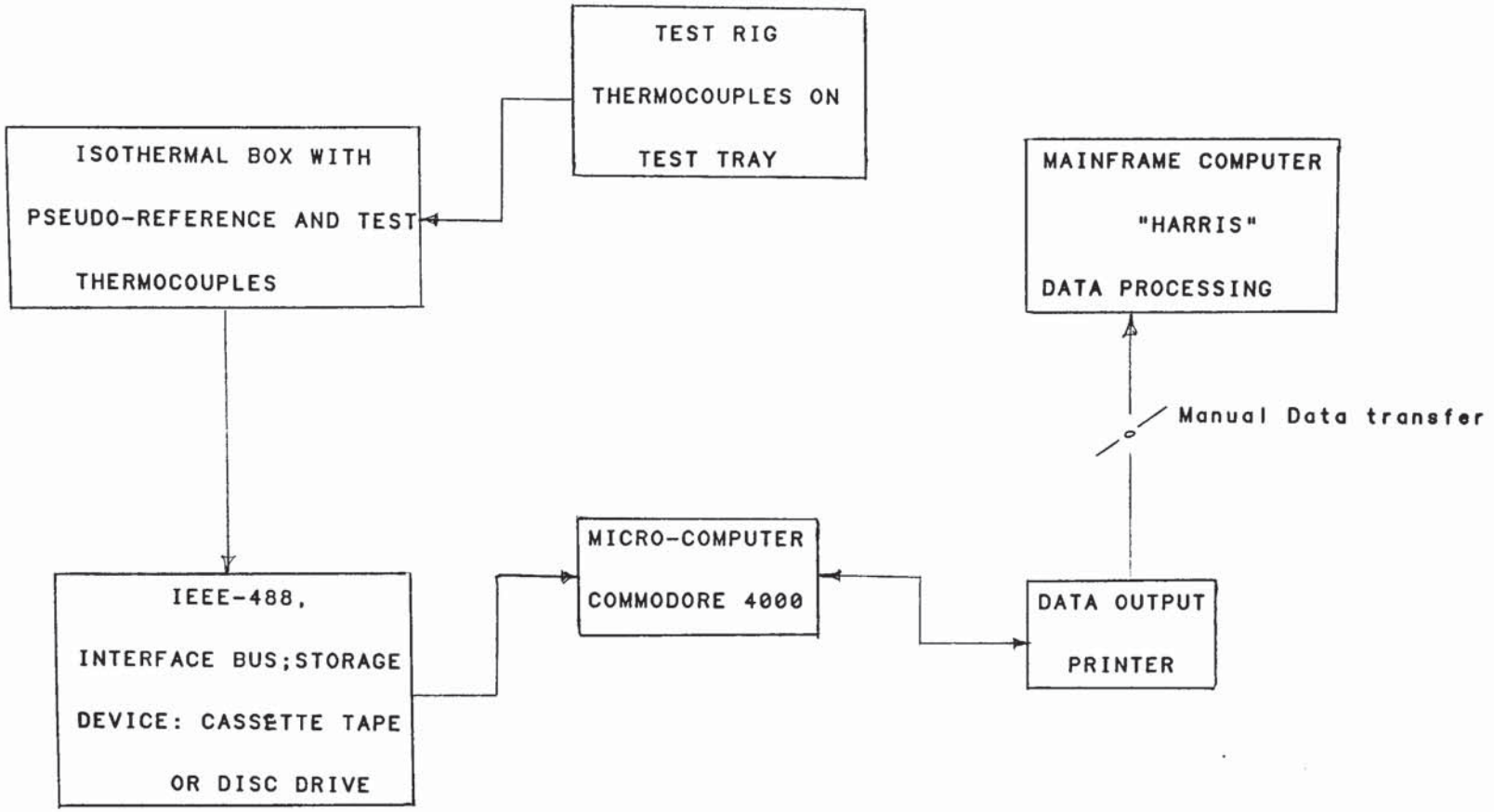

Figure 4.9 Information Flow Sheet for Data Logging Instruments

4.7.2 Peripheral Devices

The peripheral devices include:

i.An isothermal box with provision for 16 thermocouples, including a reference one, was located close to the test rig. The box was made of die-cast aluminium and lined with polystyrene for insulation. A platinum resistance sensor built into the box served as the reference thermocouple. The isothermal box was connected to the microlink through a ribbon cable assembly. A more detailed description of the box is given in Appendix C

ii. A cassette tape drive was connected to the computer (controller) to collect, store and retrieve data.

iii. A printer was used on-line to output information into hardcopy.

The equations used to convert voltages into temperatures in C are given in Appendix C.

Details of a computer program written to collect data are also given in Appendix C, program C1.

4.8 Temperature Profiles from the Revamped Column.

The temperature profiles measured from the revamped tray are shown in figure 4.10. The skewed temperature profiles shown in the figure is evidence of nonuniform flow patterns on the tray. Dye studies were carried out on the tray by blocking the holes with a thin white surface thus enabling the path of dye to be visualised. The dye movements showed that the tray was not "level". It may be noted at this point that the detection of nonuniformity in the flow pattern by means of the temperature profiles in itself provides justification for investigating temperature profiles by water cooling. It had been reported in literature that this amounts to a malalignment or an out-of-levelness of the tray which can arise during installation [120]. This fact led to further precautions being taken to level the tray.

4.8.1 Methods used to Improve Tray Levelness.

The tray support rings were adjusted according to :

a. visual observations from i. a spirit level (not sensitive enough) and ii. dye movements from water only experiments and

b. further measurements of temperatures for evidence of skewness

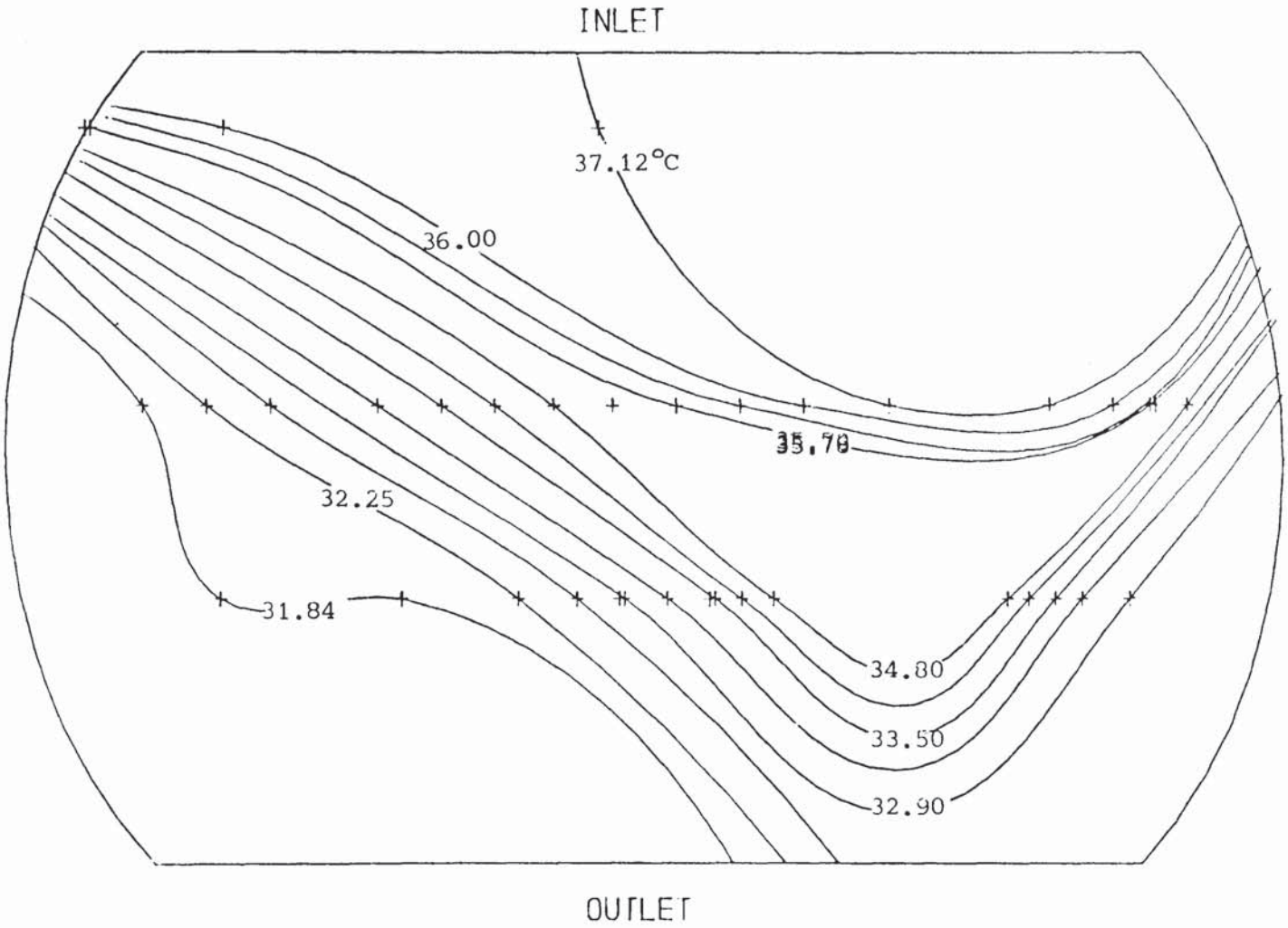

FIGURE 4.10 : SKEWED TEMPERATURE PROFILES (MIXED)
Csb=0.092m/s ;q/b=0.960E-2m3/sm

Other precautions taken include i. an examination of the outlet weir for levelness at all points across the length and ii. measurements of distances between the inlet downcomer and the outlet weir to ensure equidistances along all lines parallel to the flow axis.

None of these modifications completely removed the maldistributed liquid flow as shown by the skewed shape of the temperature profiles.

4.9 The Use of Spacers to Restore Symmetrical Temperature Profiles

Although the modifications succeeded in achieving reproduction and improved confidence in the temperature measurements the profiles were still unsymmetrical. It would seem that as far as placement of the tray on the support ring could be done, sufficient care was already taken with the modifications described above.

However, the lack of symmetry was finally solved by providing two equal size spacers between the bottom of the downcomer and the tray floor. The spacers were 14mm high. These are shown in figure 4.11. This caused the temperature profiles associated with the flow patterns to be symmetrical as expected. A symmetrical profile is shown in figure 4.12. Figure 4.13 and figure 4.14 are temperature profiles in the Mixed regime and Spray regime respectively, from the level tray.

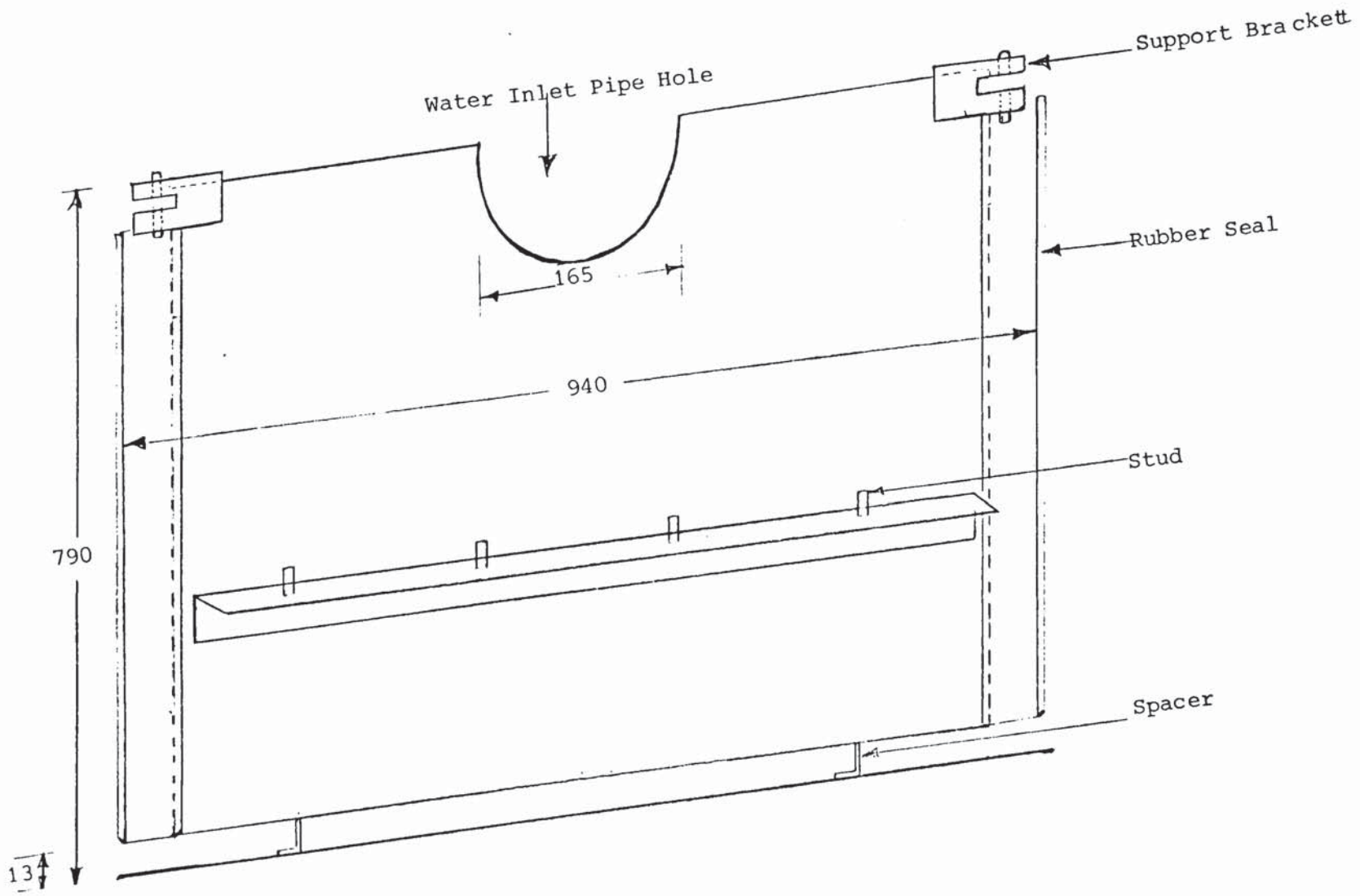

FIG:4.11 "Standard" Downcomer Showing Spacers and Water Pipe Inlet Point

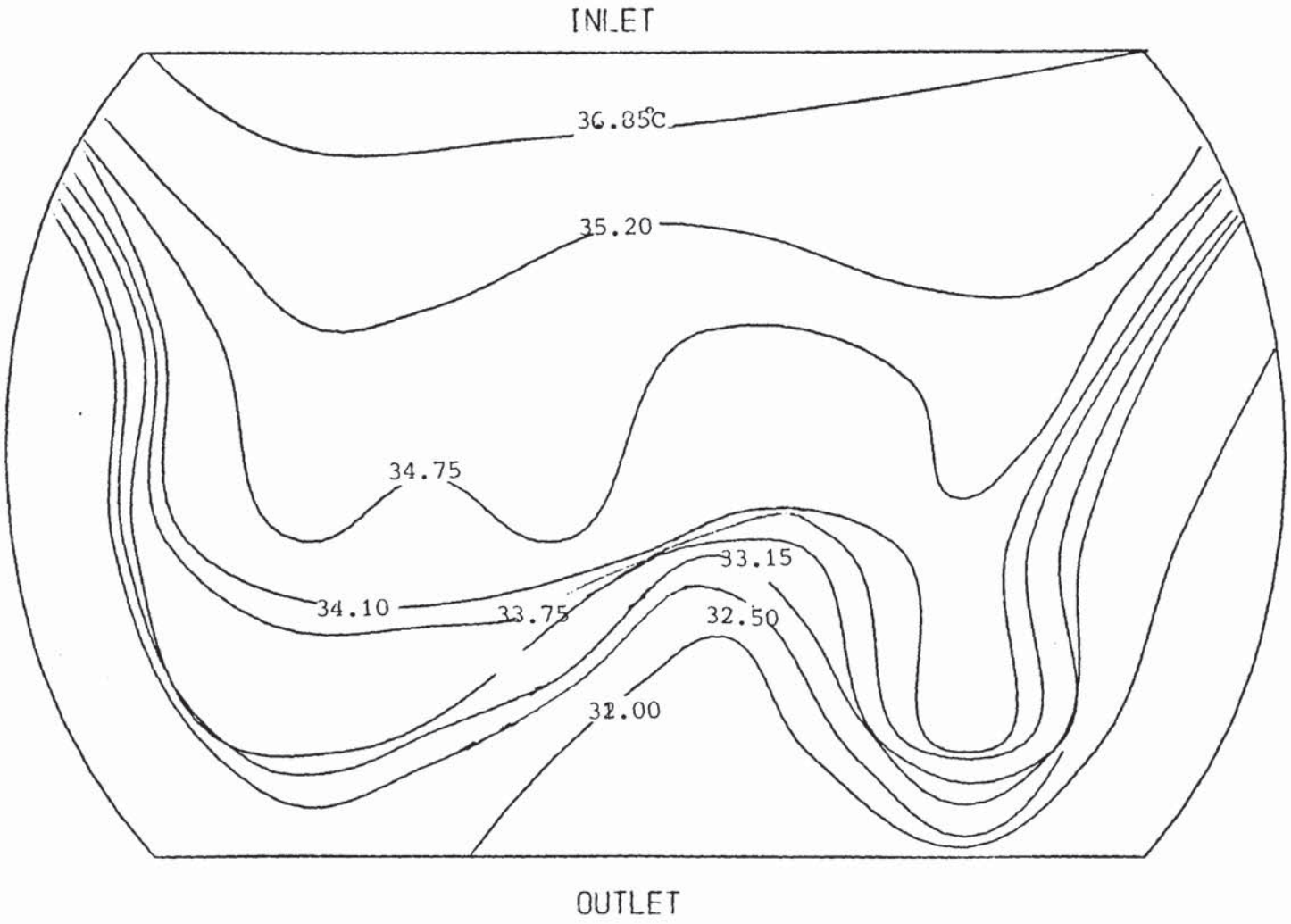

FIGURE 4.12 : TEMPERATURE PROFILES ON A LEVEL TRAY

Csb=0.092m/s ;q/b=0.960E-2m3/sm

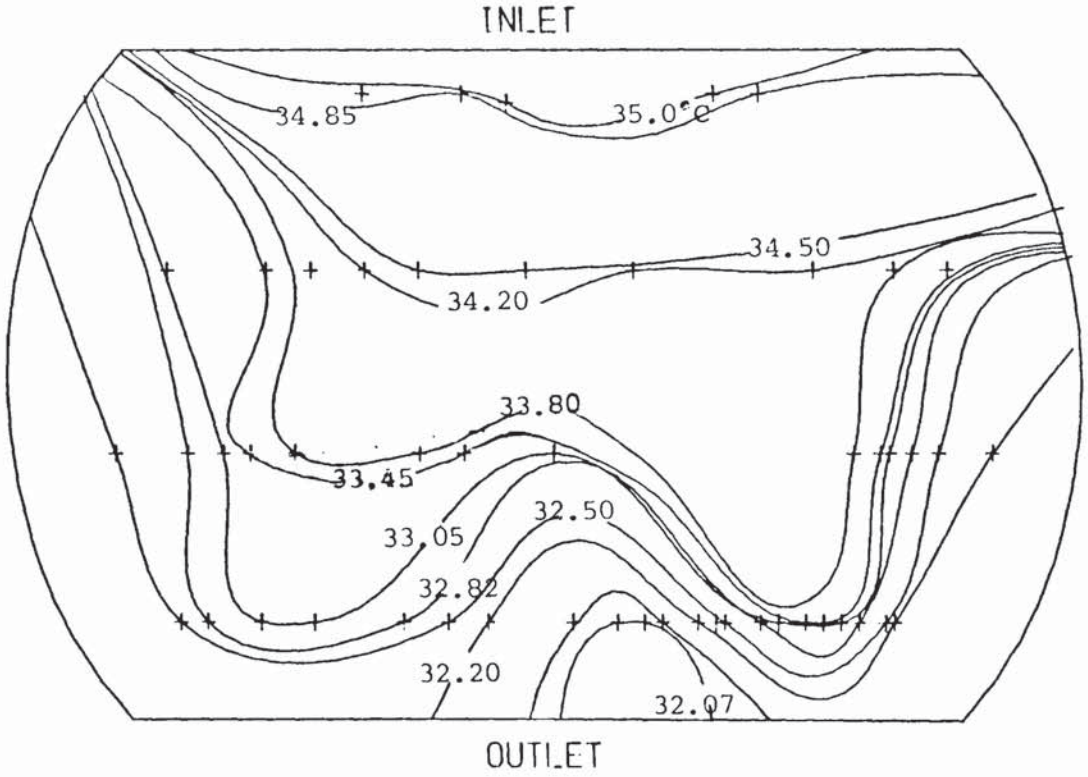

FIGURE 4.13 : TEMPERATURE PROFILES IN MIXED REGIME
Csb=0.078M/S ; q/b=1.069E-2m3/sm

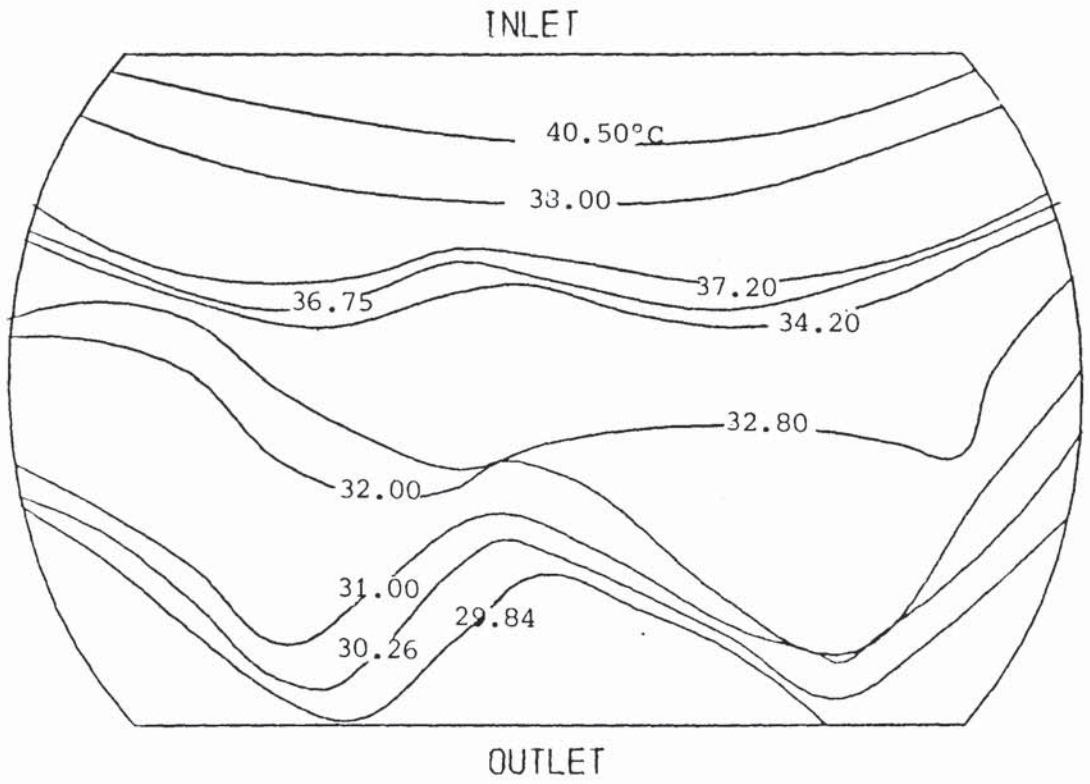

FIGURE 4.14 : TEMPERATURE PROFILES IN SPRAY REGIME
Csb=0.084m/s ;q/b=0.450E-2m3/sm

4.10 Additional Experiments

4.10.1 Measurement of Uniformity of Flow Over the Weir

There is no record in published literature, where consideration was given to the possible variation of flow of liquid per unit length across the outlet weir. This is always assumed to be uniform. This may yet be another important factor in the flow patterns across trays.

A project was devised for this work, in which the flow across the weir was investigated.

A compartmentalised box, approximately the length of the weir was built to fit into the outlet downcomer. Holes were made at the bottom of each compartment so that "all" liquid crossing the weir passed through the box and out through the holes. The presence of the holes meant that a head of liquid always formed inside the box. The liquid flow rate through each compartment was estimated from the head of liquid formed.

The box is shown in the figure 4.15 below.

In the following sections the method of calculations and interpretation of the results from the water cooling apparatus described in this section is dealt with.

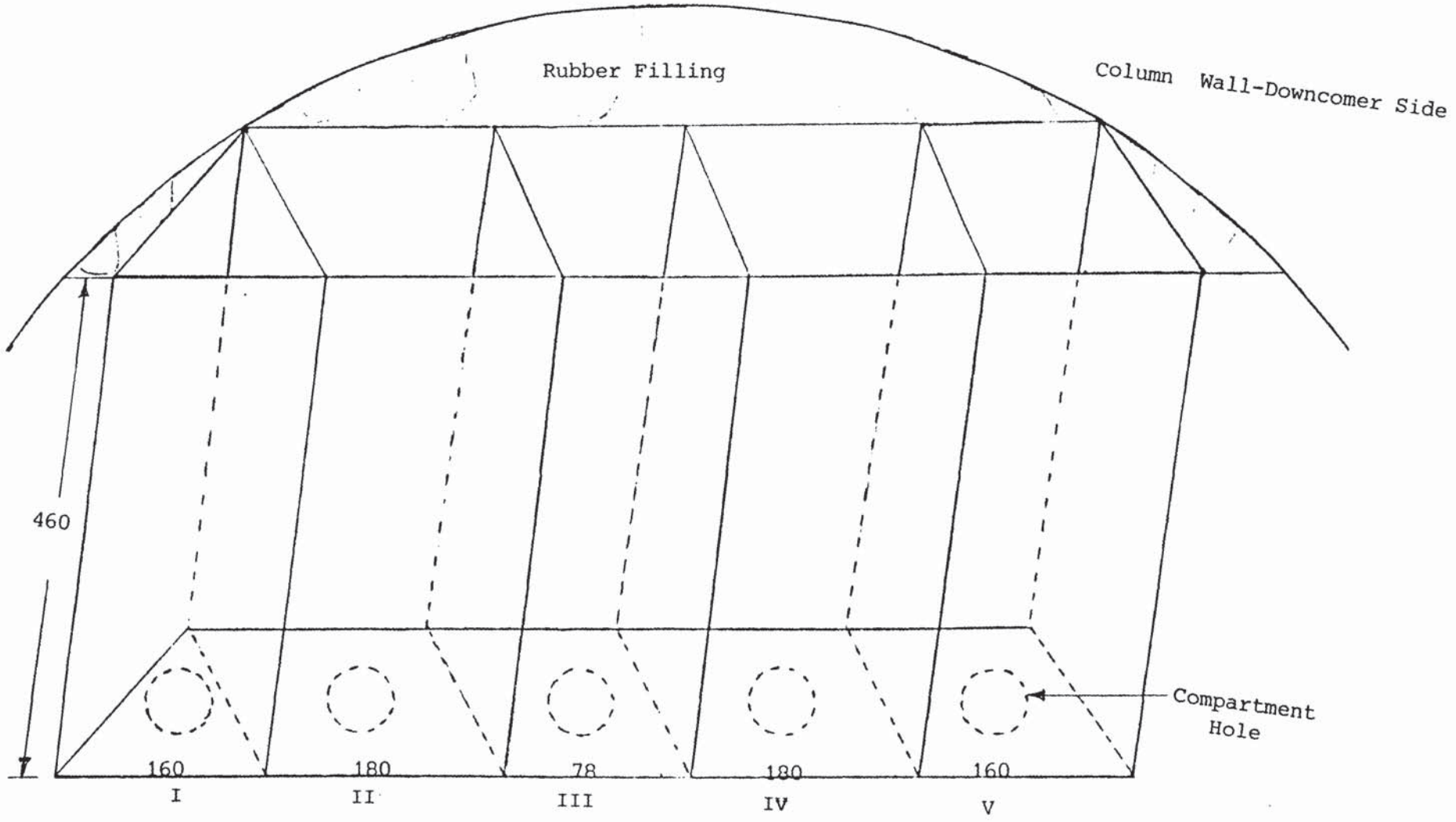

FIG:4.15 WEIR COLLECTOR ILLUSTRATING FIVE COMPARTMENTS(Symmetry about III)
Dimensions in mm

5. DATA PROCESSING

The temperature measurements were made on the tray so as to represent a temperature field. In order to "best fit" the temperature measurements to the hypothetic field an interpolation technique was required. Further, the determination of the wet-bulb temperature described in Section 4 and hence the air enthalpy meant that the efficiencies could be determined for the water cooling process. In this section the calculation method used to derive the temperature profiles on the temperature "field" is desribed. This is followed by a description of the calculation method for efficiency.

5.1 A Description of the Temperature Surface Problem

The problem is a three dimensional one, with the dimensions as: the direction of flow of liquid, the transverse direction, and the temperature (or height) as the dependent variable. It is assumed that the column wall is an impermeable membrane and that the temperature gradient across it is negligible, compared to that across the tray. The temperature gradient across the outlet weir is also assumed to be negligible. These are represented mathematically as:

i. for the column wall $$\frac{dT}{dr} = 0 \qquad 5.1$$

ii. for the outlet weir $$\frac{dT}{dz} = 0 \qquad 5.2$$

where T is temperature and r is distance across the tray in the radial direction (r=0.0; at tray centre) and z is the distance in the direction of flow of liquid (at the inlet downcomer / bubbling area interface : z = 0). A diagramatic representation of the boundary conditions is shown in figure 5.1.

It may be noted that similar boundary conditions are used in the models of mass transfer on circular trays.

5.2 Methods of Curve and Surface Approximation

Traditionally, the methods favoured for approximating curved lines and surfaces involve the use of straight line segments and planar polygons [8]. Two related difficulties were always encountered. First, the resulting images were objectionable even for very fine line segments or polygons at the borders between adjacent polygons. Also, they required excessive amounts of computational storage which often were fixed and thus not flexible. The more modern methods developed to overcome these limitations include i. the Hermitite Interpolation and Coons Surfaces [21], ii. Bezier Curves and Surfaces [12], and iii. Beta-Spline Curves and Surfaces [8] and iv. B-Spline Curves and Surfaces [22].

The ultimate choice of B-Spline Curves and Surfaces for this work was based on its increasing application to solving Engineering problems and the added convenience of a tested Computer Package [81] adaptable for use in the University Mainframe Computer.

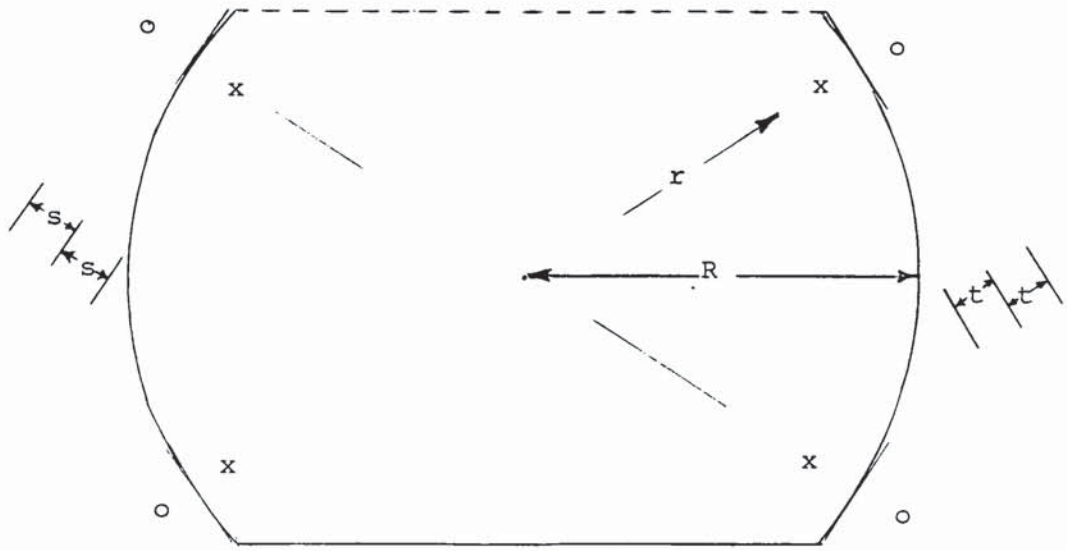

a. Wall boundary conditions: $\frac{dT}{dr} = 0$

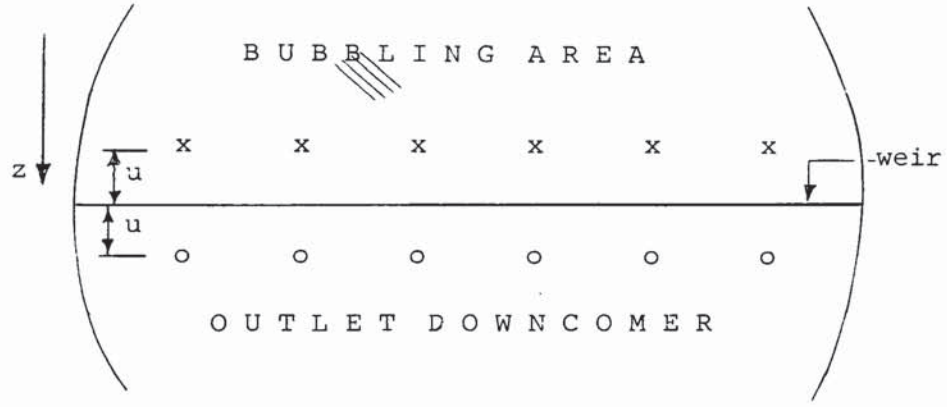

b. Weir boundary conditions: $\frac{dT}{dz} = 0$

FIG:5.1 Representation of the boundary conditions used in the calculation method

x- temperature measurement point
o- extrapolated point

5.3 Cubic B-Splines Curves and Ssurfaces

Although a computer package was used for the spline curves and surfaces in this work, it is appropriate to describe the method.

5.3.1 Description and use of Splines

Splines are devices used by draftsmen and shipbuilders to draw curves [8]. They attach weights to the spline, which essentially is a thin plastic material, to obtain the right distribution so as to make the spline pass through all the points required. The translation of this physical device into a calculus problem was first attempted by Schoenberg [106]. The author showed that the curvature of the spline may be approximated by a second derivative while minor flexes or deflections can be described by the first derivative of a polynomial. Often a close approximation to such a function can only be attained by using a high degree polynomial but then this results in oscillations in the function. The spline approximation method is devised to minimise this.

For a cubic spline a set of cubic polynomials is passed through each point of the function. The object is to achieve continuity in the slope and the curvature at the boundaries between adjacent points. It is thus required that the first derivative which gives the slope and the second which gives the curvature be numerically equal at the boundary. This condition is satisfied by the cubic spline. Its other advantage is that it can accomodate a multiple - valued curve or surface. Surfaces are infact two dimensional

curves. The degree of continuity at the joints between segments and the borders between surface segments can be controlled by the spline without affecting the whole function. This is called local control. This flexibility makes for very efficient computation [21,43,46,64].

5.3.2 Mathematical Development of Splines

Definition

A spline function S(x) of order n (or degree n-1) with knots $x_1, x_2, \ldots, x_n$, is a function possessing the following two properties.

1. In each of the intervals

$$x < x_1;\ x_{j-1} < x_j\ ;\ (j = 2,3,,\ldots,m)\ ;x_m < x,$$

S(x) is a polynomial of degree n-1 or less

2. S(x) and its derivatives of orders $1,2,\ldots,n-2$ are continuous. There is discontinuity in the (n-1)th derivative at each of the points $x = x_j, j = 1,2,\ldots,m$.

Consider a cubic spline or n = 4, degree 3. This has a unique representation in the form [35]:

$$S(x) = \sum_{k=0}^{3} \alpha_k x^k + \sum_{i=1}^{h} \beta_i (x - x_i)_+^3 \qquad 5.3$$

where $x_+^{n-1} = \begin{cases} x^{n-1} & x > 0 \\ 0, & x < 0 \end{cases}$

Suppose that x lies within some finite boundary, $a < x < b$, then the left-hand sum in equation 5.3 provides the cubic polynomial in the interval $a < x < x_1$ and the right-hand sum provides a discontinuity in the third derivative at each knot and a different cubic polynomial in each of the intervals. In order to determine the coefficient of the spline α_k and β_i as represented in the equation, the observation equations employed tend to be numerically unstable. A further difficulty arises from a loss of accuracy due to cancellation in the matrix of S(x). B-Splines were developed primarily to overcome these problems [23,44].

B-splines or Cubic B-splines differ from cubic splines in that in the latter only four adjacent intervals between knots have a non-zero value. A cubic B-spline $M_i(x)$ is defined as a cubic spline with knots x_{i-4}, x_{i-3}, x_{i-2}, x_{i-1}, and x_i which is zero outside the range $x_{i-4} < x < x_i$.

Due to this condition only eight Knots (2x order) are introduced to the function. In practice they are often chosen to coincide with the end values of the function.

5.3.3 Bicubic B-splines For Surface Fitting

A bicubic spline S(x,y) is a function which is a bicubic polynomial of the form:

$$\sum_{s=1}^{3} \sum_{0}^{3} \alpha_{s,t} x^s y^t \qquad 5.5$$

which has continuity up to the second derivative everywhere within a given area of the function.

In its bicubic B-spline notation, setting the knots for x as $x_1, x_2, \ldots, x_h$ and for y as $y_1, y_2, \ldots, y_k$, the equation is given as a set of cross-products of one function from the other set, thus:

$$s(x,y) = \sum_{i=1}^{h+4} \sum_{j=1}^{k+4} \alpha_{ij} M_i(x) N_j(y) \qquad 5.6$$

As with the cubic B-spline each set of knots is augmented with 4 additional knots at the ends of each range. They are again non-zero over a limited range only. At any given point (x,y), only 16 basis functions are non-zero.

Suppose the data points are (x_r, y_r, f_r) the observation equations would be:

$$\sum_{i=1}^{h+4} \sum_{j=1}^{k+4} \alpha_{ij} M_i(x_r) N_j(y_r) = f_r \qquad r=1,2,\ldots,m \qquad 5.7$$

A cubic spline with knots $x_1, x_2, \ldots, x_h$ has a unique representation in the range $a < x < b$ of the form defined by Schoenberg [106] as,

$$S(x) = \sum_{i=1}^{h+4} \alpha_i . M_i(x) \qquad 5.4$$

$M_i(x)$ is often normalised.

5.3 The Importance of Knots in Evaluating Splines.

Knots are arbitrary boundaries for the polynomial arcs or segments. They are specified and must fulfill the only condition that they be in a non-decreasing order. In specifying a set of knots over a polynomial of order k, the same value cannot appear more than k times. When a knot appears more than once it is called a multiple knot. Specifying too many knots in a spline curve to improve accuracy can also lead to discontinuity. The method of choice of knots within a given range of data is by trial and error and by a graphic examination of the behaviour of the curve (or surface). It is useful to choose knots in segments where the shape of the curve or surface is suspected to be nonuniform. So in this work as much as possible the knots were chosen close to the expected boundaries between the "active and stagnant" zones of the tray.

In the matrix notation this maybe written as

$$A.\aleph = f \qquad 5.8$$

with A as a matrix having m rows and (h+4)(k+4) columns. Equation (3.7) of reference [46] shows the form of matrix A. It shows that each observation matrix of A is a rectangular matrix of a band form. The advantage of this peculiar band form matrix is that use can be made of the Householder Transformations [50] to solve for matrix A.

It is adequate to evaluate bicubic B-splines as individual one dimensional cubic B-splines and to find the product as in equation 5.6 above.

5.3.5 Methods of Evaluating B-Splines

A general way of expressing equation 5.4 is the form:

$$S(x) = \sum_{i=1}^{m+n} c_i M_{nl}(x) \qquad 5.9$$

such that S(x) is expressed as a linear combination of B-splines $M_{nl}(x)$.

It can be proved that the relation [22]:

$$M_{ni}(x) = \frac{(x - x_{i-n}).M_{n-1,i-1}(x) + (x_i - x).M_{n-1,i}(x)}{x_i - x_{i-n}} \qquad 5.10$$

holds for all values of x.

The following conditions apply:

In general;

$$M_{ni}(x) = \begin{cases} M_{ni} & x_{i-n} < x_i \\ 0 & \text{otherwise} \end{cases} \qquad 5.11$$

And

$$M_{1j}(x) = \begin{cases} 1/(x_j - x_{j-1}), & x_{j-1} < x < x_j \\ 0, & \text{otherwise} \end{cases} \qquad 5.12$$

For any order n, the relation in equation 5.10 can be written in a triangular array. However, by using equation 5.11 and equation 5.12 some of the elements become zero.

Thus for the range $x_{i-3} < x < x_{i-3}$ and n = 4 the following form evolves:

$$
\begin{array}{ccccc}
M_{1,i-3} & & & & \\
 & M_{2,i-2} & & & \\
M_{1,i-2} & & M_{3,i-1} & & \\
 & M_{2,i-1} & & M_{4,i} & \\
M_{1,i-1} & & M_{3,i} & & \\
 & M_{2,i} & & & \\
M_{1,i} & & & &
\end{array}
\qquad 5.14
$$

by using equation 5.10 it gives;

$$
\begin{array}{ccccc}
0 & & & & \\
 & M_{2,i-2} & & & \\
M_{1,i-2} & & M_{3,i-1} & & \\
 & M_{2,i-1} & & M_{4,i} & \\
0 & & M_{3,i} & & \\
0 & 0 & & &
\end{array}
\qquad 5.15
$$

Since all the terms on the right side of the equation 5.10 are positive or zero, the problem of cancellation is eliminated. The equation for $M_{nl}(x)$ is reduced to that of a linear combination of the terms in the array of equation 5.14. Each of the elements on the right of the array is obtained by the two elements immediately

to its left. Thus $M_{2,i-2}$ is obtained from $0(M_{1,i-3} = 0)$ and $M_{1,i-2}$ and so forth. This method ensures that there is numerical stability, consequently, it is called the stable method.

Once the evaluation of the B-Splines $M_i(x)$ for a curve or the product of B-Splines for $M_i(x).N_j(x)$ for a surface is complete these then form the matrix A in the observation equations. The equations are then evaluated by the least-squares solution method.

5.3.6 The Least-Squares Solution of the Observation Equation

The least-squares solution of the observation equation involves a cumbersome evaluation of complex matrix algebraic equations resulting in vast amounts of substitution and elimination which often tends to become unstable. In dealing with substitution in matrix algebra the process is further complicated by the rank status (full or deficient) of the matrix. The rank of a matrix is defined as its maximum number of linearly independent row vectors [34]. Now in observation equations derived from Engineering practice and as indeed is the case in the water cooling experiments it is common to find that data is irregularly spaced. This results in the matrix being rank deficient. Thus the solution developed for a full rank case is slightly modified to accomodate the rank deficient case. The method is further explained below.

5.3.6.1 Solution for the Full Rank Matrix A

The observation equations are:

$$A\,v = f \qquad 5.8$$

Consider A to be of size m x n (with m > n) with the vectors having n elements and f,m elements. Use is made of the Householder Transformations [50] to reduce the matrix to an Upper Triangular form which drastically simplifies the solution. To do this the matrices A and f are premultiplied by a series of orthogonal matrices [42], thus;

$$Q\,A = U = \begin{pmatrix} U_1 \\ \dot{0} \end{pmatrix} \qquad \{\text{matrix notation}\} \qquad 5.16$$

and $$Q\,f = v \qquad 5.17$$

where Q is the orthogonal matrix m x m such that

$$Q^T Q = I \qquad \{\text{the identity matrix, } Q^T \text{ is the transpose of matrix } Q\}$$

and U_1 is an upper triangular n x n matrix of full rank . The elements of the last m - n rows of U are all zero. The least-squares solution is then given by,

$$\gamma = U_1^{-1} v_1 \qquad 5.18$$

where v_1 denotes the first n elements of v. The sum of squares of residuals is given by the sum of squares of the last m - n elements of v.

The solution involves a process of column interchanges and back substitution. The Householder Matrices Q are discarded once they have operated on A and f.

5.3.6.2 Solution for A Rank Deficient Matrix A

Going back to the observation equations 5.8 above the method of solution for a rank deficient case sets out to eliminate or at least minimise the deficiency of the original matrix. The remaining matrix can then be solved as that of the full rank case above.

Suppose the matrix A has rank r < n or is n - r deficient. Upon reducing the matrix to its upper triangular form by the normal column interchanges and substitution, the reduced matrix takes the form:

$$U = \begin{pmatrix} U_1 & U_2 \\ 0 & 0 \end{pmatrix} \qquad 5.19$$

where U_1 is an upper triangular matrix r x r of rank r and U_2 is an r x (n - r) matrix

The rank deficiency is dealt with by setting to zero all the coefficients of the observation equations y_1 corresponding to the last n - r (permuted) columns of $U.U_1$ becomes the upper triangular matrix described in equation 5.16 above and v consists of the first r elements of v.

The residual sum of squares is given by the sum of squares of the last m - r elements of v.

5.3.7 Development of Curve Fitting Program

It is clear from equation 5.10 its accompanying array equations 5.14 and 5.15 and the matrix form of 5.8, that employing a least squares solution to fit polynomial splines to a number of data points requires a vast amount of calculation. Evaluation of the observation equations 5.8 in their matrix representation, by the least squares solution presents yet a different mathematical problem. This is a linear algebra problem whose translation into a computer program demands some expertise in computational techniques and programing. In spite of these difficulties, the increasing use of splines in modern engineering applications [35] has brought advanced solutions to these equations. Computer packages [81] are now available which can be used to generate splines to fit curves and surfaces with good accuracy. The computer program written, integrating the spline package is given elsewhere in Appendix C, program C2.

5.8 Calculation of Point and Tray Efficiency

Recall the definition equations of efficiencies for the water cooling process:

i. at a point on the tray, the point efficiency is,

$$E_{OG} = \frac{H_{out} - H_{in}}{H^{*} - H_{in}} \qquad 5.20$$

and ii. over the entire tray the tray efficiency is,

$$E_{MV} = \frac{\bar{H}_{out} - H_{in}}{H^{*}_{out} - H_{in}} \qquad 5.21$$

H^{*} is the equilibrium enthalpy of the in contact with the water leaving a point on the tray. For a given water temperature T, the corresponding H^{*} can either be calculated from:

$$H^{*} = m' T + c \qquad 5.22$$

or read from a pshychrometric chart [85].

The spline interpolation technique described in this section enables the calculation of T at any point on the tray to be made and hence the corresponing H^* estimated.

It is assumed that the enthalpy of the air entering the tray H_{in}, is everywhere the same. The value of the H_{in} is determined from the wet-bulb and the dry-bulb temperatures of the air stream.

An overall heat balance was made on the tray to determine the average enthalpy of the moist air leaving the tray, $\bar{H}_{out}$

5.8.1 Overall Heat Balance on the Tray

To make the overall heat balance on the tray the following assumptions were made:

i. Negligible water loss through entrainment and evaporation from the tray,

ii. Uniform enthalpy of the air entering the tray,

iii. Uniform temperature of the water within the inlet downcomer,

iv. Negligible heat loss through the column wall,

v. Uniform flow of water per unit width across the outlet weir, and

vi. Negligible temperature gradient across the tray / water interface.

The balance equations are:

$$L.c.\Delta T = G.\Delta H \qquad 5.23$$

or $$L.c.(T_{in} - \bar{T}_{out}) = G'(\bar{H}_{out} - H_{in}) \qquad 5.24$$

rearranging,

$$\bar{H}_{out} = H_{in} + (L/G').c.(T_{in} - \bar{T}_{out}) \qquad 5.25$$

5.8.1.1 Estimation of $\bar{T}_{out}$

$\bar{T}_{out}$ is the average temperature of the water crossing the outlet weir. Assumption iv. above, for uniform flow across the weir is made. The spline interpolation technique was used to calculate the temperatures at specified interval lengths across the weir and thus an average value $\bar{T}_{out}$ was determined by dividing the integral (obtained numerically) by the weir length.

5.8.3 Calculation of Tray Efficiency

The definition equation of tray efficiency water cooling was earlier given as:

$$E_{MV} = \frac{\bar{H}_{out} - H_{in}}{H^*_{out} - H_{in}} \qquad 5.26$$

where H^*_{out} is the enthalpy of the air in equilibrium with the outlet water temperature $\bar{T}_{out}$. H^*_{out} was determined from standard psychrometric charts for corresponding values of $\bar{T}_{out}$.

$\bar{H}_{out}$ was calculated from equation above and H_{in} was determined as described in subsection 5.4.1 above.

5.8.4. Calculation of Point Efficiency

The definition equation for point efficiency water cooling is,

$$E_{OG} = \frac{H_{out} - H_{in}}{H^* - H_{in}} \qquad 5.20$$

This equation was invoked to calculate the efficiency for a vast number (500) of temperature points on the tray. The average value was calculated by numerical integration methods [37].

5.8.4.1 Development of the Calculation Procedure for Point Efficiency

The equation for point efficiency above can be rearranged as:

$$H_{out} = H_{in} + E_{OG} (H^* - H_{in}) \qquad 5.27$$

The average outlet enthalpy over the entire tray is given as:

$$\bar{H}_{out} = \frac{1}{A} \int_{z=0}^{z=z_L} \int_{W=0}^{W_D} H_{out} \, dw.dz \qquad 5.28$$

The value of H_{out} can be obtained for each point on a predetermined grid on the tray, by equation 5.27 above for a given value of point efficiency, E_{OG}. These were averaged according to equation 5.28, by integrating over the tray and dividing by the tray area. The trapezoidal numerical integration method was used [38].

Now, $\bar{H}_{out}$ was also obtained from the overall heat balance in equation 5.25 above.

Since at any point H_{out} depends on the value assumed for E_{OG}, the method of calculation is by trial and error adjustment of E_{OG}, until agreement is reached between the two values of H_{out}.

In the sections following an outline of the experiments involving the water cooling method is discussed. This is followed by a discussion of the results.

6. PROGRAM OF EXPERIMENTS

A program of experiments was drawn up to determine the use of the water cooling technique for investigating:

1. The effects of the liquid flow patterns on tray mass transfer. That is, can the effects of the flow patterns on mass transfer be shown by changes in the temperature profiles?. And,

2. Point and Tray efficiency

These will be described and discussed separately.

6.1 The Effects of Liquid Flow Patterns on Tray Mass Transfer

Stichlmair and Weisnam [120] satisfactorily employed temperature measurements on small trays to detect and thus improv$tray out-of-levelness. It has been shown in Section 4 of this work, that skewed temperature profiles were associated with "malaligned" trays only. It is concluded that the measurements of temperature profiles provide an adequate means for investigating tray installation and mechanical design. Further, temperature profiles from a 3mm holes sieve tray were carried out (and reported elsewhere in reference [3]) in this rig. The results showed that areas of the tray where cold water was observed were shown to correspond to areas of the tray where the dye tracers used was retained for relatively longer periods than the others.

From these observations it is to be expected that the hydraulic behaviour and therefore the liquid flow pattern on a tray can be represented by the temperature profiles from a water cooling experiment.

6.1.1 Temperature Profile Experiments

a. In all temperature profile experiments the minimum air flow rate was set above the incipient weeping limit so as to avoid weeping. Random weeping is common in real trays and if this happens the enthalpy of the incoming air can no longer be uniform. This would have unpredictable effects on the temperature profiles.

b. Some FRI systems were simulated. A system is defined here as a family of points along a line of constant flow ratio number, that is;

$$(q/b) \;/\; (C_{sb}) = s \text{ a constant.} \qquad 6.1$$

Unlike in practically all distillation systems, the ratio of air to water densities ρ_V/ρ_L (in the variable C_{sb}) remains constant. It is noted here that no account is given in published literature, where the approach using the flow ratio number has been adopted in simulating distillation systems using air and water. This approach is akin to distilling under total reflux or at a constant reflux ratio, that is, L/V. Here the FRI systems were simulated simply by adjusting the flow rates of air and water, see reference [90].

c. Flow rates were chosen to investigate differences between the temperature profiles of separate flow regimes. The recommendation for the transition between the flow regimes was based on the correlation using the flow ratio number in reference [90]. The limits of the experimental flow rates are indicated in figure 6.1 below.

d. The effects of flow control devices on the liquid flow patterns were investigated.

6.1.2 Experimental Procedure

The following procedure was adopted for each experiment carried out;

i. Switch on electronics system at least 15 minutes before start-up. This is recommended by the instruments manufacturers [122].

ii. Start air fan and set butterfly valve position to correspond with the required value of air flow rate.

iii. Start water pump to lift water to test tray and set the rate to required value.

iv. Introduce steam into water circulating through the pipe to the test tray.

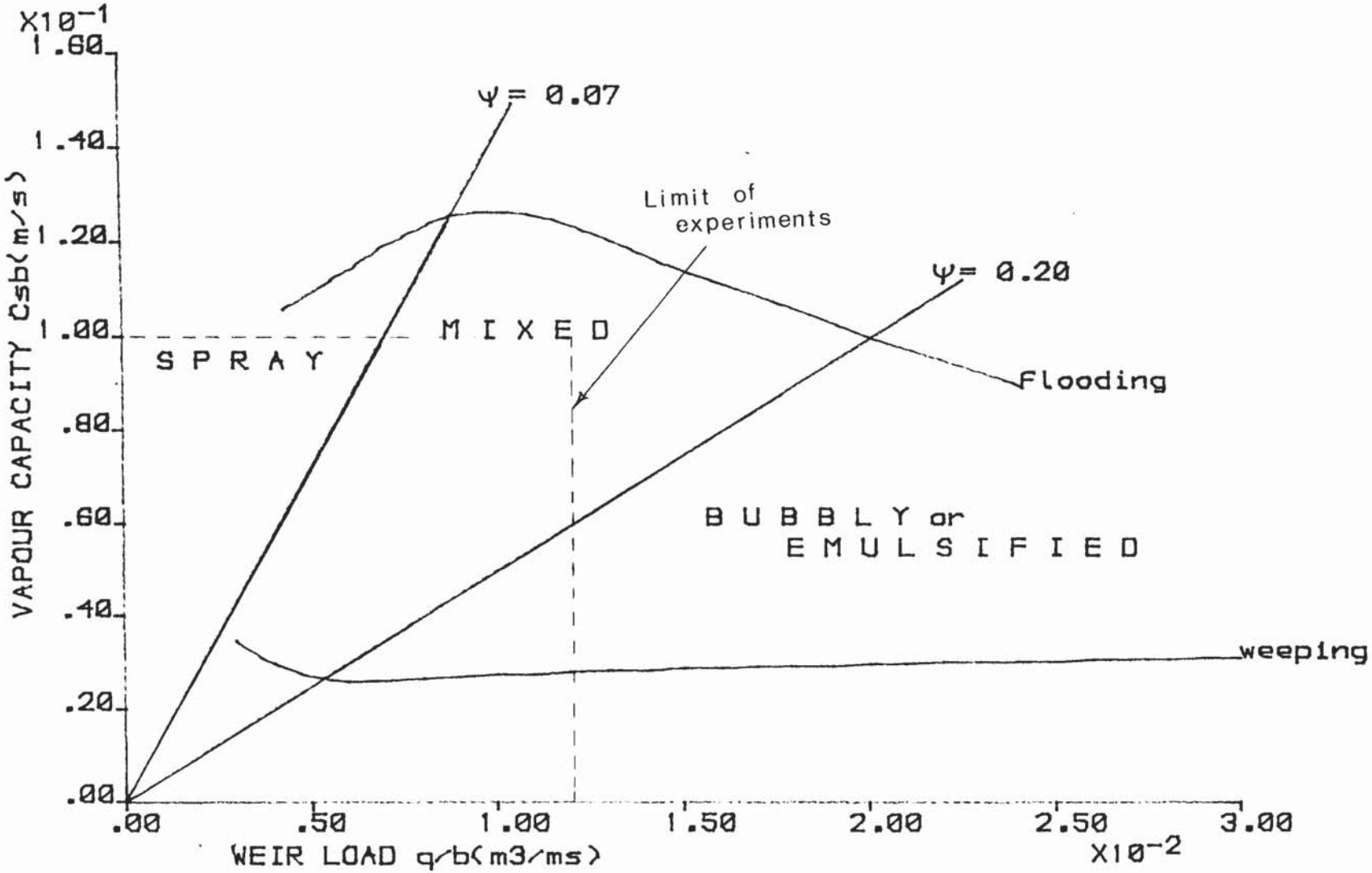

FIG 6.1 FLOW REGIMES TRANSITION LINES (PORTER/JENKINS)

v. Run computer program to display temperatures on the VDU (visual display unit or computer screen) and observe for changes in temperatures.

vi. Reduce steam valve as the tray inlet temperature approaches 40 C and observe for further changes.

vii. Adjust steam valve till temperature at tray inlet is steady to 0.5 C for five minutes.

viii. Check for no change in wet-bulb temperature.

ix. Feed data sampling commands into computer and retrieve data (can set number of runs;time intervals between runs ;averaging option over total number of runs made and coarse display on the VDU of shaded areas represnting temperature range - incorporated into program by courtesy of reference [2]. An example of the final measurements is given in Appendix B, Table A:B3.

6.1.3 Experimental Results on Temperature Profiles

The temperature profiles shown are typical of the two regimes investigated in this work, thus: figure 6.2 shows the profiles for the Mixed regime while figure 6.3 and figure 6.4 are both representing the Spray regime profiles. In figure 6.4, the profiles are identified as those of an intense Spray regime. It is worth noting here that the U-shapes in figure 6.4 for intense Spray are a new phenomenon whose shape bears a resemblance to the U-shapes hitherto identified with the Bubbly and Mixed regimes only. The

Measured Temperature Profiles on a Sieve Tray

(Temperature °C)

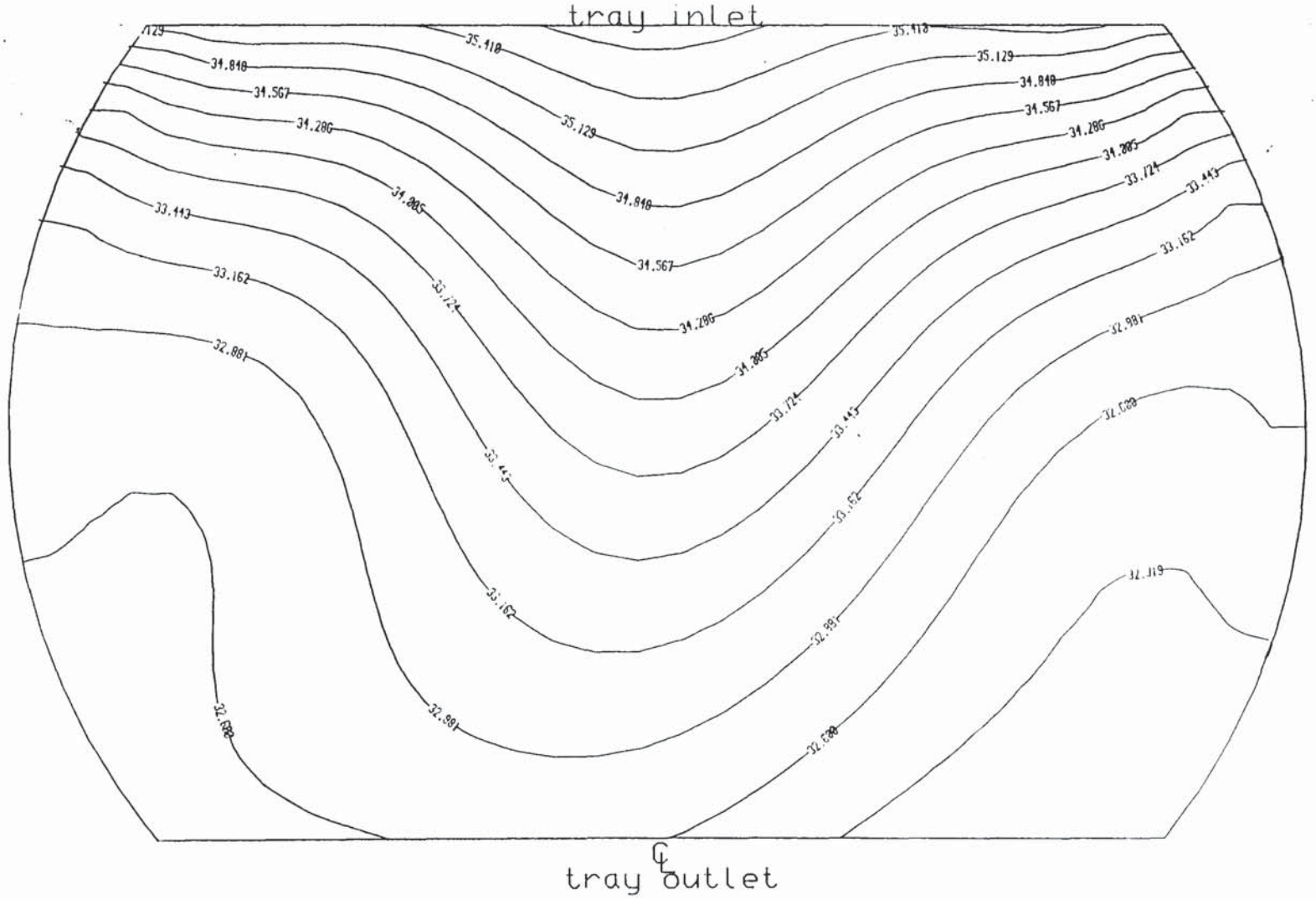

FIG:6.2 Mixed Regime
Csb= .0660m/s q/b= .01227m3/sm
STANDARD TRAY

Measured Temperature Profiles on a Sieve Tray

(Temperature °C)

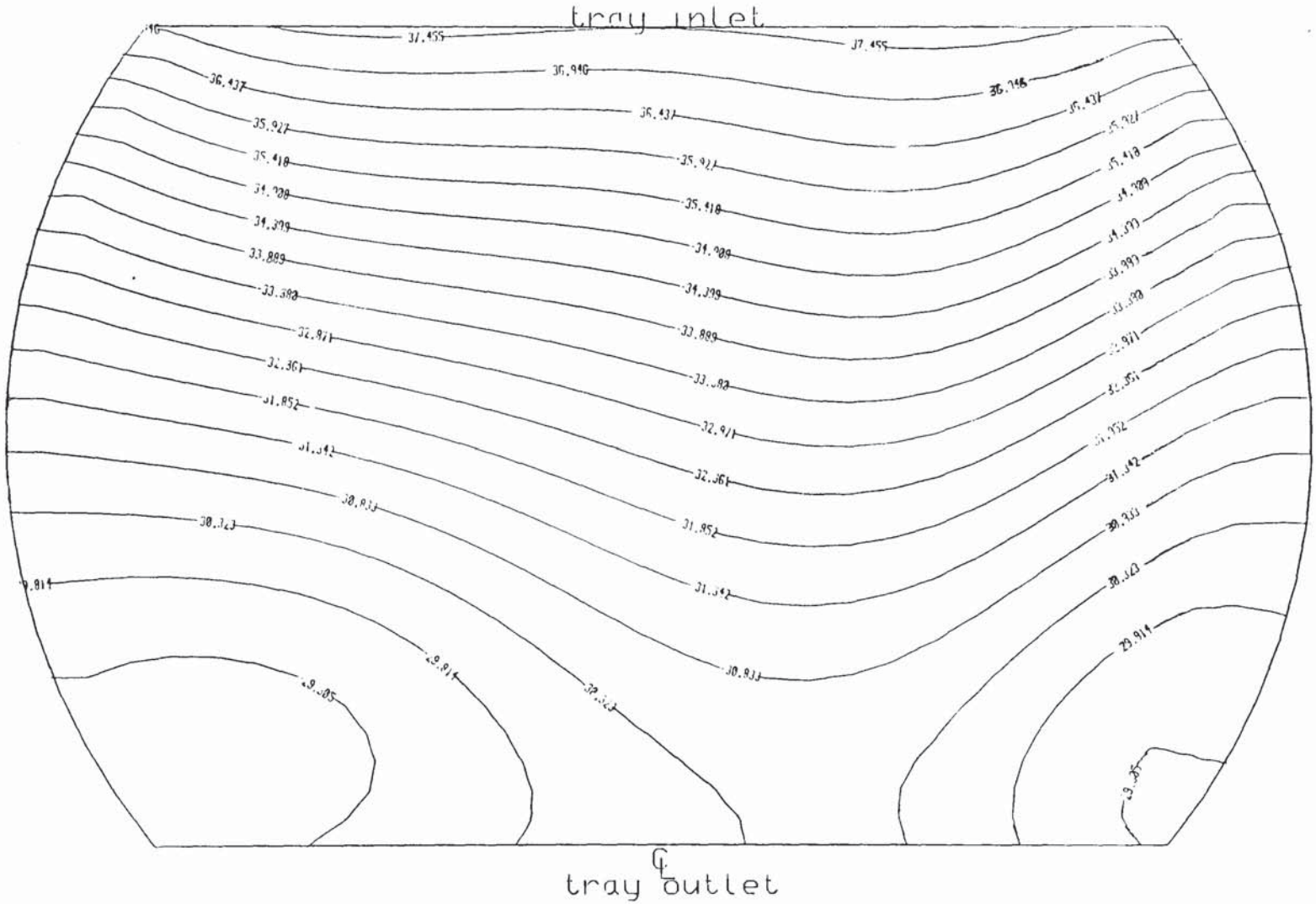

FIG:6·3 Spray Regime
Csb= .0915m/s q/b= .00322m3/sm
STANDARD TRAY

Measured Temperature Profiles on a Sieve Tray

(Temperature °C)

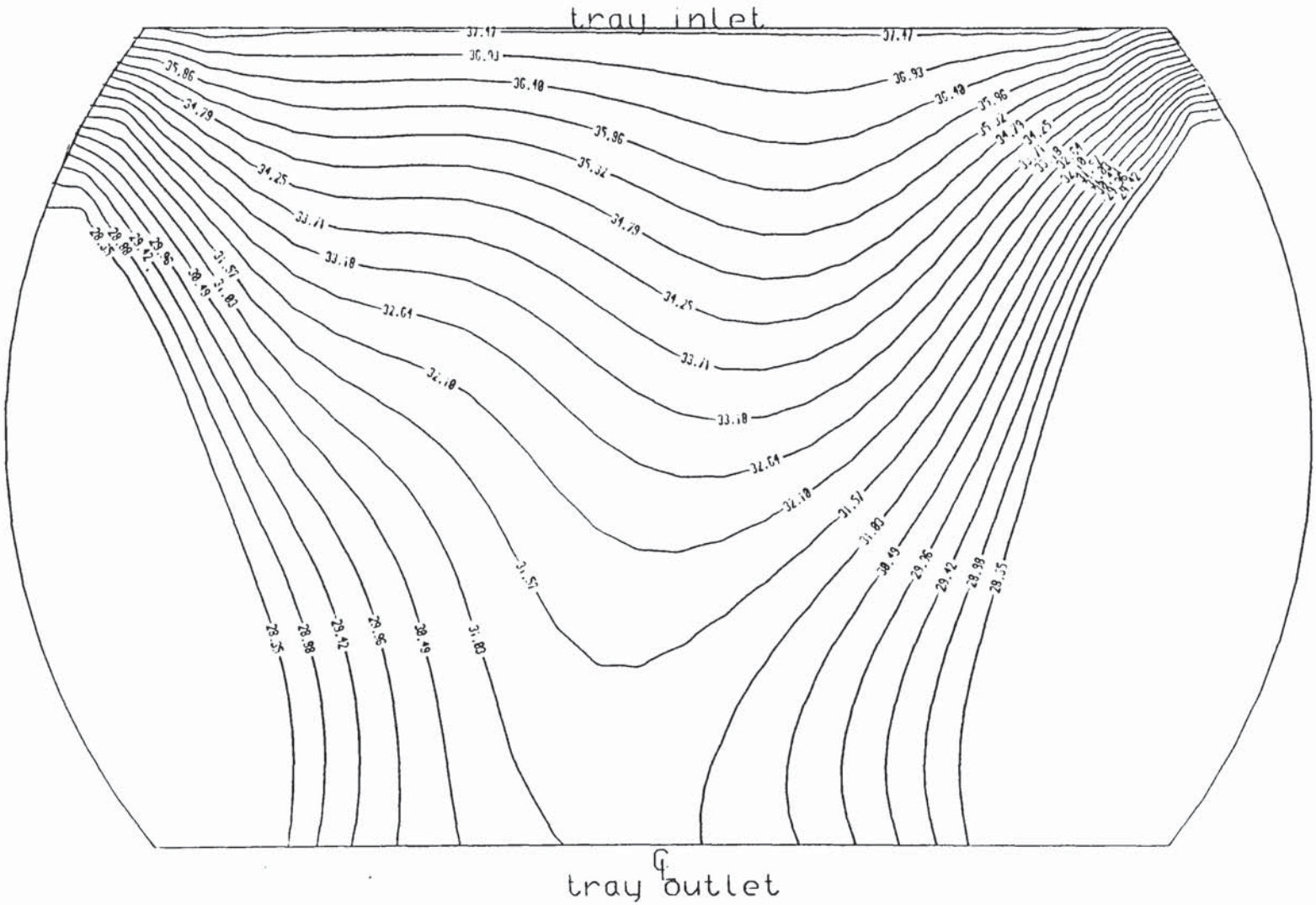

FIG:6·4 Spray Regime
Csb= .0670m/s q/b= .00233m3/sm
STANDARD TRAY FRI FLOW RATES

rest of the experimental data is given in Appendix A. The temperature profiles are further discussed below.

6.2 Measurement of Uniformity of Flow Over the Weir

The procedure for the experiments follows from the description of the apparatus made and described in subsection 4.10

The water outlet hole made at the bottom of each compartment, was varied by inserting into it rubber bungs fitted with copper tubes of required sizes. The copper tubes were individually calibrated in each compartment, in order to relate the height of liquid therein directly to the flow rate of liquid passing through the hole for each tube size. A scale was attached to each compartment wall to measure the height of liquid within.

The box was carefully lowered into the downcomer. The column was run at different air and water flow rates. The flow rate per unit width was found by dividing the flow rate corresponding to the height of liquid by the width of the compartment. No steam was used.

6.2.1 Results of Measurements of Flow Over the Weir.

The results of the measurements are shown in part in figure 6.5 to figure 6.10.

At high liquid loading (> 0.45 x $10^{-2}m^3/s$) channelling at the centre of the weir is high. This reduces at intermediate flow rates, but then at low liquiud loading (< 0.06 x $10^{-2}m^3/s$), there is less liquid flow at the central part of the weir and more liquid at the sides. It was thought that the reason for this is partly due to the method used to measure the flow. As such stronger conclusions can only be made from further experiments and perhaps by employing smaller size compartments. The experiments are currently undertaken in this laboratory [3].

6.3 Discussion of Results on Effect of the Liquid Flow Pattern on Tray Mass Transfer

The theoretical work by Porter and Jenkins [90], suggests that there would be differences between concentration profiles for the Bubbly flow, that is, the Mixed and Emulsified flow regimes and that for the Spray regime. The shape of the profiles in the Spray regime is expected to be straight (or flat). Furthermore, the concentration profiles would remain the same everywhere along a systems line. The correlation equations given by the authors for the transition between the various flow regimes is strictly adhered to in this work.

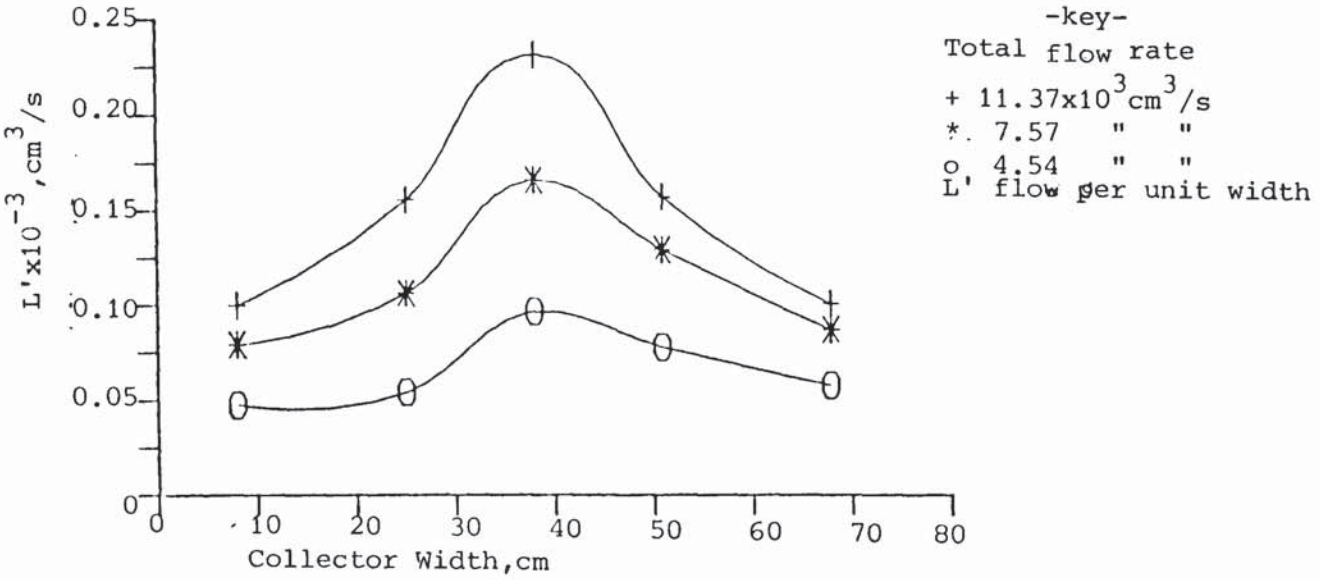

FIG: 6.5 Results of Flow per unit width of Weir experiments
Air superficial velocity U_{sb} = 1.74m/s ;hole size 25.4mm

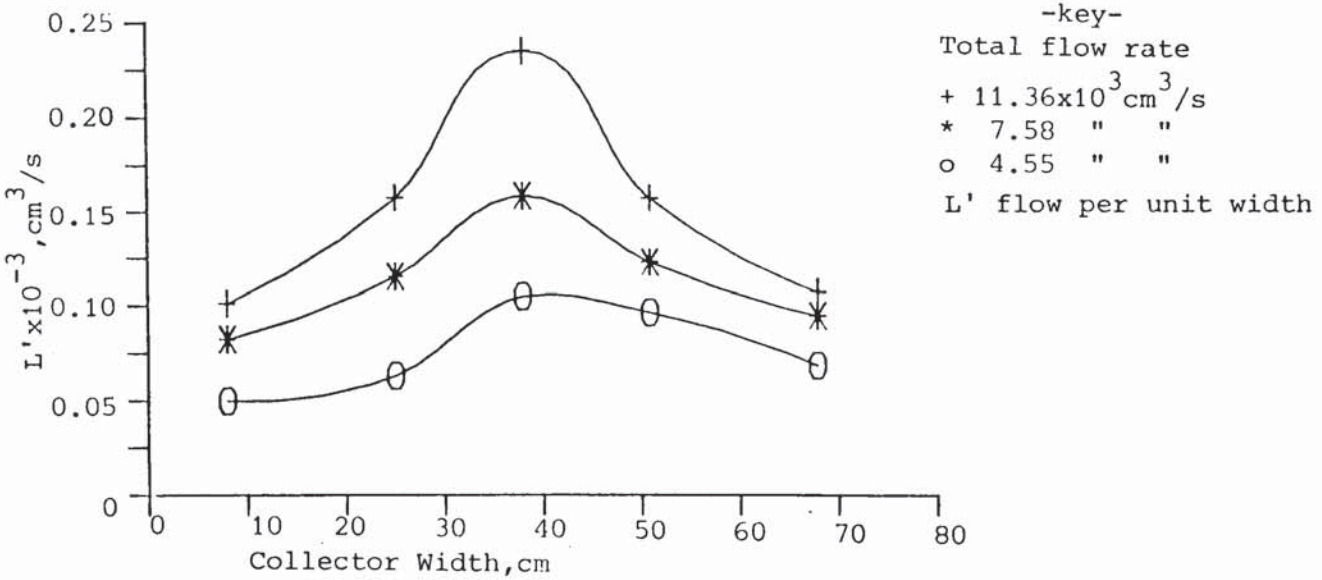

FIG: 6.6 Results of Flow per unit width of Weir experiments
Air superficial velocity U_{sb}= 2.24m/s ;hole size 25.4mm

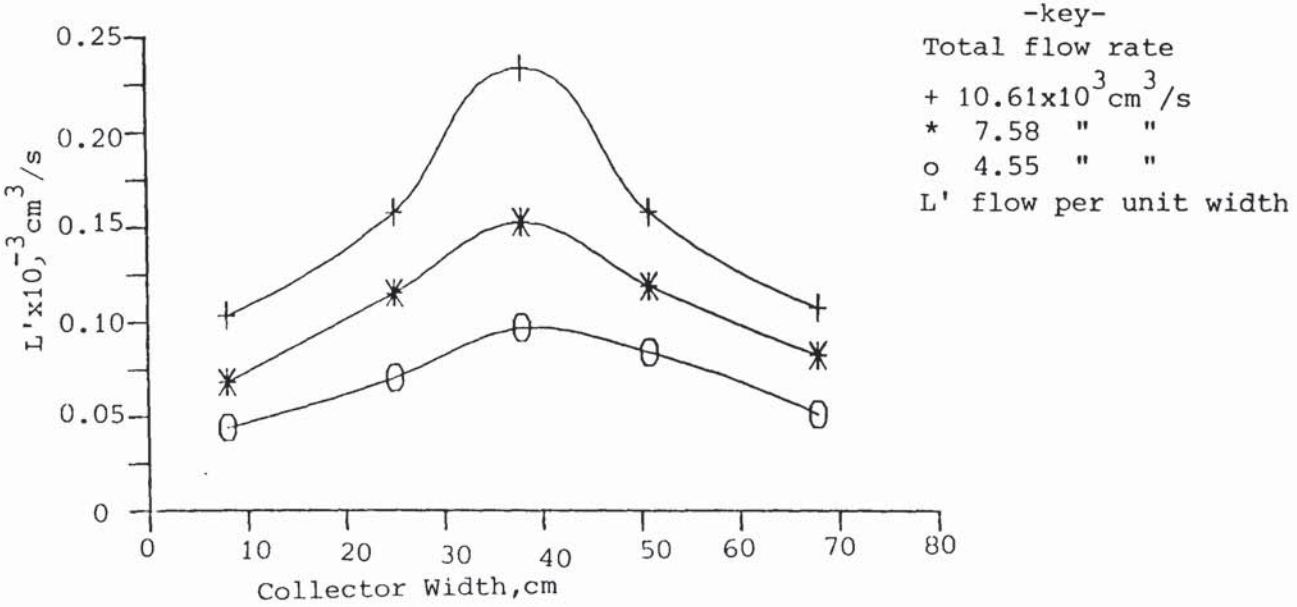

FIG: 6.7 Results of Flow per unit width of Weir experiments
Air superficial velocity U_{sb} = 2.64m/s; hole size 25.4mm

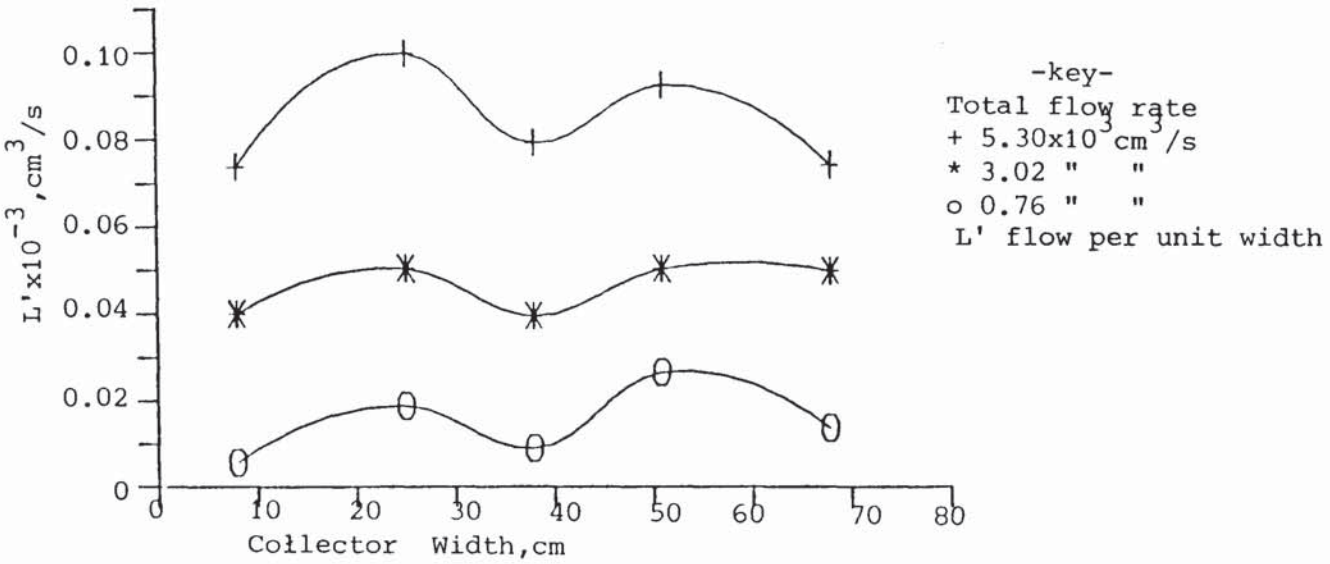

FIG: 6.8 Results of Flow per unit width of Weir -experiments
Air superficial velocity U_{sb} = 1.74m/s; hole size 35.0mm

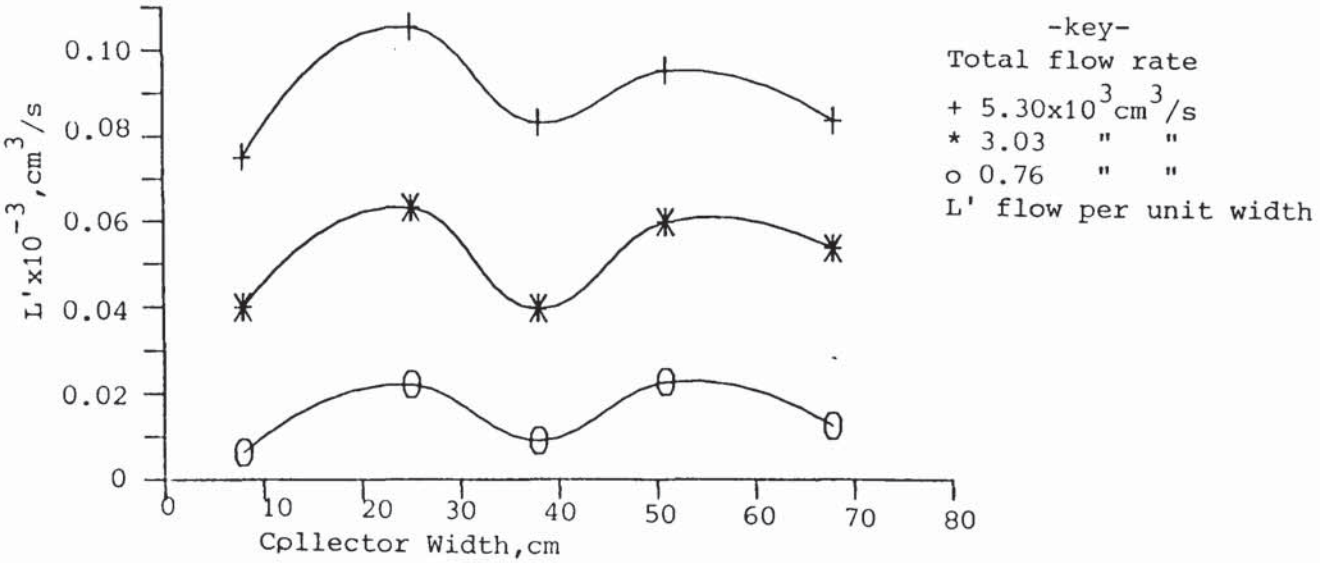

FIG: 6.9 Results of Flow per unit width of Weir experiments
Air superficial velocity U_{sb} = 2.24m/s ; hole size 35.0mm

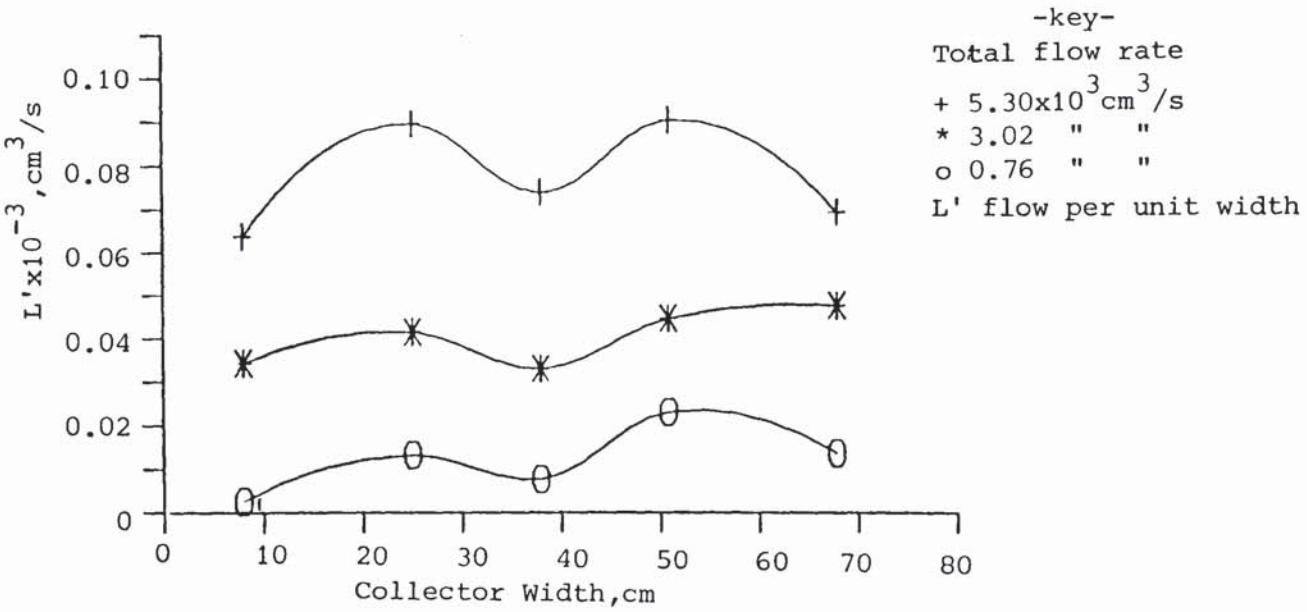

FIG: 6.10 Results of Flow per unit width of Weir experiments
Air superficial velocity U_{sb} = 2.64m/s; hole size 35.0mm

This is displayed on a weir load versus capacity factor plot in figure 6.1.

6.3.1 Definition of U- and Straight (Flat) Profiles

In practice, a variety of shapes of profiles can occur for any particular experiment on a tray. It seems reasonable to define and illustrate the criteria used to describe a single or group of profiles as U-shaped, Straight (or Flat) or otherwise in this work.

Note : Profile reference line is not always parallel to the weir. The profile reference line is a straight line, drawn from the beginning of a profile on the side of the tray, to where it first terminates on the tray.

The criteria used were:

1. An ideal straight profile is one that is parallel to the profile line and satisfies criteria 3 below.

2. From figure 6.11a above, when;

$$a > (1/3 * b) \qquad 6.2$$

the profile is considered as U-shaped.

a

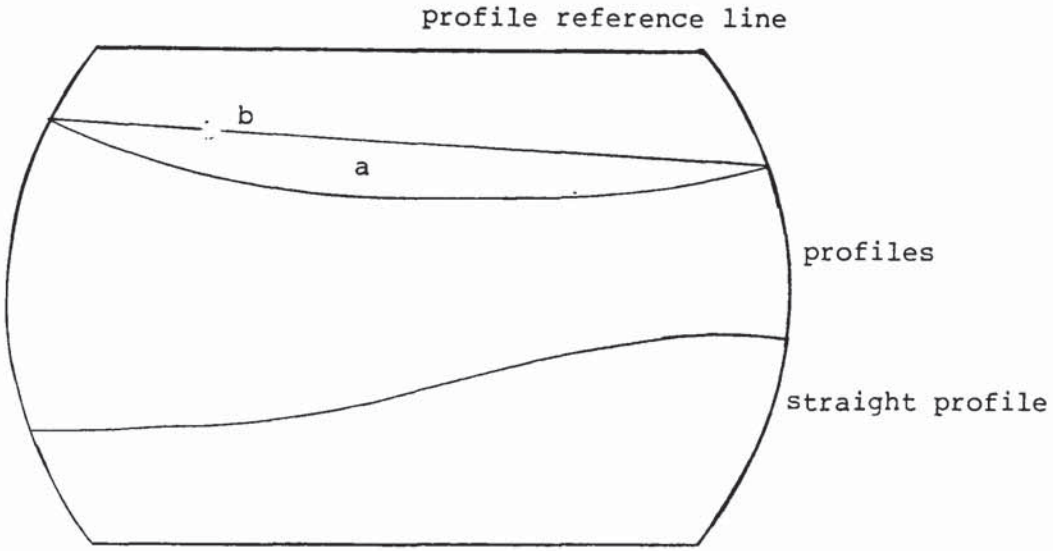

b

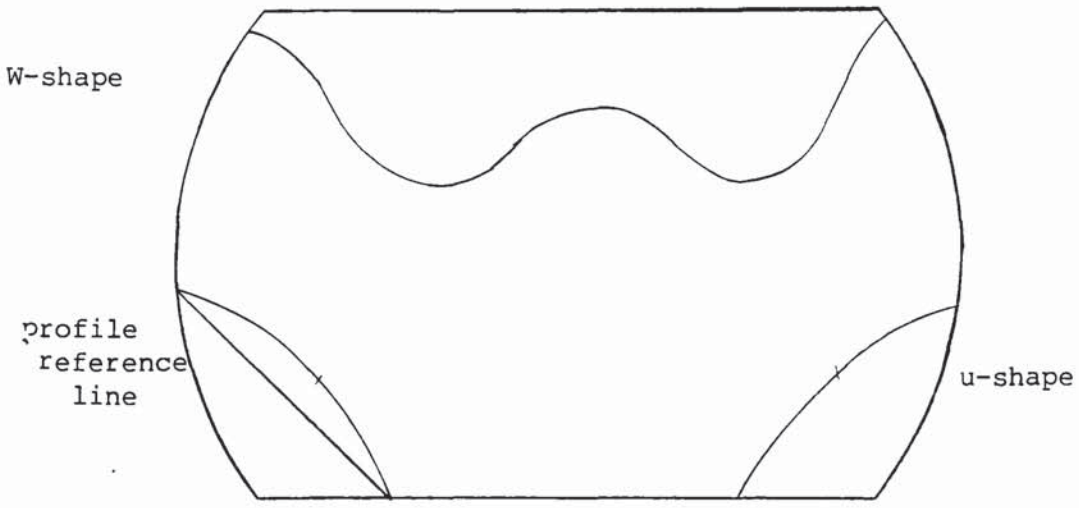

Fig.6.11 Criteria for definition of temperature profiles on tray

3. From figure 6.11a above, when;

$$a < (1/3 * b) \qquad 6.3$$

the profile is considered as straight.

4. Profiles that dip into the outlet weir are potentially U-shaped, and are labelled as such, see figure 6.11b above.

5. Others, like the W-shape is shown in figure 6.11b above.

6. For a group of profiles, when greater than 50% of the tray area is occupied by profiles that could be described by any one shape, then the general pattern on the tray is labelled as same.

In the next subsection the flow patterns for the flow regimes are discussed separately using the criteria above.

6.3.2 Temperature profiles in the Mixed Regime

A mixture of flow patterns shown by the temperature profiles were evident in this regime. They were predominantly U-shaped but flat and irregular (W) shapes were also observed. At the gas flow rate, C_{sb} = 0.0605m/s (or U_{sb}=1.75m/s), the temperature profiles are distinctly U-shaped although at the tray inlet flat profiles are observed. This is shown in figure 6.12. By increasing the liquid rate the shape of the profiles is affected in the second half of the tray only. These are shown in figure 6.13, to be relatively more U-shaped thus suggesting that the relatively high liquid momentum in this regime is insufficient to overcome the retrograde (opposite flow) forces often thought to emanate from the weir.

An important feature of the Mixed regime profiles is that at low gas rates the profiles are sometimes irregular and skewed, inspite of the precautions taken to level the tray during installation. These are shown in figure 6.14 and figure 6.15. Since out-of-leveiness of the tray as well as poor distribution of liquid from the inlet downcomer result in skewed temperature profiles, the observation suggests that trays operating at low gas rates will tend to become out-of-level during operation.

The predominantly U-shapes and other shapes found together in this regime further suggests that there might be regions on the tray of differing flow patterns. Temperature profiles have been found showing lower temperatures along the centre-line. This observation

Measured Temperature Profiles on a Sieve Tray

(Temperature °C)

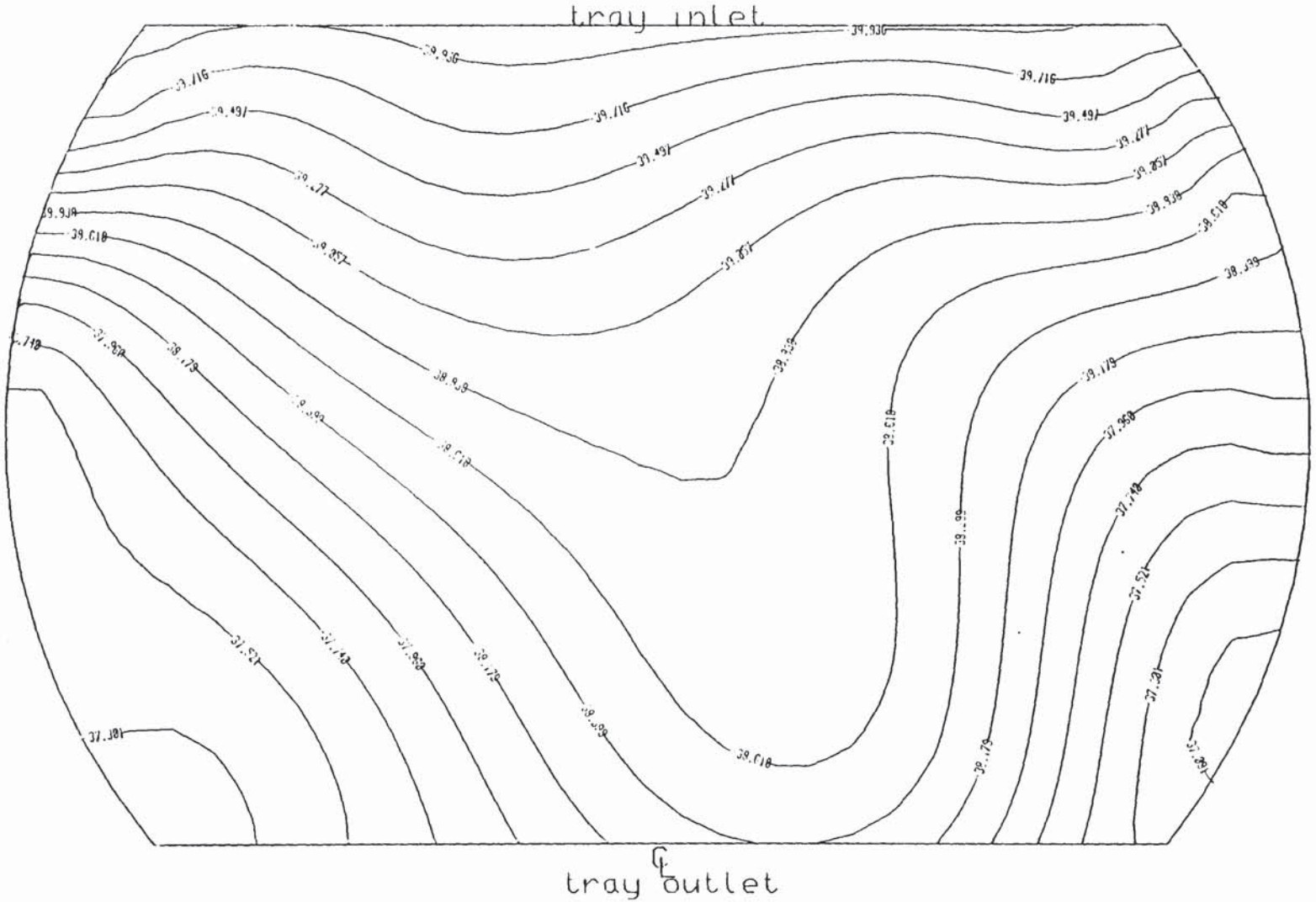

FIG:6·12 Mixed Regime
Csb= .0605m/s q/b= .00806m3/sm
STANDARD TRAY

Measured Temperature Profiles on a Sieve Tray

(Temperature °C)

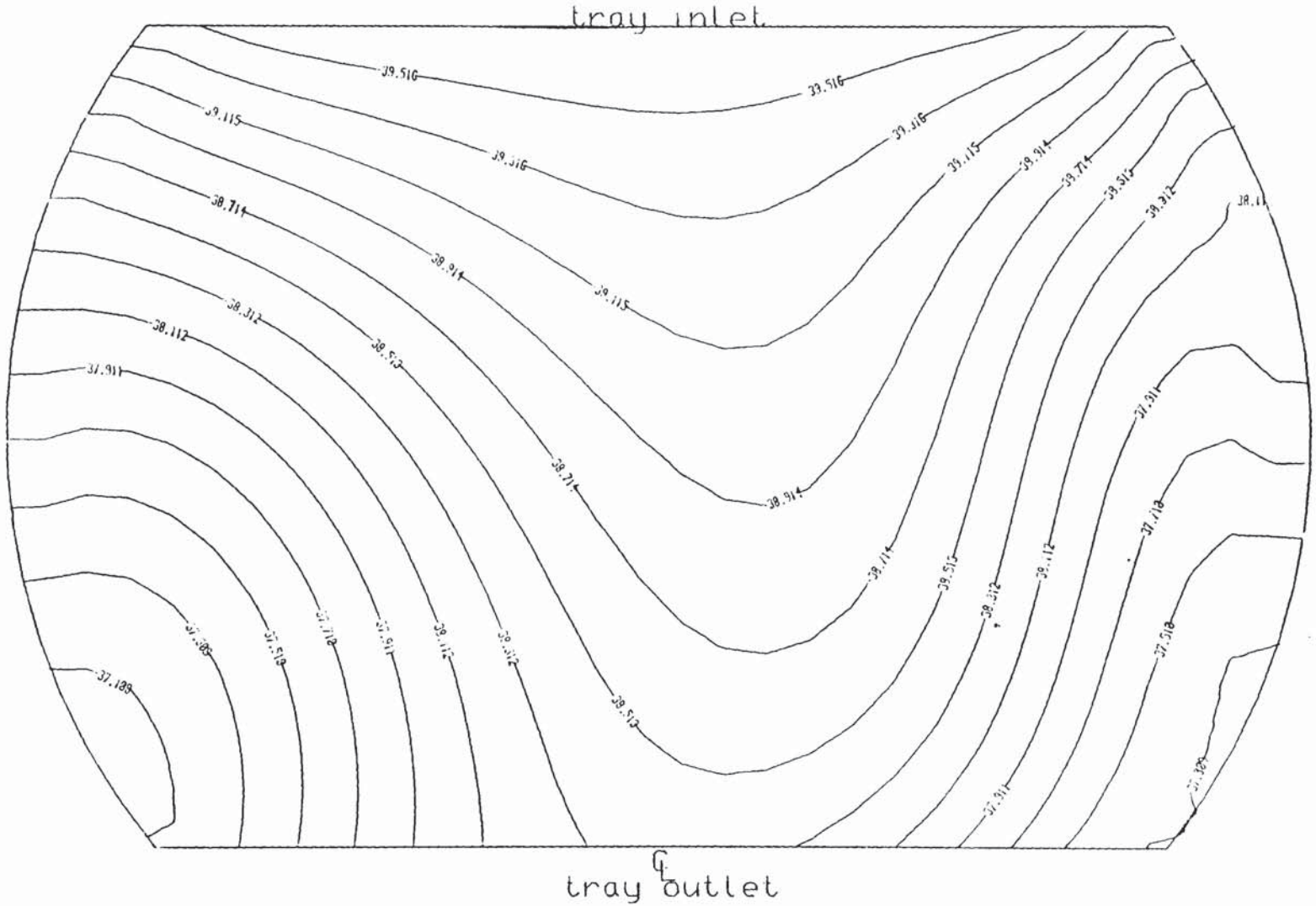

FIG 6.13 Mixed Regime
Csb= .0605m/s q/b= .00967m3/sm
STANDARD TRAY

Measured Temperature Profiles on a Sieve Tray

(Temperature °C)

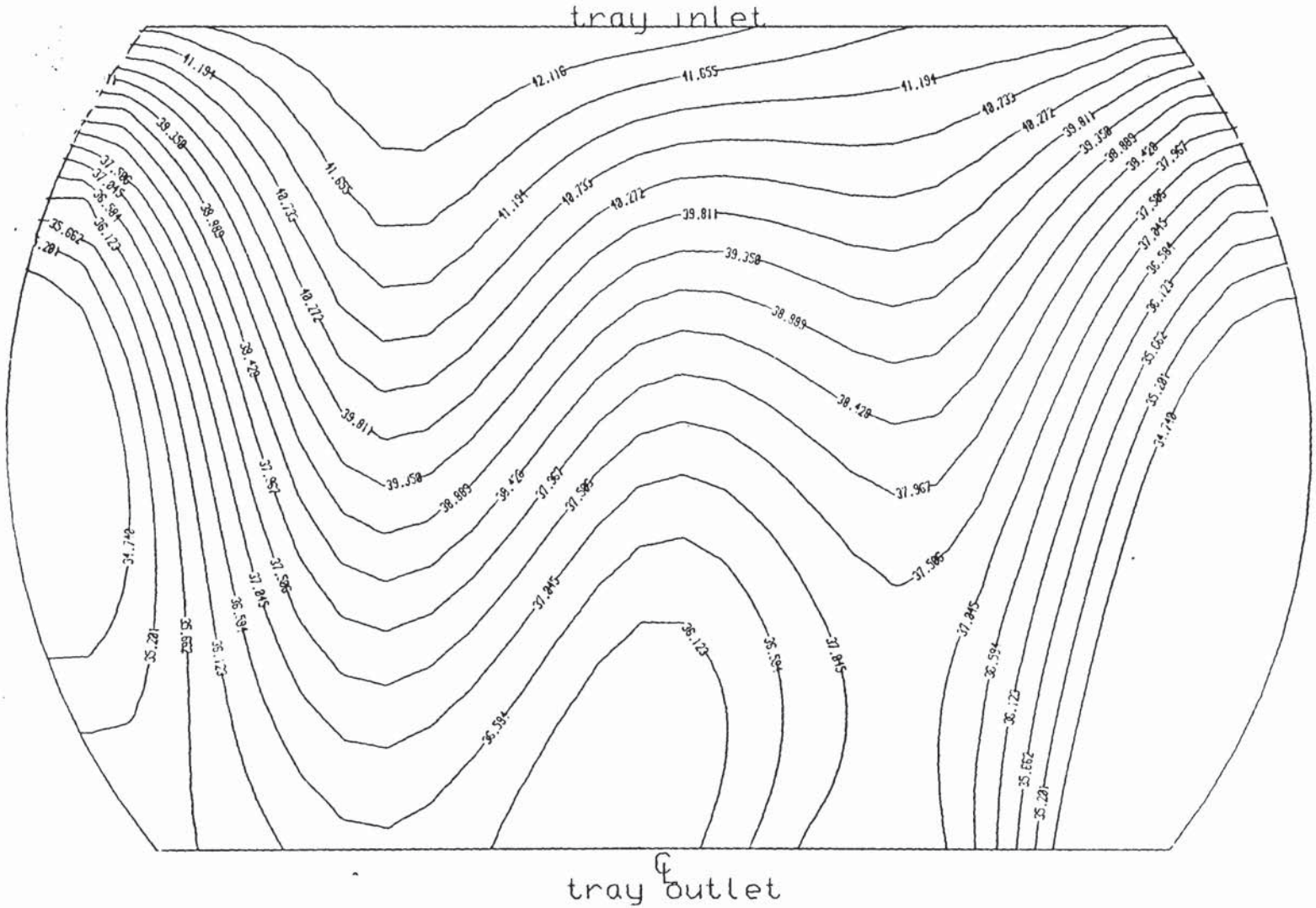

FIG:6·14 Mixed Regime
Csb= .0560m/s q/b= .00426m3/sm
STANDARD TRAY

Measured Temperature Profiles on a Sieve Tray

(Temperature °C)

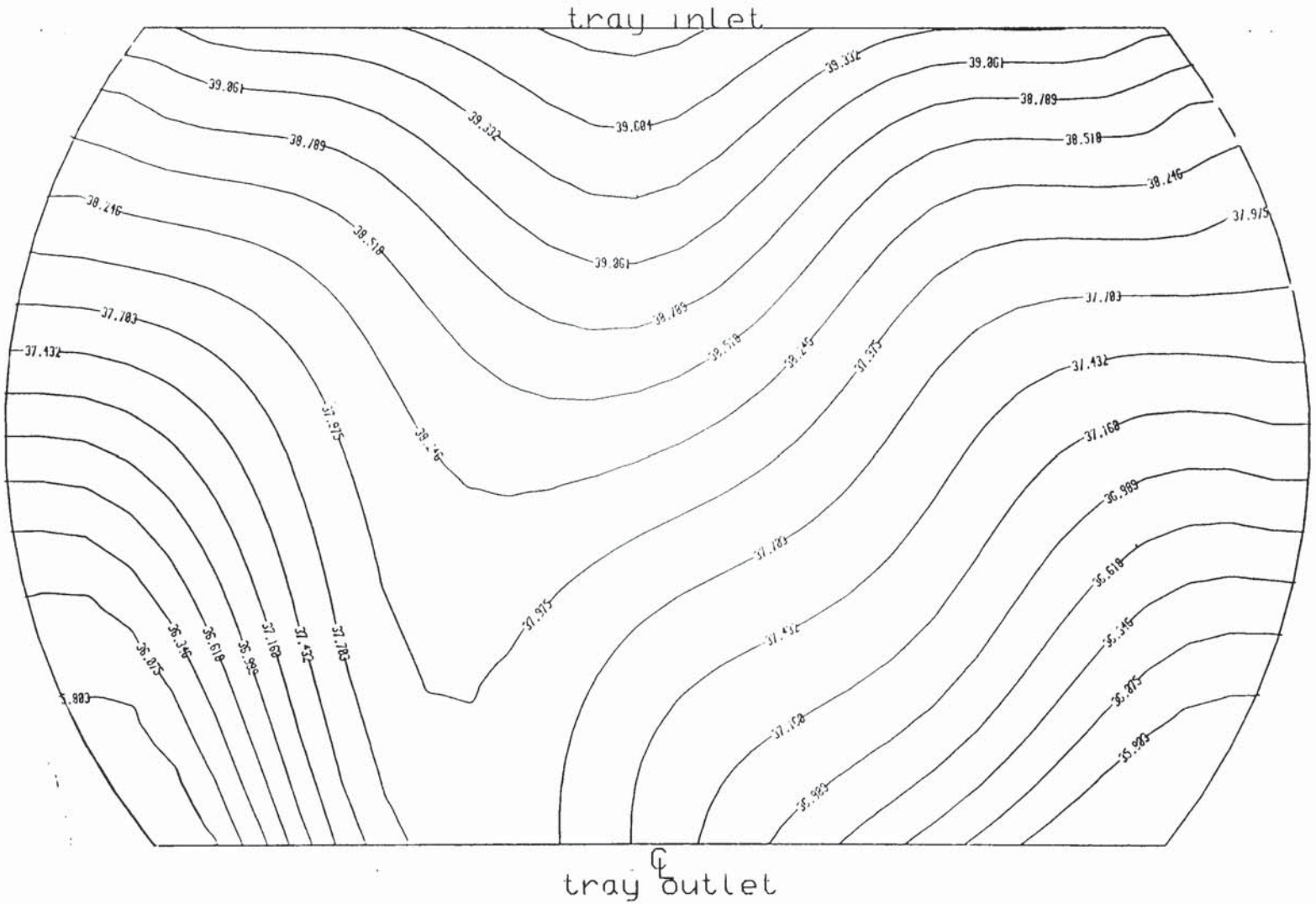

FIG 6.15 Mixed Regime
Csb= .0560m/s q/b= .00851m3/sm
STANDARD TRAY

is unexpected but it is thought that this can only happen due to the effects of the gas passing through the froth. If one accepts that oscillations in the air stream can occur then the assumption of uniform flow of air is no longer tenable. It is unclear how the oscillations will affect the overall flow patterns on the tray.

6.3.3 Temperature Profiles in the Spray Regime.

The temperature profiles in the Spray regime were predominantly straight (flat) in shape although U-shapes were also identified. It was found that as the liquid rate was increased thus bringing the conditions towards the transition line between the Spray and the Mixed regimes, the fraction of the tray area occupied by the straight profiles was increased. At the vicinity of the outlet weir the shapes of the profiles became nonuniform. Large cold regions (corresponding to low values of water temperature) were observed at the tray sides. In figure 6.16 the profiles occupying most of the tray are straight in shape while the fraction of the tray occupied by these is seen to decrease as the liquid rate is increased in figure 6.17. The presence of nonuniform flow patterns near the outlet weir is a feature of the temperature profiles consistently shown on this tray. This suggests that there is some reaction of the weir which persists in all the flow regimes investigated. This seems to confirm the notion that the weir reaction does influence the flow pattern of liquid on a tray. However, the fact that these are restricted to the last half of the tray also means that this influence may have limited significance on the overall tray efficiency since at the outlet of a typical

Measured Temperature Profiles on a Sieve Tray

(Temperature °C)

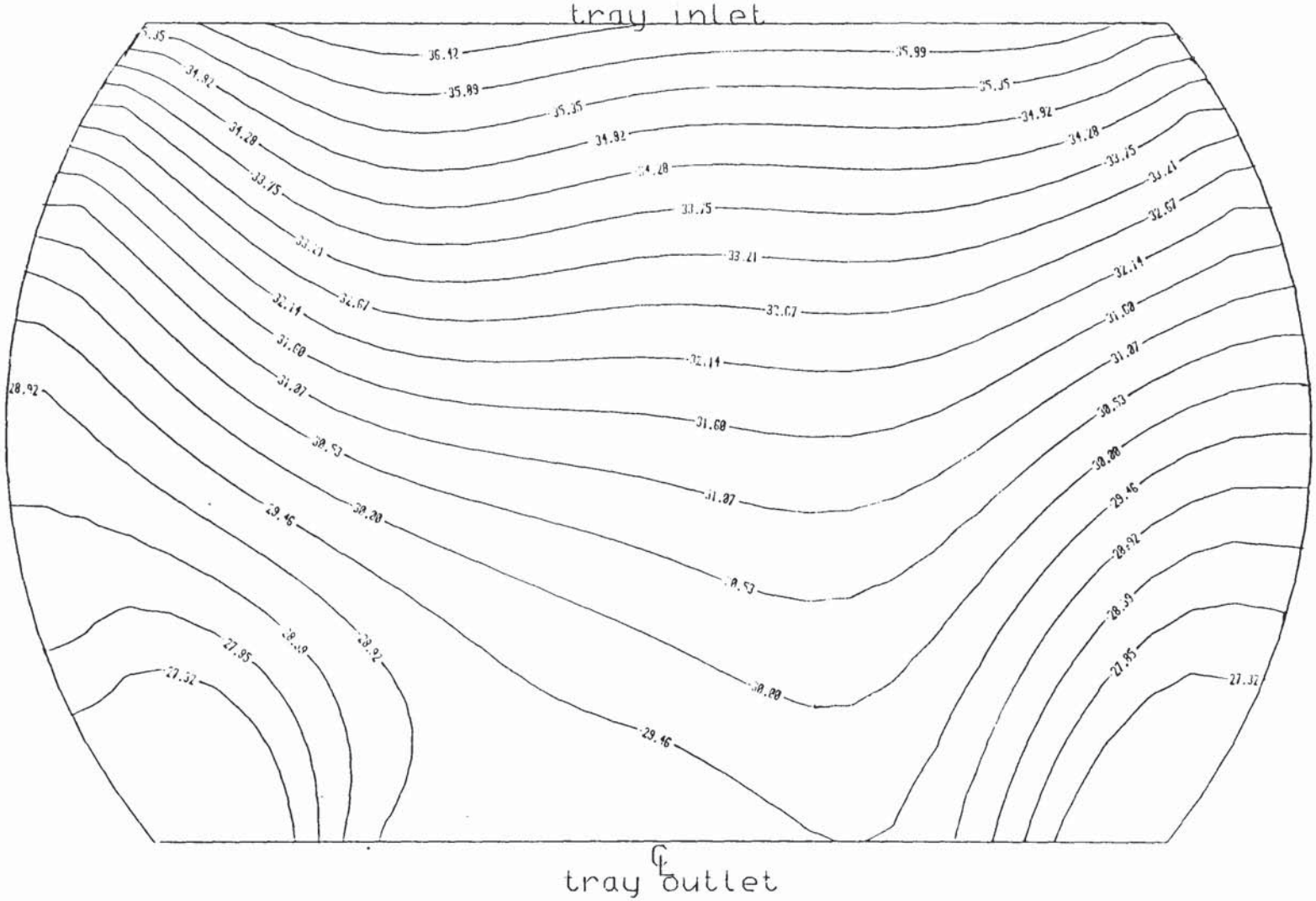

FIG:6.16 Spray Regime
Csb= .0775m/s q/b= .00161m3/sm
STANDARD TRAY

Measured Temperature Profiles on a Sieve Tray

(Temperature °C)

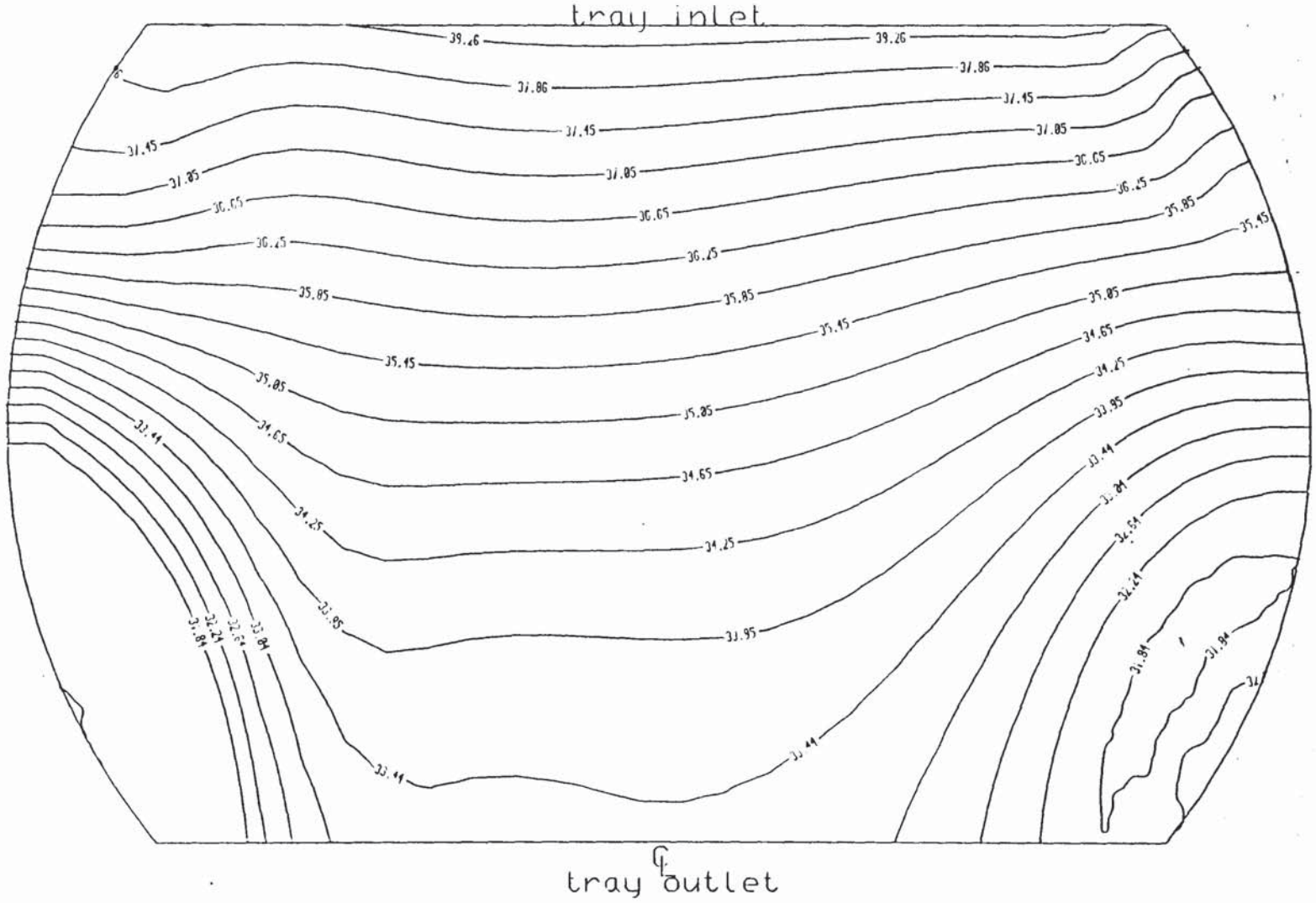

FIG:6.17 Spray Regime
Csb= .0775m/s q/b= .00508m3/sm
STANDARD TRAY FRI_FLOW RATES

Measured Temperature Profiles on a Sieve Tray

(Temperature °C)

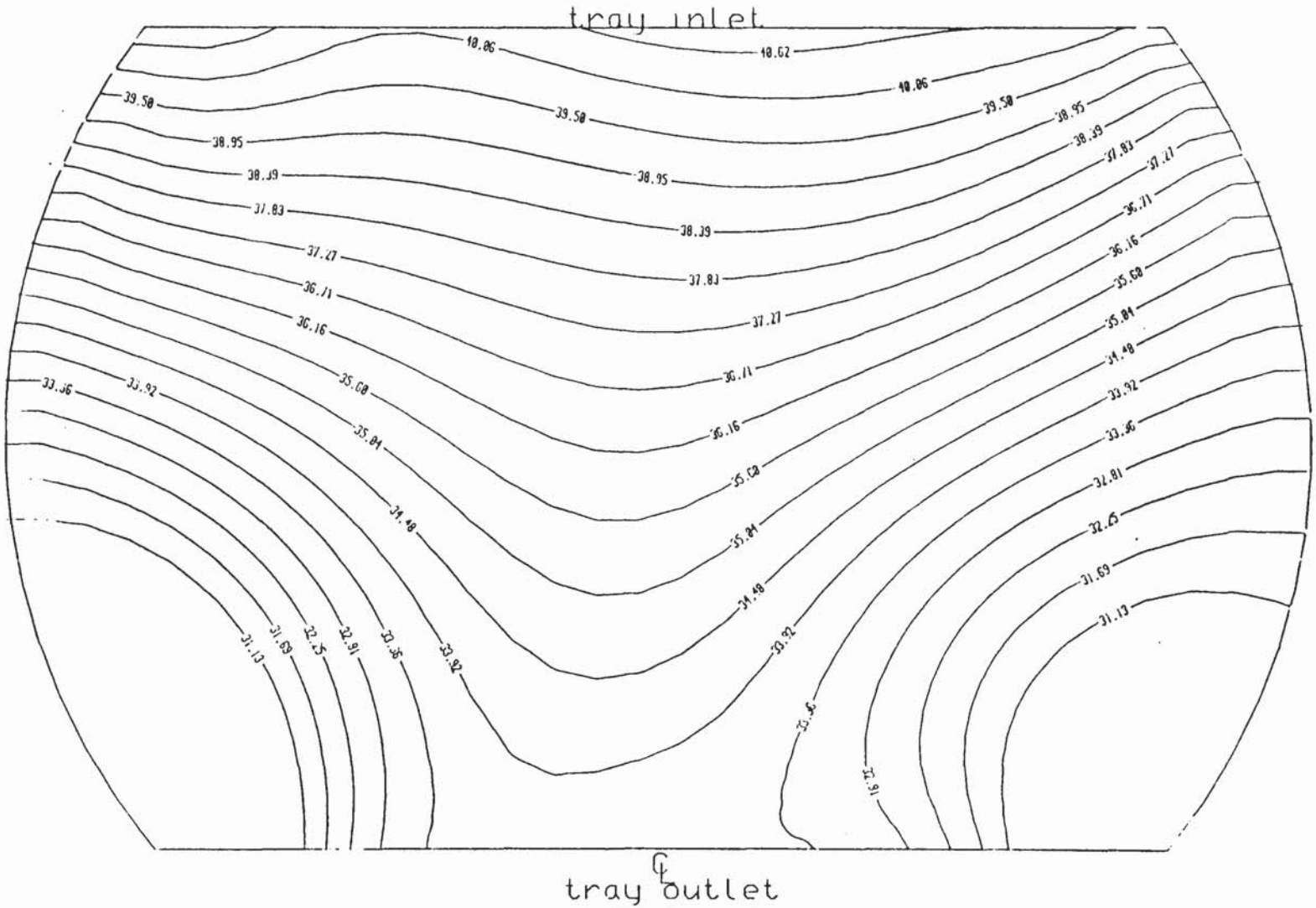

FIG:6·18 Spray Regime
Csb= .0745m/s q/b= .00426m3/sm
STANDARD TRAY

Measured Temperature Profiles on a Sieve Tray

(Temperature °C)

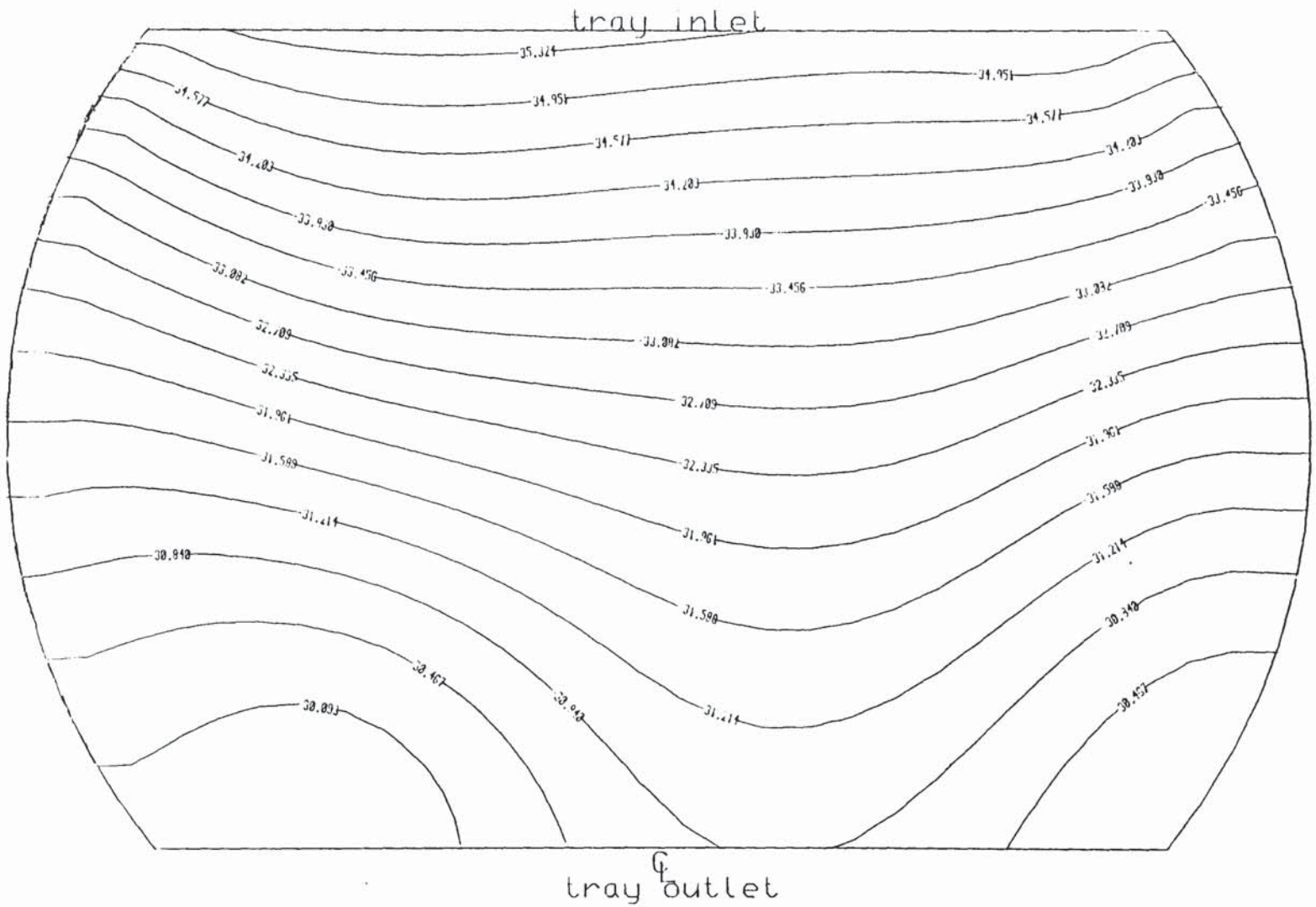

FIG:6.19 Spray Regime
Csb= .0915m/s q/b= .00484m3/sm
STANDARD TRAY

operating tray the least transfer of mass (or in this case, heat) takes place. Other straight profiles found in the Spray flow regime are shown in figure 6.18 and figure 6.19 below.

6.3.3.1 Discovery of Severe U-Shapes in Intense Spray

Perhaps the most outstanding revelation of the temperature profiles in the Spray regime is the discovery of U-shapes in conditions which are described here as intense (or severe) Spray. These are shown in figure 6.20, fogure 6.21 and figure 6.22 below. There is channelling of the liquid through the central part of the tray, leaving large chunks on both sides of the tray at relatively low temperatures. The profiles at the tray sides also suggest that the liquid therein is well mixed. Therefore in this regime, temperature gradients in the direction transverse to flow are small.

It is worth pointing out here that the conditions where this phenomenon were prevalent, are furthest from the transition curve and also close to flooding. Entrainment from the tray is expected to be quite high. The significance of these conditions is that they represent the penultimate stage to flooding by entrainment or blowing.

Measured Temperature Profiles on a Sieve Tray

(Temperature °C)

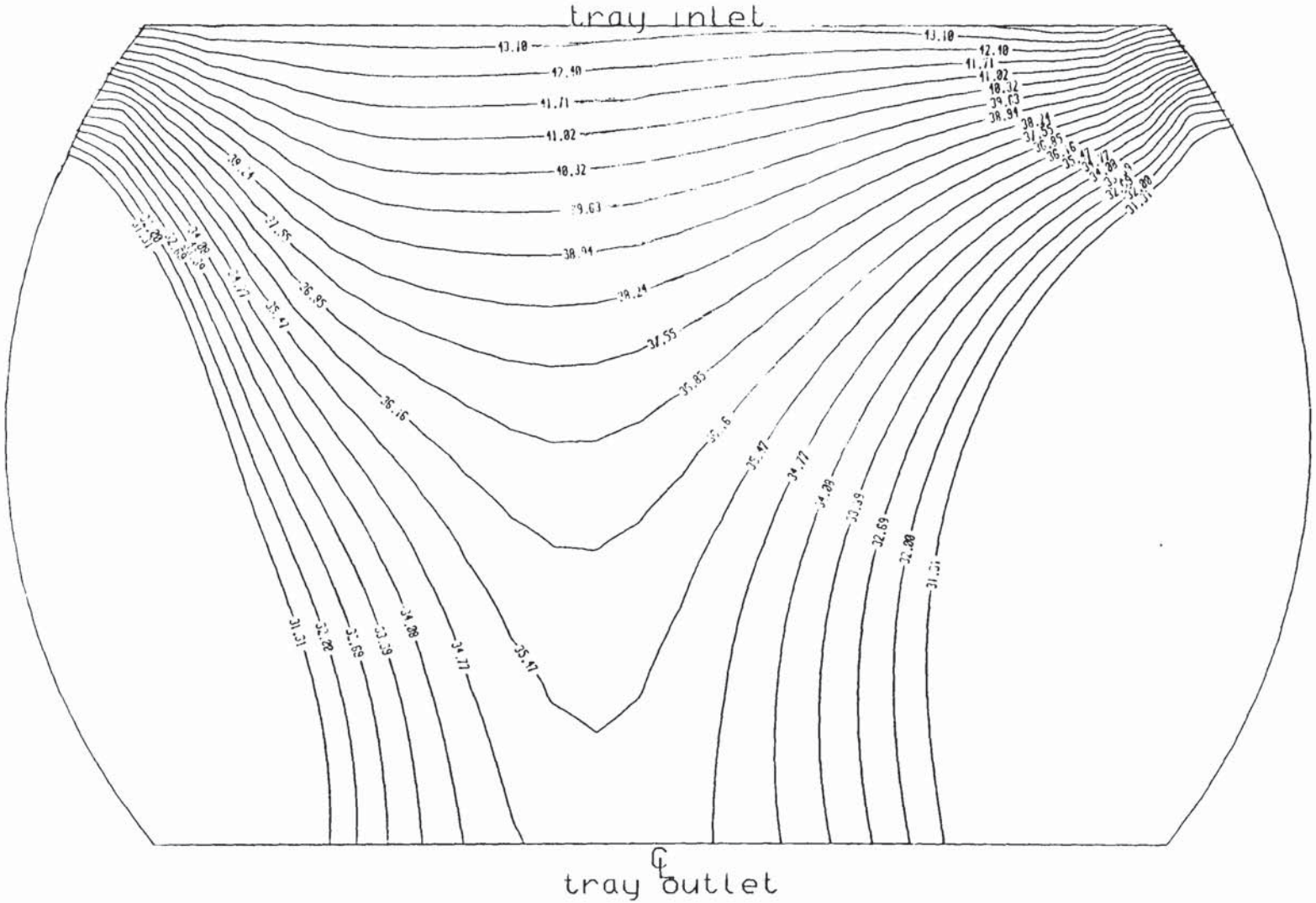

FIG:6·20 Spray Regime

Csb= .0715m/s q/b= .00258m3/sm

STANDARD TRAY FRI FLOW RATES

Measured Temperature Profiles on a Sieve Tray

(Temperature °C)

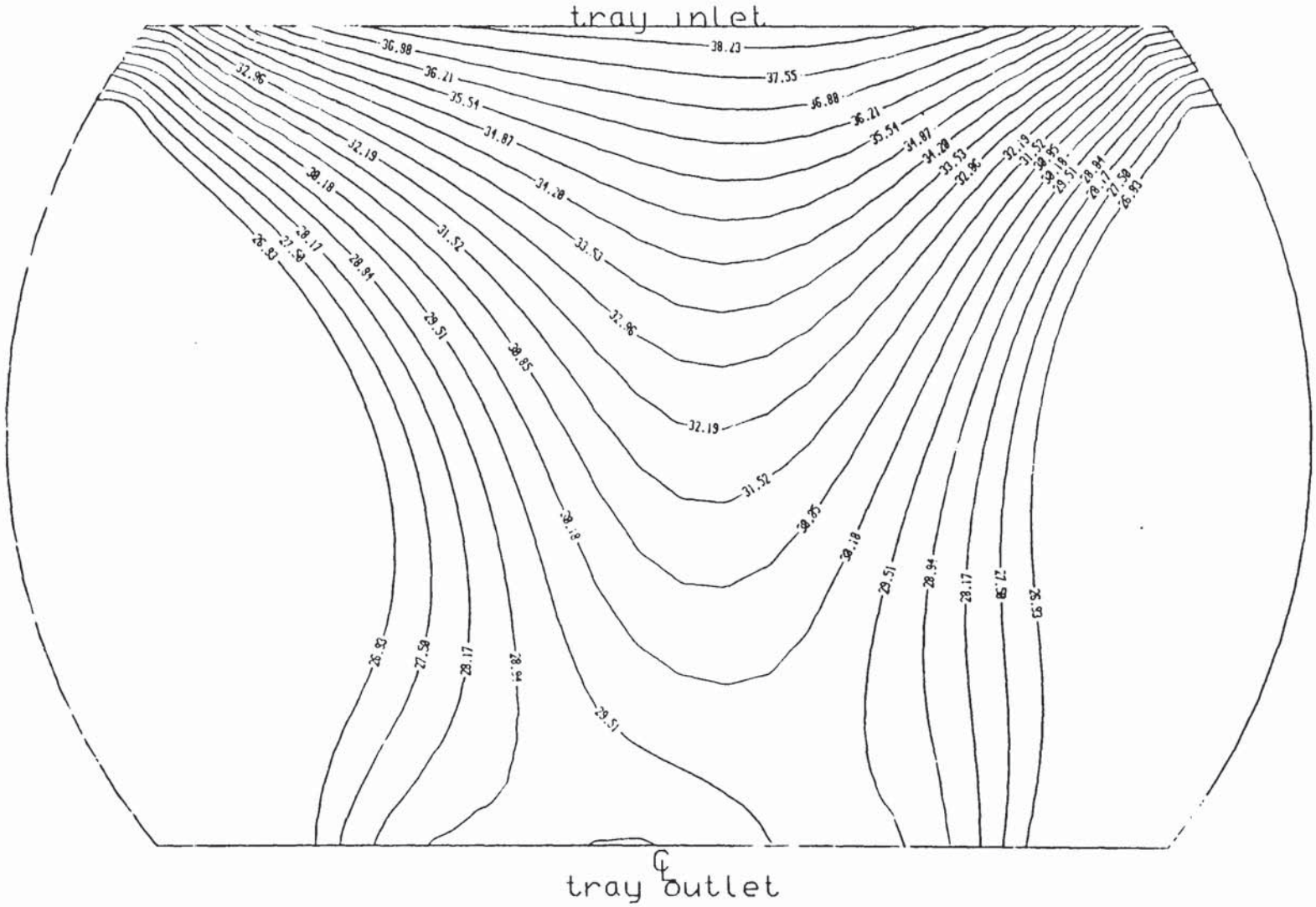

FIG:6·21 Spray Regime
Csb= .0635m/s q/b= .00110m3/sm
STANDARD TRAY

Measured Temperature Profiles on a Sieve Tray

(Temperature °C)

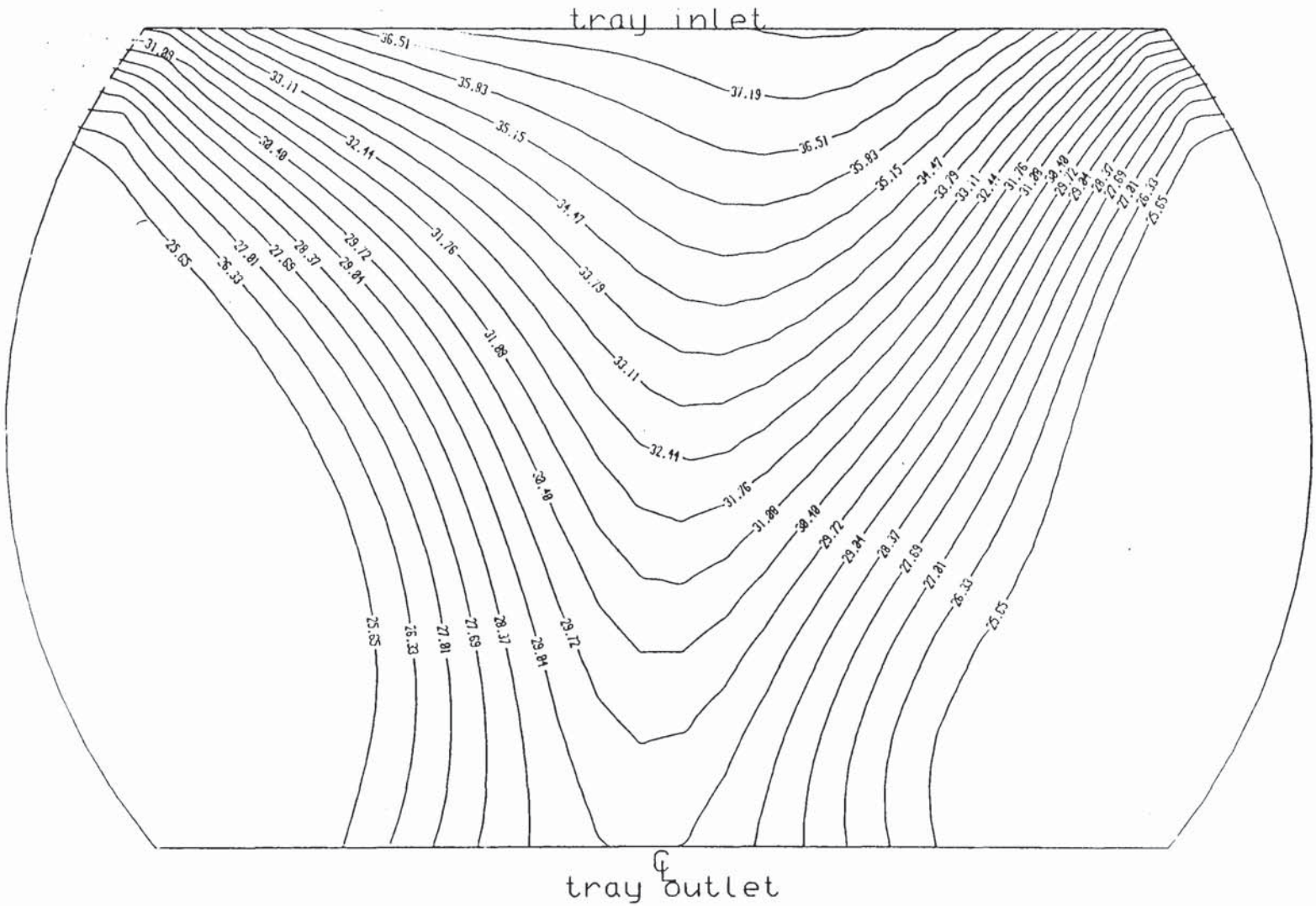

FIG:6·22 Spray Regime
Csb= .0640m/s q/b= .00149m3/sm
STANDARD TRAY

The profiles demonstrate that blowing actually commences or is most from the central part of the tray. Therefore the loss of efficiency associated with high entrainment and due to the presence of large areas of cold (low transfer of heat (or mass)) liquid on the tray sides is expected, thus making these operating conditions unattractive.

This work provides the very first evidence of this kind which shows the existence of intense U-shapes in a cross flow tray operating in the Spray regime. The fact that this was discovered from temperature profiles only and remained undetected from the conventional methods of visual and photographic studies, further justifies the use of this technique and its advantage over others.

6.3.4 Conclusion on Temperature Profiles.

The test carried out here are the first demonstration of the theoretical concepts of the liquid flow patterns on trays. In so doing they also support the Porter and Lockett channelling theory although a more detailed illustration is made later in Section 10 of this work. The evidence thus far lead to the conclusion that U-shaped temperature profiles are associated mainly with the Mixed regime while Straight temperature profiles are associated with the Spray regime. A new regime called the Intense Spray regime is discovered. This is depicted by U-shaped temperature profiles which hitherto were associated only with the Bubbly (and Mixed) regimes. These occur in conditions where the weir load is low. A mixture of flow patterns shows up in both the Spray and the Mixed

regimes. If one believes that the Mixed regime represents a transition between the Spray regime and the Bubbly (or Emulsified) regimes then this mixture is not totally unexpected.

In the next section, further advantage is taken of this technique to investigate the effects of flow control devices on flow patterns. The control devices used are compared to the standard tray fitted to the column in the conventional form.

7. FLOW CONTROL DEVICES

In large trays where nonuniform flow patterns are known to produce a significant reduction in tray efficiency, the use of certain flow control devices to straighten flow and hence increase efficiency, show encouraging results [88,101,130,118]. Straight flow patterns represent an approach to the ideal plug flow and thus enhance the tray efficiency over point efficiency. Flow nonuniformities or flow patterns that are not straight are not expected in rectangular trays. Rectangular designs ensure that the momentum of the liquid is, at least in principle, equal at all points along the flow path length which are equidistant from the weir. A natural solution would seem to be to build columns that are rectangular in cross section. However, this will pose several mechanical problems. For instance, for any given throughput and hence tray size, the thickness of the material needed to maintain the required stress is several times more in a rectangular column than it is in a circular one. Further, the material of construction of columns is steel which is costed on the basis of its weight. The use of thick materials of steel will not only drastically increase capital cost but will substantially make installation more difficult. This means that trays will continue to be built in circular columns.

The two main sources generally believed to be responsible for nonuniform flow of liquid on circular trays are; I. the maldistribution of the liquid ensuing from the dowmcomer and II. the reaction of the outlet weir to the liquid impinging directly

on it [9]. The relevance of the source to tray efficiency was first pointed out by Sohlo et al. in a series of publications [61,62,63,109,110,111].

The two sources are investigated in this work by employing two separate flow control devices. The first involved the use of a Stepflow Downcomer and the second employed a Uniform Gap under the Outlet Weir.

7.1 The Stepflow Downcomer

Most columns in industrial use employ sloped or stepped downcomers. Particular care is taken to fit the top of the downcomer into the existing arrangement of the tray above it. Often the bottom is made straight and parallel to the outlet weir. The distribution of the liquid leaving the downcomer onto the tray is such that the highest flux occurs in the central part leaving the low momentum flux at the tray sides. When designing sloped and stepped downcomer this is based on the top, and the bottom is sometimes required to be not less than one half that of the top. However, the straight bottom means that it is designed for liquid back-up inside the downcomer and not for liquid distribution from the downcomer onto the tray. The design of the Stepflow Downcomer takes into account the liquid distribution factor. The fact that the area of the bottom is designed for 1/2 the top means that the back-up effect is also accounted for.

A schema for the expected distribution from the Stepflow and the Straight (stepped or sloped) downcomers is shown in figure 7.1a below. The contact between the downcomer and the column wall is tangential. The shape of the bottom of the downcomer is circular (elliptical in this work). The clearance between the tray floor and the downcomer was set to a height of 15mm. An even distribution of the liquid momentum flux is expected from the downcomer. Since the test tray was the top tray in this simulation column the cylindrical shape of the top of the Stepflow downcomer used in this work was thought to have little relevance to the distribution from thereof. The Stepflow Downcomer is illustrated in figure 7.1b.

7.2 Modification Involving A Uniform Gap Under the Weir.

A tray arrangement which includes a uniform gap under the outlet weir is an imperative from the suggestion by Sohlo et al., Bell and, Kafarov et al. that the source of the nonuniformities may be traced to the outlet weir. The nonuniformities are seen as evidence of the reaction of the outlet weir to the impact of the liquid flowing from the tray onto the outlet downcomer. The flow nonuniformities are thought to develop upstream from the weir with the severest nonuniformities supposedly showing up nearest to their source.

If the weir reaction theory is true then it can be expected that the presence of a uniform gap between the weir and the tray floor will minimise the nonuniformities. The presence of the gap also

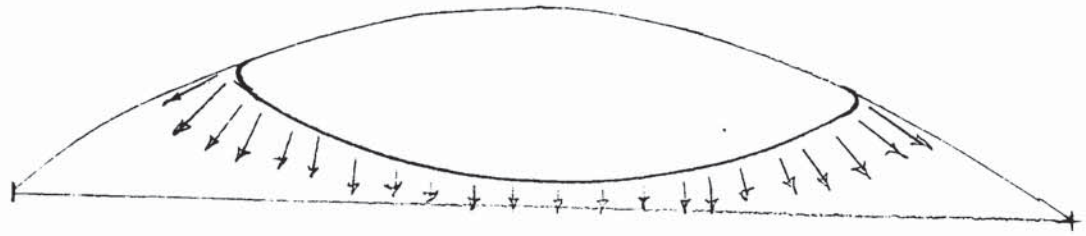

a. The expected Distribution Pattern from a Steplow Downcomer

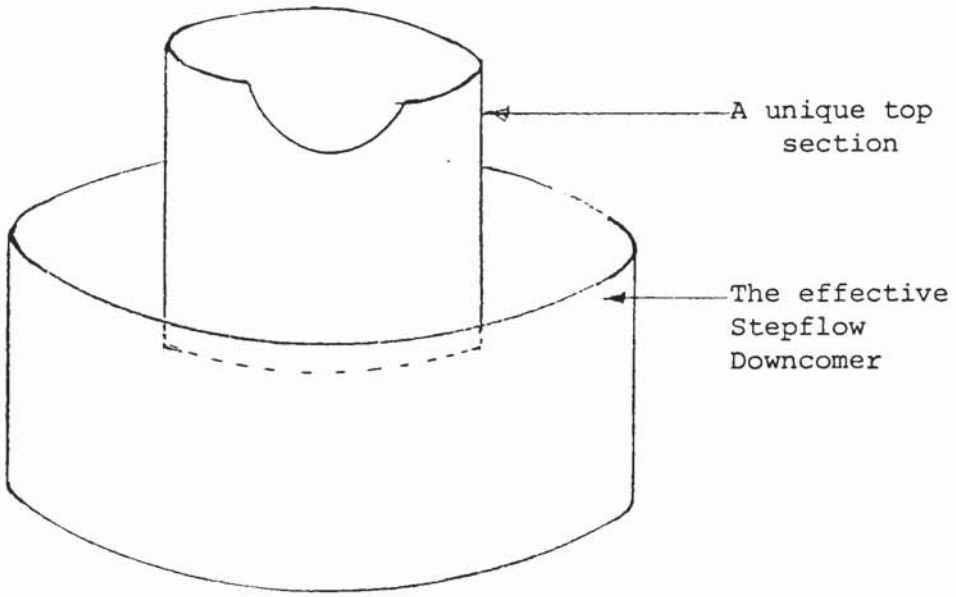

b.The Stepflow Downcomer

FIG:7.1 A schema of the Stepflow Downcomer

means that a "source" and "sink" may coexist in a froth layer at the top and the bottom of the weir respectively. The potential fraction of liquid in the retrograde flow is forced through the gap. A schema for this arrangement is shown in figure 7.2 below.

It is significant to note that no evidence is reported in published literature, where a uniform gap under the outlet weir is used to eliminate nonuniformities on the tray.

7.3 Experimental Program

Water cooling experiments described in Section 6 above were carried out on a standard tray. The experimental conditions were chosen to cover both the Spray and Mixed regimes. The same set of conditions were repeated with the tray arrangement altered to include the uniform gap under the weir and the Stepflow Downcomer separately.

For all the experiments carried out it was assumed that;

i. the distribution of the air entering the tray was even,

ii. the distribution of water inside the inlet downcomer (including the Stepflow Downcomer) remained even throughout an experimental run and that

iii. the test tray was level

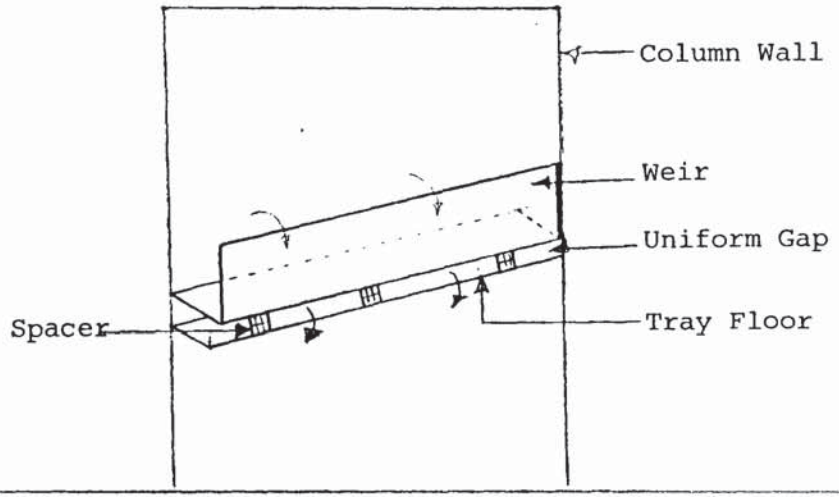

a. An angle View of the Gap Under the Weir
(Arrows indicate flow of Water)

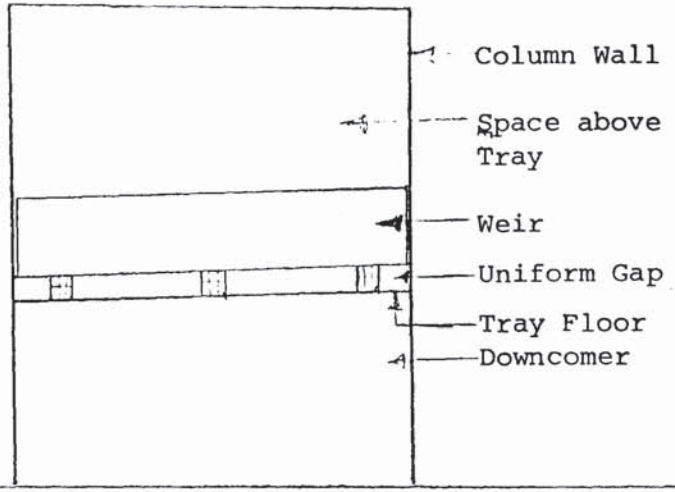

b. A plan of the Gap Under the Weir

FIG:7.2 Gap Under the Weir arrangement in the Column

7.4 Discussion of the Results

It is convenient to discuss the results of the flow patterns obtained here in terms of those found in the standard tray under similar conditions. The temperature profiles compared were derived in conditions within the Spray regime and the Mixed regime only. Two examples of the profiles in each regime are discussed, the rest of the results are given elsewhere in Appendix A.

7.4.1 Results of the Stepflow Downcomer compared to Standard Tray

Channelling of the liquid producing U-shaped profiles were observed late on the tray fitted with the Stepflow Downcomer as shown in figure 7.3b. By comparison, the profiles from the Standard Tray are U-shaped, late on on the tray, these are shown in figure 7.3a. For the second set of conditions shown in figure 7.4, the liquid rate is doubled while the gas rate is held constant. The resulting temperature profiles from the Stepflow Downcomer tray are comparatively more straight than those from the Standard tray. However, the distinction is more obvious in the last half of the tray approaching the outlet weir. Here, the non-uniformities in the Stepflow Downcomer tray are more pronounced and show unusual recirculating patterns in the central part of the tray. This phenomenon is characteristic of the tray sides where the liquid flow rate is expected to be relatively lower than that at the central part. The fact that this appears at the central part as well as on the sides suggests that the expected

redistribution of the liquid momentum flux aimed at straightening the flow all over the tray was achieved.

A similar comparison between the profiles from the two trays can be drawn from the two sets of profiles in the Mixed regime. The channeling of liquid and hence the U-shapes found in the Standard tray are straightened out in the early part of the tray which is fitted with the Stepflow downcomer. However, the nonuniformities formed at the tray sides occur much earlier on on the Steflow tray than on the Standard tray. These are shown in figure 7.5a and figure 7.5b below. As the liquid rate is increased and the gas rate held constant, in figures 7.6a and 7.6b, the similarities between the profiles from the two trays is less clear. U-shaped profiles are recorded on both trays. The tray fitted with the Stepflow downcomer develops U-shapes earlier than the Standard tray. The significance of late or early development of nonuniform profiles was pointed out by Sohlo et al.. The consequence of the nonuniformities on tray efficiency is expected to be less when nonuniformities develop and are restricted to the last part of the tray.

Measured Temperature Profiles on a Sieve Tray

(Temperature °C)

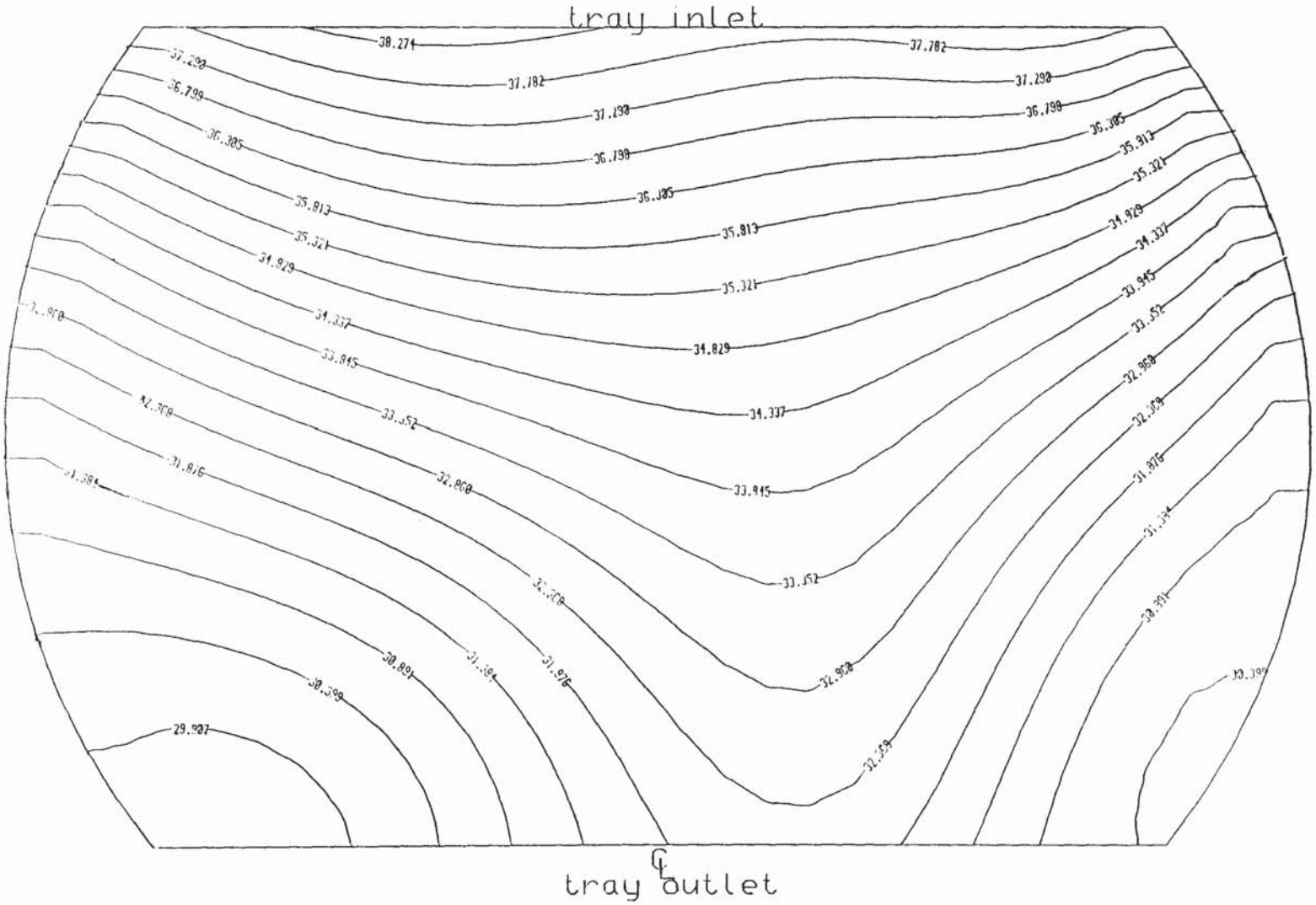

FIG:7·3a Spray Regime

Csb= .0605m/s q/b= .00161m3/sm

STANDARD TRAY

Measured Temperature Profiles on a Sieve Tray

(Temperature °C)

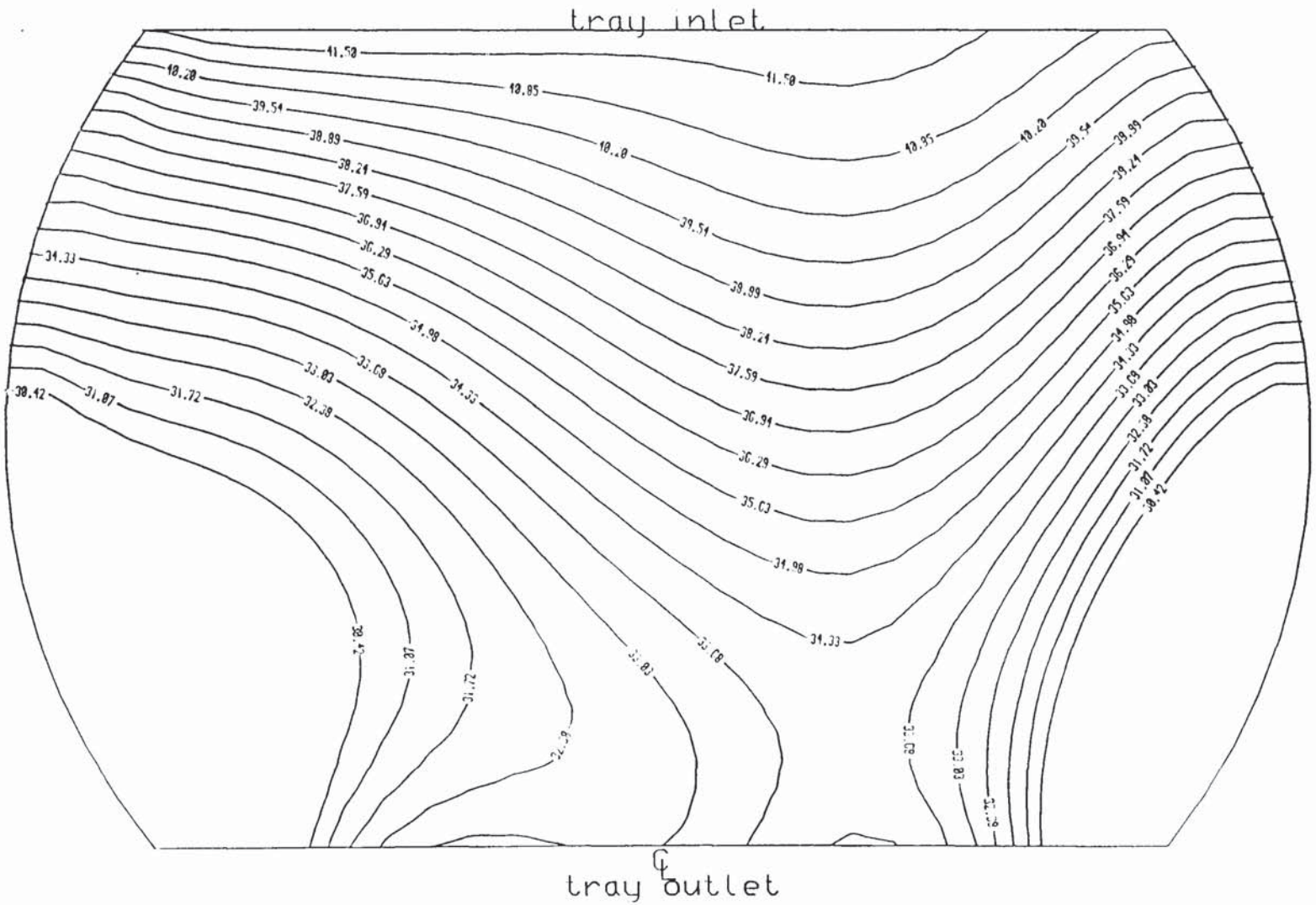

FIG:7·3b Spray Regime

Csb= .0605m/s q/b= .00161m3/sm

STEP FLOW DOWNCOMER

Measured Temperature Profiles on a Sieve Tray

(Temperature °C)

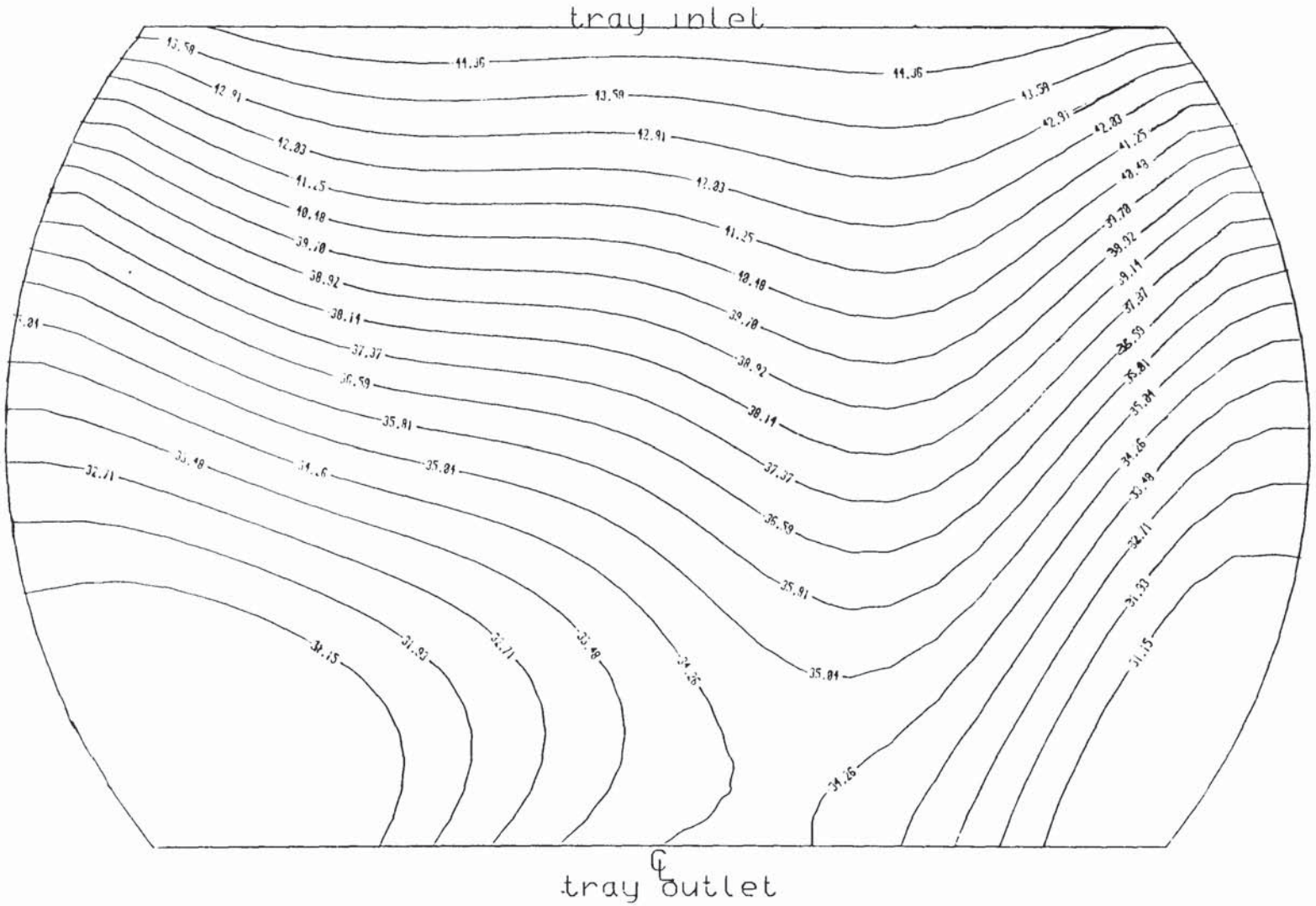

FIG:7·3c Spray Regime

Csb= .0605m/s q/b= .00161m3/sm

MODIFIED TRAY:OUTLET WEIR GAP

Measured Temperature Profiles on a Sieve Tray

(Temperature °C)

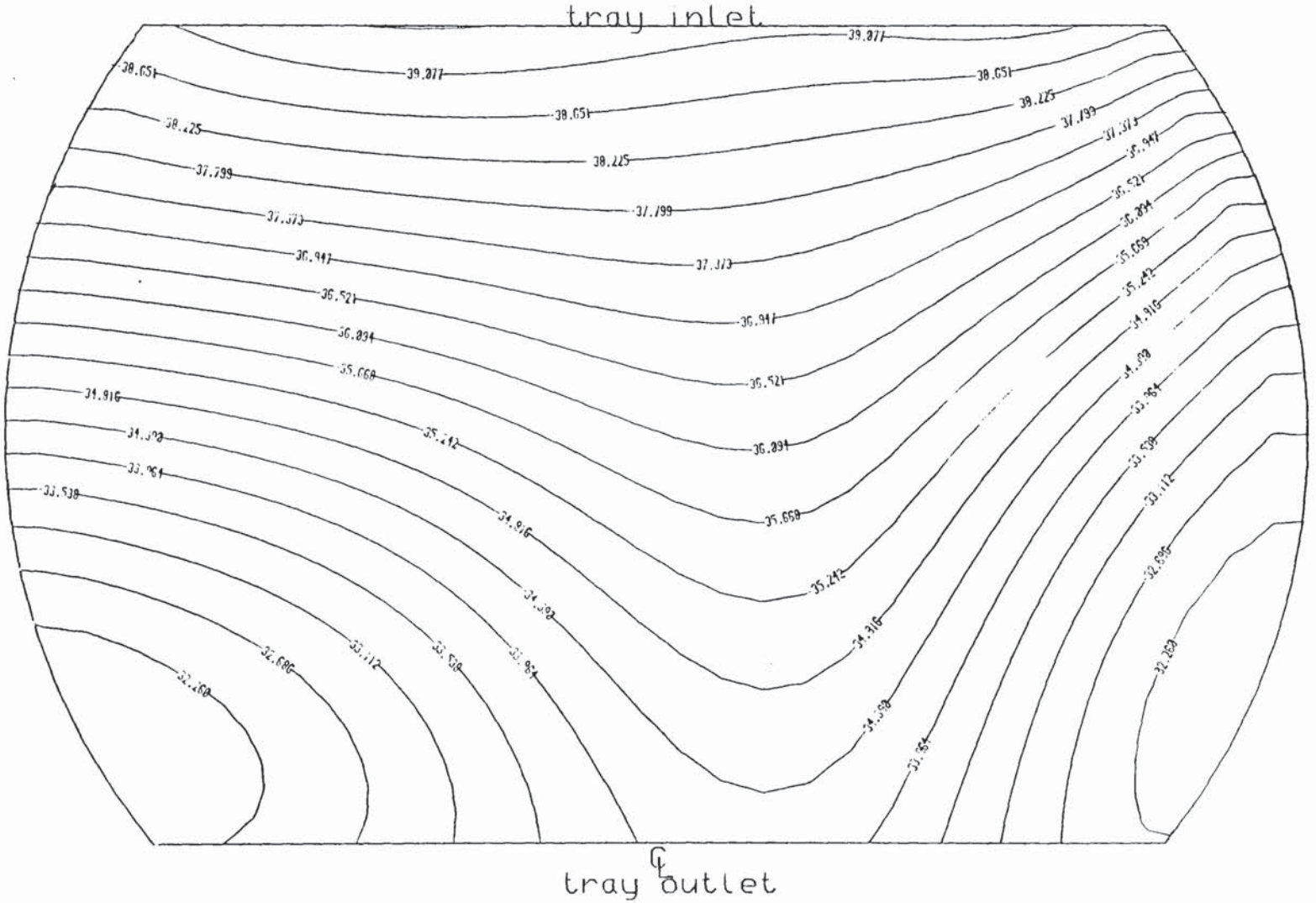

FIG:7·4a Spray Regime
Csb= .0605m/s q/b= .00322m3/sm
STANDARD TRAY

Measured Temperature Profiles on a Sieve Tray

(Temperature °C)

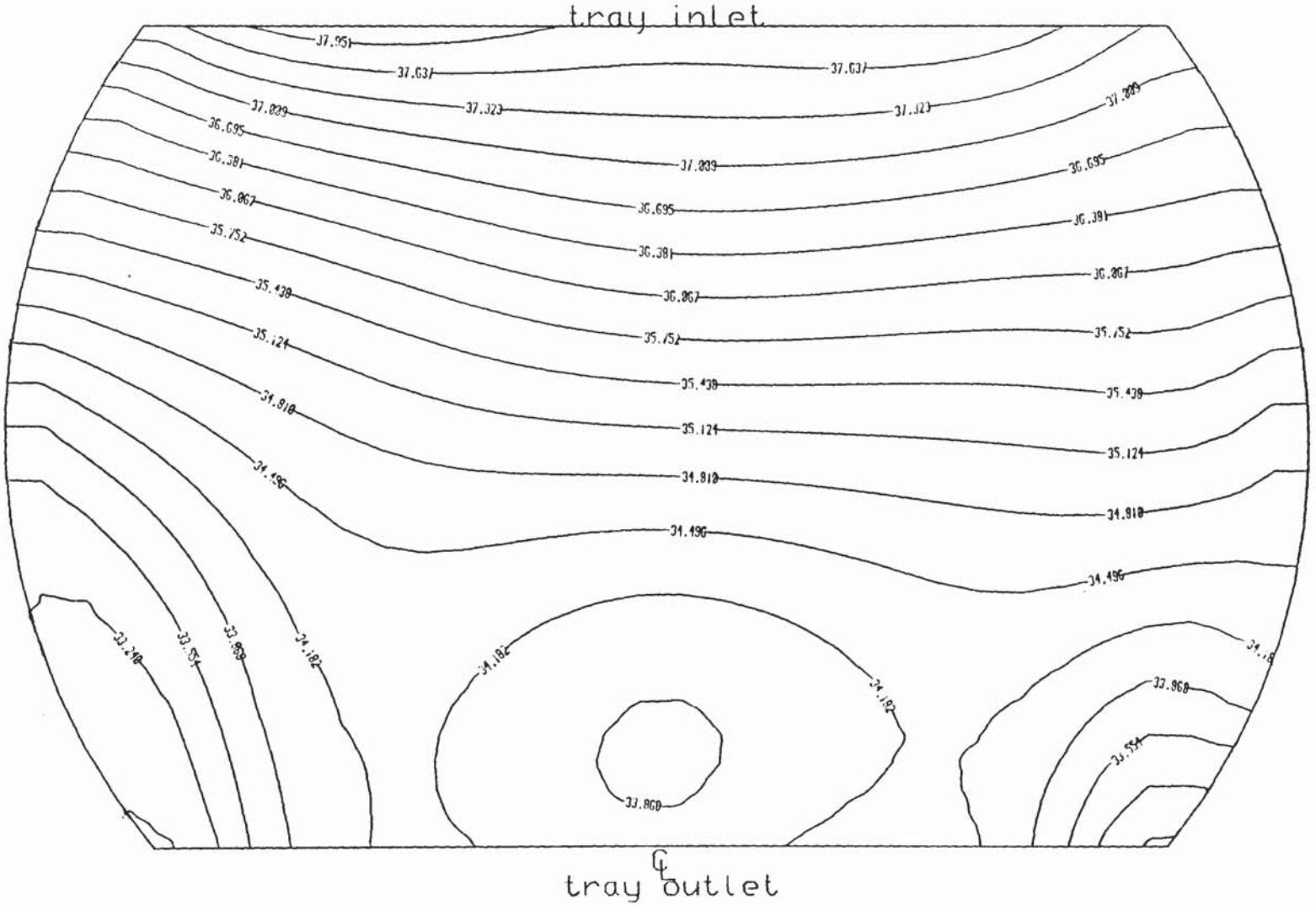

FIG:7·4b Spray Regime
Csb= .0605m/s q/b= .00322m3/sm
STEP FLOW DOWNCOMER

Measured Temperature Profiles on a Sieve Tray

(Temperature °C)

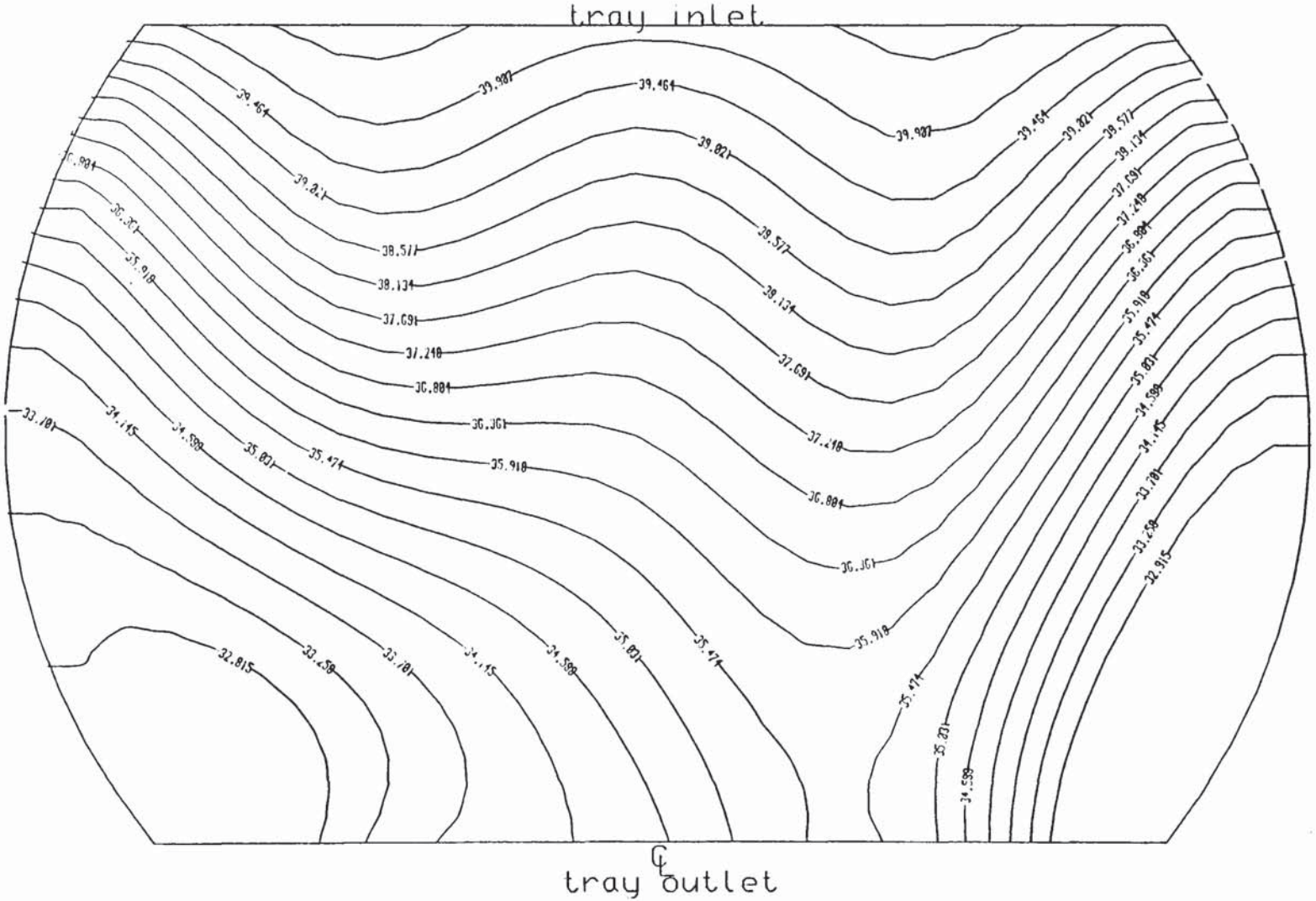

FIG:7.4c Spray Regime

Csb= .0605m/s q/b= .00322m3/sm

MODIFIED TRAY:OUTLET WEIR GAP

Measured Temperature Profiles on a Sieve Tray

(Temperature °C)

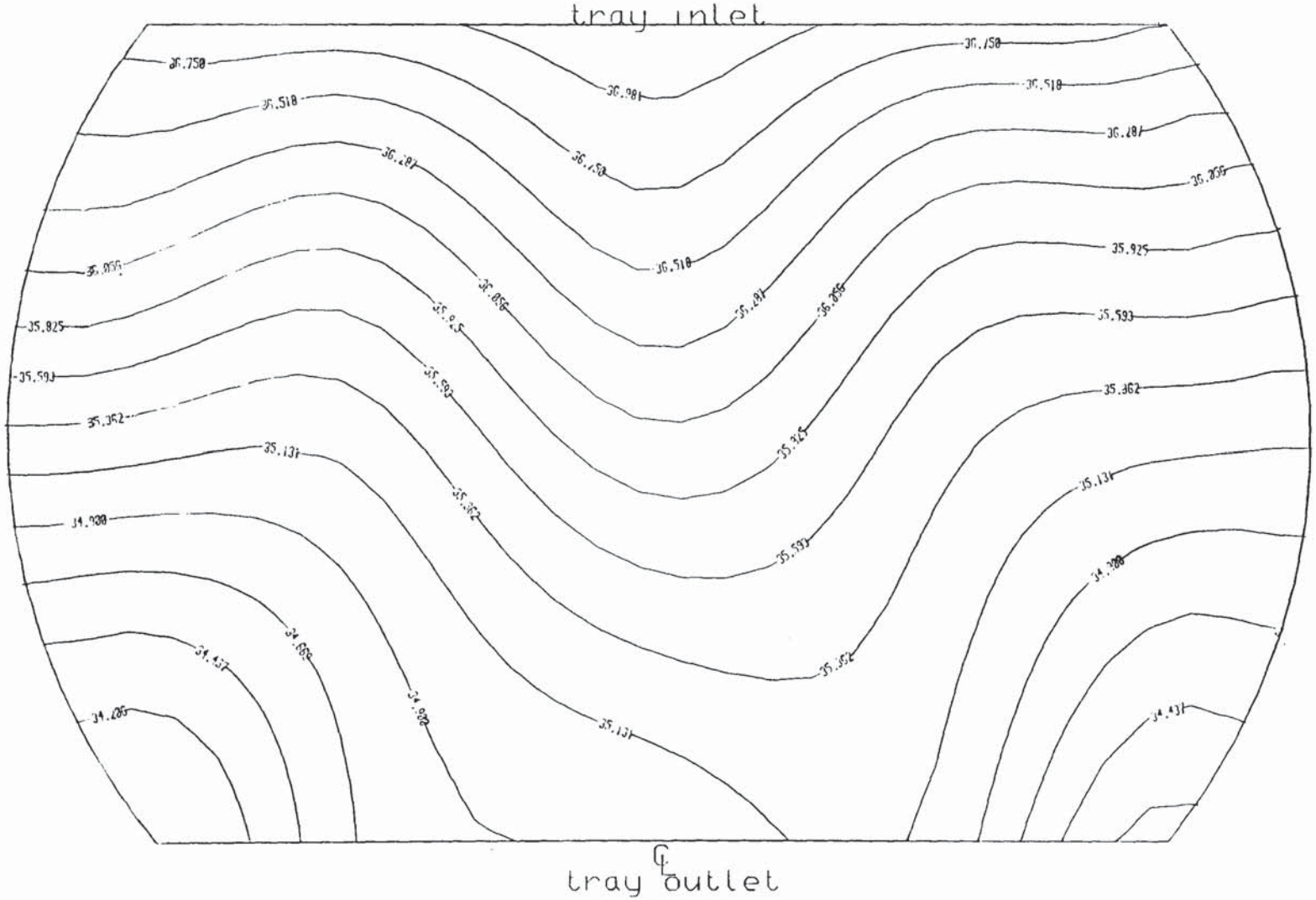

FIG 7.5a Mixed Regime
Csb= .0775m/s q/b= .00967m3/sm
STANDARD TRAY

Measured Temperature Profiles on a Sieve Tray

(Temperature °C)

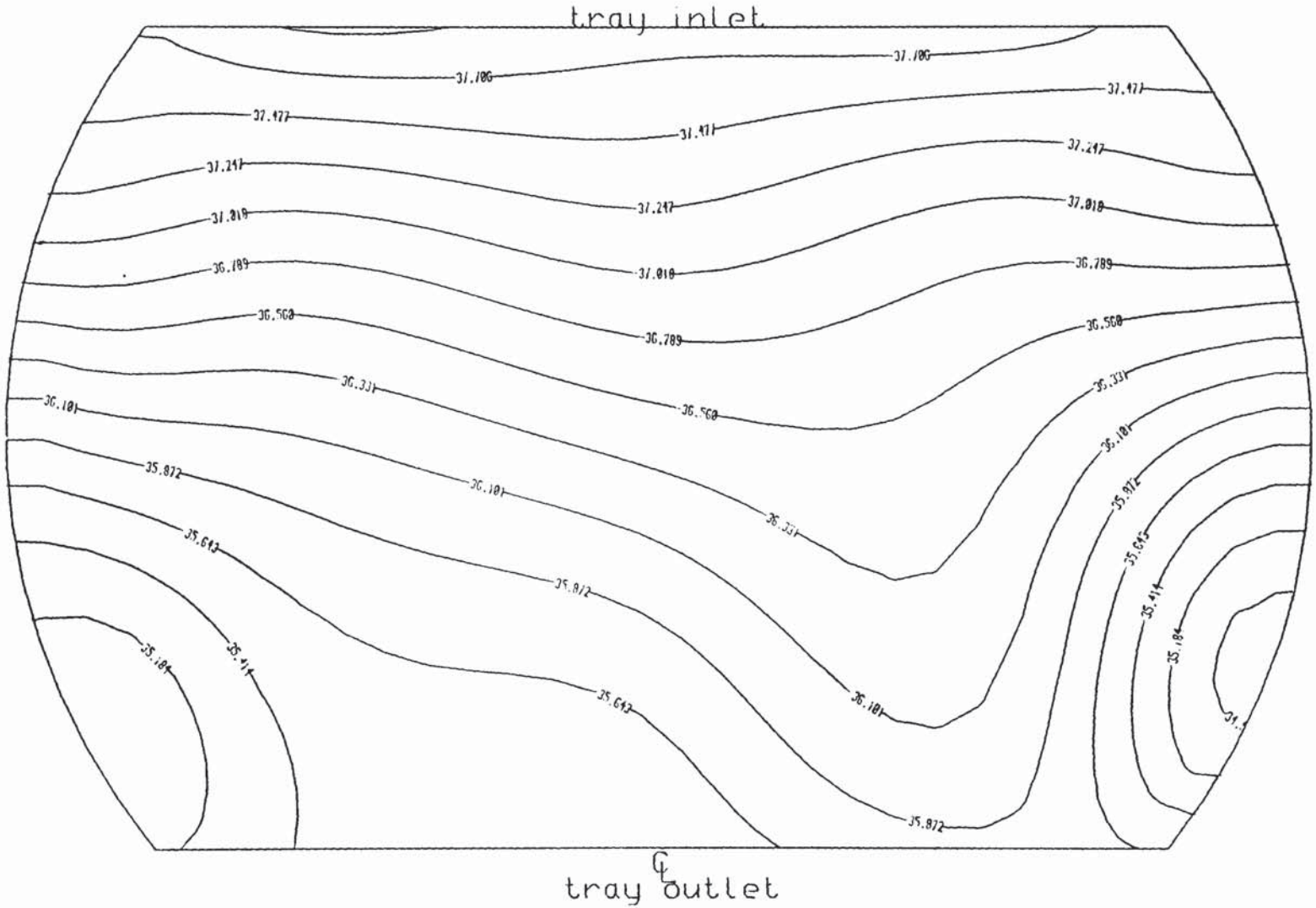

FIG:75b Mixed Regime

Csb= .0775m/s q/b= .00967m3/sm

STEP FLOW DOWNCOMER

Measured Temperature Profiles on a Sieve Tray

(Temperature °C)

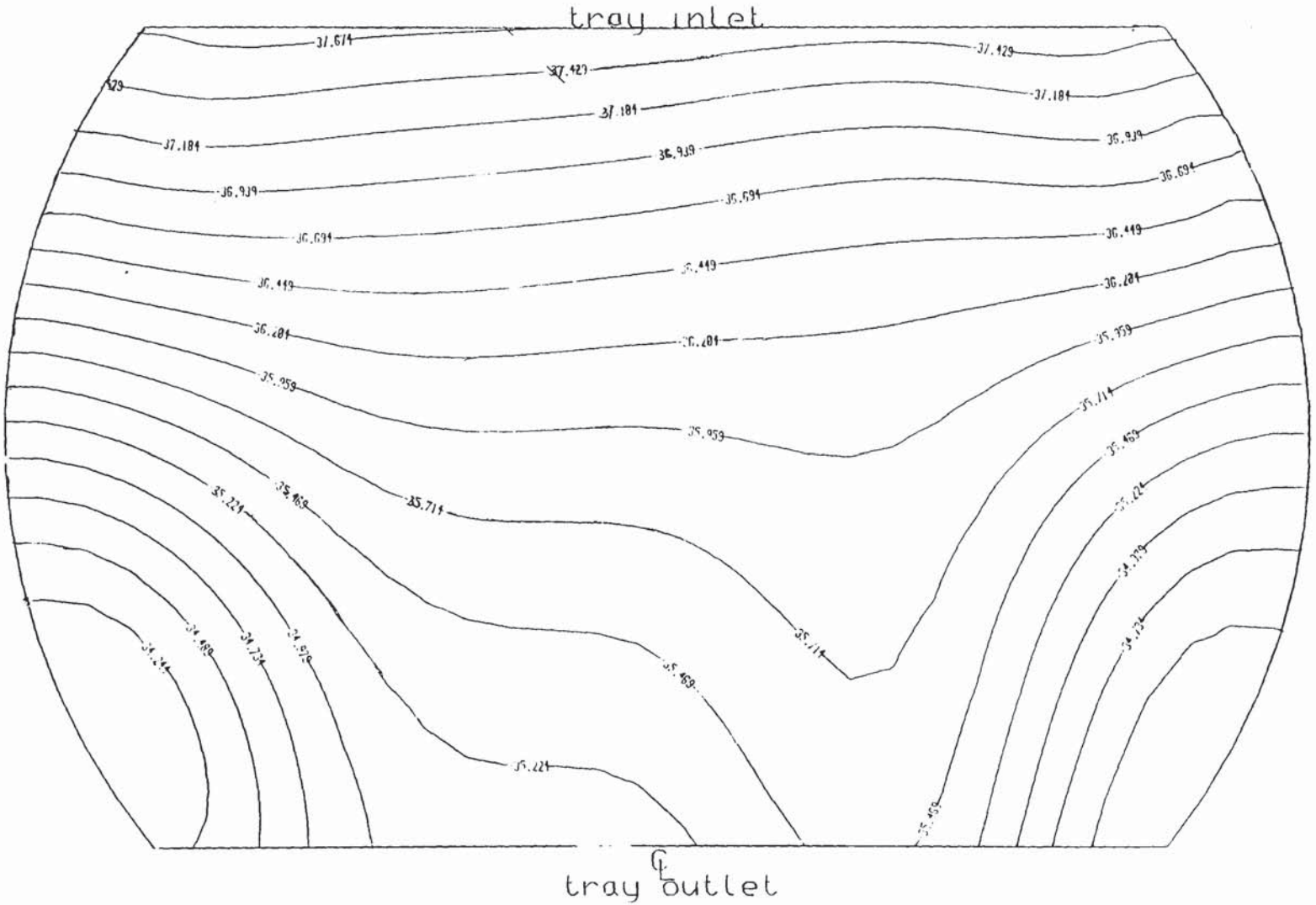

FIG:7-6c Mixed Regime

Csb= .0775m/s q/b= .00967m3/sm

MODIFIED TRAY:OUTLET WEIR GAP

Measured Temperature Profiles on a Sieve Tray

(Temperature °C)

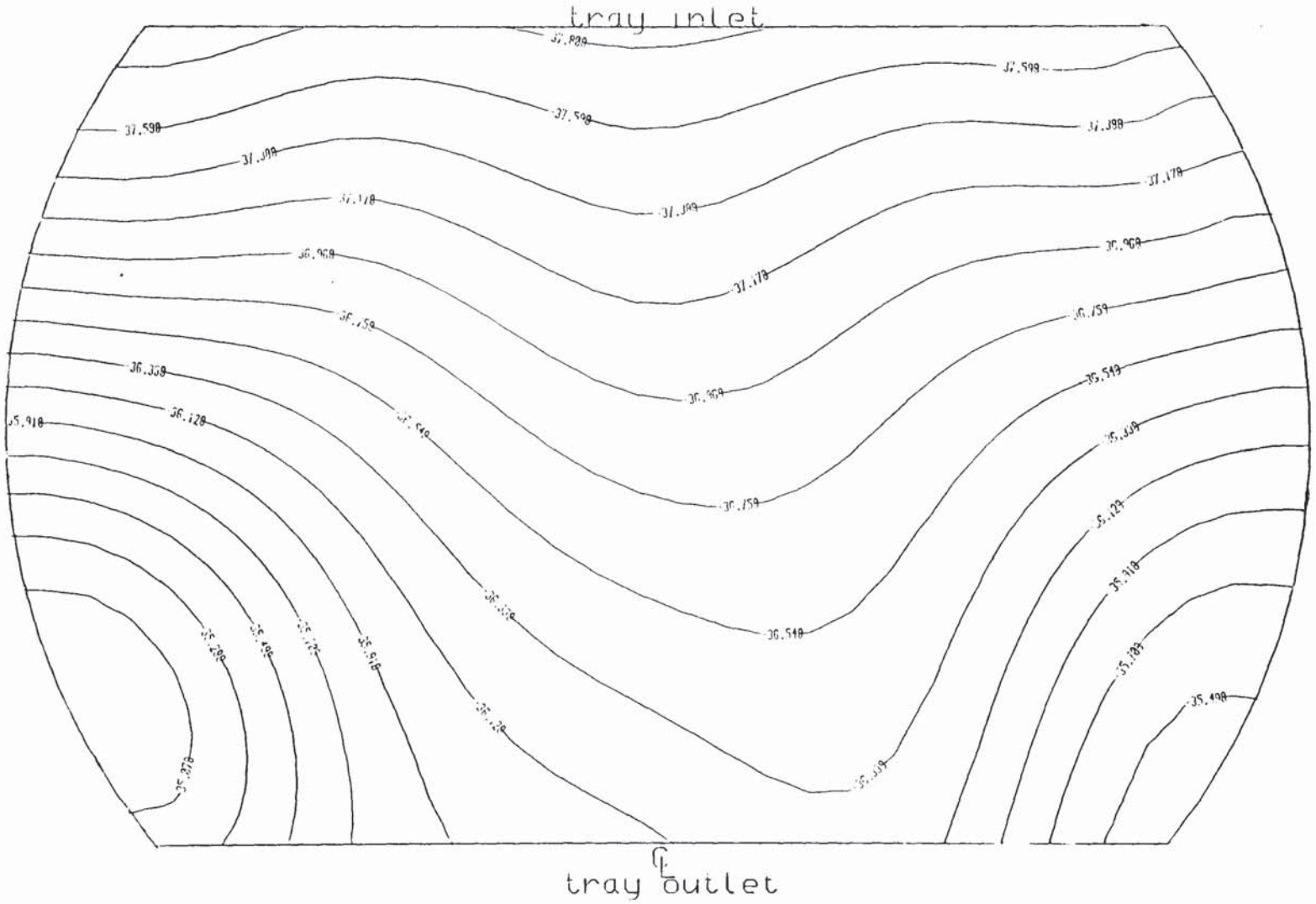

FIG 7.6a Mixed Regime

Csb= .0755m/s q/b= .01169m3/sm

STANDARD TRAY

Measured Temperature Profiles on a Sieve Tray

(Temperature °C)

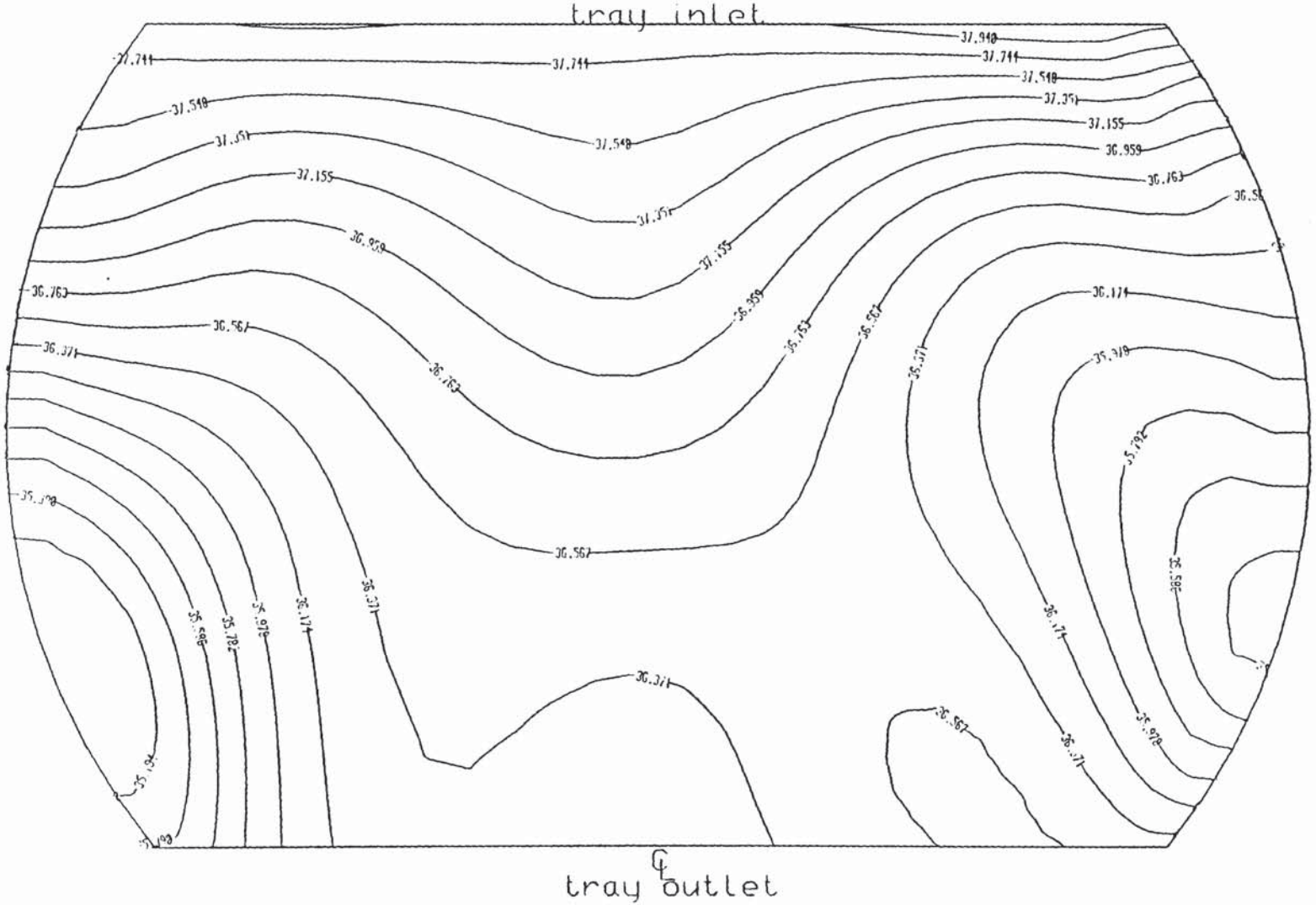

FIG:7.6b Mixed Regime

Csb= .0775m/s q/b= .01169m3/sm

STEP FLOW DOWNCOMER

Measured Temperature Profiles on a Sieve Tray

(Temperature °C)

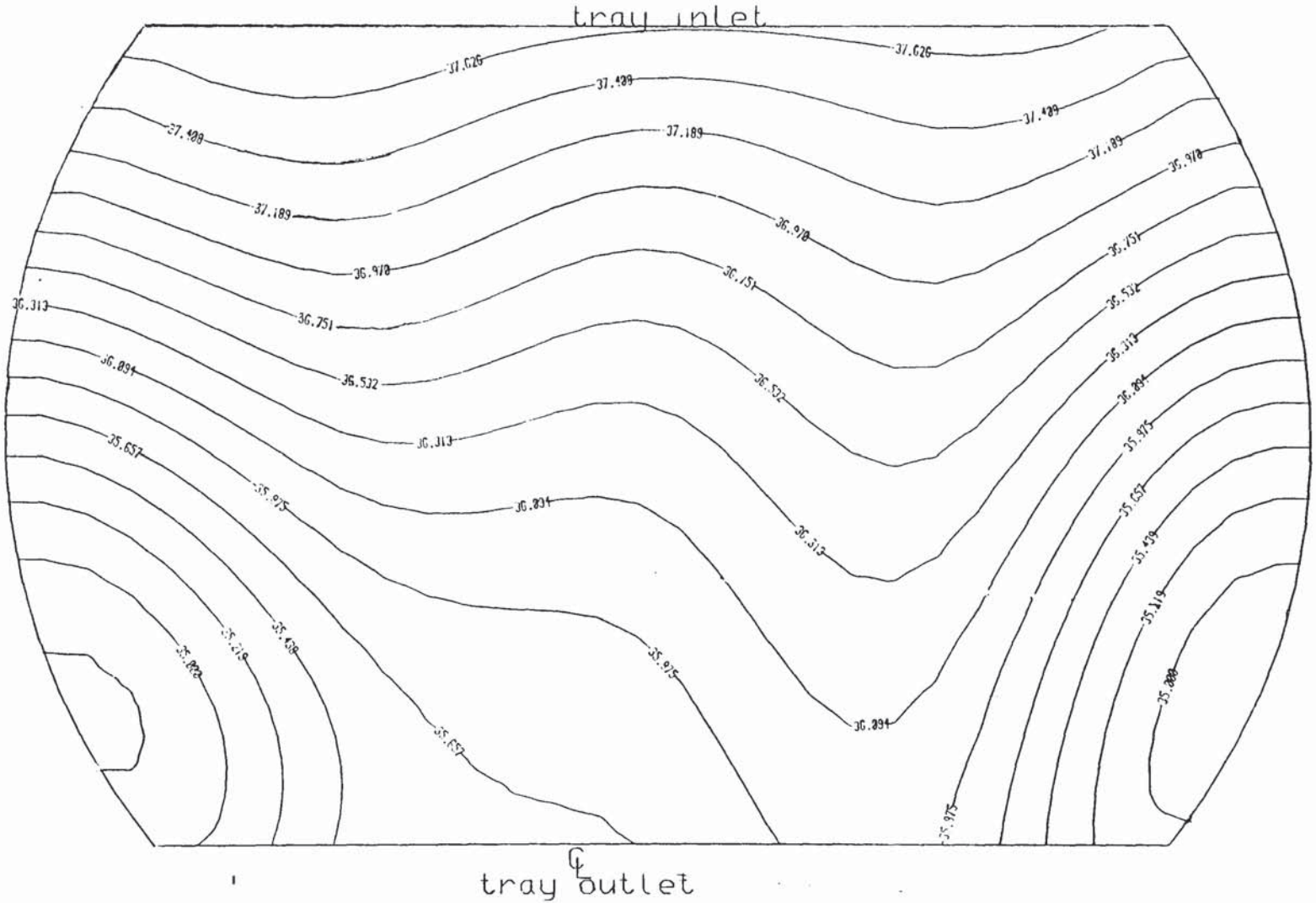

fig: 7·6c : Mixed Regime

Csb= .0775m/s q/b= .01169m3/sm

MODIFIED TRAY: OUTLET WEIR GAP

it is clear that the minor differences between the Stepflow tray and the Standard tray are insufficient to have serious implications on tray efficiency for the size of tray used in this work. Scaling-up larger trays found in industrial practice, these apparently minor effects may be larger and have much bigger influence on the overall flow patterns and thus the tray efficiencies of the trays.

7.4.2 Results of the Gap-Under the Outlet Weir compared to the Standard Tray.

By creating a uniform gap under the outlet weir when the tray is operated under conditions where the liquid momentum remains dominant over the gas momentum, the liquid streams approaching the outlet weir are expected to be channelled through the gap. If this happens then only a limited amount of mixing will occur with the liquid in the direction transverse to the flow axis. The temperature profiles would then be expected to be uniform. Some of these effects were observed on this tray, but particularly under conditions of low liquid rates.

At the low liquid rates in the Spray regime the temperature profiles from the modified tray are shown in figure 7.3C. These are similar to those obtained from the Standard tray, shown in figure 7.3a. The first half of the tray is dominated by straight profiles but the profiles in the second half of the tray change into U-shapes. As the liquid rate is increased, the temperature profiles shown in figure 7.4c and figure 7.4a are less similar.

The U-shapes obtained from the modified tray start early on on the tray and dip sharply on approach to the outlet weir. Although some cold regions at the tray sides could be found, the presence of the sharp profiles peculiar to the modified tray suggest that the "gap" is responsible for this. The "gap" may even reduce any variation in the flow of liquid per unit width of weir as the liquid leaves the tray, but the results from here are insufficient to deduce this.

As the liquid rate is increased further and the tray operated in the Mixed regime the general shapes of the temperature profiles do not show any detectable differences between the two trays. The profiles shown in figure 7.5a and figure 7.5c are similar. It is inferred that in this size of tray, the effects of this modification are too minor to draw any conclusions from them.

7.5 Conclusion

The main thrust of the experiments here is that for the first time a system s property has been measured on trays fitted with flow control devices. All previous studies have been based on visual observations and photographs of dye movements. With regards to the expected changes in flow patterns due to the flow control devices it is clear that the results were inconclusive.

Only minor differences could be seen between the temperature profiles of the Standard tray and the trays fitted with flow straightening devices in this work.

The U-shapes picked in Intense Spray were also found in the tray fitted with the Stepflow Downcomer even where they did not show up in the Standard tray. The presence of nonuniform and recirculating flow patterns across the Stepflow Downcomer tray at a zone parallel to the weir is interesting. This is not seen with the Standard tray. It suggests that some flow control may have been obtained with the Stepflow tray although ironically, at low liquid rates. As the liquid rates are increased to the Mixed regime the flow patterns from both trays become similar. The use of the Stepflow downcomer to straighten flow cannot be expected to yeild significant benefits on trays of this size. This is somewhat confirmed in this work. However, further confirmation is given to the viability of this technique to investigate the expected effects of flow straighteners on flow patterns. Applied to larger trays more firm conclusions may be arrived at.

The changes to the liquid flow patterns on a tray in which a uniform gap is created under the weir are limited to the regions of the tray which are near the outlet weir and also to conditions of low liquid rates. This leads one to believe the notion that in an operating tray there forms an accumulation of liquid at the outlet weir whose existence influences the mechanism of flow of liquid over the weir. At the relatively high liquid rates of the Mixed regime the flow patterns on both the Standard tray and the tray with the uniform gap under the weir are similar. This suggests that any accumulation of liquid at the outlet weir and / or its effects on the flow patterns is insignificant at high weir loads. The conclusion that can be drawn here is that larger trays

and possibly different tray designs would be required to observe, if any, real changes occur in the flow patterns of trays fitted with flow straightening devices. This follows from the observations made in this work that the shapes of the temperature profiles found in the standard tray were also evident on trays fitted with these devices.

8. EXPERIMENTAL DETERMINATION OF EFFICIENCIES

The new calculation methods for point and tray efficiencies described in the Section 5 and Section 6, were implemented using the temperature measurements on the tray. A comparison was made between theoretical estimates of the efficiencies and those found by the method of water cooling. The effects of the variable . = mG/L on efficiencies for water cooling was investigated. Some FRI systems were simulated and the efficiencies compared with those disclosed in the FRI data [103].

8.1 Choice of Experimental Flow Rates

The flow rates were chosen for a large number of conditions in the Spray and Mixed regimes. This was done to investigate whether the expected differences exist between the efficiencies due to the flow regimes. Further experiments were carried out to simulate certain FRI conditions disclosed in the data. The choice of FRI systems simulated was limited by the following: i. conditions above the weeping limit for air-water and ii. to enable comparisons to be made between the tray efficiencies for water cooling and those of the FRI whose efficiencies were estimated. These meant that only three systems were simulated. They include the 27.6kPa (0.27bars), 34.5kPa (0.35bars) and the 165kPa (1.65bars) cyclohexane-normal heptane. Other FRI systems in the data are provided in reference [103].

8.2 Tray Efficiencies in Spray and Mixed Regimes

In Table 8.1 the tray efficiencies and related variables are listed for conditions of both the Spray and Mixed regimes. Theoretical tray efficiencies calculated by the methods of AIChE and ideal plug flow, are also listed in the Table. Again for these theoretical estimates use was made of the point efficiencies and the parameters measured in this work.

The tray efficiencies are between 60.0% and 125.0%. Higher tray efficiencies are reported in literature. Reference to the Table shows that in general the tray efficiencies are lower in the Mixed regime than they are in the Spray regime. This observation is contrary to those found for mass transfer operations. In mass transfer operations tray efficiencies are expected to go up with liquid loading. However, as stated earlier mass transfer operations involving distillation are two-filmed control and are thus expected to show a different behaviour from the single (total gas) film control in water cooling. This is explained in the following way.

In the Spray flow regime where the gas momentum is dominant over the liquid momentum coupled with the large 12.7mm (1/2in) hole size tray discrete droplet formation is favoured. It is likely that the structure of Spray in the space above the tray seriously affects the water cooling process and hence the overall efficiency.

Table 8.1 Experimental and Theoretical Efficiencies

Regime	C_{sb} m/s	q/b(m^3/ms)	λ	Pe	$E_{OG,e}$	$E_{MV,e}$	$E_{MV,p}$	$E_{OG,p}$	$E_{OG,P1}$	$E_{MV,P1}$	$E_{MV,1}$
Mixed	0.0605	0.00967	0.2982	24.9	60.9	64.0	62.1	58.6	49.5	66.8	83.8
"	0.0775	0.01169	0.3159	17.0	69.3	75.6	72.0	67.8	56.3	77.4	99.9
"	0.0605	0.00806	0.3577	25.9	56.4	60.7	58.1	54.9	47.4	62.5	75.8
"	0.0915	0.01169	0.3730	12.0	92.5	102.2	107.3	86.6	70.4	110.5	152
"	0.0775	0.00967	0.3819	18.2	68.5	76.5	78.8	67.1	56.8	78.3	98.4
"	0.0605	0.00645	0.4469	23.6	73.8	85.3	87.9	72.3	61.7	87.5	109
"	0.0915	0.00967	0.4508	11.2	98.0	116.2	117.6	93.5	77.1	123.2	166
"	0.0775	0.00806	0.4581	19.7	67.7	74.9	77.9	64.4	55.9	79.4	96.8
"	0.0915	0.00806	0.5410	13.9	90.9	106.3	111.8	84.0	72.4	117.4	148
"	0.0775	0.00645	0.5726	17.8	65.1	77.3	76.8	64.0	57.3	78.9	91.7
"	0.0605	0.00484	0.5956	22.6	65.6	74.8	76.8	61.9	55.9	80.3	92.7
Trans	0.0915	0.00645	0.6759	12.2	77.8	97.7	97.2	75.0	68.2	102.3	118
Spray	0.0775	0.00484	0.7630	12.2	68.4	82.3	88.2	63.9	60.1	89.8	98.2
"	0.0605	0.00322	0.8953	19.2	66.8	80.3	88.2	60.5	58.9	91.4	95.0
"	0.0915	0.00484	0.9009	10.9	82.1	103.7	110.8	73.3	71.2	109.4	127
"	0.0775	0.00322	1.1468	8.4	72.8	94.2	103.4	63.9	66.4	113.8	107
"	0.0915	0.00322	1.3541	9.3	79.0	107.8	124.1	66.5	73.2	141.5	120
"	0.0605	0.00161	1.7904	15.4	46.7	60.1	69.1	40.8	47.1	73.0	59.5
"	0.0775	0.00161	2.2933	5.7	64.8	96.4	96.5	50.9	67.5	149.0	91.1

Entrainment which is expected under these conditions and which has a deleterious effect on efficiency is not present on this single test tray. All this suggests that the importance of gas residence time on efficiency for water cooling is a lot more than it may be for mass transfer. This phenomenon is probably responsible for the trend between efficiency and gas loading being opposite to the established theories which are based on mass transfer.

A further comparison between the calculated tray efficiencies and those determined from this work proves the point that, although the Simple Backmixing concept oversimplifies the flow patterns in general this effect is minimal on trays of this size.

8.3 Tray Efficiencies for Simulated FRI Systems

Estimates of the tray efficiencies for the simulated FRI systems are listed in Table 8.3 below. Of the three systems simulated the 27.6kPa and 34.5kPa cyclohexane/n-heptane corresponds to the Spray regime while at 165kPa the conditions are those of the Mixed regime.

Table 8.3 Simulated FRI Tray Efficiencies

Distillation Mixture : Cyclohexane/Normal Heptane

System	C_{sb}(m/s)	q/b(m^3/sm)	E_{MV}	E_{MV}(FRI)
27.6kPa	0.0500	0.00177	85.7	71.3
"	0.0695	0.00242	106.7	80.9
"	0.0960	0.00322	83.1	77.2
34.5kPa	0.0833	0.00242	118.9	75.3
"	0.0670	0.00233	127.0	78.0
"	0.0715	0.00258	122.2	77.9
165kPa	0.0875	0.00645	106.7	97.4
165kPa	0.0975	0.00725	83.1	96.7

The efficiencies are plotted against gas loading in Figure 8.1 below. The trend is the same for both the distillation systems and the simulated systems. Above C_{sb} = 0.07m/s the tray efficiencies decrease after going through a maximum at the lower gas rates. However, the discrepancies is as high as 52%, being higher from this work than the distillation systems. Further, the reported FRI efficiencies show a definite increase with the liquid flow rate for the two systems at 34.5kPa and 165kPa. This is not observed with the efficiencies from this work.

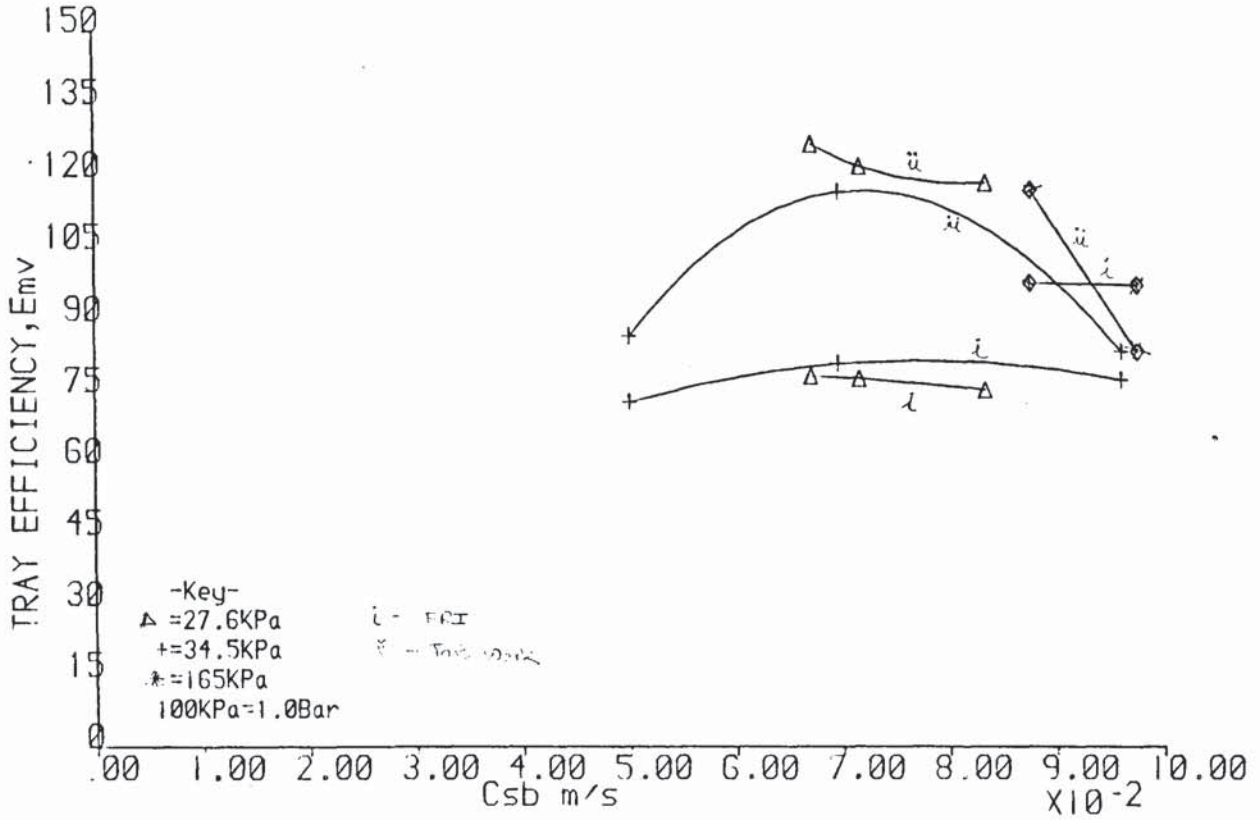

FIG:8.1 TRAY EFFICIENCY COMPARED WITH FRI SYSTEMS

8.4 Expected Point Efficiency from Semi-empirical Correlations

It is reasonable to precede the discussion on experimental point efficiencies, with an analysis of point efficiencies estimated from the principles of heat and mass film transfer coefficients. Semi-empirical relationships that relate efficiency to film coefficients and interfacial area were obtained from literature and applied to the water cooling process. The assumption of gas film control was again made use of. The classic assumption in the theory that the dimensionless group, the Lewis number, is equal to unity is invoked. Thus:

$$\frac{K'_{OG} c_w}{K' c_{pm}} = 1 \qquad 8.1$$

where c_w and c_{pm} are the specific heats of water and moist air respectively expressed in kcal/kg C. K'_{OG} is the overall coefficient of heat transfer, air side (kcal/kg C) and K' is the overall coefficient of mass transfer in the air phase kg/sm^2

Next, use is made of the semi-empirical relationship of Sharma and Gupta [105] for which for air-water systems $K_G = k_G = 0.063$ m/s (assuming gas film control):

note the units ; $K' = k_G \cdot \rho_G$ (kg/m^{2}s)

$= 0.0756$ kg/m^{2}s

From the Lewis equation above, noting that c_w= 1.0 kcal/kg C

$$K_{OG} = K' c_{pm} \qquad 8.2$$

For saturated air c_{pm}= 0.45 kcal/kg C

Therefore K_{OG}= 0.0756 x 0.45

= 0.03402 kcal/kg C

In water cooling processes it may be stated that the number of gas film transfer units:

$$H_{OG} = K_{OG} a' \qquad 8.3$$

from which:

$$E_{OG} = 1 - \exp(-H_{OG}) \qquad 8.4$$

By assuming that $a' = 25\ m^2/m^3$ from reference [105] it is deduced that the point efficiency water cooling is in the region (because of the above assumptions) of 60%. This value is similar to the "mode" of point efficiencies determined in the experiments in this work. The results of the water cooling point efficiencies are discussed in the next subsection.

8.5 Results of Point Efficiencies.

Point efficiencies determined from the water cooling experiments are listed in Table 8.2 below. The table includes values of the essential parameters used to calculate the point efficiency.

Table 8.2 Experimental Point Efficiencies

Regime	C_{sb} m/s	q/b m^3/sm	T_{in} °C	$\bar{T}_{out}$ °C	H_{in} kcal/kg	E_{OG}	λE_{OG}
Spray	0.0640	0.1490	38.30	26.26	12.05	86.6	1.773
"	0.0695	0.1100	40.43	27.59	12.20	64.4	1.770
"	0.0775	0.1610	42.17	29.67	12.03	65.5	1.502
"	0.0900	0.2500	44.35	31.31	12.42	98.96	1.027
"	0.0660	0.2128	39.32	31.37	10.97	59.70	0.955
"	0.0490	0.2150	40.54	29.90	11.68	81.61	0.886
"	0.0745	0.4260	42.00	31.78	12.06	96.34	0.803
"	0.0560	0.2660	42.20	32.91	11.60	65.57	0.658
Tran.	0.0695	0.4730	42.18	34.76	12.30	70.90	0.496
Mixed	0.0560	0.4260	42.90	35.63	11.32	77.29	0.484
"	0.0560	0.6380	41.30	35.81	12.00	86.90	0.363
"	0.0727	0.9750	37.29	33.71	11.59	80.54	0.286
"	0.0560	0.8510	40.10	36.34	11.86	80.31	0.252
"	0.0745	0.8670	36.96	32.16	10.67	89.11	0.406

A simple plot of point efficiency E_{OG} against the flow ratio number is shown in figure 8.2. Taken as it is the graph is difficult to discern, because the points are scattered and regular patterns are not apparent. For instance, it is unclear why at the flow ratio number $\Psi = 0.053\ m^{-1}$ the disparity between the two point efficiencies E_{OG}= 82.1% for C_{sb}= 0.0915m/s and q/b = 0.484 x $10^{-2}m^3/sm$ and E_{OG}= 66.7% for C_{sb}= 0.0605m/s and q/b = 0.322 x $10^{-2}m^3/sm$ is as large as it is. On the other hand, reference to Ψ= 0.021 m^{-1} where the flow rates were repeated (by coincidence) give two similar point efficiencies at E_{OG}= 64.7% and 65.5%. This confusing set of experimental results leads to further analysis and comparisons of the results with theory.

8.6 Comparisons Between Experimental and Theoretical Efficiencies

The efficiencies determined experimentally as well as those calculated from theoretical models are listed in Table 8.1

Use was made of the E_{OG} determined in this work and calculated from the computer program to calculate the tray efficiencies by the graphical method recommended in reference [1]. The mixing parameter or Peclet number were estimated from the correlations given in the reference. The agreement between tray efficiencies calculated in this way $E_{MV,AIChE}$ and those determined in this work

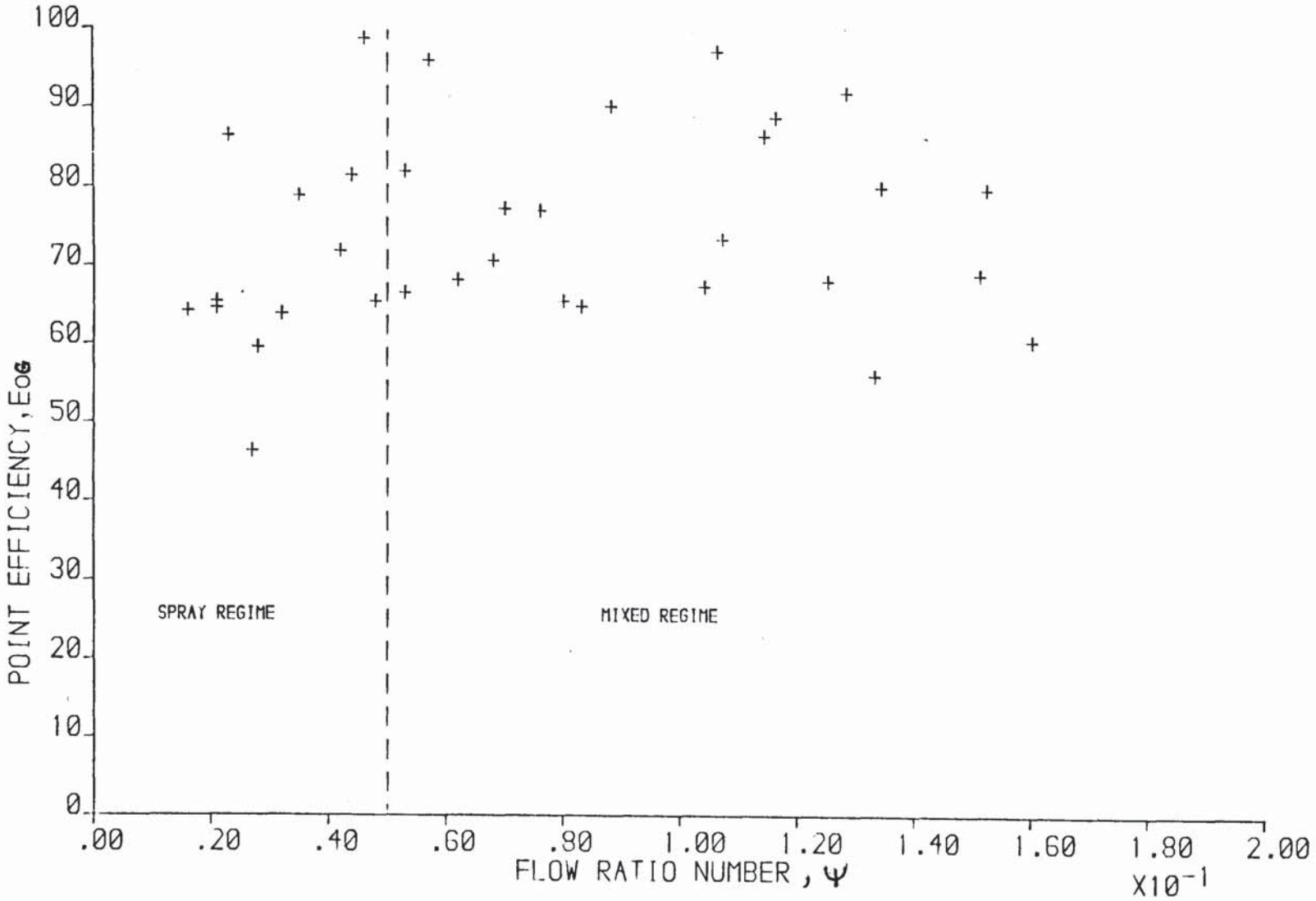

FIG:8.2 POINT EFFICIENCY FOR MIXED & SPRAY SYSTEMS

leads one to conclude that the experimental tray efficiencies are within reasonable limits. Also it shows that the performance of this tray is similar to that of a "Simple Backmixed" tray. It has already been pointed out that inspite of the shapes of the flow patterns which are nonuniform, the effects of such on tray efficiencies is not significant on this size of tray.

There is a remarkable difference between the water cooling operating variables and those for the mass transfer and in particular distillation systems. Unlike in distillation, a particular system in water cooling is defined simply by keeping a constant reflux ratio or L/V and λ would remain fixed. This variable λ occurs as an independent variable in the equations for efficiencies and may therefore have considerable and uncontrolled effects on efficiency for water cooling.

Now, it is difficult to represent the peculiar flow patterns found in this work by a model which would enable the effect of λ on efficiency to be calculated analytically. However, suppose that this effect may be eliminated by a method of calculation or computation. This can best be explained by means of the plug flow model. One might imagine an experimental determination of E_{MV} at some arbitrary value of λ which may be connected to the value of E_{MV} which would have been obtained had λ been equal to unity. That is $E_{MV,\lambda=1}$. The relative changes in efficiencies can be

demonstrated by an approximation using the calculation procedure in the following way:

i. the point efficiency, E_{OG} is calculated as described in subsection 5.4.4 and

ii. tray efficiencies, E_{MV} are calculated for the normal value of and then for $\lambda = 1$.

The variation shown, Table 8.1, between the two values of E_{MV} for each experiment is due to the . effects.

The procedure may be extended to the point efficiency, E_{OG}. The calculation may proceed thus:

i. Starting with an experimental estimate of E_{MV}, calculate the E_{OG} by the plug flow model. One recalls that for plug flow:

$$E_{MV} = \frac{1}{\lambda}(\exp(.E_{OG}) - 1) \qquad 8.5$$

and,

ii. Now assume $\lambda = 1$, that is

$$E_{MV} = \exp(E_{OG}) - 1 \qquad 8.6$$

to calculate E_{OG}.

It is implicit in this procedure that the point efficiency E_{OG} is assumed not to depend on λ which would be true only for a totally gas filmed controlled system. The overall mass transfer unit equations,

$$\frac{1}{N_{OG}} = \frac{1}{N_G} + \frac{\lambda}{N_L} \qquad 8.6$$

For gas filmed controlled systems, $N_L >> N_G$

$N_{OG} = N_G$, therefore independent of λ,

$$N_G = N_{OG} = -\ln(1 - E_{OG}) \qquad 8.7$$

and, $$E_{OG} = \ln(1 + E_{MV}) \text{ for } \lambda = 1 \qquad 8.8$$

In mass transfer this assumption does not hold since $N_G \approx N_L$. There is an interesting inference that may be gleaned from the values of point efficiencies, E_{OG} in the Table, particularly when the values which include the dependence on λ are compared with those calculated for plug flow with $\lambda = 1$. The highest discrepancies, 22% (compared to 10% or less) are shown for the experimental point efficiencies of 90% and above. This discrepancy suggests that for the water cooling process, point efficiencies as high as 90% are outside reasonable limits.

The effects of λ on the efficiencies can be judged from the Table 8.1.

Considering that E_{MV} experimental, was used to calculate the plug flow version of E_{OG} for $\lambda = 1$, it is noted that irrespective of the ratio E_{MV}/E_{OG} experimental, the difference between $E_{OG,pf}$ for $\lambda = 1$ and $E_{OG,exp}$ is of the same order of magnitude and cannot be correlated with the experimental value of $\lambda E_{OG,exp}$ is always greater than $E_{OG,\lambda=1}$ for all $\lambda < 1$ and vice-versa for $\lambda > 1$. The fact that the variations observed are of the same order of magnitude irrespective of changes in λ suggests that the assumption of gas filmed control is a valid one. The consistent discrepancy is a result of the plug flow model employed. This model may be more suitable for high λ or Spray and hence the relatively lower difference between the two point efficiencies.

A similar conclusion may be drawn for tray efficiencies shown in the Table. However, the pattern is different in that,

for $\lambda > 1$, $E_{MV,expt} < E_{MV,pf}$ for $\lambda = 1$

$\lambda < 1$, $E_{MV,expt} > E_{MV,pf}$ for $\lambda = 1$

An attempt has been made to demonstrate the effects . might have on tray efficiencies. Although it is difficult to represent these effects by an adequate model that describes the flow patterns found in this work, nevertheless it is shown by using the ideal plug flow model that λ affects efficiencies in the same way except where the point efficiencies exceed 90%. This suggests that the true point efficiencies are below 90% for water cooling experiments. By its definition, point efficiency cannot exceed 100%.

8.6 Conclusion

Based on existing knowledge efficiencies determined by the water cooling experiments and the calculation methods involving spline approximation are within expected limits. However, point efficiencies as high as 90% and above show unusually large discrepancies once compared with those predicted by established theoretical methods. All values above this range are not reliable.

A comparison between the experimental and theoretical efficiencies using the ideal plug flow model for which total gas film control is assumed (putting $\lambda = 1$, to underline no effect of λ) shows that there is no correlation between changing values of λ and the magnitudes of the difference between the two efficiencies. This leads to the conclusion that the assumption of total gas film control for water cooling is correct.

Now, although certain trends may be detected, nevertheless there is a disappointing scatter in the results of the efficiencies. Thus further experiments and calculations were carried out to explain this.

These include:

i, experiments to measure liquid hold-up at 20 different points on the tray

ii, an analysis of the repeatability of experiments and

iii, an analysis of the effects of measurement errors on the calculations of point and tray efficiencies.

These are described in the next section.

9. BACKGROUND STUDIES ON EFFICIENCY DETERMINATION

It was pointed out in Section 8 that large unexplained differences were found between the trends in the efficiencies determined in this work. The object of this Section is to present further experimental findings relevant to efficiencies, and to explain or trace the source(s) of the discrepancies in both the experimental methods and the calculation procedure used. In the second part of this Section the discrepancies are investigated by using some basic mathematical methods for errors analysis.

Measurements of liquid hold-up on the tray were made in order to examine changes in point efficiency with this parameter; repeated experiments were investigated for reproducibility of liquid flow patterns; and finally, errors analysis on water cooling efficiencies were determined. The results of these studies have far reaching consequences on the viability of this technique for simulating distillation systems.

9.1 Liquid Hold-up Measurements

An assumption made in this and all published calculation methods is that point efficiency is constant everywhere on an operating tray. If this is not so then the calculation methods adopted so far may be inadequate. It is known that point efficiency depends strongly on gas residence time which in turn depends on the liquid hold-up. Thus in these experiments the liquid hold-up was determined from 20 positions on the sieve tray used for this work.

9.1.1 Description of Apparatus for Liquid Hold-up Measurements

20 Stainless Steel tappings were welded flush with the tray floor at the locations displayed in figures 9.1 to 9.3. The tappings were connected through PVC tubings onto separate glass manometer tubes, bore 4mm. The manometers were placed on a wooden board fixed to the laboratory wall at the height of the test tray. A manifold was used to link the glass manometers to the vapour space above the test tray. The PVC tubings were led out of the column through several holes made in the column wall so as to minimise air maldistribution caused by a pack of the tubings. Gaps in the column holes were filled to prevent air from leaking out of the column.

9.1.2 Experimental Procedure

The manometer lines were cleared of air bubbles by purging them with large quantities of water under pressure. The lines were then filled with water the individual static zeros (datum) recorded for each manometer. Passing air through the test tray resulted in a slight drop in the manometer readings from their static zero positions. This later reading was taken preceding every experimental run and recorded as the effective zeros, [26]. Three fixed air rates were chosen corresponding to capacity factors, C_{sb} = 0.0605 (fig.9.1), 0.0775 (fig.9.2), and 0.0915m/s (fig.9.3). Six or Seven different water rates were used for each gas rate.

9.1.3 Experimental Results

The experimental results are displayed in figures 9.1 to 9.3. The average values were calculated by fitting a spline to the hold-up values at the individual measurement points. A Simpson's method [38] was used to integrate over the tray area and the average found by dividing the integral by the tray area. Liquid hold-up correlations in literature are listed in Table 9.1. In Table 9.2 the values resulting from the correlations are given together with the average values found in this work.

LOAD FACTOR C_{sb} = 0.0605m/s

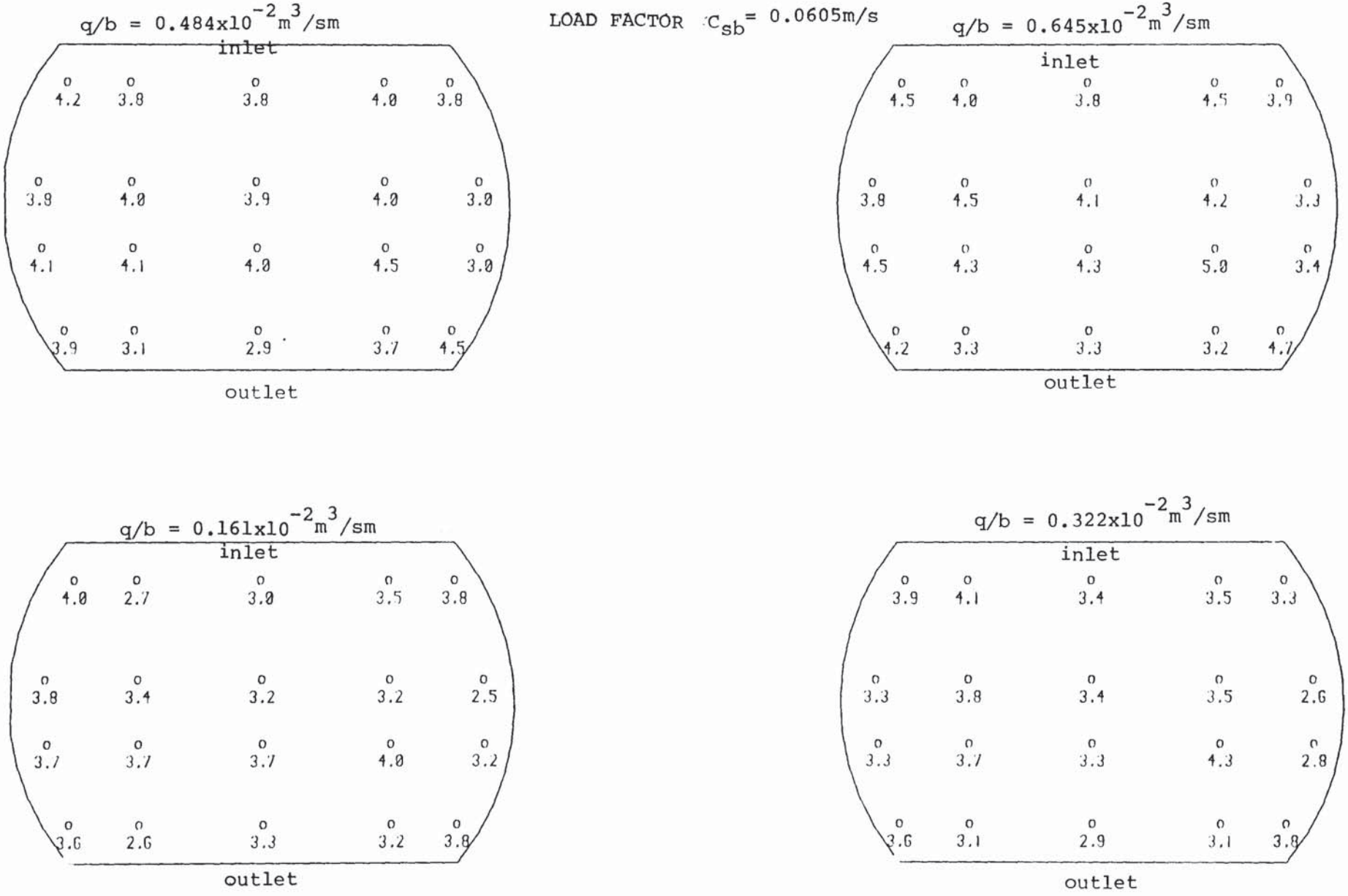

FIG: 9.1 Point measurememnts of liquid holdup on the tray

LOAD FACTOR C_{sb} = 0.0605m/s

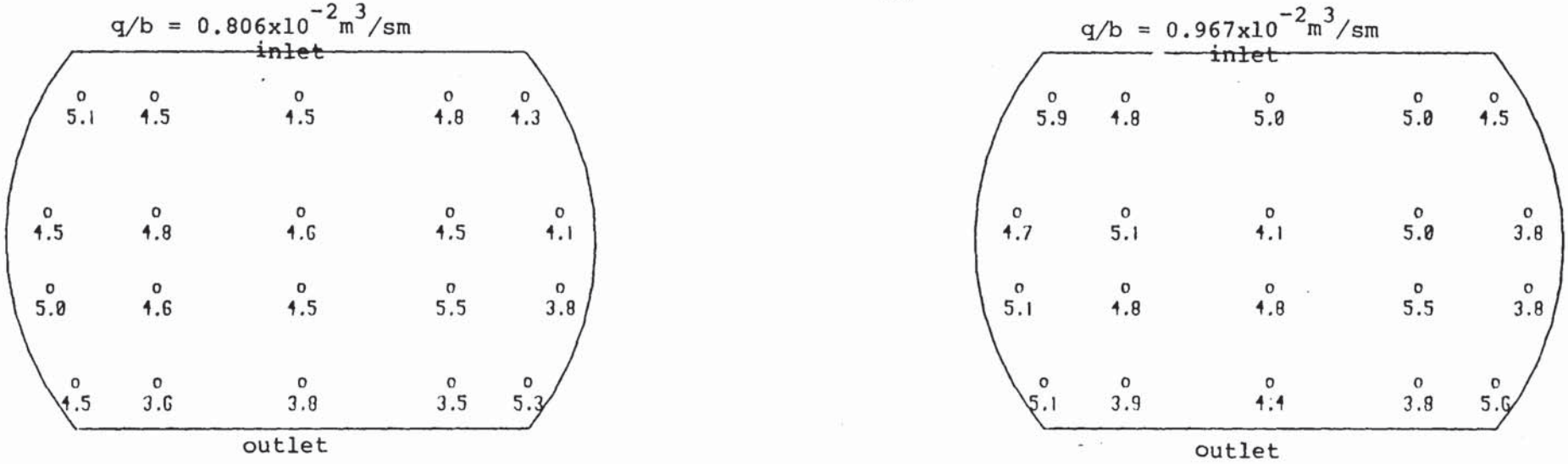

FIG: 9.1 Point Measurements of liquid holdup on the tray

LOAD FACTOR C_{sb} = 0.0775m/s

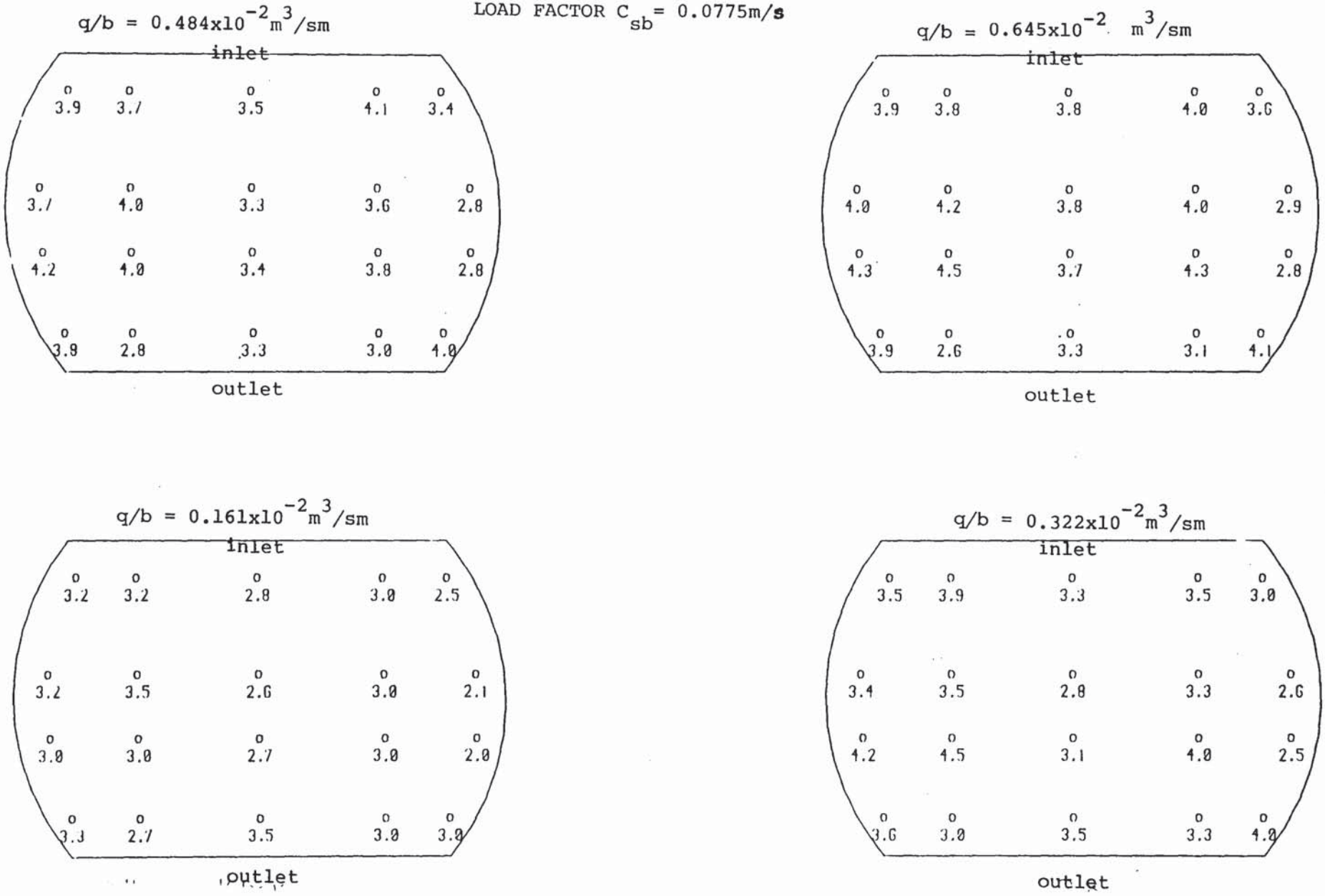

FIG: 9.2 Points measurements of liquid holdup on the tray

LOAD FACTOR C_{sb} = 0.0775m/s

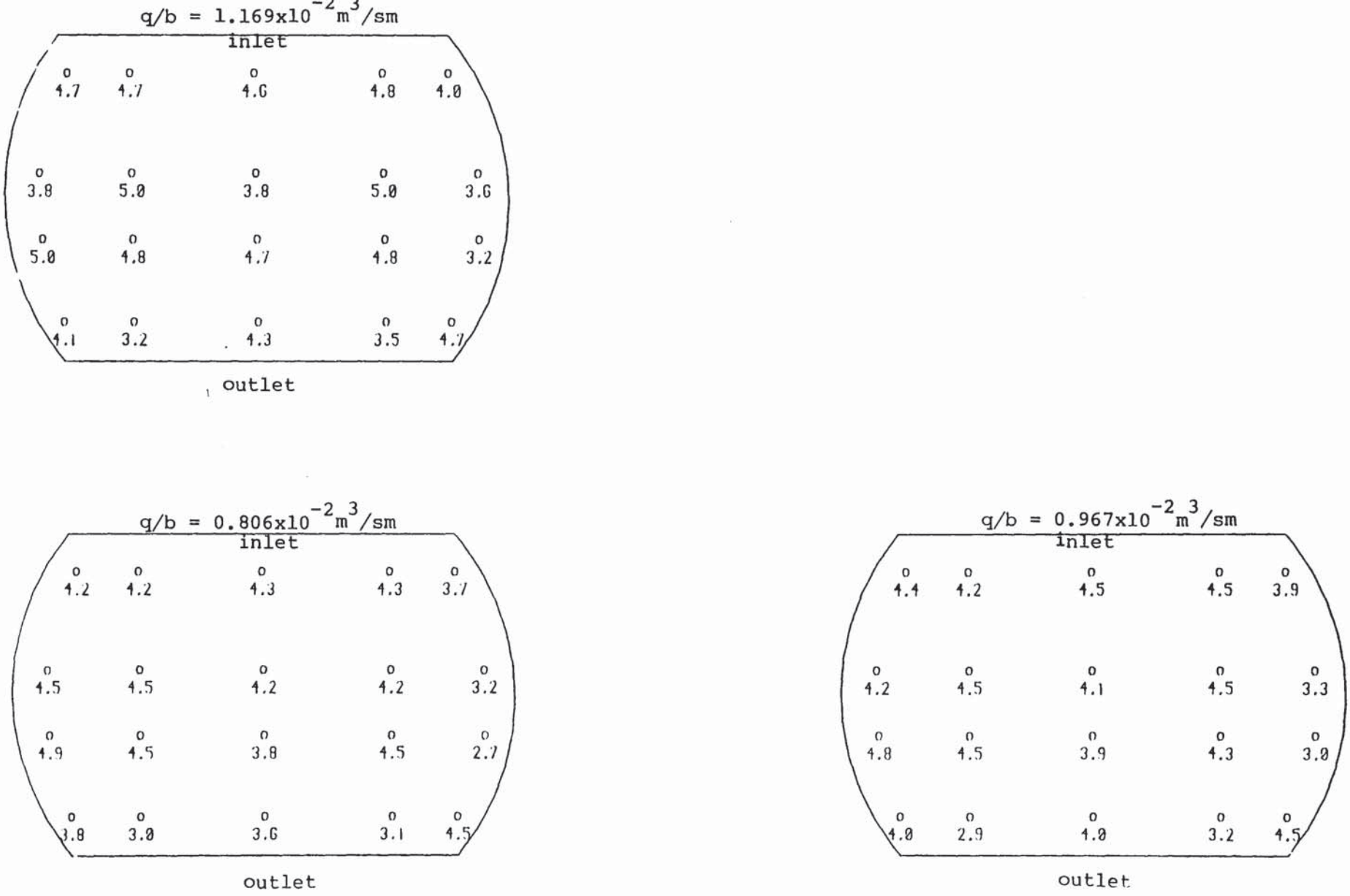

FIG: 9.2 Point measurements of liquid holdup on the tray

LOAD FACTOR C_{sb} = 0.0915m/s

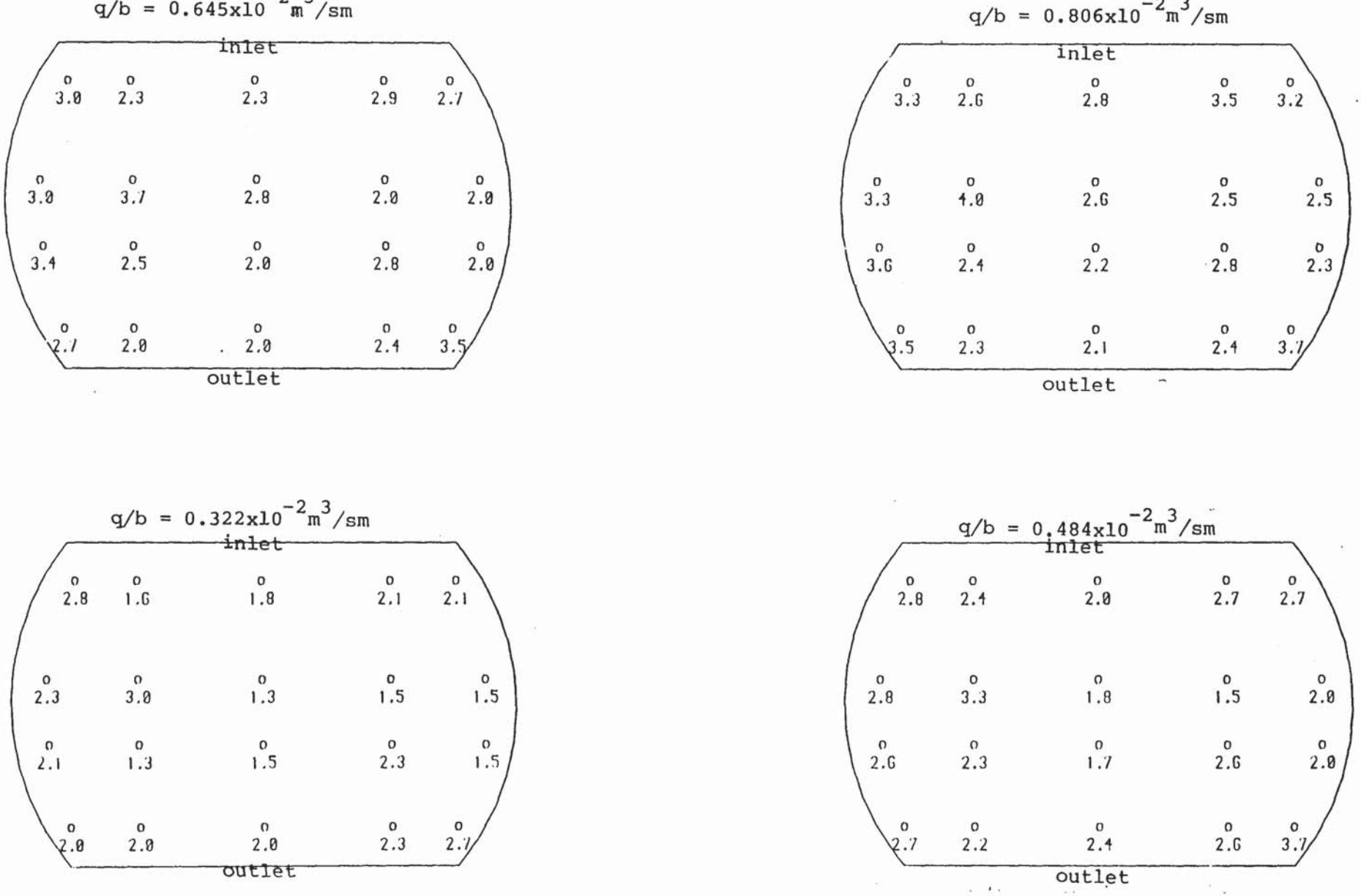

FIG: 9.3 Point mesurements of liquid holdup on the tray

LOAD FACTOR C_{sb} = 0.0915m/s

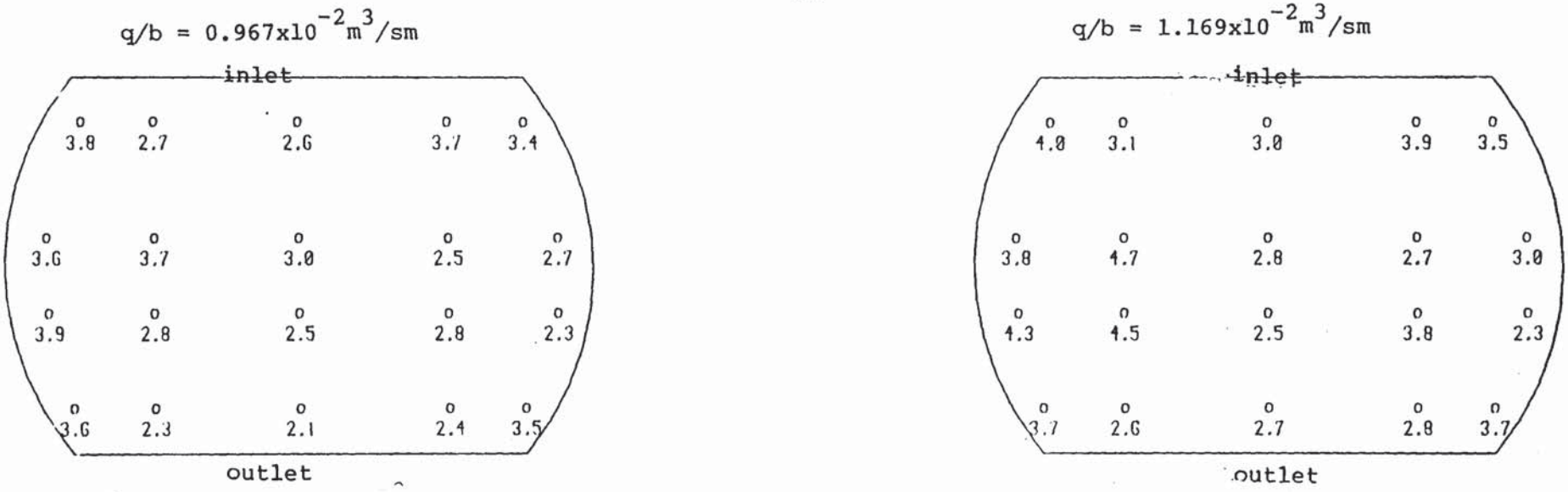

FIG: 9.3 Point measurements of liquid holdup on the tray

9.1.4 Discussion on Liquid hold up Experiments

There is generally good agreement between the correlations in literature and the values determined from this work. It is worth noting that the method adopted by Hofhuis and Zuiderweg [49] involved the integration of the froth density in the tray bed.The froth density having been obtained by the gamma ray absorption technique. The good agreement found here underlines the observations made by Payne and Prince [93] that for clear liquid height the cheap and relatively simple dynamic head measurements also used in this work will suffice.

One of the features of these measurements is the disparity of the values found at the points on the tray. Under low liquid rates $q/b=0.161x10^{-2}m^3/sm$ and $0.322x10^{-2}m^3/sm$ the average hold-up variation between the inlet (first) row and the outlet (last) row is often quite negligible. The point measurements at the tray sides and at the inlet and outlet rows suggest a build up of liquid for most of the flow rates in the experiments. This observation may explain the consistent cold regions found towards the outlet weir and the tray sides in the temperature profiles measurements.

Table 9.1 Some Hold-up Correlations

Author[ref]	Hold-up Correlation	Unit	Equip. Size
Barker and Self [7]	$h_L = 0.24 + 1.74L + 0.0372W - 0.012U_G$ L gal/min.ft of weir, W-in, U_G -ft/s	ft	1.74m x 0.34m
AIChE Bubble Tray Design Manual [1]	$h_L = 1.65 + 0.19W - 0.65F + 0.020L$ L gal/min.ft of weir, W-in, F ft/s $(lb/ft^3)^{0.5}$	in3/in2 bubbling area	-
Hofhuis and Zuiderweg H/Z [49]	$h_L = 0.6W^{0.5}P^{0.25}b^{-0.25}(FP)^{0.25}$ {0.25 < W < 100mm} W - m, P -m, b-m	m	1.0m
Harris and Roper[47]	$h_L = 0.25 + 0.58W + 0.03L - 0.28WF$	in	1ft dia.

Note: "Symbols applied here only"

L - Liquid flow rate over weir

W - weir height

U_G- superficial gas velocity

P - pitch

b - weir length

F - F-factor U_G/ρ_G

FP - flow parameter

There is no obvious correlation between the individual point measurements of liquid hold-up (fig.9.1 to fig.9.3), and the point efficiencies determined in this work and discussed in Section 8.

Table 9.2

Liquid Hold-up from Measurements and Literature Correlations

Source	C_{sb} m/s	h_L (cm) q/b x 10^{-2} m^3/sm						
		0.161	0.322	0.484	0.645	0.806	0.967	1.200
Thesis		3.39	3.45	3.83	4.10	4.49	4.69	
B/S		3.23	3.52	3.80	4.09	4.38	4.66	
AIChE	0.0605	3.54	3.87	4.20	4.86	5.19	5.60	
H/Z		3.03	3.61	3.99	4.28	4.53	4.74	
Thesis		2.88	3.43	3.53	3.83	4.04	4.09	4.40
B/S		2.59	2.88	3.17	3.45	3.74	4.03	4.38
AIChE	0.0775	2.88	3.21	3.54	3.87	4.20	4.53	4.94
H/Z		2.85	3.39	3.76	4.03	4.26	4.47	4.69
Thesis			1.84	2.25	2.52	2.71	2.83	3.36
B/S			2.07	2.36	2.65	2.93	3.22	3.51
AIChE	0.0915		2.66	2.99	3.32	3.65	3.98	4.39
H/Z			3.25	3.60	3.86	4.09	4.27	4.49

9.2 Repeatability of Temperature Measurements

The question whether the experimental measurements of temperatures were reproducible is one that has far reaching consequences to the conclusions that may be drawn from this work. Possible causes for nonreproducibility of the experimental observations are:

i. faulty measurement techniques (devices),

ii. errors in the measurements of individual parameters (use of devices) and

iii. instability in the experiment.

It is the object in this section to investigate causes i. and ii above. The question of instability inherent in the experiments was dealt with in subsection 4.4. It is assumed that all other errors are similar in magnitude for all repeated experiments. The investigation is carried out by repeating a number of experiments over a broad range of flow rates in the Spray regime as well as the Mixed regime. Each experiment was repeated after a time interval (usually up to and beyond 24hrs). The procedure used was the same as that described in subsection 6.1.

9.2.2 Interpretation of the Results.

Since no efforts were made throughout these experiments to adequately control the temperature of the water entering the test tray, this temperature could vary for each experimental run. Further, changes in the wet-bulb temperature and thus the cooling driving force could change from one experiment to another. To overcome this problem the results of the temperature measurements were normalised thus;

A reduced temperature defined as

$$T_r = \frac{t - t_{wb}}{t_{in} - t_{wb}} \qquad 9.1$$

was used. This meant that for the all experiments the reduced temperature at the inlet was automatically set to unity and all temperature measurements represented as a fraction.

A further simplistic approach was used to compare the repeated temperature measurements. In this, the difference between the reduced temperatures at each point on the tray was treated as an independent variable. It is thus implied that the effects of the neighbouring points on the temperatures of any point are the same over a repeated experiment. An analysis of variance is made and is confined to the difference between the reduced temperatures thereby isolating all other possible effects. A statistical test of confidence at 95% confidence level is carried out [116]. The results of the analyses are listed in Table 9.3 below.

Table 9.3 Statistical Errors Analysis

Flow Rates

A : C_{sb} (m/s) B : q/b x 10^2 (m^3/sm)

	(1)	(2)	(3)	(4)	(5)	(6)
A:	0.0635	0.0695	0.0695	0.0695	0.0975	0.0695
B:	0.110	0.161	0.473	0.484	0.742	0.766
$T_{in,i}$ °C	39.89	41.30	41.80	41.20	35.93	37.44
$t_{wb,i}$ °C	20.33	19.69	22.74	23.15	20.02	19.51
$T_{in,f}$ °C	40.57	38.25	42.74	42.74	36.33	38.43
$t_{wb,f}$ °C	20.60	17.11	24.57	24.07	19.96	20.51
T_r °C	±0.0266 ±0.004	±0.0730 ±0.0183	±0.0348 ±0.0047	±0.0276 ±0.0089	±0.0038 ±0.0016	±0.006 ±0.00084
$Var(\Delta T_r)$ $(°C)^2$	0.00205	0.00943	0.00242	0.00452	0.00082	0.00043

Note: subscripts i is initial measurement

ii is repeated measurement

9.2.3 Discussion of the Results

Numbers on the tray locations corresponding to measurements points as shown in figures 9.4 to 9.9. The nomenclature is such that i.the top reduced temperature is due to the initial experimental run, ri and the bottom reduced temperature is due to the repeated experimental run, rf. In the second set of figures, the reduced temperature difference between the initial and final measurements at a point and the variance calculated for that position are displayed. At the top, the value displayed is that of the difference, $T_r = T_{ri} - T_{rf}$.

At the bottom, the value displayed is the variance, $Var(\Delta T_r)$.

A predictable trend may be seen from the reduced temperatures diplayed. First, it is appropriate to allocate the flow regimes to the various conditions of the experiments. Figures 9.4 to 9.6, are for conditions in the Spray regime. Figure 9.7 lies on the transition line while figures 9.8 and 9.9 are in the Mixed regime. A cursory look at the values shows that the maximum drop in the reduced temperatures across the tray occurs in the Spray regime by as much as 50% and is below 30% in the Mixed regime. While this is not meant to reflect reproducibility, the magnitude of the fractional drop is relevant to the magnitudes of the errors incurred.

a) Reduced Temperatures

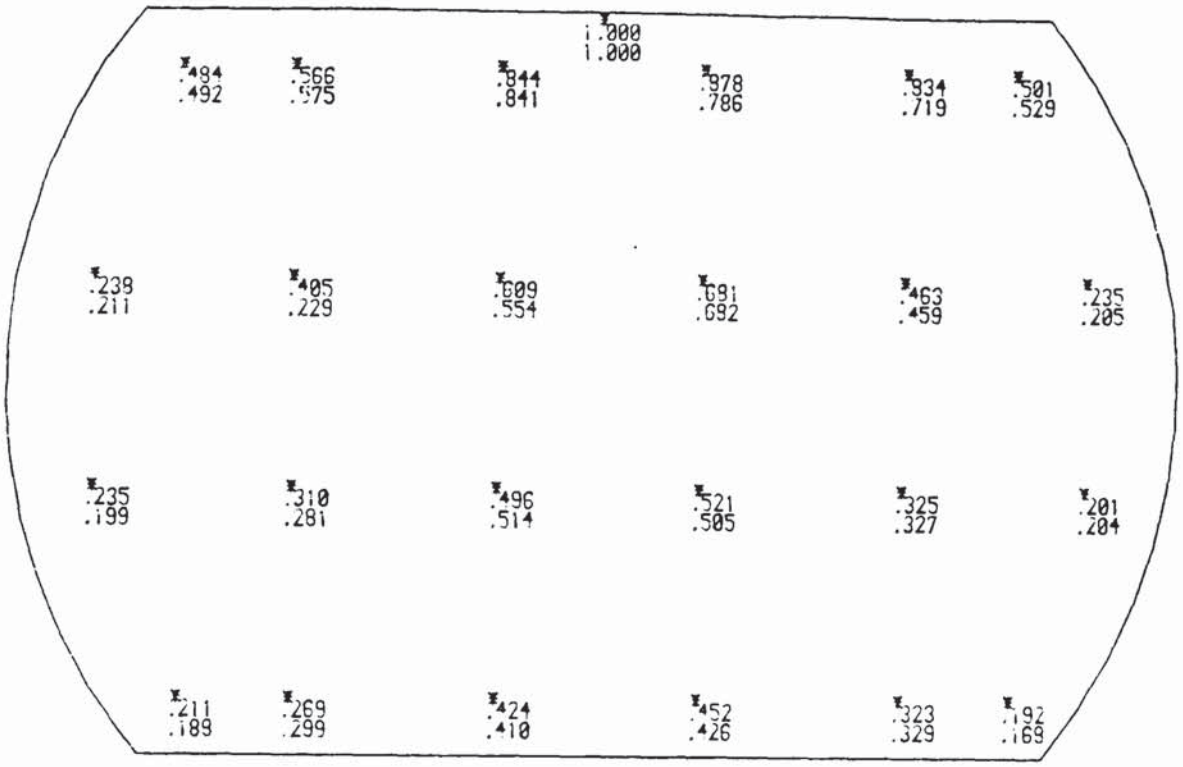

b) Reduced temperatures difference and variance

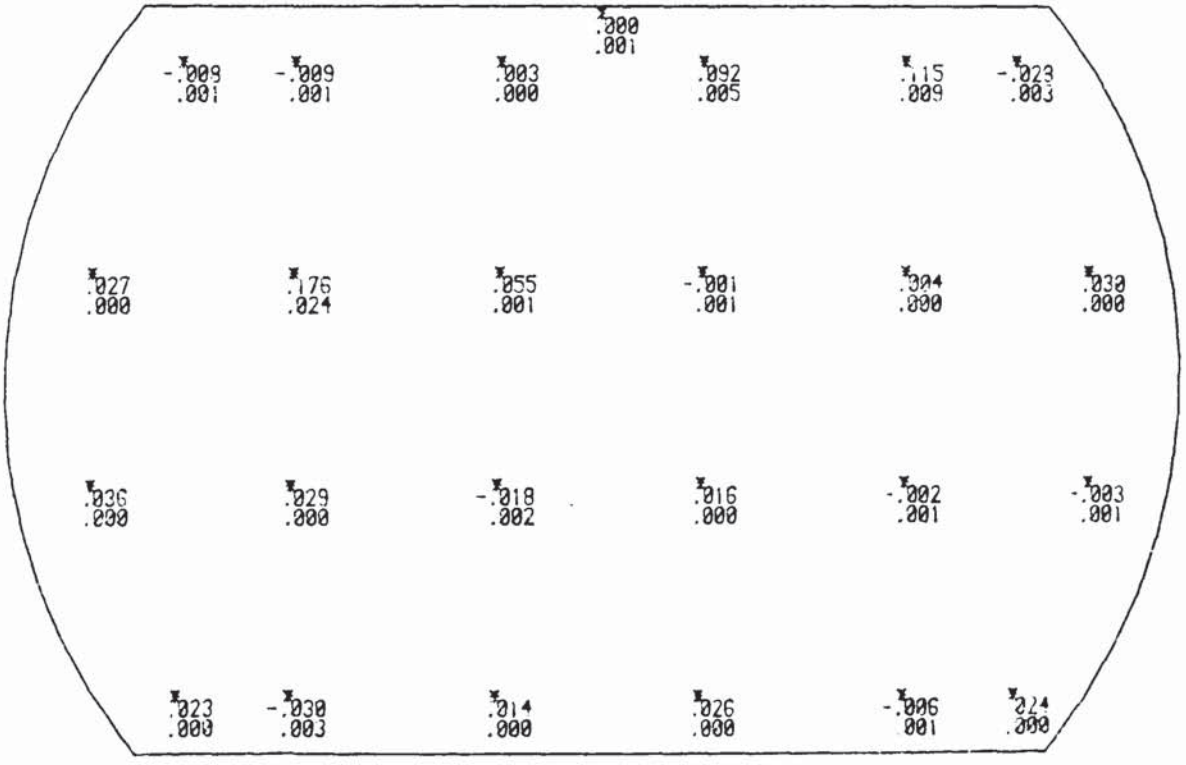

FIGURE:9.4 REPEATED WATER COOLING EXPERIMENTS

Flow Rates: $\lambda = 2.748$ $q/b = 0.110 \times 10^{-2}$ m^3/sm $C_{sb} = 0.0635$ m/s

a) Reduced Temperatures

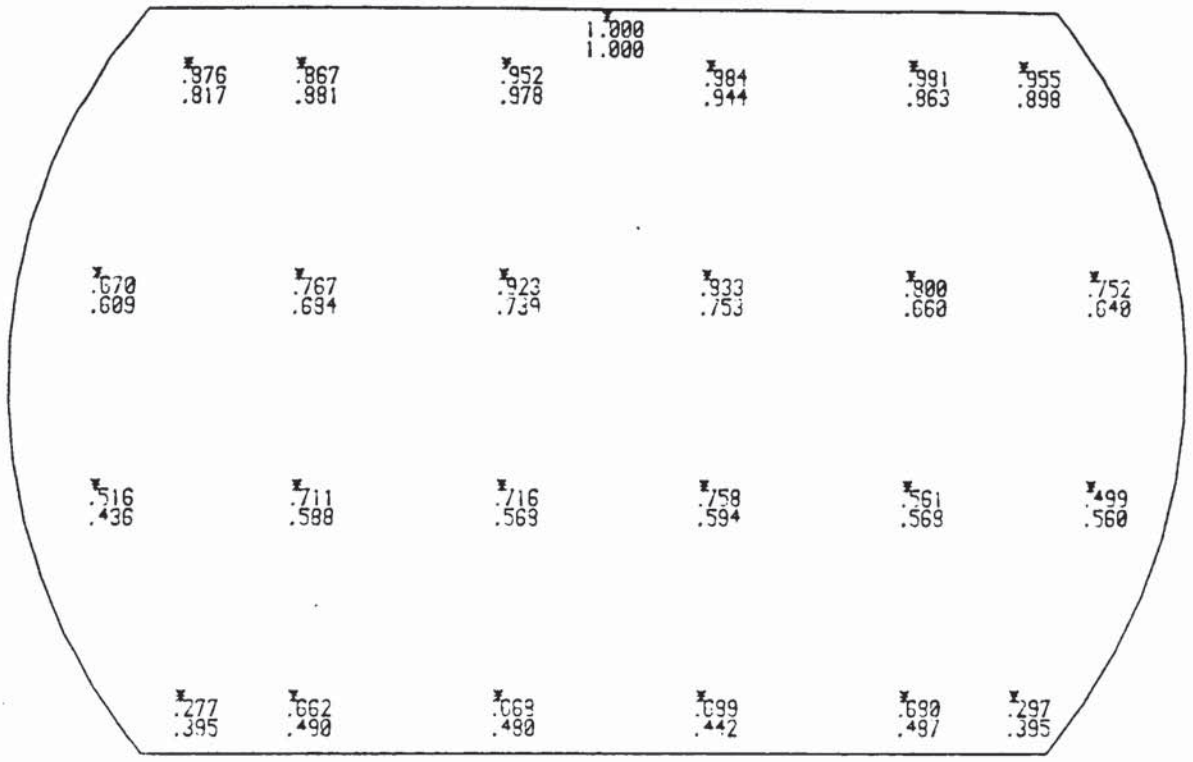

b) Reduced temperatures difference and variance

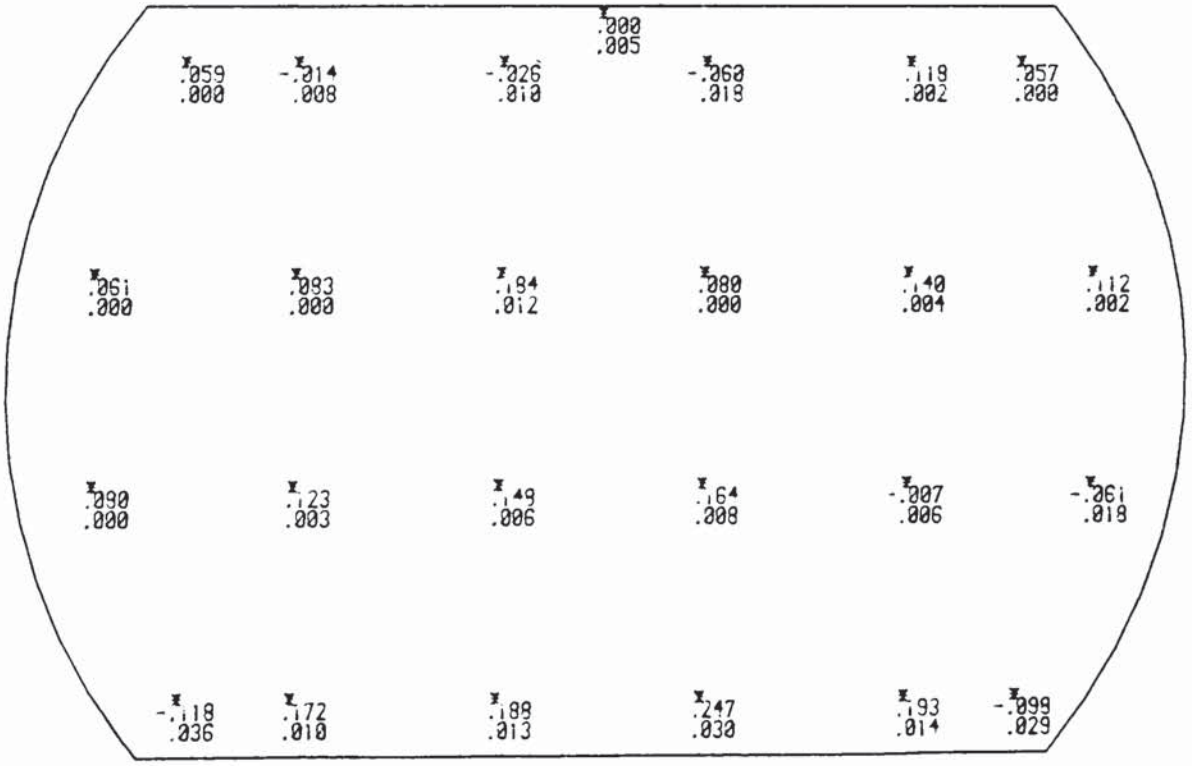

FIGURE:9.5 REPEATED WATER COOLING EXPERIMENTS

Flow Rates: $\lambda = 2.055$ $q/b = 0.161 \times 10^{-2}$ m^3/sm $C_{sb} = 0.0695$ m/s

a) Reduced Temperatures

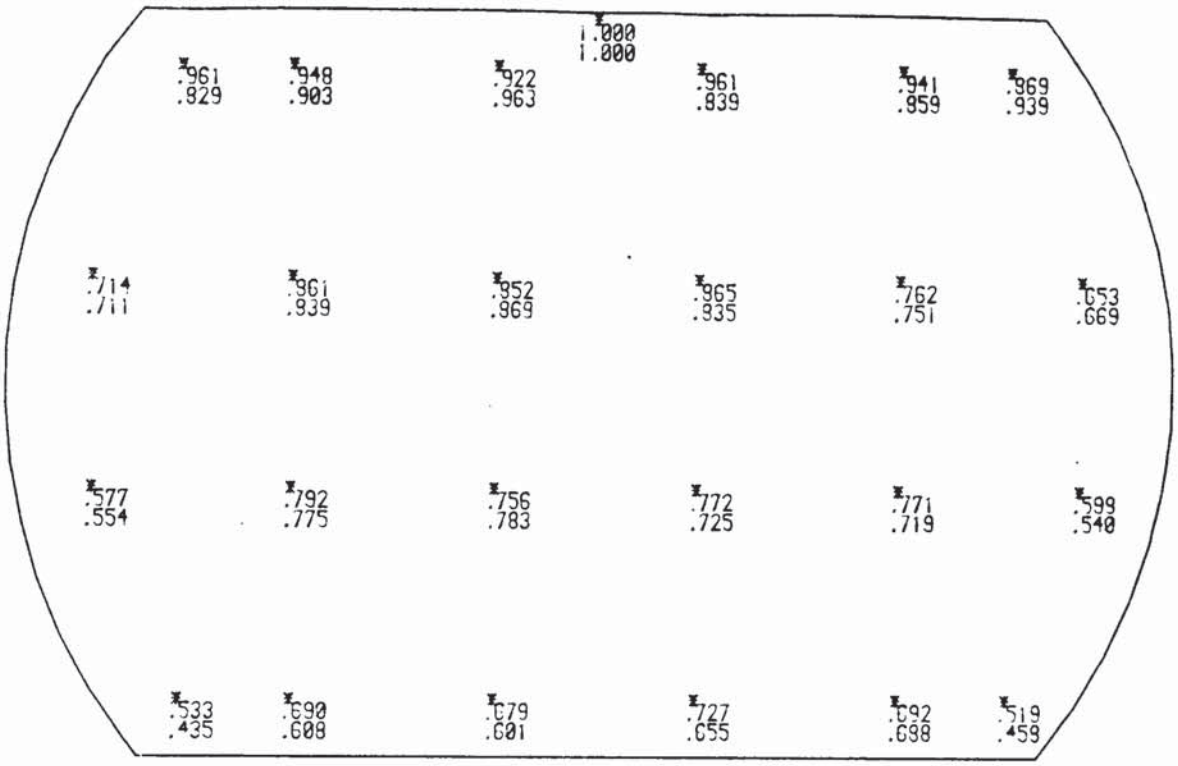

b) Reduced temperatures difference and variance

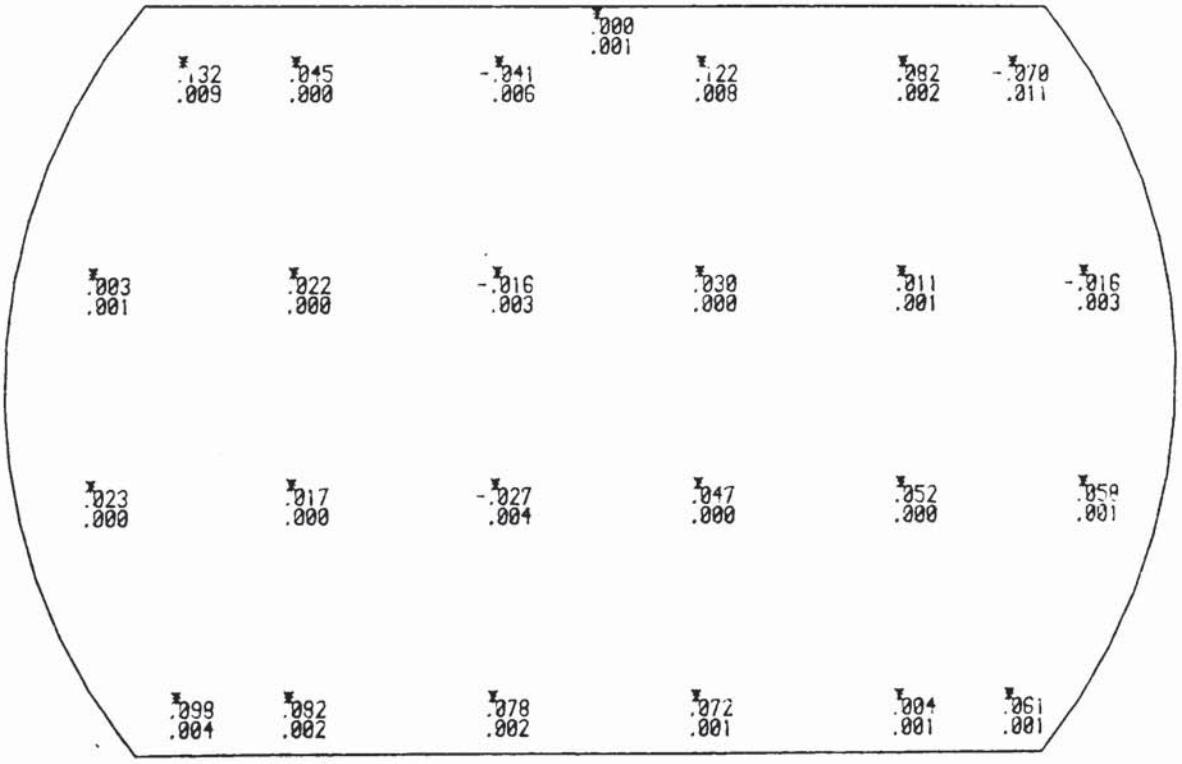

FIGURE:9·6 REPEATED WATER COOLING EXPERIMENTS

Flow Rates: $\lambda = 0.699$ $q/b = 0.473 \times 10^{-2}$ m^3/sm $C_{sb} = 0.0695$ m/s

a) Reduced Temperatures

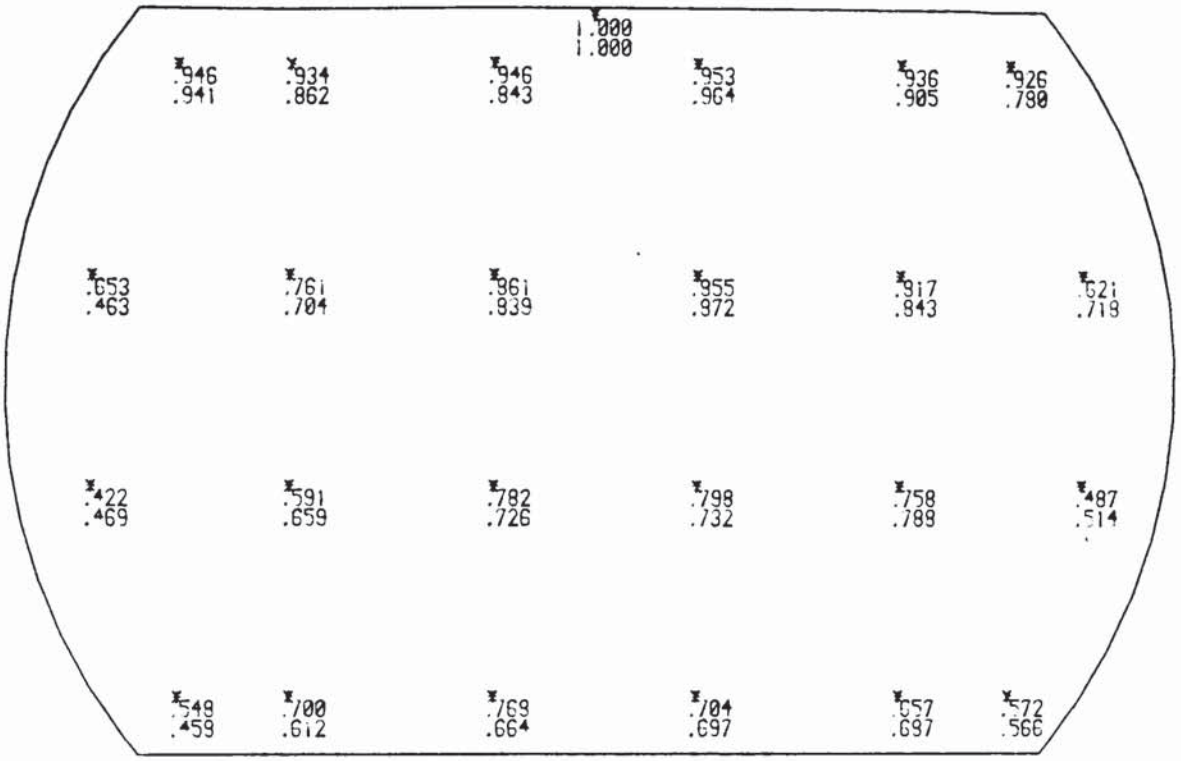

b) Reduced temperarures difference and variance

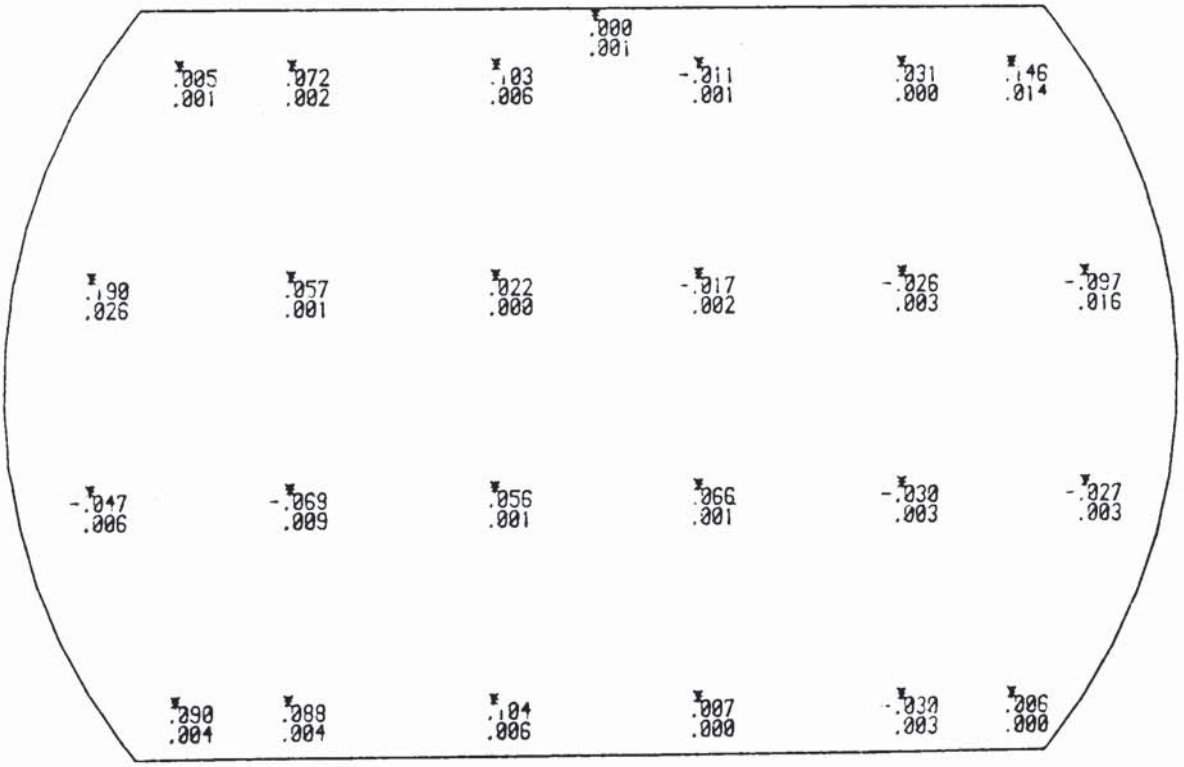

FIGURE:9·7 REPEATED WATER COOLING EXPERIMENTS

Flow Rates: $\lambda = 0.684$; $q/b = 0.484 \times 10^{-2}$ m^3/sm; $C_{sb} = 0.0695$ m/s

a) Reduced Temperatures

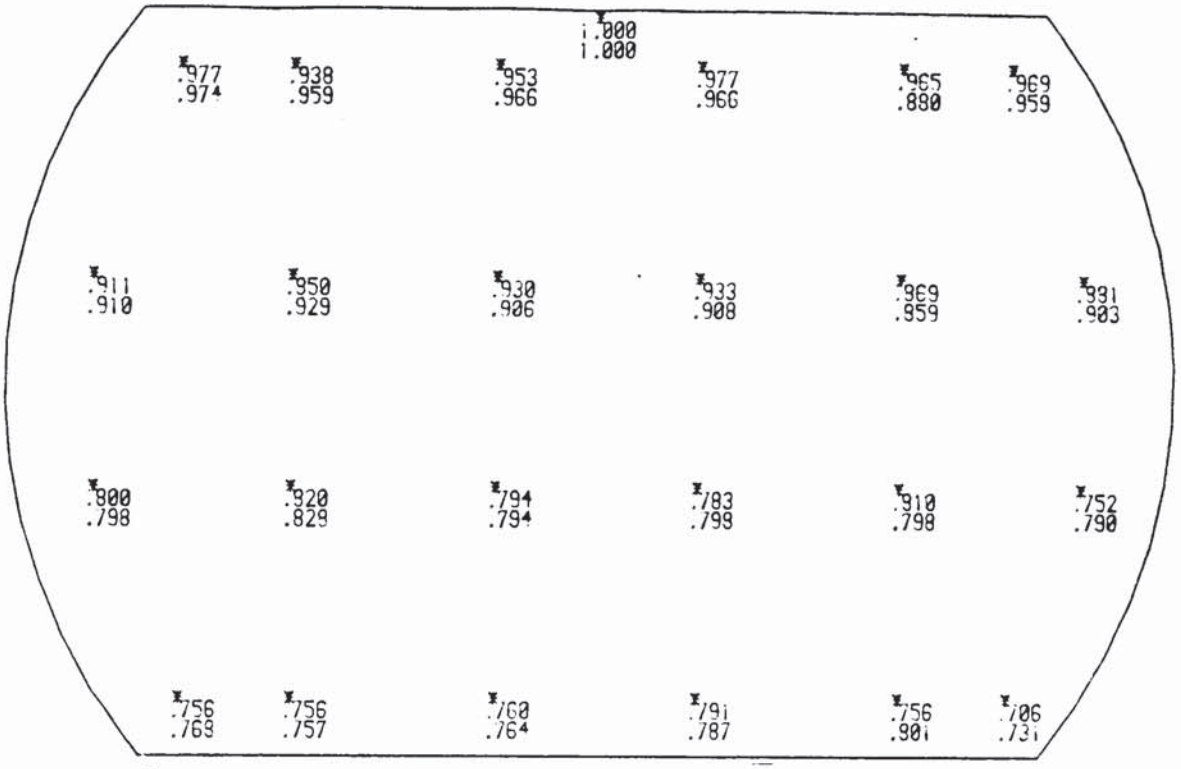

b) Reduced temperatures difference and variance

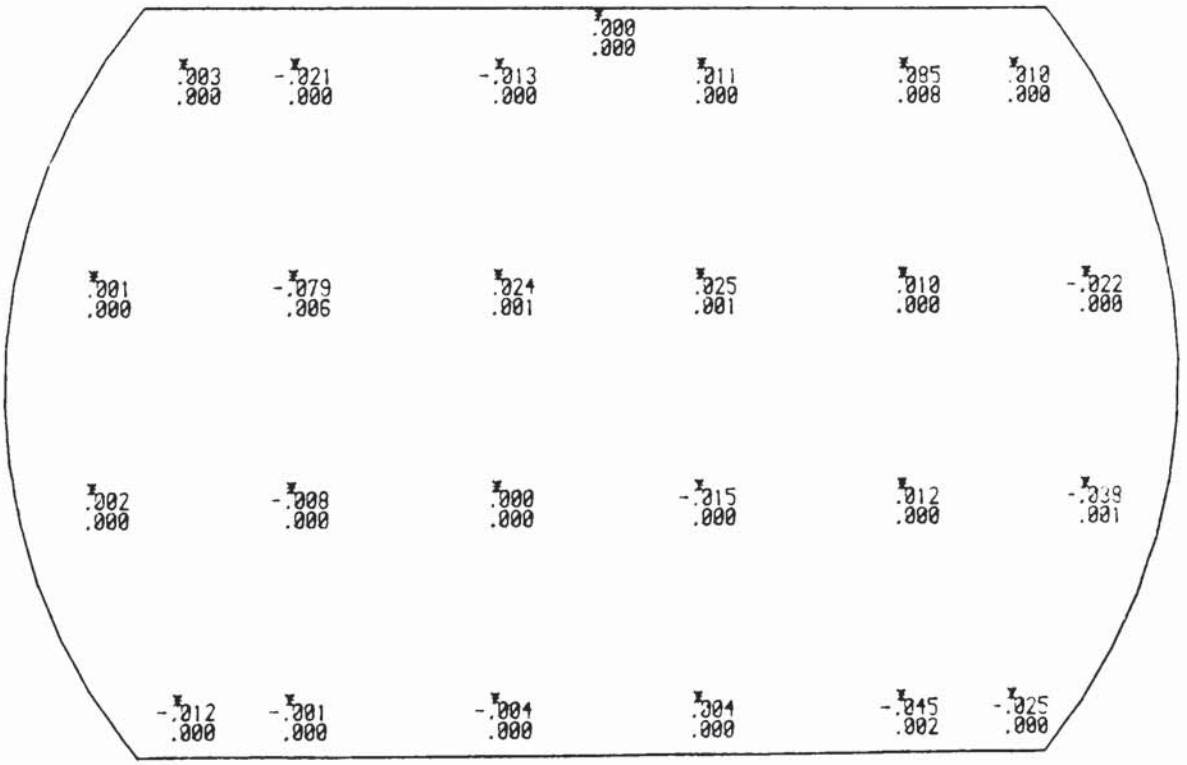

FIGURE:9.8 REPEATED WATER COOLING EXPERIMENTS

Flow Rates: $\lambda = 0.626$; $q/b = 0.742 \times 10^{-2}$ m^3/sm; $C_{sb} = 0.0975$ m/s

a) Reduced Temperatures

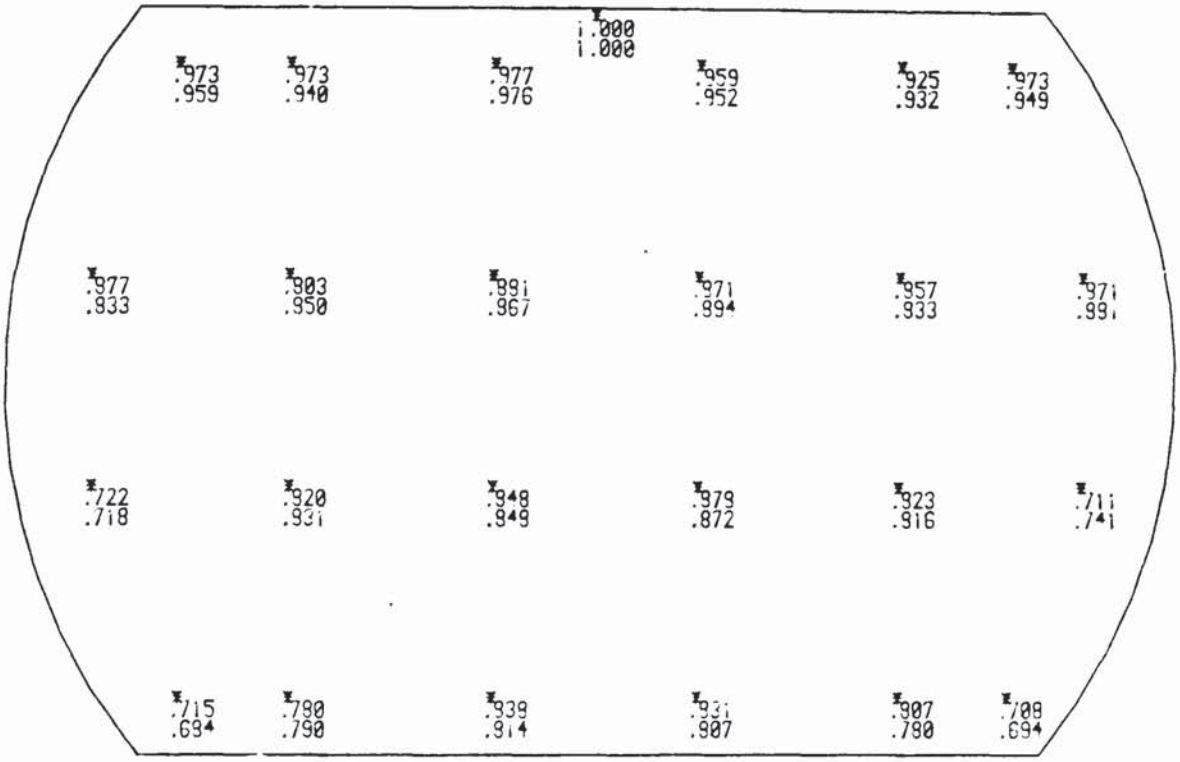

b) Reduced temperatures difference and variance

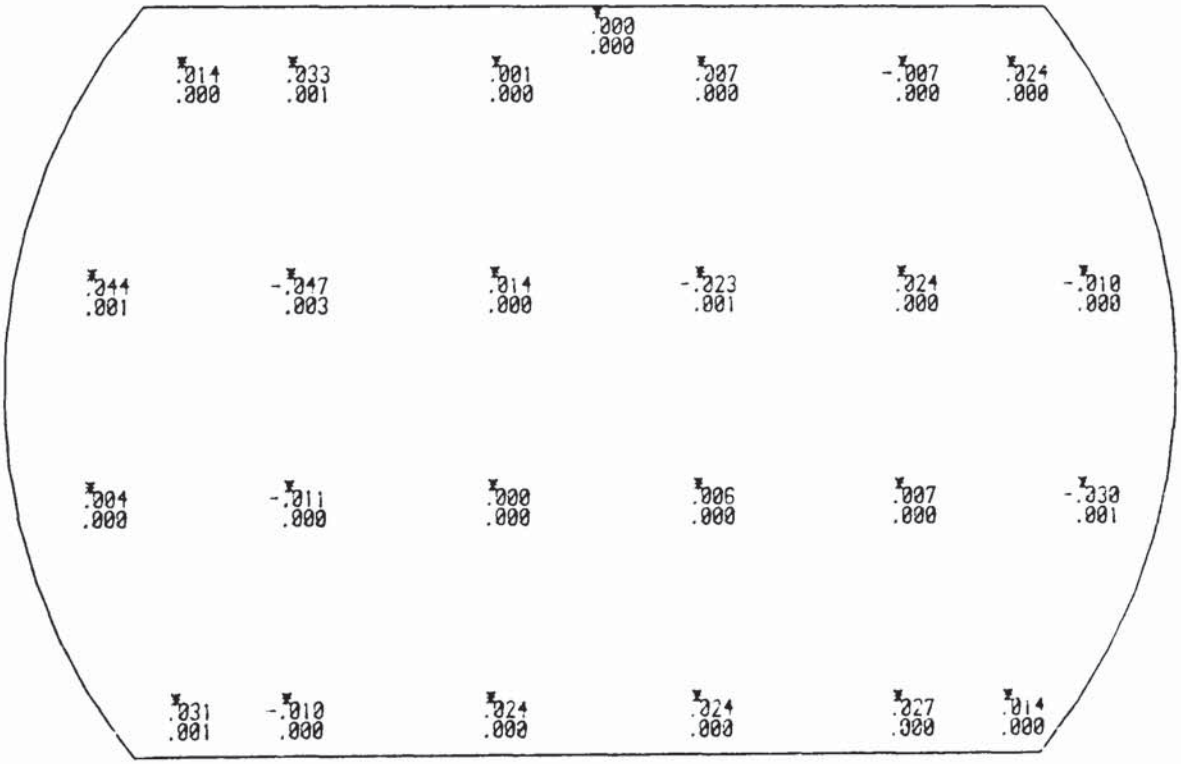

FIGURE: 9·9 REPEATED WATER COOLING EXPERIMENTS

Flow Rates: $\lambda = 0.432$; $q/b = 0.766 \times 10^{-2}$ m^3/sm; $C_{sb} = 0.0695$ m/s

It may be noted that the difference between the reduced temperatures of the repeated experiments show very good agreement. This is more so in the Mixed regime where the temperature drop is below 30%. The worst case of nonreproducibility occured in the Spray regime, figure 9.5. This is particularly poor at the outlet which may be due to the approach of the water temperatures to the wet-bulb temperature. However, it is worth noting that the difference between the wet-bulb temperature is exceptinally high for this measurement at 15%. The variance which represents a measure of the deviation from the mean is generally 4 x higher in the Spray regime than it is in the Mixed regime.

9.2.4 Conclusion on Repeatability of Temperature Measurements

The agreement between the reduced temperatures over repeated experiments confirms the reliability of this technique when used to determine temperature profiles on a tray. Although smaller temperature changes generally occur in the Mixed regime than in the Spray regime, the results are more reliable in the former than in the latter. This is probably because the temperatures in the Mixed regime unlike those in the Spray do not approach the wet-bulb temperature of the inlet air. However, the results of the repeated temperatures in the Spray regime also show reproducibility.

It is expected that in view of the reproducibility of the temperature measurements, the tray efficiencies will also be reproducible. This leads to a reevaluation of the water cooling efficiencies in the next section.

9.3 Evaluation of Reproducibility of Tray Efficiency

The conditions shown to reproduce temperatures on the tray were evaluated for tray efficiencies to investigate, if like temperatures, tray efficiency is also reproducible. The procedure for repeating the experiments was outlined in subsection 9.2.2 above. The method of calculation of tray efficiency is approximated in this section. It involves the arithmetic averaging of the temperatures at the outlet row of thermocouples to determine the outlet temperature, knowledge of the inlet temperature and the flow rates to determine λ. The heat and material balance equation derived later in subsection 9.4.2 as:

$$E_{MV} = \frac{1}{\lambda} \cdot \left[\frac{T_{in}}{T_o} - 1\right] \qquad 9.22$$

is used. But the same was applied to repeated experiments therefore errors inherent in the simplification are assumed to be the same for each experiment.

The results obtained are listed in Table 9.3 below.

Table 9.3: Repeated Experiments for Tray Efficiency

C_{sb}(m/s)	q/b(m^3/sm)	λ	t_{in}	t_{ot}	t_{wb}	E_{MV}	[ΔE_{MV}]
0.0635	0.110×10^{-2}	2.748	38.89	26.43	20.33	74.3	
			40.57	26.66	20.60	83.5	9.2
0.0695	0.161×10^{-2}	2.055	41.30	31.48	19.69	40.5	
			38.25	26.56	17.11	60.2	19.8
0.0695	0.473×10^{-2}	0.699	42.74	35.01	24.57	105.9	
			41.80	34.94	22.74	80.4	25.5
0.0695	0.484×10^{-2}	0.684	41.20	35.03	23.15	75.9	
			42.74	35.53	24.07	92.0	16.1
0.0975	0.742×10^{-2}	0.626	36.33	32.53	19.96	48.3	
			35.93	32.02	20.02	52.1	3.8
0.0695	0.766×10^{-2}	0.432	37.44	33.49	19.51	65.4	
			38.43	34.15	20.51	72.6	7.2

It is noticeable that the tray efficiencies calculated here are on the average lower than those determined by the computational method used elsewhere in this work, see subsection 8.1. Two related reasons are responsible for this, namely i. the simple averaging of the outlet row temperatures to represent the outlet temperature of the liquid leaving the tray decreases the value of T and ii. the location of the outlet row of temperatures is about 100mm (or 13% of the flow path length) from the outlet weir from where the liquid actually leaves the tray.

All this amounts to an underestimation of the overall drop in liquid temperature across the tray and thus a lowering of the overall tray efficiency. However, since this procedure is applied to the repeated experiment it is convenient to assume here that the errors due to this will be the same for each experiment.

The results of the calculated tray efficiencies and the corresponding difference between the values of each repeated experiment show an interesting trend. Half of the six (6) conditions examined show good reproducibility since the difference between the tray efficiencies is below 8%. These are conditions of both low and high liquid rates. At intermediate liquid rates the disparity between the tray efficiencies is large at between 14% and 26%. The tray efficiencies are thus not reproducible. The most serious case of nonreproducibility corresponds to the least values of wet-bulb temperatures of the air entering the tray. This suggests that the tray efficiency is more sensitive to the wet-bulb temperature than it is to temperature profiles on the tray.

An errors analysis carried out in the next subsection should clarify this a little further.

9.4 Errors Analysis

The errors analysis made in this section was intended to illustrate the sensitivity of the efficiencies to the parameters measured in this work. The liquid flow pattern was simplified to the ideal plug flow model so as to show the relationship between the point efficiencies and the point measurements of temperatures on the tray. The model used for tray efficiency was derived from the usual heat balance on the tray. Typical values of individual parameters were substituted into the model equations along with some arbitrary margins of error. The combined effects of the errors on efficiencies was estimated from the model equations.

9.4.1 Derivation of the Ideal Plug Flow Model for Point Efficiency

A heat balance was made over an element of froth on the tray. The assumptions made are that, there is::

i. no liquid mixing in any direction

ii. negligible transfer of heat between the froth and the tray floor and

iii. there is uniform flow of liquid across the width of the tray at any distance from the tray inlet

A schema of the element of froth is shown in figure 9.10 below.

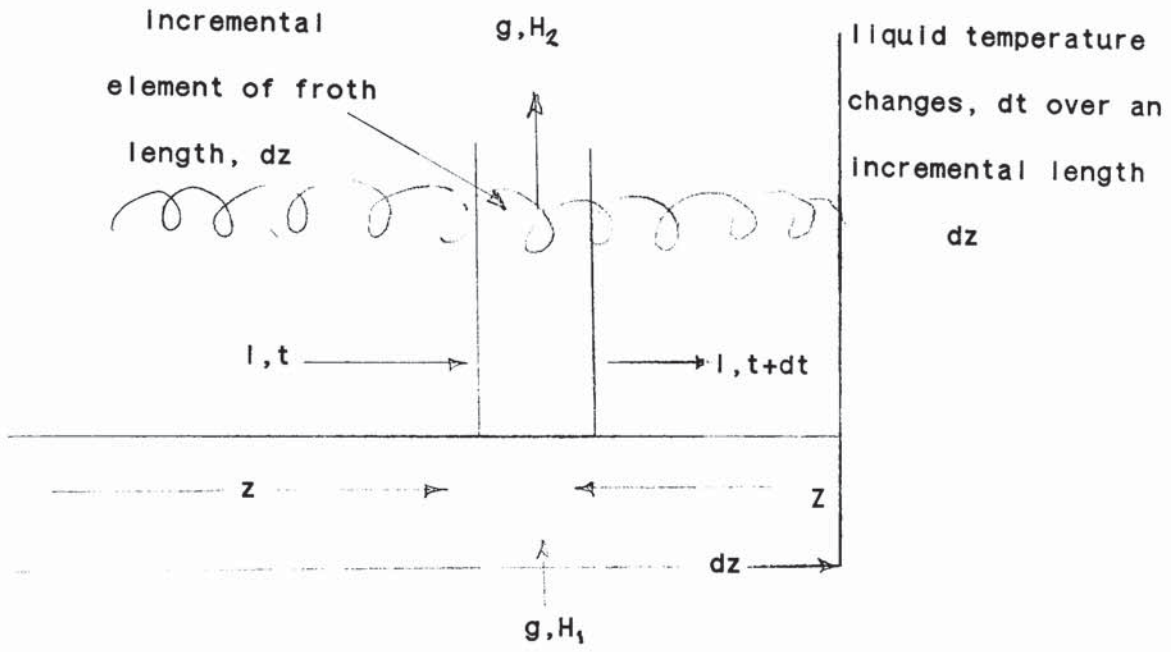

Figure 9.10: Froth Incremental Diagram

Symbols used are:

l is liquid crossflow in moles/unit width of flow path =L/W

g is vapour flow through the froth in moles/unit area of tray = G/(WZ)

t is liquid temperature at distance z from the liquid inlet

H_1, H_2 are the enthalpies of air entering and leaving the froth a distance z from the inlet.

A heat balance on the element would give:

$$l.dt = g.(H_1 - H_2).dz \qquad 9.2$$

The saturation air enthalpy in equilibrium with the liquid of temperature t, (with no temperature gradient in the froth vertical direction) is:

$$H^* = m't + c \qquad 9.3$$

Consider the wet-bulb temperature t_{wb} as the temperature of the liquid saturated with (or in equilibrium with) the entering vapour, such that;

$$H_1 = m' t_{wb} + c \qquad 9.4$$

The definition of point efficiency is given as, see subsection 5.4,

$$E_{OG} = \frac{H_2 - H_1}{H^* - H_1} \qquad 9.5$$

or

$$E_{OG} = \frac{(H_2 - H_1)}{m'(t - t_{wb})} \qquad 9.6$$

Rearranging :

$$H_2 - H_1 = E_{OG}.m'.(t - t_{wb}) \qquad 9.7$$

the heat balance equation 9.2 above then becomes:

$$l.dt = g.E_{OG}.m'.(t - t_{wb}).dz \qquad 9.8$$

Separating the variables,

$$\frac{dt}{t - t_{wb}} = (\frac{m' g}{l}).E_{OG}.dz \qquad 9.9$$

Put

$$\underline{Z} = \frac{z}{Z} \qquad 9.10$$

$$d\underline{Z} = \frac{1}{Z}\, dz \qquad 9.11$$

$$T = t - t_{wb} \qquad 9.12$$

$$dT = dt \qquad 9.13$$

and considering the definition:

$$= \frac{m' \cdot G}{L} \qquad 9.14$$

Equation 9.9 can be solved to yeild:

$$\int \frac{dT}{T} = E_{OG} \int dZ \qquad 9.15$$

$$\ln T \Big|_{T_{in} = t_{in} - t_{wb}}^{T_O = t_O - t_{wb}} = E_{OG} \cdot Z \Big|_0^1 \qquad 9.16$$

Therefore, the final equation becomes:

$$\frac{T_o}{T_{in}} = \exp(E_{OG}) \qquad 9.17$$

where $0.0 < \frac{T_o}{T_{in}} < 1.0$

9.4.2 Model for tray efficiency

The Murphree tray efficiency water cooling is defined as:

$$E_{mv} = \frac{H_1 - \bar{H}_2}{H_1 - H^*_{out}} \qquad 9.18$$

where,

$$H^*_{out} = m' T_{out} + c \qquad 9.19$$

An overall heat balance gives

$$G.(\bar{H}_2 - H_1) = L.c.(t_{out} - t_{in}) \qquad 9.20$$

(Note, for water, c = 1.0kcal/kg).

$$H^*_{out} - H_1 = m' .(t_{out} - t_{wb}) \qquad 9.21$$

Substituting into equation 9.18 above, and rearranging, yields:

$$E_{mv} = \frac{1}{\lambda} \cdot [\frac{T_{in}}{T_o} - 1] \qquad 9.22$$

Errors analysis are based on the models represented by equation 9.17 and equation 9.22. These are rules that govern the errors of a product, a quotient, a coefficient and an exponent [121,124].

9.4.3 Derivation of the Equations for Errors Calculations

Assign: $\delta s = sf(s)$ 9.23

where, δs is error (or deviation) in s and f(s) is the fractional error in s. For convenience, this shall be expressed in percentage. The following common laws of errors are invoked, reference [121]:

$$x = a + b \qquad 9.24$$

$$f(x) = \frac{\delta a^2 + \delta b^2}{a + b} \qquad 9.25$$

Now, the equation for point efficiency:

$$E_{OG} = -\frac{1}{\lambda} \ln(s) \qquad 9.26$$

where s takes the value;

$$s = \frac{T_o}{T_{in}} \qquad 9.27$$

The equation for tray efficiency is:

$$E_{MV} = -\frac{1}{\lambda}(\frac{1 - s}{s}) \qquad 9.28$$

So: $$f(E_{MV}) = \frac{-f(s)}{1 - s} \qquad 9.29$$

and $$f(E_{OG}) = f(\ln(s)) \qquad 9.30$$

Put, $$g = \ln(s) \qquad 9.31$$

and, $$p = 1 - s \qquad 9.32$$

By the logarithmic series expansion,

$$\ln(s) = 1 - p + 1/2(p)^2 - 1/3(p)^3 + 1/4(p)^4 - \ldots \qquad 9.33$$

It is reasonable to truncate after the fourth polynomial, on expanding, this gives:

$$g = \ln(s) = 4 - 10s + 20s^2 - 4s^3 + s^4 \qquad 9.34$$

$$f(E_{OG}) = f(g) = \frac{\delta g}{g}$$

$$= \frac{-10\delta s + 40s\delta s - 12s^2\delta s + 3s^3\delta s}{4 - 10s + 20s^2 - 4s^3 + s^4} \qquad 9.35$$

Next, assume that the absolute error in all thermocouples is the same, that is :

$$\delta t_{in} = \delta t_o = \delta t_{wb} = r\,^{\circ}C \qquad 9.36$$

The calculations yield the results tabulated in Table 9.5 below.

The accuracies of the thermocouples used in this work is set at 0.3 °C. This is deduced from the calibrations carried out in Appendix B. The results above also show the expected margins of deviations in efficiency for other arbitrary errors in temperature measurements.

Table 9.5 Estimated Errors in Efficiency from Temperature Measurement Errors

t_{in}	t_o	t_{wb}	T_{in}	T_o	λ	s	r °C	f(s)	f(E_{QG})	f(E_{MV})
40.57	38.25	24.07	16.5	14.2	0.298	0.86	0.1	1.86	3.4	13.3
							0.3	5.57	9.2	40.0
							0.5	9.28	17.0	66.0
40.10	36.34	21.90	18.2	14.4	0.314	0.79	0.1	1.74	3.1	8.3
							0.3	5.27	8.5	25.0
							0.5	8.79	15.5	41.0
42.20	32.90	21.50	20.7	11.4	1.003	0.55	0.1	1.92	2.1	4.3
							0.3	5.77	6.1	13.0
							0.5	9.62	10.5	21.3
42.20	30.40	21.00	21.2	9.4	1.478	0.44	0.1	2.17	1.7	3.9
							0.3	6.51	5.0	12.0
							0.5	10.85	8.3	19.5
40.00	29.00	22.00	18.0	7.0	1.790	0.39	0.1	2.80	1.5	4.6
							0.3	8.42	4.4	14.0
							0.5	14.03	7.4	22.9
42.17	29.67	22.00	20.3	7.67	2.294	0.38	0.1	2.53	1.2	4.1
							0.3	7.62	3.3	12.0

The fact that errors in point efficiencies are far less than those for tray efficiencies is probably due to the separate models used to evaluate each one. Essentially, two measurements only, the tray inlet and outlet average water tempertures are responsible for the disparity. By operating the logarithmic function on the measurement variables used for the point efficiency calculations, the corresponding errors are also reduced. By contrast, the procedure for tray efficiency is based on direct estimates from the inlet and outlet temperature measurements. In consequence, the magnitudes of the resulting errors are higher than its true value. The true value can be obtained by integrating the errors at several points along the flow axis.

The results show that there is a strong dependence of the correct estimates of both the point and tray efficiencies on the accuracy of temperature measurement. This in turn is dependent on the overall temperature drop across the tray. That is, the expected accuracies are much higher in certain flow regimes than others. From Section 4, and subsequent experiments of temperature profiles in Section 6 and Section 7, it was clear that the overall temperature drop in the Mixed regime is much lower than it is in the Spray regime. Higher temperature drops can also be expected in large trays due to their long liquid flow paths. Therefore, both large trays and operations in the Spray regime will yield relatively more reliable estimates of water cooling efficiencies than small trays and operations in the Mixed regime.

With regards to the thermocouples employed in this work, the calculations show that, at r = 0.3°C, they cannot be expected to give reliable tray efficiencies particularly in the Mixed regime. However, both point efficiencies and tray efficiencies within the Spray regime should be accurate to within 10%. At r = 0.1 °C, or less, water cooling efficiencies can be estimated to high levels of accuracies.

9.5 Conclusion

The work carried out in this Section is consistent with the normal procedure for evaluating tray performance and hence leads to the following conclusions:

i. the tempeartures obtained from the water cooling experiments on a sieve tray are repeatable. These are best demonstrated using the reduced temperature concept,

ii. to determine both tray efficiency and point efficiency to acceptable levels of accuracy, temperature measurements must be within 0.1°C (or a tenth of a degree). Temperature measurements with tne equipment used in this work, give r = 0.3°C and thus are expected to result in high losses of accuracy in efficiencies,

iii. in the Spray regime, where the temperature drop across the tray is higher than that in the Mixed regime, the relative accuracies fo water cooling efficiencies are better than those for the Mixed regime. It is expected that for large trays, the accuracy would be good because of expected large drop of temperature across the tray. This is due to their long liquid flow paths,

iv. experiments for which the flow variables were repeated give different efficiency results. Efficiency reproducibility is therefore unsatisfactory, but this is clearly due to the errors in the measurements of temperature.

v. the liquid hold-up measurements give similar results to the correlations in literature. Assuming therefore, that these are accurate, no direct relationship was detected between the gas phase point efficiencies and the liquid hold-up on the tray.

10. A COMPARISON OF EXPERIMENTAL TEMPERATURE PROFILES WITH THOSE PREDICTED FROM THE CHANNELLING THEORY OF PORTER AND LOCKETT.

In Section 2 it was stated that the current theoretical models for large trays all predict similar liquid flow patterns on trays. In this section the channelling model was nominated and its equations transformed to predict temperature profiles. Due to its simplicity the parameters used were few and as easy to determine in the temperature mode as they would be in the usual concentration mode. These required an estimate of the point efficiency for water cooling, which is not necessarily the same as that in the mass transfer process. The point efficiencies determined in the water cooling experiments were ploughed back into the Porter and Lockett channelling model for a single tray to calculate the flow pattern and tray efficiency.

10.1 Theory and Asumptions

It is expected that processes that determine both temperature and concentration profiles on a tray depend on the liquid flow pattern and develop in the same way. The analogy between the processes of heat and mass transfer enables one to conclude that temperature profiles derived from a water cooling experiment will be similar to the concentration profiles of a mass transfer experiment. The driving forces are i. concentration gradient for mass transfer and ii. enthalpy change for water cooling. Thus in mass transfer equations, x the mole fraction of a component in the liquid phase and y, the mole fraction of the same component in vapour phase can be

replaced by T, the water temperature of a point on the tray and H the enthalpy of an air stream passing through that point, respectively.

The assumptions are similar to those made for the channelling model, applied to a single cross-flow tray, that is:

a. the air and water entering the plate are each well mixed, and

b. the equilibrium line or the air saturation temperature is straight over the temperature range in the experiment. The equation of the saturation line is given as :

$$H^* = m'T + b$$

The justification for this is demonstrated in the plot of saturation temperature against the saturation enthalpy shown in figure A:B3.

And finally,

c. the point efficiency for water cooling is assumed to be constant over the plate. This is defined as:

$$E_{OG} = (H_2 - H_1)/(H^* - H_1) \qquad 10.2$$

or from equation 10.1 above,

$$E_{OG} = (H_2 - H_1)/m'(T - T_s) \qquad 10.3$$

where T_s is the saturation temperatureof the inlet air,

d. heat transferred through the tray is negligible compared to that transferred through the passing vapour.

e. the water flow rate per unit width of weir is constant. This is given by the equation:

$$L' = L / W \qquad 10.4$$

The implications of this assumption was investigated in subsection 6.2.

The derivations of the model in its mass transfer form was described in subsection 2.4.2.1. The water cooling analogue is derived from mass and heat balance equations over an element of froth shown in figure 10.1. The model equations for each flow stream are also indicated in the figure.

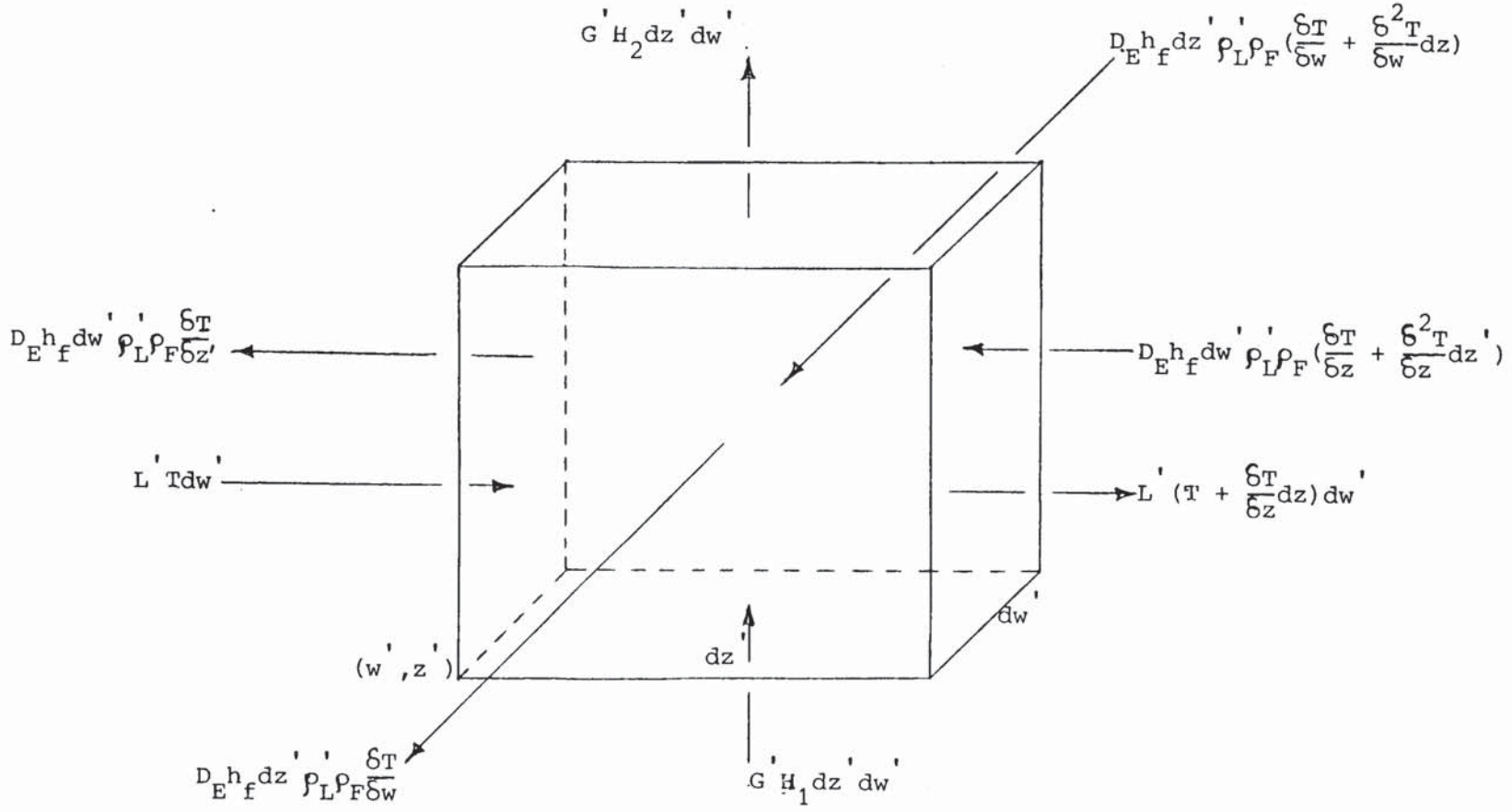

FIG:10.1 Heat and Material Balance over an Element of Froth

The Boundary Conditions are:

a. by symmetry, at the flow axis;

$$w = 0 \qquad 0 < z < z_1 \qquad \frac{\partial T}{\partial w} = 0 \qquad 10.5$$

b. at the liquid inlet, the widely used Danckwerts [24,25] mass balance equations ;

$$\text{at } z = 0 \qquad 0 < w < w_1 \qquad T_+ = 1 + \frac{1}{Pe}.\left(\frac{dT}{dz}\right) \qquad 10.6$$

c. at the liquid outlet, it is assumed that there is no air circulating inside the downcomer ;

$$\text{at } z = z_1 \qquad 0 < w < w_1 \qquad \frac{\partial T}{\partial z} = 0 \qquad 10.7$$

d. at the impermeable column wall, it is assumed that the wall material has poor heat conduction such that:

$$\frac{\partial T}{\partial n} = 0 \qquad 10.8$$

The assumption of negligible heat conduction across a column wall of poor (or good) heat conduction is investigated by making the appropriate heat balance over an element of froth and column wall, later in subsection 10.4. A simple equation which only requires knowledge of the conductivity of the material is derived.

10.2 Mathematical Development of the Model

The predictive equations are based on a heat balance over the differential element on the tray, figure 10.1 below. The equations of the model are given for each region separately as:

a. for the active region;

$$D_e\left(\frac{\partial^2 T}{\partial w^2} + \frac{\partial^2 T}{\partial z'^2}\right) - \frac{L'_1}{h_f \rho'_L \rho_F}\cdot\frac{\partial T}{\partial z'} + (H_1 - H_2)\frac{G'}{h_f \rho'_L \rho_F} = 0 \qquad 10.9$$

b. for the stagnant regions;

$$D_e\left(\frac{\partial^2 T}{\partial w^2} + \frac{\partial^2 T}{\partial z^2}\right) - (H_1 - H_2)\frac{G'}{h_f \rho_L \rho_F} = 0 \qquad 10.10$$

It is noted that L'_1 used in equation 10.9 above accounts for the specific heat of water which is 1.0 Btu/lb°F. The equations 10.9 and 10.10 above, are solved numerically by finite difference methods in the way described in reference [67] . The predicted temperature profiles resulting from the solution of the equations are shown in figure 10.1 to figure 10.3.

By integrating the predicted water temperatures at a predetermined number of points on a grid on the tray, and by integrating the exit water temperature over the width of the outlet weir to obtain the average temperature of the water leaving the tray, a final equation for the E_{MV} / E_{OG} is derived as:

$$\frac{E_{MV}}{E_{OG}} = \frac{1}{A}.\int_A T.dA \;/\; [\frac{1}{W}\int_{-w/2}^{w/2} T_2 dw^1] \qquad 10.11$$

When this equation is applied to the active region of the tray only, it reduces to the equation of the Simple Backmixing Model which is expressed as :

$$\frac{E_{MV}}{E_{OG}} = \frac{1 - \exp[-(n + Pe)]}{(n + Pe)[1 + (n + Pe)/n]} + \frac{\exp(n) - 1}{n[1 + n/(n + Pe)]} \qquad 10.12$$

where,

$$n = \frac{Pe}{2}[\ (\frac{1 + 4\lambda' E_{OG}}{Pe}) - 1] \qquad 10.12a$$

and,

$$\lambda' = mGA_1 / LA = \lambda A_1 / A \qquad 10.12b$$

Solutions to equation 10.12 were sought in the manner described in reference [67]. A computer program written by the author to predict concentration profiles [67] was adopted and transformed into one to produce temperature profiles. The most significant change to the program involved the replacement of the parameter x by T. The results obtained are shown in figure 10.2b to figure 10.4b below.

10.3 Discussion of the Results

In comparing the temperature profiles obtained by experiment with those predicted using the Porter and Lockett Channelling Model the essential parameters used are the same. These include, λ derived from the flow rates chosen, λE_{OG} from the calculation procedure using the air enthalpy and point measurements of water temperatures on the tray and the design ratio W/D = 0.77 for this tray. In Table 10.1 the conditions used together with the tray efficiencies found by experiment $E_{MV,e}$, and by the predictive method $E_{MV,t}$, are given. The temperature profiles are shown in figure 10.2 (a&b), figure 10.3 (a&b), and figure 10.4 (a&b).

Going by the definition of types of profiles in this work all three pairs with the exception of the experimental profiles of figure 10.3a are considered as flat. The temperature profiles determined by experiment are very similar to those predicted by the model. In both sets of profiles small dead or cold zones emanate from the sides of the tray at the outlet weir. U-shaped profiles are identified in the last half of the tray in figure

Predicted Temperature Profiles on a 1.22m Tray

(Temperature °C)

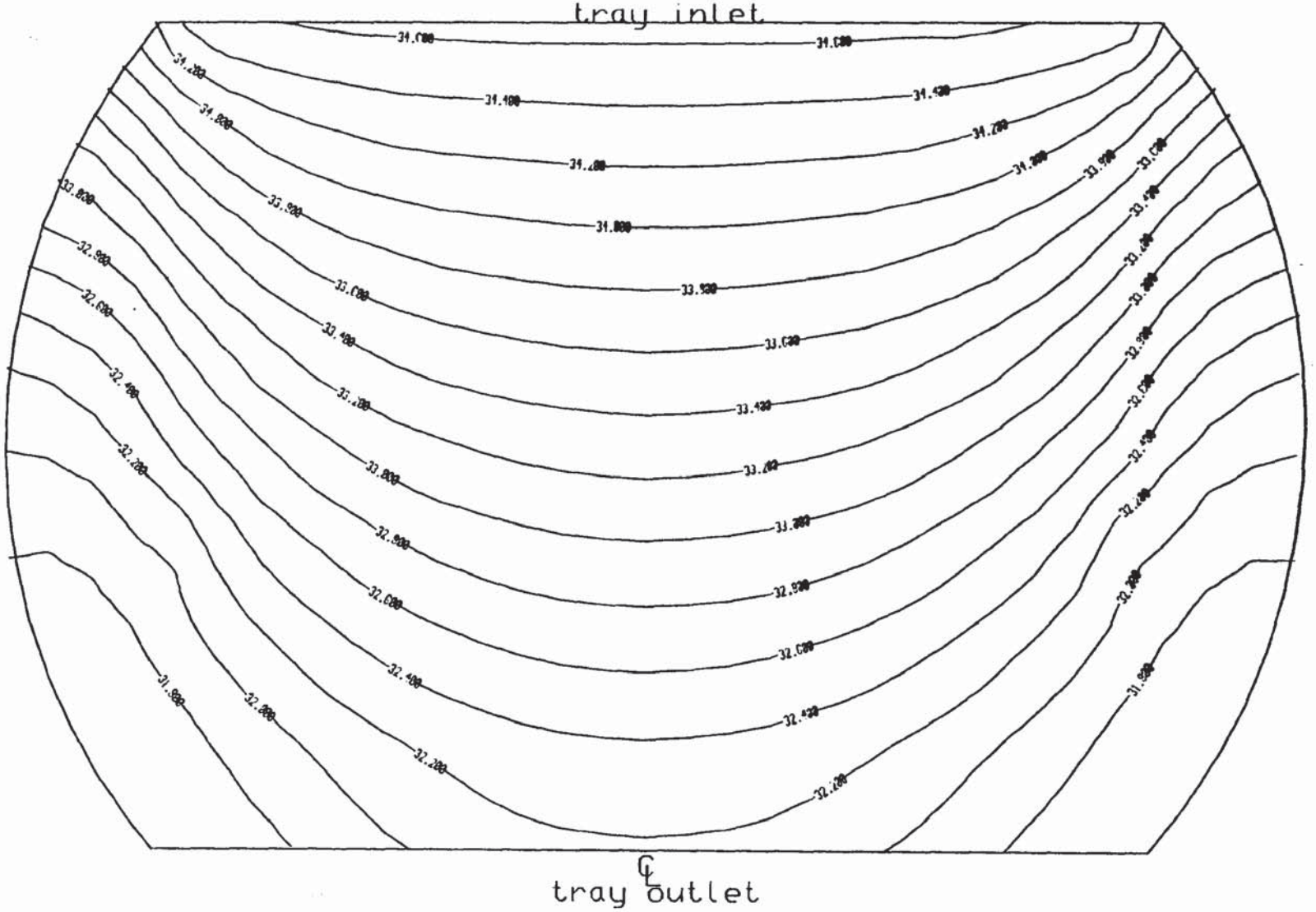

FIG:10·2a Temperature Profiles using PORTER & LOCKETT( )
Eog=92.50% λ=0.374 Pe=19.00 W/D=0.77
Predicted Emv=106.36%

Measured Temperature Profiles on a Sieve Tray

(Temperature °C)

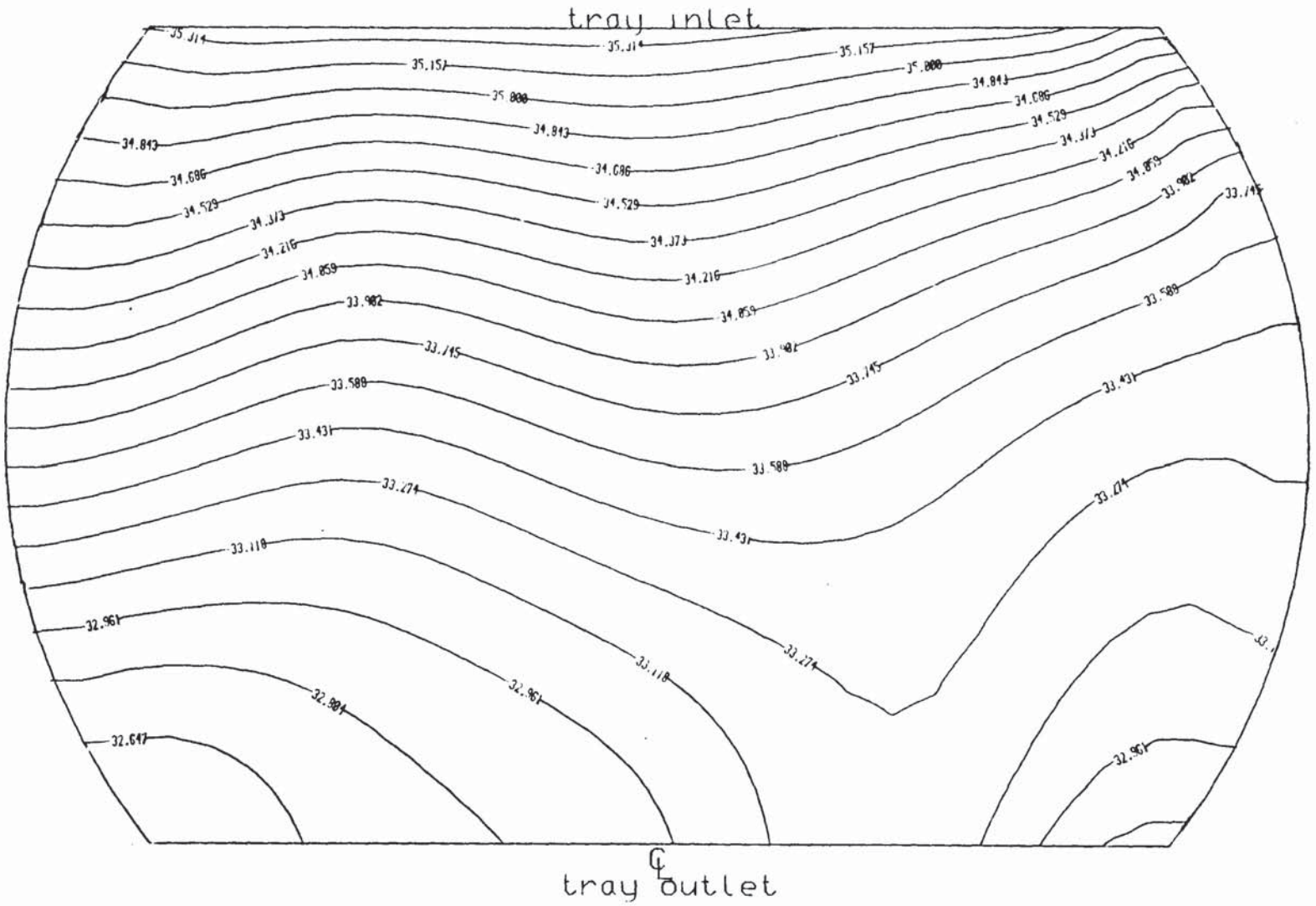

FIG: 10-2b Mixed Regime(compared with Porter & Lockett)

Csb= .0915m/s q/b= .01169m3/sm

λ = 0.374 ;Calculated Emv =102.2%

Predicted Temperature Profiles on a 1.22m Tray

(Temperature °C)

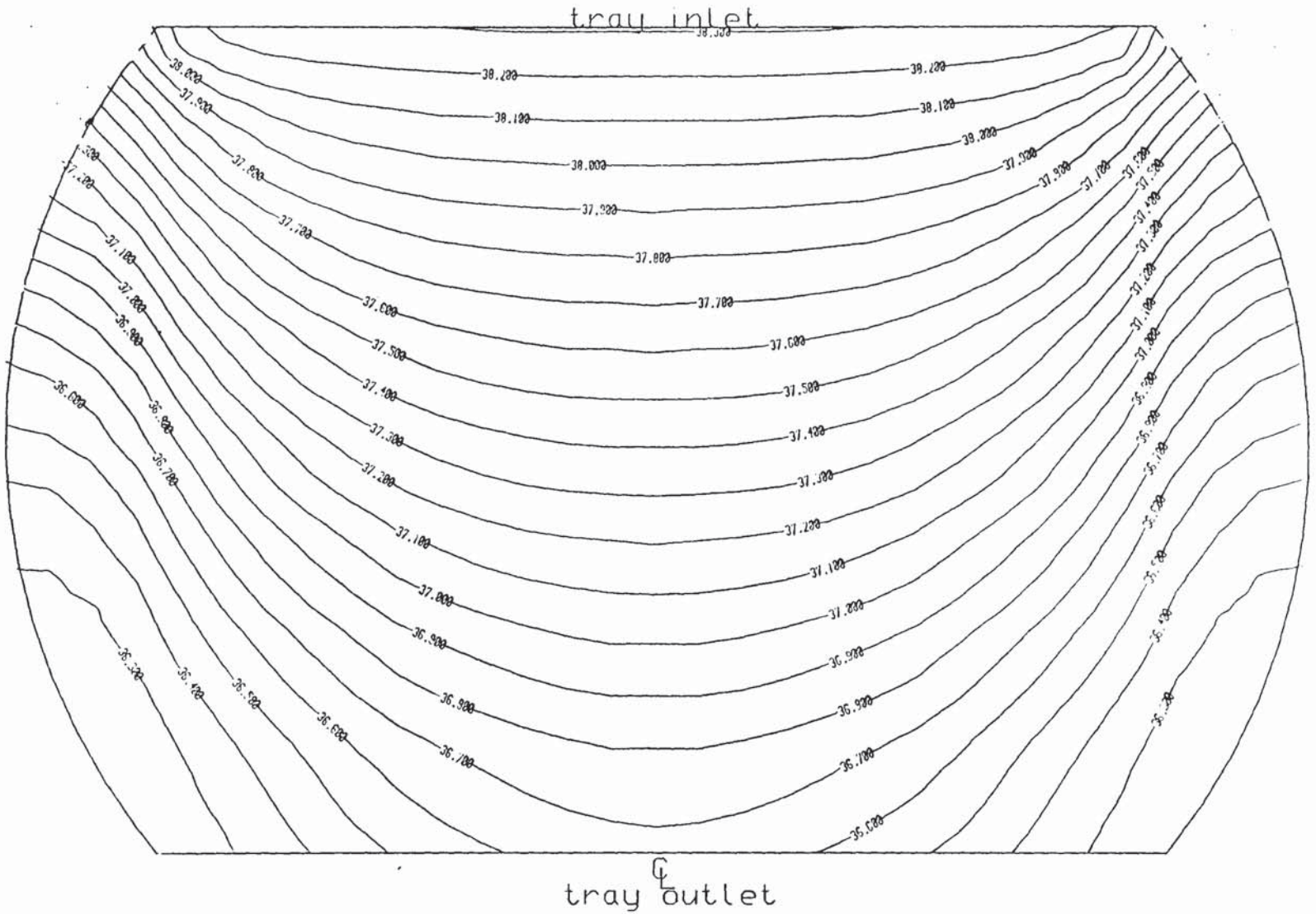

FIG:10·3a Temperature Profiles using PORTER & LOCKETT( )
Eog=65.60% λ=0.596 Pe=22.61 W/D=0.77
Predicted Emv=76.97%

Measured Temperature Profiles on a Sieve Tray

(Temperature °C)

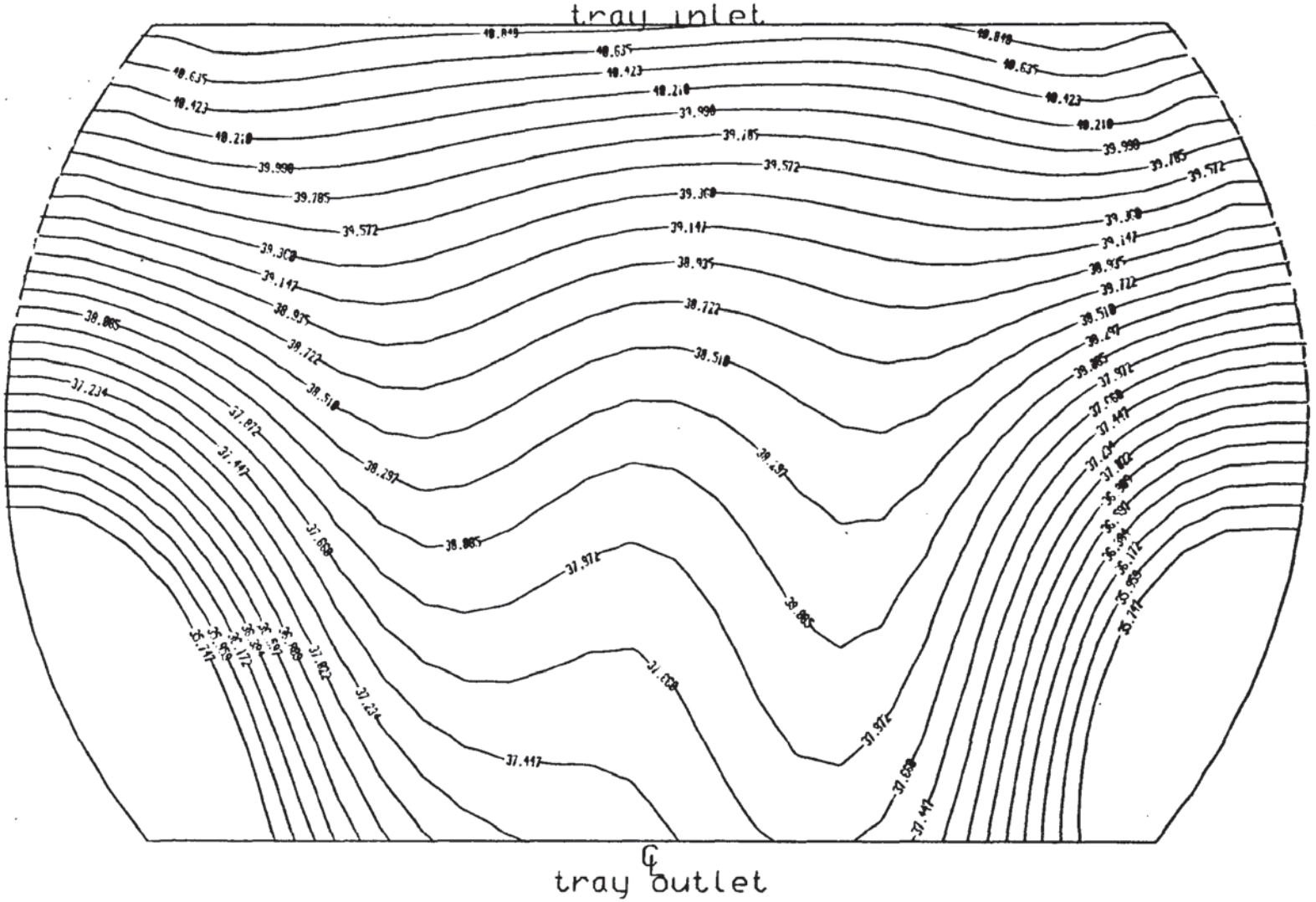

FIG:10·3b, Mixed Regime(compared with Porter & Lockett)

Csb= .0605m/s q/b= .00484m3/sm

λ = 0.596 ;Calculated Emv = 74.8%

Predicted Temperature Profiles on a 1.22m Tray

(Temperature °C)

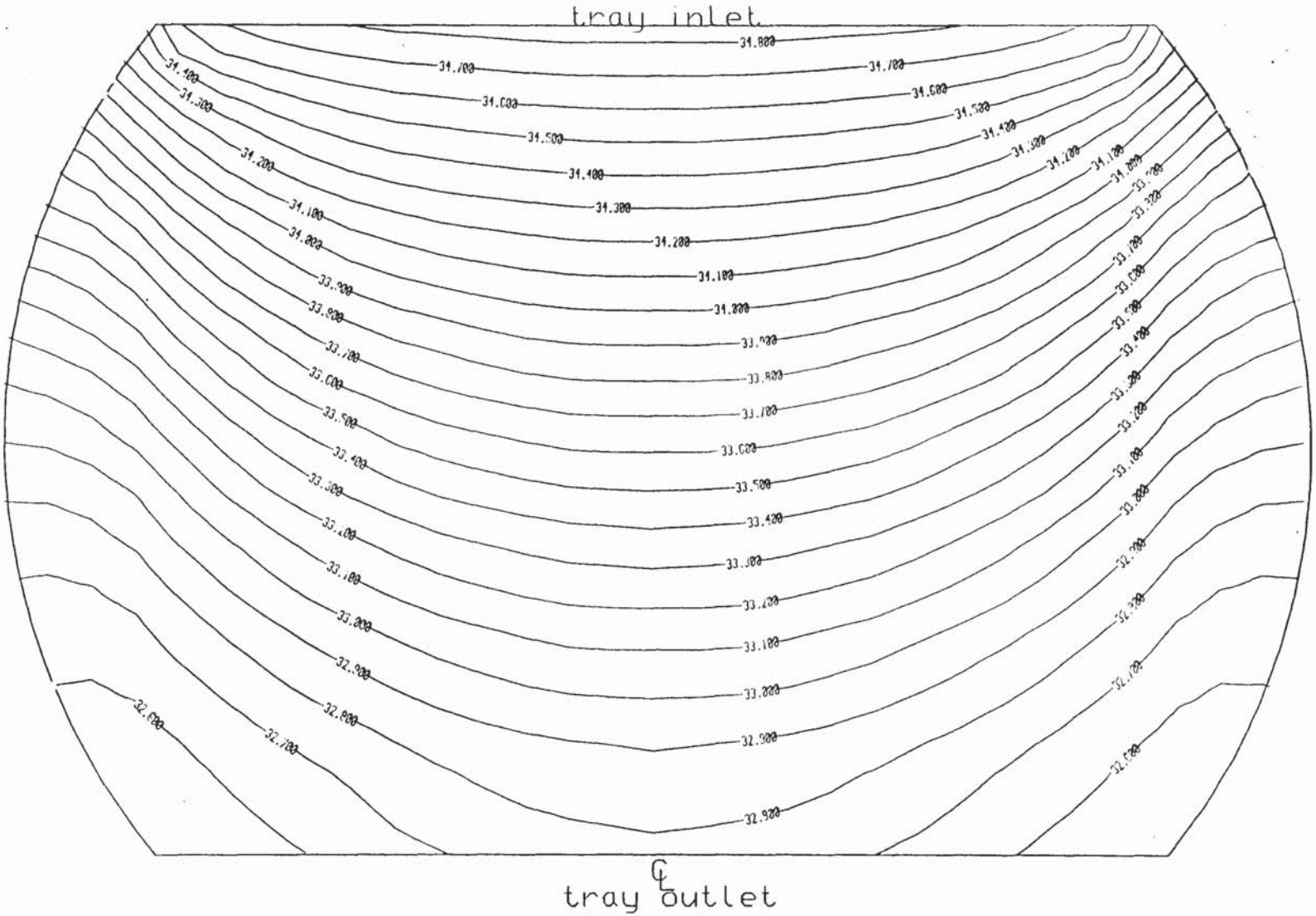

FIG 10.4a Temperature Profiles using PORTER & LOCKETT( )

Eog=68.40% λ=0.763 Pe=12.20 W/D=0.77

Predicted Emv=83.41%

Measured Temperature Profiles on a Sieve Tray

(Temperature °C)

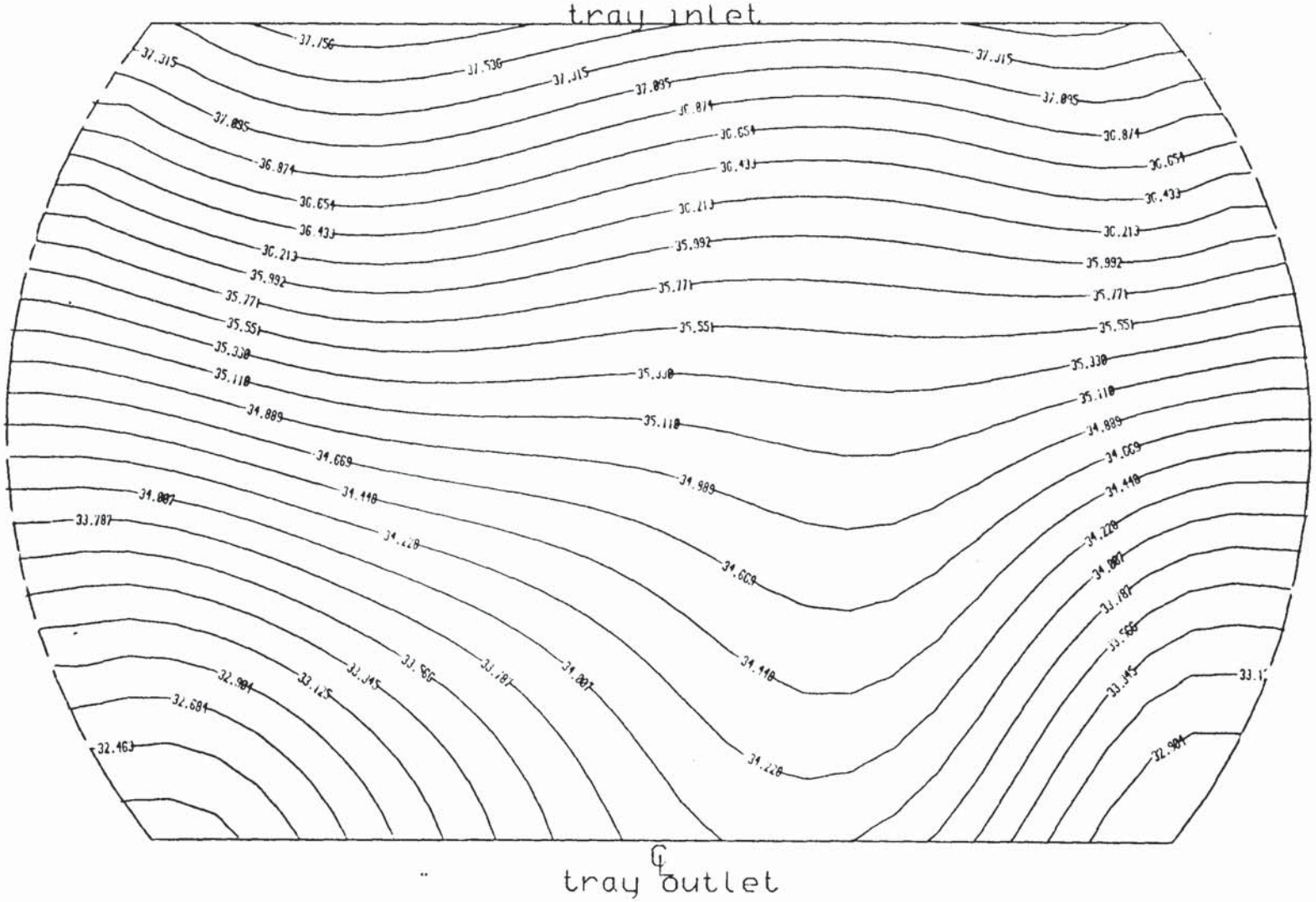

FIG:10.4b Spray Regime (compared with Porter & Lockett)

Csb= .0775m/s q/b= .00484m3/sm

λ = 0.763 ; Calculated Emv = 82.3%

10.3a. That at λ= 0.596 and a flow ratio group of ψ= 0.08, this is close to the transition line to the Spray regime has been proven in this work to have some significance to the shape but the predictive profiles do not show that distinction. The channelling model is said to be valid for systems in the Bubbly/Emulsified regime and to have limited application to systems in Spray. The experimental temperature profiles in the Spray regime in figure 10.4a are similarly flat to those for the model in figure 10.4b. The medium size of tray as well as the relatively high W/D are both expected to enhance straight profiles. Although in the water cooling technique, the value of λ is much higher in the Spray regime than it is in the Mixed regime, it will appear from the temperature profiles that the low values of the Pe number have stronger influence on the shapes of the profiles which are flat in this regime. This is because high values of the operating parameter λE_{OG} are expected to cause U-shapes rather than flat profiles while low values of Pe which means intense mixing have an opposite effect.

However, taking the comparisons a little further on account of the general findings from this work it is recalled that whereas the model does not predict severe U-shapes or indeed U-shapes for this design except for values of λE_{OG} larger than those used here, these U-shapes were also found in the experiments.

Table 10.1 Tray Efficiencies:Channelling Model & Experiment

Figure	Regime	λ	E_{OG}	$E_{MV,e}$	$E_{MV,t}$
10.1	Mixed	0.374	92.5	102.2	106.36
10.2	Spray	0.596	65.6	74.8	76.97
10.3	Spray	0.763	68.4	82.3	83.41

A noteworthy outcome of the comparisons made between the predicted channelling effects and the experimental profiles is the tray efficiencies found. The values of the tray efficiencies obtained by experiment is about the same as those derived from the model, Table 10.1. From the point of view of the technique used here the method is completely vindicated. Together with the close comparative values found by using the AIChE and the plug flow models discussed earlier in Section 8, the findings here lead to the conclusion that the flow pattern on a medium size (1.22m) tray may be approximated by the plug flow model. But perhaps for this size of tray, it is more important to determine the point efficiency accurately.

10.4 Investigating the Amount of Conductive Heat Transferred through the Column Wall

The assumption that negligible heat transfer occurs through the column wall is not a general one. It depends strongly on the material(s) of construction of the column. The object of this section is to show that for a perspex column this assumption is valid.

To do this, a hypothetical elemental strip of the froth through which the heat transferred by vapour passage is equivalent to the total quantity of heat transferred through the column wall is considered. The fraction of the tray occupied by the "strip" is directly proportional to the fraction of heat loss from strip compared to tray.

A heat balance over an element of the froth including the section of the column wall adjacent to the froth shown in figure 10.4 is made.

First the assumptions are that:

i. uniform temperature throughout the froth within the strip,

ii. negligible heat transfer to the column wall by conduction through the edge of the tray,

iii. uniform enthalpy of the air entering the tray and,

iv. heat conduction through the column wall is in the direction of the plane of the tray only.

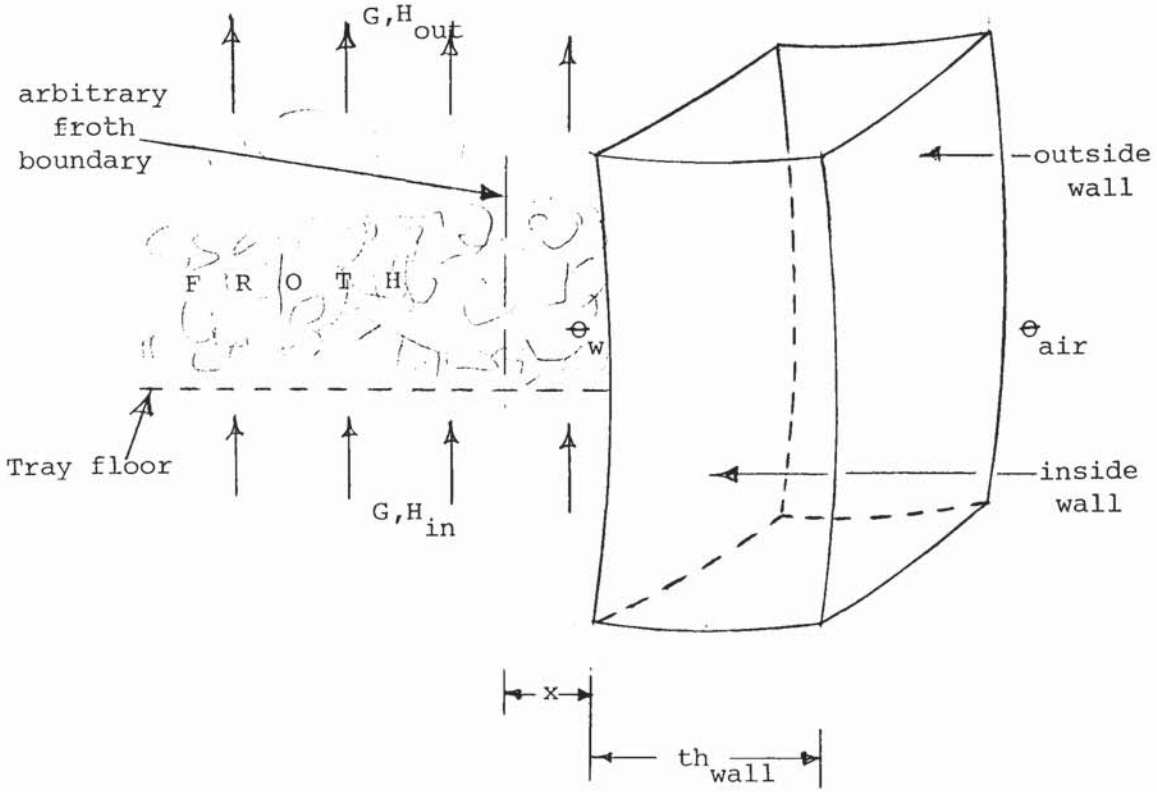

FIG:10.5 Differential element of froth and column wall used in heat balance equations

The model equation for air is ;

$$q_{air} = A_s . G'' . \Delta H \qquad 10.13$$

where G'' is the gas flow rate per unit area of tray kg / $m^2 s$. An overall balance through the element yeilds:

$$L_1 . c . \Theta = G'' . \Delta H \qquad 10.14$$

where L_1 is the liquid flow rate per unit area of tray $kg/m^2 s$. For a unit length the area of the strip is given as:

$$A_s = 1.0 * x$$

where x is the thickness of the strip (assumed rectangular).

The model of heat transfer through the column wall is given as

$$q_{wall} = K . \frac{\Theta_w - \Theta_{air}}{th_{wall}} \qquad 10.15$$

where th_{wall} is the wall thickness (m).

Rearranging;

$$x = \frac{\Theta_w - \Theta_{air}}{th_{wall}} . \frac{K}{G'' \Delta H} \qquad 10.16$$

or $$x = \frac{\Theta_w - \Theta_{air}}{th_{wall}} . \frac{K}{L_1 . c . \Theta}$$

The maximum value of x is evaluated by considering the highest possible difference in $\theta_w - \theta_{air}$ and the lowest value of $L_1.c.\Delta T$ possible from this work, simultaneously.

a. Air temperature outside the column is minimum at $\theta_{air} = \theta_{rm}$; θ_{rm} = 21.0°C. Take a highest wall temperature θ_w = 37.0°C equivalent to the water temperature at the immediate vicinity of the wall. A highest possible difference $\theta_w - \theta_{air}$ = 16.0°C is found.

b. $Q = L_1 .c.\Delta\theta$; θ_{min} = 2°C was found in the experiments in the Mixed regime.

$$L_1 .c = (0.16 - 1.5)\times10^{-2} \times 4.2$$

$$Q_{min} = L_{1,m} \times c \times \theta_{min} = 1.344\times10^{-2} kJ$$

c. Constants: i. wall thickness th_{wall} = 0.003m (1/8")

ii. K_{pers} = 1.0 - 15.0×10^{-8} kJ/s m K, reference [123].

substituting these values into the equation for x yelids

$$x = \frac{16.0}{0.003} \times \frac{15.0 \times 10^{-8}}{1.344 \times 10^{-2}}$$

$$= 5.6\times10^{-2} m$$

or $x = 5.6$ cm

So under the worst (and least probable) conditions the heat transfered through a column wall of perspex is under 10% of the total heat loss through vapour passage, which is substantial. However, if one considers the true value of K_{pers} to be 10 to 15 x less than the value assumed for the calculation above [123], the temperature difference across the wall to be half of that given and a temperature change across the tray to be up to 5x that used, then the real width of the strip would be of the order of magnitude of 0.056cm, which is negligible compared to the tray radius. That is, the wall effects have an insignificant effect on the overall flow pattern on the tray.

10.5 Estimation of the Model Parameters

The parameters W and D are fixed by the tray design.

The values of point efficiencies were those found in this work.

The slope of the equilibrium line, m is derived from the saturated air enthalpy - water temperature plot given in figure A.23. The values used for the plot were obtained from standard psychrometric charts.

The height of the froth was estimated visually, its lower limit being the height of the clear liquid on the tray.

The estimate of the froth density posed the greatest problems. This is generally defined as the ratio of the volume of clear liquid on the tray to the volume of the froth and is thus dimensionless. It is always in the range $0.0 < \rho_f < 1.0$. Low values of this parameter are expected in the Spray regime while higher values are associated with the Bubbly regime. For all practical purposes it suffices to use the ratio of the clear liquid height on the tray to the total height of froth, that is about 0.3.

Eddy diffusivity De, liquid phase is estimated by the correlation recommended in the AIChE Bubble Tray Design Manual [1].

Eddy diffusivity vapour phase was more difficult to determine confidently. There is a limited amount of information available in literature on this parameter. This may be because vapour mixing between trays is considered to play an insignificant role in the performance of trayed columns. However, the vlue of 0.093 (0.1 sq.ft/s) square meters per second is recommended in reference [71] and was adopted in this work.

10.6 Conclusions

The model equations for concentration profiles in mass transfer can be transformed to predict temperature profiles on a sieve tray.

Temperature profiles predicted from the equations all show "semi-plug flow" with no distinct stagnant regions on the tray. This conforms with the predictions for concentration profiles for a medium size 1.22m diameter tray. The experimental temperature profiles are similar in shape to those predicted by the model. However, the theory does not predict severe U-shapes of the type found in intense Spray, see Section 6.

The assumption of an impermeable wall in mass transfer theories is only valid in water cooling when poor conductivity materials such as perspex are used to construct the wall. This does not constitute a major drawback to the technique since for metal walls in industrial use, the walls can be extensively lagged.

The experimental tray efficiencies found agree with those from the channelling model thus vindicating the use of the water cooling technique for simple tray simulation experiments. Of far greater importance is the conclusion that up to this size of tray emphasis must be on the accurate determination of point efficiency rather than flow pattern.

11. DISCUSSION

The use of water cooling to investigate the performance of trays is a new technique for simulating distillation processes. It enables certain questions hitherto unanswerable by the traditional methods of study involving mass transfer variables only, to be determined in a consistent manner. These traditional methods have proved unsatisfactory due mainly to the practical limitations to the determination of the variables. These limitations do not arise when the water cooling technique is used. It is found that there is no interference to the flow of material or to heat (and mass transfer) processes on the tray, when the water cooling devices are installed. The implications of the results to tray design theory are discussed in this section. The identified limitations of the technique follow from the incoherence in the patterns of the results. These are further discussed in this section.

11.1 The Liquid Flow Patterns Related to Tray Performance

The serious gaps that exist in tray studies were considered by Porter and Jenkins [90] to be partly due to lack of an adequate classification of variables against which the performance estimates can be made. The classification adopted by the authors was also used by Zuiderweg [137]. Thus the flow ratio number was successfully used to correlate the vast FRI data. The result which separates the Spray regime, the Mixed regime and the Bubbly or Emulsified regimes has been applied to the water cooling technique in this work. The temperature profiles have shown different flow

patterns for each flow regime. Thus the flow patterns in Spray are flat or straight whereas those in the Mixed regime are U-shaped. This distinction shown by the temperature profiles is given in Section 4 and Section 6.

The implications of the distinction to tray design is far reaching. First, it is now established in literature that the structure of froth on the tray which hitherto formed the basis for distinguishing flow regimes has strong influence on the magnitude of the point efficiencies and would therefore require specific methods of estimation for each flow regime. This then demands that the flow regimes be confidently identified and distinguished and then, to fit to it the appropriate model for point efficiency. The point efficiency together with the flow pattern are used in the calculation equations for tray efficiency. The experimental results from this work go some way to confirm the notion, attributed to Porter, Lockett and Safekourdi, that separate flow patterns exist for each flow regime, and that as a result, no single generalised model can be used for all flow conditions or systems.

It was pointed out by Lockett [69] and also by Porter and Jenkins [90] that the correlations given in literature for the transition from the Spray regime are nearly all completely different. Evidence of this is presented in figure 2.13, Section 2. To the exclusion of other correlations, the results from this work showing that the flow patterns for the Spray regime are different from the ones in the Mixed regimes, justify the use of the Porter and

Jenkins correlations. Admittedly, the other correlations do not identify a Mixed regime to be between the Spray and Bubbly regimes. There is no evidence in published literature, known to this author, which shows distinctive flow patterns for separate flow regimes. Further, there is as yet no evidence of work involving the flow regimes by the correlations of Porter and Jenkins. What makes this unique correlation of particular interest to this author is that, the transition from Spray to Mixed was derived from the entrainment data of FRI and is based on the flow ratio group classification.

It was discovered and described in Section 4 and 6 that under intense Spray conditions flow patterns remniscent of severe channelling are found. Since this occurs particularly in conditions of low liquid rates and high vapour rates, high rates of entrainment are expected. Thus, this phenomenon precedes column flooding by entrainment and can therefore be used to a) simulate the point of incipient flooding in a distillation system and b) determine the mechanism of flooding by entrainment; that is, it may be detected that liquid disappears from certain areas of the tray earlier than others.

It was pointed out in Section 9 that λ changes over a wide range in water cooling when flow rates are altered while in mass transfer changes in system properties compensate for changes in flow rates within a particular system such that the range of λ is limited. However, it is predicted in both the channelling and the retrograde models described in Section 2 that U-shaped profiles

will increase with the operating parameter λE_{OG}, that is, effectively with λ. Since this is irrespective of the flow regime of the system, the discovery of the severe U-shapes in intense Spray conform to this prediction because under these conditions λ is high.

There is no question that it is only a matter of time before flow straightening devices will either be built into trays and columns or trays designed for flow straightening. An easy check for a device chosen can be made by applying the water cooling technique to it. Although the devices tested in this work and described in Section 7 showed only minor and inconclusive evidence for their effectiveness, nevertheless flow patterns from the trays were obtainable and the reasons for the unclear results are attributed to the size of the tray.

11.2 The Effect of Flow Patterns on Tray Design and Installation.

An immediate benefit of the technique could be the results in Section 4, where the experiments showed that when an operating tray is even slightly tilted, or the gap under the inlet downcomer is nonuniform, the corresponding temperature profiles were considerably skewed, see figure 4.10. As far as possible trays would be installed level but this is not always realised. Thus tray tolerance limits for installing large commercial trays can be fixed by applying this simple technique.

An implicit advantage stems from the fact that trays are designed for capacity and maximum throughput. At present there is apparent uncertainty in the relationship between hole size on sieve trays and capacity. The main advantage for designing for large holes is mechanical. It is quite clear that large holes are easier and even cheaper to fabricate and less prone to fouling which means, less maintenance requirement. However, since it is possible to change the systems flow regime simply by changing the hole size on the tray, a detailed series of water cooling experiments can lead to some useful correlation between hole size and flow regimes.

11.3 The Efficiencies

The tray performance index is its efficiency rating. Two related methods are traditionally employed to determine tray efficiency. A theoretical method, which combines point efficiency with an expected flow pattern, can be considered to be of limited reliability since neither the point efficiency nor the flow pattern is satisfactorily determined at present. A practical solution involves taking samples of separating materials at the downcomers plus a knowledge of the vapour compositions below and above the tray in question [33]. Often, these are approximated by assuming tray to tray composition gradients from the concentrations determined at the top and at the bottom of the column only. Taking samples of separating materials from an operating column presents numerous problems. Clearly both of these methods present serious difficulties and are, at best, mere approximations.

It was shown in this work, that both point and tray efficiency can be determined with little difficulty using the water cooling technique. The results of efficiencies were presented and described in Section 8. The range of values found in this work compares favourably with the ones of mass transfer and those determined by Sakata and Yanagi [102] using the Fenske-Underwood calculation method [33]. When compared specifically, with the plug flow model and the Simple Backmixing model attributed to the AIChE [1], it was found that the tray efficiencies were very nearly reproduced in both cases. This means that it suffices to use the simple plug flow model for this tray. A similar conclusion was arrived at by Zuiderweg [137] although the author used mass transfer variables in correlating the FRI data. Furthermore, when the point efficiencies and λ obtained in this work were used in the channelling model, the tray efficiencies predicted were again nearly reproducing the experimental efficiencies. What this means is that the influence of the point efficiency is dominant over flow patterns in the calculation of tray efficiency using this tray. And this is independent of the flow regime.

Although the values were satisfactory, the trend of point efficiency and indeed tray efficiency plotted against the flow ratio number was disappointing. It was found that the tray efficiencies fail to be reproduced under repeated conditions. Discrepancies as high as 25% were found. This was particularly true for low values of the wet-bulb temperature. Temperatures on the tray meanwhile were reproducible which means that the flow patterns are reliable. An errors estimate made to investigate the anomaly in efficiencies

revealed that this is due to errors in measurements of temperature. Efficiencies are very sensitive to temperature measurements. However, accurate estimates for efficiencies can be made when temperatures are measured to $\pm$ 0.1 C.

When simulating distillation systems using the water cooling technique it is identified here that the flow variable λ can have significant effects on the values of the efficiencies. The water cooling method is gas filmed control and thus similar systems in mass transfer would be expected to have point efficiencies which are not strongly dependent on λ. This is discussed in some detail in Section 8. And, unlike in mass transfer, λ can vary by as much as 10x for a given system in water cooling. Consideration must be given to this fact when simulating mass transfer systems.

11.4 Calculation Method and the Splines

It is normal to attribute any inconsistencies found in such measurements as the efficiencies to the method of calculation. The Spline approximation technique described in Section 5, an established method, was applied to this technique to calculate both the temperature profiles and the point measurements for the saturation enthalpies used for point efficiencies. Dye studies carried out on a set of trays (the large holes on this test tray meant it was not suitable to carry out similar tests on it) and reported elsewhere [3], conclusively showed that areas on the tray where the dye movement was slow, corresponded to those areas for which the temperature profiles had the least values. The results of tray

efficiencies using the various theoretical models have shown remarkable similarity with the experimental values arrived at by the calculation method. These results demonstrate that the calculation method used in this work is adequate. Furthermore, the theoretical tray efficiencies compare favourably with the experimental ones. This result means that the experimental point efficiencies used in the calculation for the theoretical tray efficiencies, were determined by correct calculation methods.

11.5 Other Experiments Relevant to Tray Design

The unfinished and thus inconclusive experiments to determine the flow over the weir described in Section 4 and Section 6 may provide some interesting information on the liquid flow pattern across the tray. It is perhaps just as important to understand the way liquid crosses the weir as it is to ensure that liquid entering the tray is evenly distributed. The weir reaction theory which proposes that liquid nonuniformities emanate from the weir, Sohio et al. has some connotations on the choice of flow straighteners used on trays. Among the devices proposed are the ones involving the uniform gap under the weir, tested and described in Section 7, and significantly the NON-uniform gap under the weir proposed by Union Carbide [130,131]. If the flow across the weir is found to be nonuniform and if it can be established that the weir reaction theory is valid then a NON-uniform gap under the weir seems attractive. However, as pointed out in Section 6 the measurements made here require further refinements to the apparatus before firm conclusions can be made on the results.

Although the results of the liquid hold-up in Section 9 were found to agree quite well with the semi-empirical correlations in literature, a detailed look at the point hold-up measurements on the tray, displayed in figure 9.1 shows that liquid accumulation appears on the tray sides appraoching the weir. Detailed measurements of this kind can be applied to investigate the "hold-up concentration gradient" proposed in the Spray Diffusion model of Porter, Lockett and Safekourdi [91]. Further use of this can be gained in correlating point efficiency with hold-up measurements and thus the now classic assumption that "point efficiency is the same everywhere on the tray" can be investigated.

The conclusions that can be drawn from this work are described in the next section.

12. CONCLUSION

The following conclusions can be drawn from this work, that:

1. the water cooling technique would give a good representation of the liquid flow patterns on a distillation tray.

2. the temperature profiles are sensitive to the tray levelness, and to the liquid distribution from the downcomer. Thus this technique can be employed as a means of setting commercial tray installation standards.

3. the temperature profiles are straight or flat for conditions in the Spray regime and U-shaped in the Mixed regime. Properly applied they can be used to identify flow regimes.

4. A new flow regime was identified in conditions of intense Spray. It is distinguished by the severe U-shapes of its temperature profiles. It occurs under low liquid loading.

5. when the stepflow downcomer and the uniform gap under the weir were incorporated onto the tray, positive changes in the flow patterns from those on the standard (conventional) tray were not evident. However, this may be due to the size of the test tray which is not sufficiently large for the effects to show on it.

6. temperature profiles predicted by the Porter and Lockett channelling model for a single tray, were similar to those found in the experiments except for the intense Spray.

7. predicted tray efficiencies are similar in magnitude to the experimental tray efficiencies. Although this is an expected result, nevertheless it justifies the use of the technique as well as the calculation method by Spline approximation.

8. unlike in mass transfer for a gas film control process, it was found that point efficiency changed with the flow variable λ in water cooling.

9. whereas repeated experiments would give similar temperature profiles, the tray efficiencies are not reproducible. This is because the acuracy requirement for measurements of temperature ffor tray efficiency was inadequate in the experiments. The level of accuracy required for temperature measurements is at least a tenth of a degree centigrade (0.1 C) in order to implement this technique to determine efficiencies.

10. Conditions favouring high temperature drops across the tray, give reliable water cooling efficiencies. Such conditions are found in the Spray regime and are expected in large trays.

SYMBOLS USED

Symbols defined and used locally are not included here.

a	interfacial area of froth
A	bubbling area of tray (m^2)
b	weir length (m)
c	specific heat (kcal/(kg°C))
CF	capacity factor, $CF = u_{sb}/\sqrt{(\rho_V/\rho_L - \rho_V)}$, (m/s)
C_{sb}	load factor: $u_{sb}\sqrt{\left(\frac{\rho_V}{\rho_L - \rho_V}\right)}$ (m/s)
d_h	tray hole diameter (m)
D	tray diameter (m)
D_e	eddy diffusivity (m^2/s)
F	F-factor= $u_{sb}\sqrt{(\rho_V/\rho_L)}$ (m/s)
E_{MV}	Murphree tray efficiency, vapour phase
E_{OG}	Point efficiency, vapour phase
E_o	overall column efficiency
G	-mass transfer; vapour rate (kg mole/s)
	-heat transfer; vapour rate (kg/s)
h_L	liquid hold-up (cm)
h_F	height of froth (m)

H enthalpy of vapour (kcal/kg)

H^* saturation enthalpy of vapour (kcal/kg)

K_{OG} overall mass transfer coefficient in gas phase (m/s)

k_L mass transfer coefficient in liquid phase (m/s)

k_G mass transfer coefficient in gas phase (m/s)

L - in mass transfer; liquid rate (kg mole /s)

- in heat transfer; liquid rate (kg/s)

Le Lewis number = $\frac{Sc}{Pr}$

m - in mass transfer; slope of the equilibrium concentration line

- in heat transfer; slope of the saturation enthalpy line

N number of actual trays in column

N_T number of theoretical trays in column

N_G number of gas phase transfer units

N_L number of liquid phase transfer units

N_{OG} overall number of transfer units, gas phase

Pe Peclet number

r finite length element in radial direction

t temperature (°C)

T temperature function (°C)

th wall thickness (m)

u gas velocity (m/s)

x liquid concentration mole fraction

x_l liquid concentration leaving plate no. l

x_e^* liquid concentration in equilibrium with vapour

X dimensionless liquid concentration

y vapour concentration mole fraction

y^* concentration of vapour in equilibrium with liquid

Z distance between downcomers (m)

$\lambda = \frac{mG}{L}$

ρ_F froth density (m^3 of liquid / m^3 of froth)

ρ_G or ρ_V vapour density (kg/m^3)

ρ_L liquid density (for clear liquid) (kg/m^3)

ψ flow ratio group $= (q/b)\sqrt{\left(\frac{\rho_V}{\rho_L - \rho_V}\right)}$

Subscripts

in inlet

l initial

f final

r reduced

o(out) outlet

G gas

L liquid

OG overall gas

A Glossary of Terms

AIChE The American Institution of Chemical Engineers

FRI Fractionation Research Incorporated - An American Research Organisation based in California

RTD Residence Time Distribution

FLOODING occurs when an excessive amount of liquid is carried over from one tray to the next, or when the system is not able to convey the liquid from one tray to the one below it.

WEEPING occurs when the vapour rate is not large enough to hold all the liquid on the tray, so that only part of it flows over the outlet weir while the rest falls through the openings in the tray.

CROSSFLOW is the term used to denote the relative directions of the planes of travel of the liquid and gas (vapour) phases, within a contacting device.

by PHYSICAL PROPERTIES, the properties referred to are density; normal boiling point; surface tension; viscosity and molecular weight.

REFERENCES

[1] AIChE "Bubble Tray Design Manual:Prediction of Fractionation Efficiency" 1958 (New York:American Institution of Chemical Engineers)

[2] Ani,C.C. M.Sc. thesis 1984,University of Aston in Birmingham

[3] Ani,C.C. 17th Annual Chem.Engng.Dept. Symp.,1986 Univ. of Aston, Birmingham

[4] Arnold,D.S.,Plank,C.A.,Schoenborn,E.M. Chem.Eng.Progr., 1952,48,633

[5] Balfour,A.,Marwick,D.H. Programming in Standard Fortran 77, 1979 (ed) Heinemann Educational Books:London

[6] Barber,A.D.,Wijn,E.F. Instn.Chem.Engrs Symp.Ser., 1979,56,3.1/15

[7] Barker,P.E.,Self,M.F. Chem.Engng.Sci.,1962,17,541

[8] Barsky,B.A. IEEE CG & A,1984,38

[9] Bell,R.L. AIChE Journal,1972,18,No.3,491

[10] Bell,R.L. AIChE Journal,1972,18,No.3,498

[11] Bell,R.L.,Solari,R.B. AIChE Journal,1974,20,688

[12] Bezier,P.E. Emploi des Machines a Commande numerique.Masson et Cie.,Paris,1970.Published in English as : Numerical Control-Mathematics and Applications, Robin A. Forest and Anne F. Pankhurst,trans., John Wiley and Sons:London,1972

[13] Biddulph,M.W.,Stephens,D.J. AIChE Journal,1974,20,No.1,60

[14] Burgess,R.G.,Robinson,K. Instn.Chem.Engrs.Symp Ser., 1969,32,2:34

[15] Carrier,W.H. Trans ASME,1911,33,1025

[16] Carrier,W.H. Trans ASHVE,1918,24

[17] Chandrasekhar,S. Reviews of Modern Physics,1943,15,4

[18] Chase,J.D. Chem.Eng.1967,74,No.16,105,No.18,139

[19] Computer Aided Design Centre,Cambridge,U.K

[20] Comark Electronics Limited, England

[21] Coons,S.A. "Surface Patches and B-Spline Curves," Computer Aided Geometric Design,Robert E. Barnhill and Richard F. Riesenfeld,eds.,1974,pp.95-126, Academic Press:New York

[22] Cox,M.G. J.Inst.Maths Applics 1972,10,134

[23] Curry,H.B.,Schoenberg,I.J. J.d Analyse Mathematique, 1966,17,71

[24] Danckwerts,P.V. Chem.Engng.Sci.,1953,2,No.1,1

[25] Danckwerts,P.V. Gas-Liquid Reactions. McGraw Hill:London 1970 (Ed.)

[26] Davies,B.T. Ph.D thesis,1965,University of Birmingham

[27] Diener,D.A. Ind.& Eng.Chem.,Process Des.& Dev.,1967,6,499

[28] Electrical Measuring Instruments Croydon Precision Instruments Co., England

[29] Fair,J.R. Petro/Chem Engr.,1961,33,Part 10,Sept,45

[30] Fair,J.R.,Smith,B.D. Design of Equilibrium Stage,Proceses, 1963,pp.551,McGraw Hill,New York

[31] Fair,J.R.,Bolles,W.L. Chem Engng. 1968,75,April,167

[32] Fane,A.G.,Sawistowski,H. Instn.Chem.Engr.Symp.Ser.,1969, 1969,32,1:8

[33] Fenske,M.R. Ind.Eng.Chem. 1932,24,482

[34] Finkbeiner,D.T.(II). Introduction to Matrices and Linear Transformations,1966,2nd Ed.,pp.88, W.H.Freeman and Company:San Francisco

[35] Forest,R.A. Computer Graphics and Image Processing, 1972,1,No.4,341

[36] Foss,A.S.,Gerster,J.A.,Pigford,R.L. AIChE Journal,1958,4,231

[37] Gautreaux,M.F.,O Connell,H.E. Chem.Eng.Progr.,1955,51,232

[38] Gerald,C.F. Applied Numerical Analysis,1978,2nd Ed., p 209-217,Addison-Wesley:London

[39] Gerster,J.A.,Hill,A.B.,Hochgraf,N.N.,Robinson,N.G. "Tray Efficiencies in Distillation Columns" Final Report from University of Delaware,1958.(New York:American Institution of Chemical Engineers)

[40] Guildline Intruments Limited,Canada (1984)

[41] Goederen,C.W.J. de, Chem.Eng.Sci.1965,20,115

[42] Golub,G. Num.Math.,1965,7,206

[43] Gordon,W.J.,Riesenfeld,R.F. Computer Aided Geometric Design, Robert E. Barnhill and Richard F. Riesenfeld,eds., 1974,pp.95-126,Academic Press:New York

[44] Greville,T.N.E. Introduction to Spline Functions:In Theory and Applications of Spline Functions,1969,eds T.N.E. Greville.New York:Academic Press

[45] Gurney,J.D.,Cotter,I.A. Cooling Towers.,1966 (ed),pp 16-58 Maclaren & Sons Ltd: London

[46] Hayes,J.G.,Halliday,J. J.Inst.Maths Applics.,1974,14,89

[47] Harris,I.J.,Roper,G.H. Can.J.of Chem.Eng.,1962,40,245

[48] Ho,G.E.,Muller,R.L.,Prince,R.G.H. Chem.Eng.Sci.,1972,27,1583

[49] Hofhuis,P.A.M.,Zuiderweg,F.J. Instn.Chem.Engrs Symp.Ser.1979, 56,2.2/1

[50] Householder,A.S. J.Ass.Comput. Mach.1958,5,339

[51] Humphreys,W.J. Physics of the Air,1940,3rd Ed., McGraw Hill:New York

[52] Hunt,C.A.,Hanson,D.W.,Wilke,C.R. 1955,AIChE Journal,1,441

[53] Hutchinson,W.K.,Spivey,E. Trans.Instn.Chem.Engrs.,1942,20,14

[54] Johnson,A.I.,Marangozis,J. Can.J.Chem.Engrs.,1958,36,161

[55] Kafarov,V.V.,Shestopalov,V.V.,Komissarov,Y.A. Instn.Chem. Engrs.Symp.Ser. 1979,56,2.3/79

[56] Kastanek,F.,Standart,G. Separation Science,1967,2,439

[57] Keller,G.J.,Yanagi,T. Film presented at 68th National Meeting AIChE 1970

[58] Kirschbaum,E. Destillier und Rektifier Technik,4^{e} Auflage Springer,Verlag,Berlin,1969

[59] Kirschbaum,E. Distillation and Rectification 1948,p.276, Chemical Publishing Co.,New York

[60] Kirschbaum,E. Forsch.Gebiete.Ingenieurer,1934,5,245

[61] Kouri,R.J.,Sohlo,J. 1981,Paper 44e,AIChE 90th National Meeting, Houston

[62] Kouri,R.J.,Sohlo,J. 1982,"The Effect of Developing Liquid Patterns on Distillation Plate Efficiency," paper presented at EFCE Working Party on Distillation,Absorption & Extraction ,Helsinki

[63] Kouri,R.J.,Sohlo,J. "The Effect of Developing Liquid Flow Patterns on Distillation Plate Efficiency" (Submitted for publication)

[64] Lane,M.J.,Riesenfeld,R.F. "Bounds on a Polynomial," BIT, 1981,21,No.1,112

[65] Lewis,W.K. Jr. Ind.Eng.Chem.,1936,28,399

[66] Lewis,W.K. Jr. Trans ASME 1922,44,325

[67] Lim,C.T. Ph.D thesis,1973,University of Manchester Institute of Science and Technology

[68] Lim,C.T.,Porter,K.E.,Lockett,M.J. Trans.Instn.Chem.Engrs., 1974,52,193

[69] Lockett,M.J. Trans.Instn.Chem.Engrs.,1981,59,26

[70] Lockett,M.J.,Lim,C.T.,Porter,K.E. Trans.Instn.Chem.Engrs., 1973,51,61

[71] Lockett,M.J.,Porter,K.E.,Basson,K. Trans.Instn.Chem.Engrs., 1975,53,125

[72] Lockett,M.J.,Spiller,G.T.,Porter,K.E. Trans.Instn.Chem. Engrs.1976,54,202

[73] Mayfield,F.P.,Church,W.L.,Green,A.C.,Lee,D.C.,Rasmussen,R.W., Ind.Eng.Chem.,1952,2238

[74] McKelvey,K.K.,Brooke,M. The Industrial Cooling Tower,1959, Elsevier:London

[75] Merkel,F.,VDI Forscchungsh.,1925,No.275

[76] Merkel,F.,VDI Zeitschrift,1926,70,No.4,123

[77] Microlink Users Manual, 1983,Biodata Limited,England

[78] Muller,R.L.,Prince,R.G.H. Chem.Eng.Sci.,1972,27,1583

[79] Murphree,E.V. J.Ind.Eng.Chem.,1925,17,747

[80] Norton Chemical Process Products (Europe) Limited
Stroke-on-Trent, England

[81] Numerical Algorithm Group Ltd,Oxford,U.K.
,NAGFLIB:1476/0:Mk6:Dec78 E02,Curve & Surface Fitting

[82] Oliver,E.D.,Watson,C.C. AIChE Journal,1956,2,18

[83] Payne,G.J.,Prince,R.G.H. Trans.Instn.Chem.Engrs.,1975,53,209

[84] Payne,G.J.,Prince,R.G.H. Trans.Instn.Chem.Engrs.,1977,55,266

[85] Perry,R.H.,Green,D. Perry s Chemical Engineers Handbook
1984,6th ed.,pp.20-6

[86] Pinckzewski,W.V.,Fell,C.J.D. Trans.Instn.Chem.Engrs.,
1972,50,102

[87] Pinczewski,W.V.,Fell,C.J.D. Trans.Instn.Chem.Engrs.,
1977,55,46

[88] Porter,K.E. "Patent on Stepflow Downcomer"
Private Communications

[89] Porter,K.E.,Lockett,M.J.,Lim,C.T. Trans.Instn.Chem.Engrs.,
1973,50,91

[90] Porter,K.E.,Jenkins,J.D. Instn.Chem.Engr.Symp.Ser.,1979,56,75

[91] Porter,K.E.,Safekourdi,A.,Lockett,M.J. Trans.Instn.Chem.
1977,55,190

[92] Porter,K.E.,Wong,P.F.Y. Instn.Chem.Engrs.Symp.Ser.,
1977,32,2:22

[93] Prince,R.G.H.,Jones,A.P.,Panic,R.J. Instn.Chem.Engrs.Symp.
Ser.,1979,56,3.1/15

[94] Raper,J.A. Ph.D. thesis, 1979, University of New South Wales

[95] Raper,J.A.,Hai,N.T.,Pinczewski,W.V.,Fell,C.J.D. Instn.Chem. Engrs.Symp.Ser.,1979,56,2.2/57

[96] Raper,J.A.,Kearney,M.S.,Burgess,J.M.,Fell,C.J.D. Chem.Engng.Sci.,1982,37,No.4.,501

[97] Raper,J.A.,Pinczewski,W.V.,Fell,C.J.D.Chem.Eng.Res.Des., 1984,62,111

[98] Reid,J.K. Comput.J. 1967,10,188

[99] Robinson,C.S.,Gilliland,E.R. "Elements of Fractional Distillation",1950,4th ed.,McGraw-Hill:New York

[100] Rush,F.E. Jr. Instn.Chem.Engrs Symp.Ser. 1979,56,4.1/1

[101] Safekourdi,A. Ph.D. thesis,1976,University of Manchester Institution of Science and Technology

[102] Sakata,M.,Yanagi,T. Instn.Chem.Engrs.Symp.Ser., 1979,56,3.2/21

[103] Sakata,M.,Yanagi,T. Data presented at : Instn.Chem.Engrs.Symp.Ser.,1979,56

[104] Shakov,Yu A.,Noskov,A.A.,Romankov,P.G. Zh.prikl.Khim., Leningr.,1964,37,2055

[105] Sharma,M.M.,Gupta,R.K. Trans.Instn.Chem.Engrs.,1967,45,T169

[106] Schoenberg,I.J. Quarterly Applied Math.,1946,4,No.1,45 & 112

[107] Schumaker,L.L. Theory and Application of Spline Functions, 1969,65-102.In T.N.E.Greville(Ed.) New York:Academic Press

[108] Silvey,F.C.,Keller,G.J. Chem.Eng.Progr.,1966,62,68

[109] Sohlo,J.,Kinnunen,S. Trans.Instn.Chem.Engrs.,1977,55,71

[110] Sohlo,J.,Kourl,R.J. 71st AIChE Annual Meeting,Miami,
1978,No.73b

[111] Sohlo,J.,Kourl,R.J. Chem.Engng.Sci. 1982,37,193

[112] Solari,R.B.,Bell,R.L. "The Effects of Transverse Eddy
Dispersion on Distillation Efficiency",
March 1978,paper No.46f presented to the
84th National Meeting AIChE,Atlanta

[113] Solari,R.B.,Bell,R.L. "Liquid Flow Patterns and Velocity
Distribution on Commercial Scale Sieve Trays",
(submitted for publication-1982)

[114] Solari,R.B.,Saez,E.,D Apollo,I.,Bellet,A. Chem.Eng.Commun.,
1982,13,369

[115] Spalding,D.B. Convective Mass Transfer,1963(Ed),
Edward Arnold:London

[116] Spiegel,M.R. Theory and Problems of Probability and
Statistics,1980,pp155-210,McGraw-Hill:London

[117] Smith,B.D. Design of Equilibrium Stage Processes,1963
pp.401 McGraw-Hill:New York

[118] Smith,V.C.,Delnicki,W.V. Chem.Engng.Progr.,1975,71,68

[119] Stamford,W.,Hill,G.B. Cooling Towers:Principles and Practice
,1966 (ed) pp 99-134 Carter Thermal Engineering
Limited;Birmingham,U.K.

[120] Stilchmair,J.,Weisnaam,E. Chemie-Ing.-Techn.45.Jahrg.
1973/Nr.5

[121] Taylor,J.R. An Introduction to Error Analysis,1982,pp 40-74, University Science Books:Mill Valley,CA,USA

[122] The Modular Computer Interface, Microlink Biodata Limited, England

[123] The TPRC Data Series:Thermodynamic Properties of Matter,1970 ,Vol.2,p.960,IFI/Plenum Data Corporation:New York

[124] Topping,J.R. Errors of Observation and their Treatment,1955, (ed) Union Brothers Limited:London

[125] Van Winkle,M. "Distillation",1967(Ed),McGraw-Hill:New York

[126] Walter,J.F.,Sherwood,T.K. Ind.Eng.Chem.,1941,33,493

[127] Warzel,L.A. Ph.D. thesis,1955,University of Michigan

[128] Weast,R.C. CRC Handbook of Chemistry and Physics,1984-1985, 65th Ed.,pp E-94.,CRC Press,Inc.:Florida

[129] Wehner,J.F.,Wilhelm,R.H. Chem.Engng.Sci.,1956,6,89

[130] Weller,D.W.,Delnicki,W.V.,England,B.L. Chem.Engng.Progr., 1971,69,67

[131] Weller,D.W.,Leanitt,F.W.,Bonnet,F.W. Paper presented at the AIChE 68th National Meeting,Houston,Feb-March,1968

[132] Williams,B.,Begley,J.W.,Wu,C.H. Tray Efficiencies in Distillation Columns,Final Report,1960 University of Michigan

[133] Wood,B.,Betts,P. Engineer,1950,189,337-349

[134] Yanagi,T. "Distillation Research in a High Vacuum Pilot Plant",AIChE 59th Annual Meeting,Detroit December,1966

[135] Yanagi,T.,Scott,B.D. Chem.Eng.Progr.,1973,69,No.10, October,75

[136] Zimmermann,O.T.,Lavine,I. Psychrometric Tables and Charts, 1945,Ind.Research Service,Dover,New Hampshire

[137] Zuiderweg,F.J. Chem.Engng.Sci. 1982,37,No.10,1441

[138] Zuiderweg,F.J.,Groot,J.H. de ,Meeboer,B.,Meer,D.van der , Instn.Chem.Engrs Symp.Ser.,1969,32(5),78

[139] Zuiderweg,F.J.,Harmens,A. Chem.Engng.Sci.,158,9,89

[140] Zuiderweg,F.J.,Hofhuis,P.A.M.,Kuzniar,J. Anaheim Meeting, AIChE,June 1982

APPENDIX A

TABLE A1

RESULTS OF TEMPERATURE MEASUREMENTS
IN THE MIXED REGIME

RUN M1:- FLOW RATES: C_{sb} = 0.0745m/s q/b = 1.543x10E-2 m^3/sm

ENTERING AIR ENTHALPY H_{in} = 11.59kcal/kg

temperature C

	37.00	37.00	37.00	37.00	37.00	37.00	
36.92	36.92	36.86	36.56	36.80	36.98	36.56	36.56
35.33	35.33	35.22	35.78	35.80	35.29	35.39	35.39
35.02	35.02	34.78	35.02	35.07	34.53	34.72	34.72
32.58	32.58	32.58	34.41	34.41	33.00	33.00	34.10
33.33	33.33	34.84	34.84	33.49	33.49	33.49	

RUN M2:- FLOW RATES: C_{sb} = 0.0660m/s q/b = 0.628x10E-2 m^3/sm

ENTERING AIR ENTHALPY H_{in} = 11.80kcal/kg

	40.05	40.05	40.05	40.05	40.05	40.05	
39.64	39.64	39.94	39.84	39.88	39.90	39.09	39.09
32.51	32.51	36.95	38.69	35.82	38.63	32.64	32.64
32.09	32.09	35.48	36.92	35.27	36.12	32.24	32.24
31.54	31.54	31.54	33.99	33.99	34.48	34.48	33.07
32.34	32.34	34.54	34.54	31.67	31.67	31.67	

RUN M3:- FLOW RATES: C_{sb} = 0.0660m/s q/b = 1.227x10E-2 m^3/sm

ENTERING AIR ENTHALPY H_{in} = 12.10kcal/kg

	36.20	36.20	36.20	36.20	36.20	36.20	
35.17	35.17	34.87	35.60	35.35	35.09	35.35	35.35
32.63	32.63	33.08	33.57	34.62	32.65	32.68	32.68
31.71	31.71	33.46	33.33	33.82	32.78	31.68	31.68
30.33	30.33	30.33	32.59	32.59	32.36	32.36	33.04
32.35	32.35	32.02	32.02	30.64	30.64	30.64	

RUN M4:- FLOW RATES: C_{sb} = 0.0745m/s q/b = 0.638x10E-2 m^3/sm

ENTERING AIR ENTHALPY H_{in} = 11.60kcal/kg

	39.35	39.35	39.35	39.35	39.35	39.35	
38.42	38.42	38.97	38.36	37.26	38.87	38.05	38.05
33.59	33.59	36.22	37.30	37.03	34.89	33.37	33.37
31.29	31.29	33.61	36.05	35.50	34.59	30.80	30.80
31.11	31.11	31.11	33.00	33.00	33.50	33.50	33.00
33.65	33.65	33.21	33.21	30.62	30.62	30.62	

TABLE A cont.

RUN M5:- FLOW RATES: C_{sb} = 0.0820m/s q/b = 1.400x10E-2 m^3/sm

ENTERING AIR ENTHALPY H_{in} = 11.46kcal/kg

	36.57	36.57	36.57	36.57	36.57	36.57	
36.19	36.19	36.19	35.80	35.77	35.58	35.64	35.64
33.51	33.51	34.86	34.37	35.01	35.34	33.60	33.60
32.18	32.18	33.87	34.18	34.00	33.70	32.00	32.00
30.95	30.95	30.95	33.57	33.57	33.65	33.65	33.78
33.67	33.67	33.12	33.12	30.40	30.40	30.40	

RUN M6:- FLOW RATES C_{sb} = 0.0745m/s q/b = 0.867x10E-2 m^3/sm

ENTERING AIR ENTHALPY H_{in} = 11.90kcal/kg

	36.96	36.96	36.96	36.96	36.96	36.96	
36.58	36.58	36.46	36.58	36.40	36.11	36.03	36.03
33.96	33.96	34.81	35.74	34.26	33.81	33.44	33.44
33.18	33.18	33.63	33.91	33.79	33.66	33.02	33.02
31.89	31.89	31.89	32.69	32.69	33.18	33.18	32.84
32.76	32.76	32.15	32.15	31.65	31.65	31.65	

RUN M7:- FLOW RATES: C_{sb} = 0.0695m/s q/b = 0.649x10E-2 m^3/sm

ENTERING AIR ENTHALPY H_{in} = 11.18kcal/kg

	39.30	39.30	39.30	39.30	39.30	39.30	
38.75	38.75	38.32	37.59	37.28	38.24	38.93	38.93
31.48	31.48	36.79	37.74	36.87	36.39	32.20	32.20
31.04	31.04	34.26	37.01	35.23	36.15	31.81	31.81
30.96	30.96	30.96	34.20	34.20	34.81	34.81	34.67
33.63	33.63	35.54	35.54	30.69	30.69	30.69	

RUN M8:- FLOW RATES: C_{sb} = 0.0745m/s q/b = 1.064x10E-2 m^3/sm

ENTERING AIR ENTHALPY H_{in} = 10.99kcal/kg

	38.00	38.00	38.00	38.00	38.00	38.00	
37.28	37.28	36.79	37.28	37.53	36.85	36.85	36.85
33.92	33.92	35.08	35.56	35.00	35.75	34.02	34.02
33.65	33.65	34.96	35.32	34.96	35.14	33.79	33.79
32.18	32.18	32.18	34.16	34.16	34.77	34.77	33.02
33.98	33.98	34.65	34.65	32.75	32.75	32.75	

TABLE A cont.

RUN M9:- FLOW RATES: C_{sb} = 0.0745m/s q/b = 0.745x10E-2 m^3/sm

ENTERING AIR ENTHALPY H_{in} = 11.60kcal/kg

	38.75	38.75	38.75	38.75	38.75	38.75	
38.40	38.40	37.66	38.09	38.33	38.34	38.03	38.03
32.43	32.43	35.77	36.54	34.92	36.57	35.47	35.47
32.11	32.11	34.49	36.08	34.45	34.37	32.29	32.29
30.46	30.46	30.46	33.45	33.45	33.63	33.63	33.53
33.82	33.82	33.67	33.67	31.00	31.00	31.00	

RUN M10:- FLOW RATES: C_{sb} = 0.0565m/s q/b = 0.638x10E-2 m^3/sm

ENTERING AIR ENTHALPY H_{in} = 11.00kcal/kg

	41.30	41.30	41.30	41.30	41.30	41.30	
40.75	40.75	40.26	40.02	40.93	38.92	40.02	40.02
35.31	35.31	39.83	39.29	39.59	39.66	35.50	35.50
35.38	35.38	36.82	36.97	37.21	37.19	35.63	35.63
35.87	35.87	35.87	35.99	35.99	37.03	37.03	37.33
37.03	37.03	36.25	36.25	34.77	34.77	34.77	

RUN M11:- FLOW RATES: C_{sb} = 0.0800m/s q/b = 0.604x10E-2 m^3/sm

ENTERING AIR ENTHALPY H_{in} = 12.07kcal/kg

	39.49	39.49	39.49	39.49	39.49	39.49	
37.96	37.96	38.15	39.12	38.39	38.94	38.45	38.45
36.80	36.80	37.17	36.68	36.80	36.13	36.00	36.00
32.75	32.75	35.19	35.00	35.37	33.08	31.06	31.06
32.38	32.38	32.38	33.72	33.72	34.09	34.09	32.50
33.84	33.84	32.56	32.56	30.42	30.42	30.42	

RUN M12:- FLOW RATES: C_{sb} = 0.0540m/s q/b = 0.403x10E-2 m^3/sm

ENTERING AIR ENTHALPY H_{in} = 10.90kcal/kg

	40.66	40.66	40.66	40.66	40.66	40.66	
39.92	39.92	39.52	38.88	39.49	40.11	39.36	39.36
35.10	35.10	38.15	38.03	38.21	38.50	35.28	35.28
34.09	34.09	37.14	36.84	36.41	34.42	32.29	32.29
33.72	33.72	33.72	34.94	34.94	35.80	35.80	32.99
35.25	35.25	33.97	33.97	31.83	31.83	31.83	

TABLE A1 cont.

RESULTS OF TEMPERATURE MEASUREMENTS
IN THE SPRAY REGIME

RUN S1:- FLOW RATES ; C_{sb} = 0.0500m/s q/b = 0.177E-2m^3/sm

ENTERING AIR ENTHALPY H_{in} = 11.57kcal/kg

temperature C

	45.99	45.99	45.99	45.99	45.99	45.99	
41.07	41.07	43.27	44.04	43.51	42.30	40.10	40.10
34.57	34.57	37.60	40.94	40.05	38.76	34.18	34.18
33.81	33.81	35.55	38.07	38.01	36.24	34.20	34.20
32.24	32.24	32.24	35.50	35.50	36.35	36.35	35.27
36.63	36.63	33.19	33.19	32.44	32.44	32.44	

RUN S2:- FLOW RATES ; C_{sb} = 0.0695m/s q/b = 0.242E-2m^3/sm

ENTERING AIR ENTHALPY H_{in} = 11.00kcal/kg

	44.44	44.44	44.44	44.44	44.44	44.44	
40.89	40.89	43.09	43.00	42.36	41.69	40.68	40.68
35.00	35.00	35.21	38.94	37.27	35.10	32.10	32.10
32.17	32.17	34.31	36.02	33.15	33.00	32.05	32.05
32.05	32.05	32.05	33.50	33.50	34.31	34.31	32.23
33.07	33.07	32.29	32.29	31.60	31.60	31.60	

RUN S3:- FLOW RATES ; C_{sb} = 0.0960m/s q/b = 0.322E-2m^3/sm

ENTERING AIR ENTHALPY H_{in} = 12.00kcal/kg

	34.47	34.47	34.47	34.47	34.47	34.47	
36.31	36.31	36.19	36.31	36.43	36.31	36.29	36.29
34.17	34.17	34.36	34.14	33.66	33.75	33.17	33.17
30.30	30.30	32.31	32.43	32.70	32.44	31.40	31.40
28.30	28.30	28.30	30.23	30.23	31.00	31.00	29.87
32.00	32.00	30.96	30.96	29.80	29.80	29.80	

RUN S4:- FLOW RATES ; C_{sb} = 0.0815m/s q/b = 0.242E-2m^3/sm

ENTERING AIR ENTHALPY H_{in} = 11.50kcal/kg

	40.48	40.48	40.48	40.48	40.48	40.48	
38.10	38.10	38.89	38.91	38.83	38.97	38.75	38.75
27.60	27.60	35.84	35.90	35.84	31.81	25.33	25.33
27.47	27.47	30.85	33.35	34.39	30.48	25.40	25.40
26.83	26.83	26.83	28.77	28.77	31.46	31.46	31.40
32.13	32.13	29.38	29.38	25.45	25.45	25.45	

TABLE A1 cont.

RUN S5:- FLOW RATES ; C_{sb} = 0.0900m/s q/b = 0.250E-2m^3/sm

ENTERING AIR ENTHALPY H_{in}= 10.75kcal/kg

	39.32	39.32	39.32	39.32	39.32	39.32	
37.34	37.34	38.16	37.99	37.70	37.16	37.06	37.06
34.89	34.89	34.91	34.88	34.84	34.22	33.99	33.99
32.07	32.07	33.34	33.08	33.06	33.07	32.68	32.68
30.57	30.57	30.57	30.84	30.84	32.28	32.28	32.05
32.95	32.95	32.75	32.75	30.37	30.37	30.37	

RUN S6:- FLOW RATES ; C_{sb} = 0.0695m/s q/b = 0.319E-2m^3/sm

ENTERING AIR ENTHALPY H_{in}= 10.62kcal/kg

	44.35	44.35	44.35	44.35	44.35	44.35	
38.90	38.90	40.00	42.51	43.43	39.76	38.40	38.40
33.32	33.32	35.67	39.38	38.95	34.49	33.42	33.42
30.40	30.40	32.84	36.63	36.63	34.19	30.52	30.52
29.48	29.48	29.48	31.27	31.27	32.13	32.13	32.12
32.60	32.60	31.98	31.98	29.09	29.09	29.09	

RUN S7:- FLOW RATES ; C_{sb} = 0.0490m/s q/b = 0.215E-2m^3/sm

ENTERING AIR ENTHALPY H_{in}= 12.00kcal/kg

	40.54	40.54	40.54	40.54	40.54	40.54	
38.90	38.90	39.32	39.87	40.12	38.59	38.50	38.50
35.88	35.88	35.60	37.41	37.41	33.26	34.06	34.06
33.02	33.02	33.12	35.28	33.32	32.53	32.06	32.06
29.90	29.90	29.90	30.31	30.31	30.65	30.65	30.02
30.70	30.70	30.20	30.20	29.61	29.61	29.61	

RUN S8:- FLOW RATES ; C_{sb} = 0.0660m/s q/b = 0.213E-2m^3/sm

ENTERING AIR ENTHALPY H_{in}= 11.20kcal/kg

	42.20	42.20	42.20	42.20	42.20	42.20	
40.33	40.33	40.88	39.62	40.27	40.43	39.80	39.80
29.76	29.76	37.73	39.63	38.27	37.86	31.32	31.32
29.67	29.67	35.93	36.58	35.13	34.38	30.47	30.47
29.08	29.08	29.08	31.07	31.07	31.05	31.05	30.26
31.81	31.81	30.17	30.17	29.86	29.86	29.86	

TABLE A1 cont.

RUN S9:- FLOW RATES ; C_{sb} = 0.0640m/s q/b = 0.149E-2m^3/sm

ENTERING AIR ENTHALPY H_{in}= 11.20kcal/kg

	38.30	38.30	38.30	38.30	38.30	38.30	
30.30	30.30	36.90	37.55	37.95	36.84	30.37	30.37
25.16	25.16	26.60	31.82	33.81	29.28	24.74	24.74
24.75	24.75	26.20	30.43	31.05	26.75	24.45	24.45
24.06	24.06	24.06	25.97	25.97	28.24	28.24	29.87
28.23	28.23	25.03	25.03	24.07	24.07	24.07	

RUN S10:- FLOW RATES ; C_{sb} = 0.0560m/s q/b = 0.426E-2m^3/sm

ENTERING AIR ENTHALPY H_{in}= 11.60kcal/kg

	42.90	42.90	42.90	42.90	42.90	42.90	
42.75	42.75	41.92	42.51	42.69	39.08	41.41	41.41
34.93	34.93	40.06	39.54	38.13	40.27	34.92	34.92
35.57	35.57	38.60	38.50	35.69	37.52	34.04	34.04
35.84	35.84	35.84	36.06	36.06	36.27	36.27	36.27
36.30	36.30	37.10	37.10	33.00	33.00	33.00	

RUN S11:- FLOW RATES ; C_{sb} = 0.0516m/s q/b = 0.426E-2m^3/sm

ENTERING AIR ENTHALPY H_{in}= 11.60kcal/kg

	37.00	37.00	37.00	37.00	37.00	37.00	
36.97	36.97	35.23	36.48	35.99	35.44	35.32	35.32
32.90	32.90	34.65	35.43	33.66	34.70	32.79	32.79
32.50	32.50	33.55	33.78	33.14	32.76	31.89	31.89
31.83	31.83	31.83	32.93	32.93	32.95	32.95	32.55
32.88	32.88	32.18	32.18	30.97	30.97	30.97	

RUN S12:- FLOW RATES ; C_{sb} = 0.0830m/s q/b = 0.282E-2m^3/sm

ENTERING AIR ENTHALPY H_{in}= 10.90kcal/kg

	42.52	42.52	42.52	42.52	42.52	42.52	
40.56	40.56	40.62	40.76	40.75	40.61	40.48	40.48
30.73	30.73	37.45	38.24	37.45	35.74	29.25	29.245
29.51	29.51	33.28	36.46	35.73	34.02	28.01	28.01
30.00	30.00	30.00	31.82	31.82	33.47	33.47	32.73
32.79	32.79	31.51	31.51	28.21	28.21	28.21	

TABLE A2

TEMPERATURE MEASUREMENTS ON STANDARD TRAY AND TRAYS FITTED WITH FLOW STRAIGHTENERS

RESULTS FROM THE STANDARD TRAY, "SD"

RUN SD1:- AIR RATE:C_{sb}= 0.0605 m/s WEIR LOAD:q/b=0.161E-2m^3/sm

ENTERING AIR ENTHALPY H_{in}= 12.46 kcal/kg

temperature C

	38.93	38.93	38.93	38.93	38.93	38.93	
38.03	38.03	37.43	38.79	37.23	37.88	38.05	38.05
32.78	32.78	34.85	34.50	34.35	34.67	31.98	31.98
30.73	30.73	31.90	32.72	33.58	33.98	30.94	30.94
29.72	29.72	29.72	30.46	29.46	31.36	31.36	31.68
32.06	32.06	31.29	31.29	30.47	30.47	30.47	

RUN SD2:- AIR RATE:C_{sb}= 0.0605 m/s WEIR LOAD:q/b=0.322E-2m^3/sm

ENTERING AIR ENTHALPY H_{in}= 12.46 kcal/kg

	39.87	39.87	39.87	39.87	39.87	39.87	
38.88	38.88	38.60	39.63	38.36	38.95	38.98	38.98
36.31	36.31	36.56	36.99	36.39	36.63	33.67	33.67
32.55	32.55	33.72	34.94	35.30	35.43	32.37	32.37
32.38	32.38	32.38	32.97	32.97	33.63	33.63	33.81
34.19	34.19	33.36	33.36	32.40	32.40	32.40	

RUN SD3:- AIR RATE:C_{sb}= 0.0605 m/s WEIR LOAD:q/b=0.484E-2m^3/sm

ENTERING AIR ENTHALPY H_{in}= 11.68 kcal/kg

	41.55	41.55	41.55	41.55	41.55	41.55	
40.60	40.60	40.33	41.11	40.30	40.74	40.55	40.55
38.50	38.50	39.09	38.55	38.36	38.92	38.25	38.25
35.81	35.81	38.09	38.38	38.38	38.12	36.09	36.09
35.29	35.29	35.29	36.27	36.27	37.27	37.27	37.27
37.54	37.54	36.96	36.96	35.88	35.38	35.38	

Table A2 cont.

RUN SD4:- AIR RATE:C_{sb}= 0.0605 m/s WEIR LOAD:q/b=0.645E-2m^3/sm

ENTERING AIR ENTHALPY H_{in}= 11.50 kcal/kg

	41.24	41.24	41.24	41.24	41 24	41.24	
40.42	40.42	40.44	40.73	40.18	40.26	40.24	40.24
38.72	38.72	38.99	39.04	38.58	38.86	38.37	38.37
36.59	36.59	38.61	38.71	38.64	38.20	36.70	36.70
36.26	36.26	36.26	37.03	37.03	37.55	37.55	37.72
38.08	38.08	36.81	36.81	36.42	36.42	36.42	

RUN SD5:- AIR RATE:C_{sb}= 0.0605 m/s WEIR LOAD:q/b=0.806E-2m^3/sm

ENTERING AIR ENTHALPY H_{in}= 10.46 kcal/kg

	40.28	40.28	40.28	40.28	40.28	40.28	
39.81	39.81	39.61	40.17	39.57	39.94	39.79	39.79
38.27	38.27	38.66	39.20	38.50	38.43	38.20	38.20
37.64	37.64	37.97	39.03	38.90	38.87	37.48	37.48
36.94	36.94	36.94	37.84	37.84	38.02	38.02	37.96
38.20	38.20	38.16	38.16	37.19	37.19	37.19	

RUN SD6:- AIR RATE:C_{sb}= 0.0605 m/s WEIR LOAD:q/b=0.967E-2m^3/sm

ENTERING AIR ENTHALPY H_{in}= 11.00 kcal/kg

	39.91	39.91	39.91	39.91	39.91	39.91	
39.46	39.46	39.42	39.85	39.28	39.73	38.48	38.48
38.27	38.27	38.20	39.21	38.89	38.66	38.19	38.19
37.50	37.50	37.68	38.83	39.03	38.73	37.62	37.62
37.10	37.10	37.10	37.95	37.95	38.18	38.18	38.12
38.41	38.41	37.68	37.68	37.33	37.33	37.33	

RUN SD7:- AIR RATE:C_{sb}= 0.0775 m/s WEIR LOAD:q/b=0.161E-2m^3/sm

ENTERING AIR ENTHALPY H_{in}= 10.85 kcal/kg

	37.25	37.25	37.25	37.25	37.25	37.25	
36.04	36.04	36.63	37.13	36.40	35.88	35.31	35.31
29.69	29.69	31.57	31.95	31.82	31.93	31.06	31.03
29.16	29.16	30.21	30.71	31.57	31.05	29.03	29.03
25.53	25.53	25.53	28.55	28.55	29.33	29.33	28.91
29.11	29.11	28.49	28.49	26.41	26.41	26.41	

Table A2 cont.

RUN SD8:- AIR RATE:C_{sb}= 0.0775 m/s WEIR LOAD:q/b=0.322E-2m^3/sm

ENTERING AIR ENTHALPY H_{in}= 11.30 kcal/kg

	40.10	40.10	40.10	40.10	40.10	40.10	
39.06	39.06	39.70	40.07	39.12	38.43	38.81	38.81
34.91	34.91	35.65	35.85	35.50	35.97	35.29	35.29
32.06	32.06	33.48	34.04	34.87	34.39	32.29	32.29
32.36	32.06	32.06	32.03	32.03	32.37	32.37	32.81
33.35	33.35	32.49	32.49	31.53	31.53	31.53	

RUN SD9:- AIR RATE:C_{sb}= 0.0775 m/s WEIR LOAD:q/b=0.484E-2m^3/sm

ENTERING AIR ENTHALPY H_{in}= 10.50 kcal/kg

	38.03	38.03	38.03	38.03	38.03	38.03	
37.43	37.43	37.94	37.96	37.27	37.43	37.31	37.31
35.49	35.49	35.38	35.49	35.17	35.49	35.53	35.53
33.83	33.83	34.53	34.90	35.06	35.26	34.07	34.07
32.18	32.18	32.18	32.63	32.63	33.61	33.61	33.64
34.07	34.07	33.33	33.33	32.82	32.82	32.82	

RUN SD10:- AIR RATE:C_{sb}= 0.0775 m/s WEIR LOAD:q/b=0.645E-2m^3/sm

ENTERING AIR ENTHALPY H_{in}= 12.20 kcal/kg

	37.07	37.07	37.07	37.07	37.07	37.07	
36.77	36.77	36.36	37.06	36.85	36.57	36.37	36.37
35.43	35.43	35.12	35.96	35.75	35.09	35.04	35.04
34.20	34.20	34.86	34.86	35.07	35.03	34.04	34.04
32.69	32.69	32.69	33.21	33.21	33.83	32.83	32.76
34.12	34.12	33.63	33.63	33.04	33.04	33.04	

RUN SD11:- AIR RATE:C_{sb}= 0.0775 m/s WEIR LOAD:q/b=0.806E-2m^3/sm

ENTERING AIR ENTHALPY H_{in}= 12.00 kcal/kg

	36.26	36.26	36.26	36.26	36.26	36.26	
35.98	35.98	35.80	36.19	36.13	35.89	35.77	35.77
34.77	34.77	34.58	34.88	34.80	34.64	34.73	34.73
33.28	33.28	33.83	34.85	34.91	34.88	34.04	34.04
33.09	33.09	33.09	33.50	33.50	33.21	33.21	33.27
34.33	34.33	33.91	33.91	33.33	33.33	33.33	

Table A2 cont.

RUN SD12:- AIR RATE:C_{sb}= 0.0775 m/s WEIR LOAD:q/b=0.967E-2m^3/sm

ENTERING AIR ENTHALPY H_{in}= 12.46 kcal/kg

	37.21	37.21	37.21	37.21	37.21	37.21	
36.70	36.70	36.75	37.17	37.09	36.76	36.69	36.69
35.83	35.83	35.55	35.91	36.12	35.30	35.52	35.52
34.85	34.85	34.99	35.83	35.71	35.61	35.03	35.03
34.10	34.10	34.10	34.67	34.67	34.86	34.86	34.81
35.18	35.18	34.74	34.74	34.21	34.21	34.21	

RUN SD13:- AIR RATE:C_{sb}= 0.0775 m/s WEIR LOAD:q/b=1.169E-2m^3/sm

ENTERING AIR ENTHALPY H_{in}= 10.90 kcal/kg

	37.99	37.99	37.99	37.99	37.99	37.99	
37.87	37.87	37.53	37.99	37.70	37.76	37.54	37.54
36.73	36.73	36.78	36.97	36.79	36.79	36.65	36.65
35.27	35.27	35.86	36.86	36.82	36.62	35.93	35.93
35.42	35.42	35.42	35.73	35.73	36.01	36.01	35.93
36.29	36.29	35.90	35.90	35.53	35.53	35.53	

RUN SD14:- AIR RATE:C_{sb}= 0.0915 m/s WEIR LOAD:q/b=0.322E-2m^3/sm

ENTERING AIR ENTHALPY H_{in}= 11.00 kcal/kg

	37.98	37.98	37.98	37.98	37.98	37.98	
37.22	37.22	37.89	37.85	37.85	37.45	37.51	37.51
32.40	32.40	32.45	33.08	33.69	33.87	32.50	32.50
29.97	29.97	30.44	31.26	32.40	31.26	30.50	30.50
29.26	29.26	29.26	29.71	29.71	29.91	29.91	29.83
30.73	30.73	29.94	29.94	29.62	29.62	29.62	

RUN SD15:- AIR RATE:C_{sb}= 0.0915 m/s WEIR LOAD:q/b=0.484E-2m^3/sm

ENTERING AIR ENTHALPY H_{in}= 10.85 kcal/kg

	35.82	35.82	35.82	35.82	35.82	35.82	
35.21	35.21	35.11	35.74	35.07	35.06	34.84	34.84
32.27	32.27	32.90	32.85	32.95	33.06	32.65	32.65
30.96	30.96	31.00	32.00	32.17	31.92	31.05	31.05
29.93	29.93	29.93	29.94	29.94	30.44	30.44	30.57
30.93	30.93	30.44	30.44	30.29	30.29	30.29	

Table A2 cont.

RUN SD16:- AIR RATE:C_{sb}= 0.0915 m/s WEIR LOAD:q/b=0.645E-2m^3/sm

ENTERING AIR ENTHALPY H_{in}= 11.15 kcal/kg

	34.59	34.59	34.59	34.59	34.59	34.59	
34.53	34.53	34.25	34.54	34.34	34.44	34.15	34.15
33.11	33.11	33.49	33.68	33.44	32.77	32.30	32.30
30.97	30.97	31.46	32.00	32.00	31.85	31.22	31.22
30.19	30.19	30.19	30.21	30.21	30.68	30.68	30.69
31.05	31.05	30.82	30.82	30.51	30.51	30.51	

RUN SD17:- AIR RATE:C_{sb}= 0.0915 m/s WEIR LOAD:q/b=0.806E-2m^3/sm

ENTERING AIR ENTHALPY H_{in}= 12.00 kcal/kg

	34.62	34.62	34.62	34.62	34.62	34.62	
33.18	33.18	33.98	34.43	33.86	33.95	33.87	33.87
32.49	32.49	32.33	33.64	32.75	32.49	32.34	32.34
31.26	31.26	31.62	31.98	31.99	31.99	31.29	31.29
30.54	30.54	30.54	30.69	30.69	31.12	31.12	31.09
31.30	31.30	31.09	31.09	30.87	30.87	30.87	

RUN SD18:- AIR RATE:C_{sb}= 0.0915 m/s WEIR LOAD:q/b=0.967E-2m^3/sm

ENTERING AIR ENTHALPY H_{in}= 11.00 kcal/kg

	35.60	35.60	35.60	35.60	35.60	35.60	
35.06	35.06	34.92	35.35	34.99	34.98	34.84	34.84
33.90	33.90	33.93	33.99	33.91	33.95	33.65	33.65
32.55	32.55	32.57	33.23	33.35	33.35	32.63	32.63
31.68	31.68	31.68	31.93	31.93	32.16	32.16	32.27
32.48	32.48	32.13	32.13	32.00	32.00	32.00	

RUN SD19:- AIR RATE:C_{sb}= 0.0915 m/s WEIR LOAD:q/b=1.169E-2m^3/sm

ENTERING AIR ENTHALPY H_{in}= 10.90 kcal/kg

	35.70	35.70	35.70	35.70	35.70	35.70	
35.22	35.22	35.41	35.42	35.34	35.10	34.87	34.87
34.16	34.16	33.59	33.79	33.86	33.48	33.41	33.41
33.25	33.25	33.34	33.39	33.60	33.61	33.37	33.37
32.55	32.55	32.55	32.70	32.70	32.83	32.82	32.80
33.20	33.20	33.00	33.00	32.75	32.75	32.75	

Table A2 cont.

RESULTS FROM GAP UNDER THE WEIR, "WG"

RUN WG1:- AIR RATE:C_{sb}= 0.0605 m/s WEIR LOAD:q/b=0.161E-2m^3/sm

ENTERING AIR ENTHALPY H_{in}= 12.06 kcal/kg

	45.59	45.59	45.59	45.59	45.59	45.59	
44.57	44.57	44.92	45.43	45.23	44.57	44.74	44.74
35.49	35.49	36.90	38.82	38.89	39.25	35.27	35.27
32.02	32.02	33.14	33.56	36.46	36.80	32.50	32.50
29.80	29.80	29.80	31.23	31.23	34.31	34.31	30.48
34.97	34.97	31.85	30.48	30.48	30.48	30.48	

RUN WG2:- AIR RATE:C_{sb}= 0.0605 m/s WEIR LOAD:q/b=0.322E-2m^3/sm

ENTERING AIR ENTHALPY H_{in}= 12.00 kcal/kg

	40.57	40.57	40.57	40.57	40.57	40.57	
40.40	40.40	40.23	40.24	40.37	40.29	40.25	40.25
34.87	34.87	37.38	37.41	37.42	37.89	34.65	34.65
33.70	33.70	34.14	35.79	36.11	36.36	33.14	33.14
31.96	31.96	31.96	33.21	33.21	34.32	34.32	34.81
34.95	34.95	34.69	34.69	31.58	31.58	31.58	

RUN WG3:- AIR RATE:C_{sb}= 0.0605 m/s WEIR LOAD:q/b=0.484E-2m^3/sm

ENTERING AIR ENTHALPY H_{in}= 10.50 kcal/kg

	42.04	42.04	42.04	42.04	42.04	42.04	
41.25	41.25	41.36	41.36	41.62	41.95	41.55	41.55
38.62	38.62	39.95	39.41	39.54	39.68	38.60	38.60
35.73	35.73	37.88	38.57	38.50	38.63	35.95	35.95
35.42	35.42	35.42	36.49	36.49	37.18	37.18	37.25
37.45	37.45	37.22	37.22	35.29	35.29	35.29	

RUN WG4:- AIR RATE:C_{sb}= 0.0605 m/s WEIR LOAD:q/b=0.645E-2m^3/sm

ENTERING AIR ENTHALPY H_{in}= 10.90 kcal/kg

	40.97	40.97	40.97	40.97	40.97	40.97	
40.08	40.08	40.09	40.90	40.08	40.45	40.71	40.71
38.01	38.01	39.31	39.70	38.99	37.99	37.85	37.85
36.36	36.36	37.91	38.40	38.25	38.31	36.24	36.24
36.21	36.21	36.21	37.02	37.02	37.25	37.25	37.30
37.53	37.53	37.36	37.36	36.29	36.29	36.29	

Table A2 cont.

RUN WG5:- AIR RATE:C_{sb}= 0.0605 m/s WEIR LOAD:q/b=0.806E-2m^3/sm

ENTERING AIR ENTHALPY H_{in}= 11.50 kcal/kg

	41.06	41.06	41.06	41.06	41.06	41.06	
40.66	40.66	40.82	40.99	40.62	40.57	40.54	40.54
38.02	38.02	39.21	39.94	39.11	38.99	37.99	37.99
36.90	36.90	38.22	38.80	38.90	38.21	37.03	37.03
36.28	36.28	36.28	37.86	37.86	37.77	37.77	37.94
38.06	38.06	38.06	38.06	37.34	37.34	37.34	

RUN WG6:- AIR RATE:C_{sb}= 0.0605 m/s WEIR LOAD:q/b=0.967E-2m^3/sm

ENTERING AIR ENTHALPY H_{in}= 11.18 kcal/kg

	42.55	42.55	42.55	42.55	42.55	42.55	
42.29	42.29	42.05	42.22	41.83	42.49	42.24	42.24
40.40	40.40	40.92	40.63	40.63	40.41	39.55	39.55
39.46	39.46	40.79	40.00	40.39	40.12	39.64	39.64
39.44	39.44	39.44	40.56	40.56	40.65	40.65	40.55
40.82	40.82	40.90	40.90	39.96	39.96	39.96	

RUN WG7:- AIR RATE:C_{sb}= 0.0775 m/s WEIR LOAD:q/b=0.161E-2m^3/sm

ENTERING AIR ENTHALPY H_{in}= 11.00 kcal/kg

	39.25	39.25	39.25	39.25	39.25	39.25	
36.73	36.73	36.83	38.65	36.95	36.84	36.81	36.81
26.76	26.76	29.68	30.10	31.10	32.94	28.67	28.67
26.30	26.30	26.87	28.87	30.12	31.00	26.30	26.30
25.00	25.00	25.00	26.07	26.07	28.13	28.13	28.28
29.21	29.21	29.19	29.19	25.30	25.30	25.30	

RUN WG8:- AIR RATE:C_{sb}= 0.0775 m/s WEIR LOAD:q/b=0.322E-2m^3/sm

ENTERING AIR ENTHALPY H_{in}= 10.50 kcal/kg

	40.66	40.66	40.66	40.66	40.66	40.66	
39.44	39.44	39.60	39.46	39.74	39.69	39.55	39.55
35.08	35.08	36.71	36.43	36.73	36.79	35.50	35.50
31.44	31.44	32.34	34.22	34.99	34.78	31.36	31.36
30.22	30.22	30.22	31.09	31.09	33.00	33.00	33.40
34.05	34.05	33.52	33.52	30.12	30.12	30.12	

Table A2 cont.

RUN WG9:- AIR RATE:C_{sb}= 0.0775 m/s WEIR LOAD:q/b=0.484E-2m^3/sm

ENTERING AIR ENTHALPY H_{in}= 11.50 kcal/kg

	38.10	38.10	38.10	38.10	38.10	38.10	
37.51	37.51	37.28	38.06	37.75	37.64	37.32	37.32
35.55	35.55	35.64	35.71	35.84	35.55	35.30	35.30
32.59	32.59	33.66	34.45	34.51	34.56	32.84	32.84
31.69	31.69	31.69	32.54	32.54	33.19	33.19	33.38
33.70	33.70	33.35	33.35	32.02	32.02	32.02	

RUN WG10:- AIR RATE:C_{sb}= 0.0775 m/s WEIR LOAD:q/b=0.645E-2m^3/sm

ENTERING AIR ENTHALPY H_{in}= 11.00 kcal/kg

	37.90	37.90	37.90	37.90	37.90	37.90	
37.56	37.56	37.68	37.88	37.85	37.51	37.34	37.34
35.96	35.96	35.98	35.91	35.88	35.86	35.56	35.56
33.92	33.92	34.58	35.30	35.25	35.19	33.61	33.61
33.00	33.00	33.00	34.00	34.00	33.51	33.51	34.00
34.07	34.07	34.03	34.03	33.14	33.14	33.14	

RUN WG11:- AIR RATE:C_{sb}= 0.0775 m/s WEIR LOAD:q/b=0.806E-2m^3/sm

ENTERING AIR ENTHALPY H_{in}= 10.85 kcal/kg

	37.98	37.98	37.98	37.98	37.98	37.98	
37.70	37.70	37.69	37.90	37.45	37.49	37.48	37.48
36.30	36.30	36.40	36.33	35.86	36.03	35.81	35.81
34.26	34.26	35.15	35.67	35.66	35.63	34.49	34.49
33.63	33.63	33.63	34.26	34.26	34.57	34.57	34.72
34.91	34.91	34.85	34.85	33.76	33.76	33.76	

RUN WG12:- AIR RATE:C_{sb}= 0.0775 m/s WEIR LOAD:q/b=0.967E-2m^3/sm

ENTERING AIR ENTHALPY H_{in}= 10.25 kcal/kg

	37.99	37.99	37.99	37.99	37.99	37.99	
37.59	37.59	37.64	37.74	37.46	37.39	37.40	37.40
36.16	36.16	36.23	36.04	36.03	35.99	35.89	35.89
34.57	34.57	35.44	35.98	35.95	35.96	34.97	34.97
34.43	34.43	34.43	34.90	34.90	35.07	35.07	35.10
35.36	35.36	35.13	35.13	35.36	35.36	35.36	

Table A2 cont.

RUN WG13:- AIR RATE:C_{sb}= 0.0775 m/s WEIR LOAD:q/b=1.169E-2m^3/sm

ENTERING AIR ENTHALPY H_{in}= 12.00 kcal/kg

37.89	37.89	37.89	37.89	37.89	37.89		
37.69	37.69	37.74	37.85	37.69	37.60	37.43	37.43
36.51	36.51	36.81	36.44	36.31	36.95	36.31	36.31
35.13	35.13	35.61	36.39	36.24	36.39	35.19	35.19
35.17	35.17	35.17	35.55	35.55	35.63	35.63	35.63
35.86	35.86	35.70	35.70	35.24	35.24	35.24	

RUN WG14:- AIR RATE:C_{sb}= 0.0915 m/s WEIR LOAD:q/b=0.322E-2m^3/sm

ENTERING AIR ENTHALPY H_{in}= 10.90 kcal/kg

	40.99	40.99	40.99	40.99	40.99	40.99	
40.30	40.30	39.77	41.09	39.90	39.99	39.56	39.56
33.46	33.46	35.63	35.63	36.23	36.16	32.90	32.90
32.12	32.12	33.52	33.66	34.37	34.28	32.00	32.00
31.06	31.06	31.06	30.78	30.78	31.88	31.88	32.22
32.65	32.65	32.20	32.20	30.92	30.92	30.92	

RUN WG15:- AIR RATE:C_{sb}= 0.0915 m/s WEIR LOAD:q/b=0.484E-2m^3/sm

ENTERING AIR ENTHALPY H_{in}= 10.50 kcal/kg

	38.25	38.25	38.25	38.25	38.25	38.25	
37.54	37.54	37.93	38.21	37.64	37.79	37.70	37.70
34.81	34.81	34.95	35.00	35.55	35.30	35.13	35.13
32.96	32.96	33.94	34.24	34.68	34.74	33.68	33.68
32.60	32.60	32.60	32.89	32.89	32.69	32.69	32.96
33.37	33.37	32.74	32.74	32.60	32.60	32.60	

RUN WG16:- AIR RATE:C_{sb}= 0.0915 m/s WEIR LOAD:q/b=0.645E-2m^3/sm

ENTERING AIR ENTHALPY H_{in}= 11.40 kcal/kg

	39.45	39.45	39.45	39.45	39.45	39.45	
38.77	38.77	38.89	39.13	38.83	38.75	38.56	38.56
36.16	36.16	36.70	36.79	36.63	36.38	36.14	36.14
33.95	33.95	35.71	36.08	36.05	36.21	34.75	34.75
33.59	33.59	33.59	34.10	34.10	34.61	34.61	34.53
34.99	34.99	34.57	34.57	33.29	33.29	33.29	

Table A2 cont.

RUN WG17:- AIR RATE:C_{sb}= 0.0915 m/s WEIR LOAD:q/b=0.806E-2m^3/sm

ENTERING AIR ENTHALPY H_{in}= 11.50 kcal/kg

	37.96	37.96	37.96	37.96	37.96	37.96	
37.51	37.51	37.79	37.78	37.88	37.60	37.41	37.41
35.98	35.98	35.69	35.67	35.55	35.42	35.48	35.48
33.96	33.96	34.45	35.68	35.53	35.80	34.57	34.57
33.57	33.57	33.57	34.10	34.10	34.44	34.44	34.39
34.77	34.77	34.41	34.41	33.80	33.80	33.80	

RUN WG18:- AIR RATE:C_{sb}= 0.0915 m/s WEIR LOAD:q/b=0.967E-2m^3/sm

ENTERING AIR ENTHALPY H_{in}= 11.00 kcal/kg

	36.91	36.91	36.91	36.91	36.91	36.91	
35.85	35.85	35.89	36.26	35.72	35.98	35.90	35.90
34.71	34.71	34.85	34.94	34.77	34.71	34.39	34.39
33.78	33.78	34.56	34.45	34.49	34.45	33.80	33.80
32.95	32.95	32.95	33.21	33.21	33.63	33.63	33.59
34.00	34.00	33.38	33.38	33.14	33.14	33.14	

RUN WG19:- AIR RATE:C_{sb}= 0.0915 m/s WEIR LOAD:q/b=1.169E-2m^3/sm

ENTERING AIR ENTHALPY H_{in}= 10.90 kcal/kg

	35.79	35.79	35.79	35.79	35.79	35.79	
34.92	34.92	34.74	35.12	34.61	34.81	34.73	34.73
33.82	33.82	33.71	33.82	33.70	33.46	33.81	33.81
33.40	33.40	33.74	33.70	33.67	33.39	33.20	33.20
32.66	32.66	32.66	32.91	32.91	33.17	33.17	33.17
33.56	33.56	33.28	33.28	32.91	32.91	32.91	

Table A2 cont.

RESULTS FROM STEPFLOW DOWNCOMER, "SF"

RUN SF1:- AIR RATE:C_{sb}= 0.0605 m/s WEIR LOAD:q/b=0.161E-2m^3/sm

ENTERING AIR ENTHALPY H_{in}= 12.46 kcal/kg

41.86

40.65	40.65	40.33	41.63	41.55	41.17	40.34	40.34
33.09	33.09	35.20	37.38	38.93	38.30	33.92	33.92
28.64	28.64	29.41	32.44	34.06	33.95	29.00	29.00
26.05	26.05	26.05	32.31	32.31	33.31	33.31	34.02
33.92	33.92	33.42	33.42	26.85	26.85	26.85	

RUN SF2:- AIR RATE:C_{sb}= 0.0605 m/s WEIR LOAD:q/b=0.322E-2m^3/sm

ENTERING AIR ENTHALPY H_{in}= 12.00 kcal/kg

37.98

37.98	37.36	37.36	37.49	37.90	37.70	37.30	37.30
34.92	34.92	35.34	35.84	35.93	35.87	35.67	35.67
33.78	33.78	34.36	34.83	33.68	35.09	34.78	34.78
33.33	33.33	33.33	33.93	33.93	34.57	34.57	34.34
33.21	33.21	34.31	34.31	33.06	33.06	33.06	

RUN SF3:- AIR RATE:C_{sb}= 0.0605 m/s WEIR LOAD:q/b=0.484E-2m^3/sm

ENTERING AIR ENTHALPY H_{in}= 11.00 kcal/kg

37.33

36.64	36.64	36.94	37.21	36.87	37.08	36.82	36.82
35.43	35.43	35.60	35.77	35.72	35.50	34.98	34.98
33.77	33.77	33.99	35.49	35.26	35.40	34.40	34.40
33.77	33.77	33.77	33.89	33.89	34.11	34.11	33.59
34.08	34.08	34.31	34.31	34.06	34.06	34.06	

RUN SF4:- AIR RATE:C_{sb}= 0.0605 m/s WEIR LOAD:q/b=0.645E-2m^3/sm

ENTERING AIR ENTHALPY H_{in}= 11.00 kcal/kg

38.69

38.06	38.06	38.26	38.54	38.15	38.29	38.20	38.20
36.82	36.82	37.02	36.79	36.84	36.96	36.79	36.79
36.61	36.61	36.70	36.72	36.48	36.92	36.78	36.78
35.81	35.81	35.81	35.84	35.84	35.76	35.76	35.87
36.09	36.09	36.28	36.28	36.02	36.02	36.02	

Table A2 cont.

RUN SF5:- AIR RATE:C_{sb}= 0.0605 m/s WEIR LOAD:q/b=0.806E-2m^3/sm

ENTERING AIR ENTHALPY H_{in}= 11.20 kcal/kg

			39.23				
38.64	38.64	38.85	39.08	38.84	38.97	38.77	38.77
37.67	37.67	37.87	37.84	37.92	37.65	37.70	37.70
37.75	37.75	37.79	37.80	37.42	37.20	37.62	37.62
37.78	37.78	37.78	37.77	37.77	37.34	37.34	37.02
37.26	37.26	37.52	37.52	37.31	37.31	37.31	

RUN SF6:- AIR RATE:C_{sb}= 0.0605 m/s WEIR LOAD:q/b=0.967E-2m^3/sm

ENTERING AIR ENTHALPY H_{in}= 10.50 kcal/kg

			37.91				
37.53	37.53	37.62	37.75	37.69	37.71	37.45	37.45
35.89	35.89	36.86	36.94	36.80	36.72	36.63	36.63
35.68	35.68	35.51	36.99	36.56	36.59	36.56	36.56
35.31	35.31	35.31	36.04	36.04	36.29	36.29	36.26
36.24	36.24	36.30	36.30	36.32	36.32	36.32	

RUN SF7:- AIR RATE:C_{sb}= 0.0775 m/s WEIR LOAD:q/b=0.161E-2m^3/sm

ENTERING AIR ENTHALPY H_{in}= 11.05 kcal/kg

			42.17				
40.61	40.61	41.93	41.48	40.90	38.34	37.82	37.82
32.09	32.09	33.47	34.27	35.76	34.52	32.28	32.28
30.63	30.62	30.91	31.87	33.25	32.46	30.80	30.80
29.28	29.28	29.28	30.01	30.01	30.36	30.36	30.02
30.63	30.63	29.99	29.99	29.65	29.65	29.65	

RUN SF8:- AIR RATE:C_{sb}= 0.0775 m/s WEIR LOAD:q/b=0.322E-2m^3/sm

ENTERING AIR ENTHALPY H_{in}= 10.90 kcal/kg

			36.30				
35.86	35.86	35.83	36.25	35.95	35.91	35.64	35.64
33.19	33.19	33.37	33.79	33.99	33.23	33.48	33.48
32.49	32.49	32.62	33.34	33.73	32.65	32.47	32.47
30.19	30.19	30.19	30.21	30.21	30.21	30.21	30.40
31.15	31.15	31.08	31.08	31.00	31.00	31.00	

Table A2 cont.

RUN SF9:- AIR RATE:C_{sb}= 0.0775 m/s WEIR LOAD:q/b=0.484E-2m^3/sm

ENTERING AIR ENTHALPY H_{in}= 11.00 kcal/kg

38.04

37.78	37.78	37.45	37.98	37.43	37.57	37.14	37.14
35.68	35.68	35.84	36.15	35.90	35.84	35.73	35.73
34.54	34.54	34.64	35.28	34.75	34.61	34.83	34.83
34.00	34.00	34.00	34.65	34.65	35.01	35.01	33.90
34.49	34.49	34.12	34.12	33.80	33.80	33.80	

RUN SF10:- AIR RATE:C_{sb}= 0.0775 m/s WEIR LOAD:q/b=0.645E-2m^3/sm

ENTERING AIR ENTHALPY H_{in}= 11.50 kcal/kg

37.86

37.52	37.52	37.45	37.74	37.49	37.36	37.11	37.11
35.79	35.79	35.90	35.80	35.73	35.67	35.72	35.72
34.80	34.80	35.00	35.48	35.48	35.00	34.80	34.80
33.83	33.83	33.83	34.56	34.56	34.22	34.22	34.63
35.13	35.13	34.83	34.83	34.19	34.19	34.19	

RUN SF11:- AIR RATE:C_{sb}= 0.0775 m/s WEIR LOAD:q/b=0.806E-2m^3/sm

ENTERING AIR ENTHALPY H_{in}= 12.00 kcal/kg

37.99

37.91	37.91	37.94	37.76	37.79	37.87	37.67	37.67
36.13	36.13	36.44	36.61	36.51	36.43	36.35	36.35
35.60	35.60	35.82	36.30	36.09	36.07	36.02	36.02
34.88	34.88	34.88	34.92	34.92	35.38	35.38	35.39
35.62	35.62	35.57	35.57	35.33	35.33	35.33	

RUN SF12:- AIR RATE:C_{sb}= 0.0775 m/s WEIR LOAD:q/b=0.967E-2m^3/sm

ENTERING AIR ENTHALPY H_{in}= 10.75 kcal/kg

37.90

37.68	37.68	37.63	37.89	37.60	37.71	37.49	37.49
36.68	36.68	36.68	36.73	36.71	36.61	36.64	36.64
35.49	35.49	35.50	36.42	36.08	36.65	35.25	35.25
35.38	35.38	35.38	35.40	35.40	35.71	35.71	35.36
35.48	35.48	35.83	35.83	35.76	35.76	35.76	

Table A2 cont.

RUN SF13:- AIR RATE:C_{sb}= 0.0775 m/s WEIR LOAD:q/b=1.169E-2m^3/sm

ENTERING AIR ENTHALPY H_{in}= 11.80 kcal/kg

			37.93				
37.72	37.72	37.63	37.87	37.65	37.67	37.60	37.60
36.69	36.69	36.72	37.06	36.77	36.34	36.21	36.21
35.39	35.39	36.44	36.38	36.92	36.04	35.48	35.48
35.74	35.74	35.74	36.15	36.15	36.40	36.40	36.20
36.31	36.31	36.57	36.57	36.57	36.57	36.57	

RUN SF14:- AIR RATE:C_{sb}= 0.0915 m/s WEIR LOAD:q/b=0.322E-2m^3/sm

ENTERING AIR ENTHALPY H_{in}= 11.40 kcal/kg

			41.99				
41.90	41.90	40.34	41.42	40.87	41.00	41.12	41.12
35.67	35.67	37.85	38.14	37.90	37.83	37.77	37.77
34.15	34.15	34.84	34.62	34.17	35.78	34.68	34.68
32.49	32.49	32.49	32.73	32.73	33.10	33.10	32.59
32.91	32.91	32.97	32.97	33.31	33.31	33.31	

RUN SF15:- AIR RATE:C_{sb}= 0.0915 m/s WEIR LOAD:q/b=0.484E-2m^3/sm

ENTERING AIR ENTHALPY H_{in}= 13.01 kcal/kg

			41.22				
40.44	40.44	40.15	41.00	40.57	40.63	39.84	39.84
35.24	35.24	36.44	36.65	37.31	36.14	36.14	36.14
33.05	33.05	33.37	34.52	35.18	36.24	33.43	33.43
32.41	32.41	32.41	33.49	33.49	33.99	33.99	33.30
33.71	33.71	33.73	33.73	33.91	33.91	33.91	

RUN SF16:- AIR RATE:C_{sb}= 0.0915 m/s WEIR LOAD:q/b=0.645E-2m^3/sm

ENTERING AIR ENTHALPY H_{in}= 11.05 kcal/kg

			39.30				
38.94	38.94	38.72	39.21	38.72	38.77	38.26	38.26
35.41	35.41	36.19	36.14	36.95	36.67	36.64	36.64
33.45	33.45	33.87	34.75	35.15	35.83	33.35	33.35
32.87	32.87	32.87	32.77	32.77	33.63	33.63	34.22
34.34	34.34	34.28	34.28	33.22	33.22	33.22	

Table A2 cont.

RUN SF17:- AIR RATE:C_{sb}= 0.0915 m/s WEIR LOAD:q/b=0.806E-2m^3/sm

ENTERING AIR ENTHALPY H_{in}= 11.20 kcal/kg

			37.95				
37.58	37.58	37.55	37.70	37.50	37.30	37.40	37.40
35.15	35.15	35.43	36.25	35.73	35.71	35.74	35.74
34.62	34.62	34.88	35.05	35.08	35.31	34.61	34.61
33.95	33.95	33.95	34.04	34.04	34.08	34.08	33.88
34.24	34.24	34.13	34.13	33.81	33.81	33.81	

RUN SF18:- AIR RATE:C_{sb}= 0.0915 m/s WEIR LOAD:q/b=0.967E-2m^3/sm

ENTERING AIR ENTHALPY H_{in}= 10.40 kcal/kg

			36.83				
36.62	36.62	36.53	36.76	36.58	36.46	36.16	36.16
35.09	35.09	35.10	35.20	35.45	35.57	35.29	35.29
34.07	34.07	34.23	34.36	34.59	34.55	34.60	34.60
33.54	33.54	33.54	33.56	33.56	33.87	33.87	33.88
34.16	34.16	33.93	33.93	33.91	33.91	33.91	

RUN SF19:- AIR RATE:C_{sb}= 0.0915 m/s WEIR LOAD:q/b=1.209E-2m^3/sm

ENTERING AIR ENTHALPY H_{in}= 10.90 kcal/kg

			41.97				
41.48	41.48	41.41	41.64	41.73	41.35	41.16	41.16
40.47	40.47	39.66	39.86	39.92	39.41	40.35	39.51
39.95	39.95	39.79	39.34	39.56	39.66	39.85	39.85
37.96	37.96	37.96	37.98	37.98	37.98	37.98	38.13
38.45	38.45	38.85	38.85	38.79	38.79	38.79	

Table A:B1 Calibration of Handmade Thermocouples against a 0.1 Resolution Mercury-in-Glass Thermometer, Hg and a Standard "K" Thermocouple.

	Temperature C				
Hg	0.00	18.20	36.05	46.00	53.15
"K"	0.22	18.45	36.20	45.90	53.27
	0.05	18.60	36.10	45.95	53.20
Average error	0.14	0.33	0.10	0.08	0.09
Corresponding readings from handmade Thermocouples					
1	2.60	18.50	36.10	45.37	53.10
2	0.00	18.50	36.20	45.76	53.30
3	1.64	18.57	36.20	45.76	53.30
4	0.03	18.51	36.27	45.80	53.27
5	0.00	18.60	36.24	45.88	53.35
6	0.05	18.57	36.24	45.84	53.33
7	0.03	18.70	36.28	45.97	53.48
8	3.40	18.60	36.27	45.95	53.30
9	0.03	18.70	36.27	45.88	53.28
10	0.00	18.70	36.21	45.90	53.26
11	0.20	18.51	36.23	45.35	53.29
12	1.20	18.60	36.25	45.38	53.31
13	0.06	18.63	36.27	45.95	53.35
14	0.50	18.55	36.29	45.87	53.25
15	0.00	18.60	36.40	45.55	53.30
16	0.09	18.67	36.18	45.60	53.31
17	1.00	18.70	36.19	45.70	53.32
18	0.00	18.68	36.25	45.85	53.33
19	0.08	18.80	36.29	45.95	53.29
20	1.07	18.59	36.35	45.60	53.28
Average Error:	0.60	0.41	0.20	0.25	0.14

* Standard refers to industrial manufacture rather than level of accuracy

"K" is an alloy of Ni-Cr/Ni-Al

Table A:B2 Calibration of Manufactered Thermocouples against a 0.001 C Platinum Resistance Electronic Thermocouple reference [40]

	Temperature C								
No.	Pt	"K"	-o-	Pt	"K"	-o-	Pt	"K"	-o-
1	0.020	0.16	-	16.041	15.51	0.531	28.030	27.80	0.230
2	0.020	0.12	-	16.041	14.27	0.771	28.030	27.74	0.290
3	0.042	1.34	-	15.502	14.73	0.772	27.906	27.96	0.054
4	0.042	1.34	-	15.502	14.98	0.522	27.906	27.63	0.276
5	0.030	0.95	-	15.831	16.06	0.229	27.894	27.62	0.274
6	0.030	0.89	-	15.831	15.95	0.119	27.894	27.58	0.314
7	0.030	0.26	-	15.621	15.84	0.219	27.760	27.50	0.260
8	0.030	1.66	-	15.621	15.43	0.191	27.760	27.70	0.060
9	0.033	1.23	-	15.712	15.12	0.592	28.653	28.82	0.167
10	0.033	0.00	-	15.712	15.08	0.632	28.653	29.17	0.083
11	0.017	0.60	-	15.660	15.83	0.170	28.231	28.55	0.319
12	0.017	1.89	-	15.660	15.64	0.020	28.231	28.54	0.309
13	0.021	0.85	-	15.701	15.62	0.081	27.772	27.92	0.148
14	0.021	1.31	-	15.701	16.08	0.379	27.772	27.84	0.032
15	0.013	1.25	-	15.820	16.03	0.210	27.882	27.57	0.312
16	0.013	0.02	-	15.820	15.81	0.010	27.882	28.12	0.238
17	0.087	1.53	-	15.590	14.93	0.660	28.019	27.75	0.269
18	0.087	1.11	-	15.590	15.20	0.290	28.019	27.91	0.109
19	0.072	1.48	-	15.483	15.39	0.093	27.778	27.78	0.002
20	0.072	0.61	-	15.483	15.23	0.253	27.778	28.18	0.402
21	0.013	0.24	-	15.620	15.26	0.360	28.010	28.05	0.050
22	0.023	0.54	-	15.620	15.16	0.460	28.010	27.70	0.310
23	0.023	0.35	-	15.403	15.00	0.403	27.502	27.26	0.242
24	0.027	0.10	-	15.403	15.49	0.097	27.502	27.34	0.162
25	0.027	0.22	-	15.370	14.81	0.560	27.728	27.44	0.288
26	0.027	0.50	-	15.370	15.02	0.350	27.728	27.80	0.072
27	0.032	0.75	-	15.674	15.21	0.464	27.030	27.35	0.320
28	0.032	0.35	-	15.674	15.57	0.104	27.030	27.07	0.040

Key: -o- is absolute value of deviation (error).
- value irrelevant to measurements in this work

Table A:B2 cont.

No.	Pt	"K"	-o-	Pt	"K"	-o-
1	38.139	38.55	0.311	48.091	48.40	0.309
2	38.139	38.37	0.231	48.091	48.07	0.021
3	38.207	38.31	0.103	48.302	48.21	0.092
4	38.207	38.46	0.253	48.302	48.09	0.212
5	38.810	38.47	0.340	50.070	49.97	0.100
6	38.810	38.55	0.260	50.070	49.97	0.100
7	38.402	38.21	0.192	49.705	50.05	0.345
8	38.402	38.28	0.122	49.705	49.61	0.095
9	35.300	35.28	0.020	48.360	48.59	0.230
10	35.300	35.53	0.230	48.360	48.42	0.060
11	38.480	38.15	0.330	50.800	51.07	0.270
12	38.480	37.57	0.110	50.800	50.82	0.020
13	39.807	39.67	0.137	50.400	50.66	0.260
14	39.807	40.07	0.263	50.400	50.28	0.120
15	40.618	40.72	0.102	48.600	48.31	0.290
16	40.618	40.59	0.028	48.600	48.50	0.100
17	40.811	40.45	0.361	50.880	50.99	0.110
18	40.811	40.94	0.129	50.880	50.80	0.080
19	37.634	37.47	0.164	49.673	50.00	0.327
20	37.634	37.59	0.044	49.673	49.34	0.333
21	37.376	37.48	0.104	48.100	48.26	0.210
22	37.376	37.76	0.384	48.100	48.34	0.240
23	38.600	38.44	0.160	49.807	50.03	0.223
24	38.600	38.42	0.180	49.807	50.06	0.253
25	37.620	37.67	0.050	50.043	49.93	0.113
26	37.620	37.87	0.250	50.043	50.00	0.043
27	38.008	38.01	0.002	50.067	50.02	0.042
28	38.008	37.92	0.088	50.067	50.04	0.027

Key: -o- is absolute value of deviation (error).
ESTIMATED ERROR IS 0.30 C

Table A:B3 A Typical Set of Final Temperature Readings for Analysis on the tray

Couple(No.)	Average	Standard Deviation
Reference	27.68	0.04
Reference	27.68	0.04
1	39.61	0.05
2	39.46	0.12
3	39.42	0.15
4	39.85	0.09
5	39.28	0.09
6	39.73	0.09
7	39.48	0.12
8	38.27	0.13
9	38.20	0.12
10	37.21	0.20
11	37.89	0.23
12	38.06	0.08
13	37.99	0.17
14	36.50	0.06
15	37.68	0.13
16	38.83	0.05
17	39.03	0.14
18	38.73	0.15
19	37.62	0.09
20	37.10	0.13
21	37.95	0.22
22	38.18	0.15
23	38.41	0.11
24	37.68	0.06
25	37.33	0.04
26	21.65*	0.04
27	28.55*	0.13
28	38.12	0.13

Total number of scans : 21 Time taken : approx. 30mins (this includes 60secs between scans and print time)

* Thermocouples 26 and 27 measure the wet-bulb and dry-bulb temperatures of the inlet air stream respectively.

The order of the Thermocouple arrangements on the tray is determined by the experimenter, see Section 4.

Table A:B4

CALIBRATION OF AIR FLOW METER
METHOD: PITOT STATIC TRAVERSE

Plane of measurement: 650mm from column top

Cross-sectional area of measurement: m^2

Manometer fluid: liquid parafin

Manometer reading H in.

$\times 10^{-3}$

125	170	180	205	215	235	250	275	320	305	330	350	375	365	350	350	345	345	325	315	270	275	270	245	235	195
180	195	205	225	245	280	280	300	325	340	350	350	370	370	360	355	335	315	305	265	260	235	255	225	225	190
185	225	230	230	235	265	275	280	315	335	345	350	365	365	360	325	325	290	285	245	230	210	205	190	205	195
235	230	220	230	245	255	270	280	325	335	330	360	370	365	355	350	320	280	245	235	185	185	180	180	195	200
245	255	250	245	245	255	275	280	315	335	350	370	375	370	360	355	320	285	250	230	190	185	175	175	180	190
250	255	260	255	270	295	295	310	325	350	365	370	380	375	370	345	340	315	280	255	215	190	180	195	185	195
270	280	270	270	280	290	305	325	340	350	370	380	375	360	350	345	325	310	285	230	215	220	200	195	200	190
275	270	270	275	275	280	290	315	315	345	355	355	355	335	310	310	315	275	275	260	235	210	220	215	220	210
275	275	270	270	280	290	290	300	315	320	340	345	355	340	325	280	255	280	275	260	245	265	235	235	240	220
270	270	245	245	270	275	280	295	300	305	320	300	285	295	265	285	245	230	260	250	245	235	245	240	255	235
230	270	255	230	210	215	230	235	250	260	275	290	280	290	290	260	245	230	245	245	250	240	255	250	255	230

Average H across plane of measurement: 0.275in.

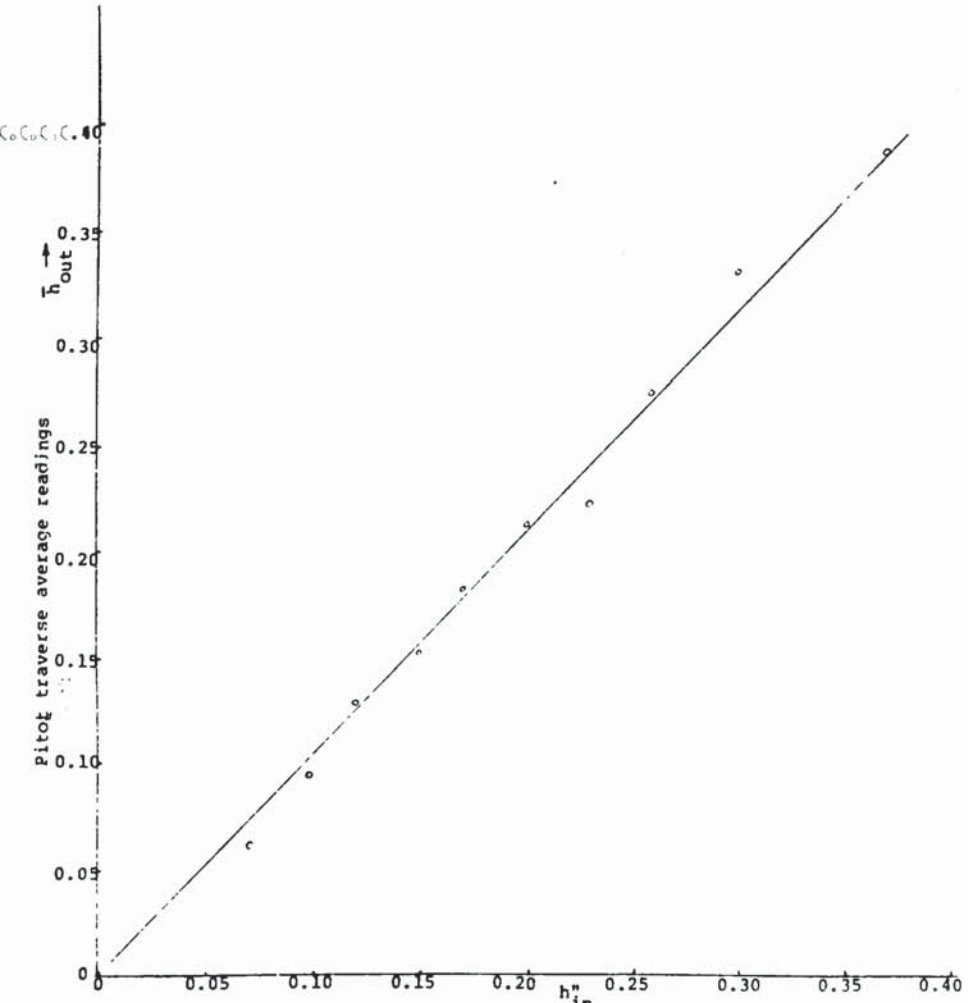

Fig.A:E1 Cal ibration of single pitot tube in duct by pitot traverse

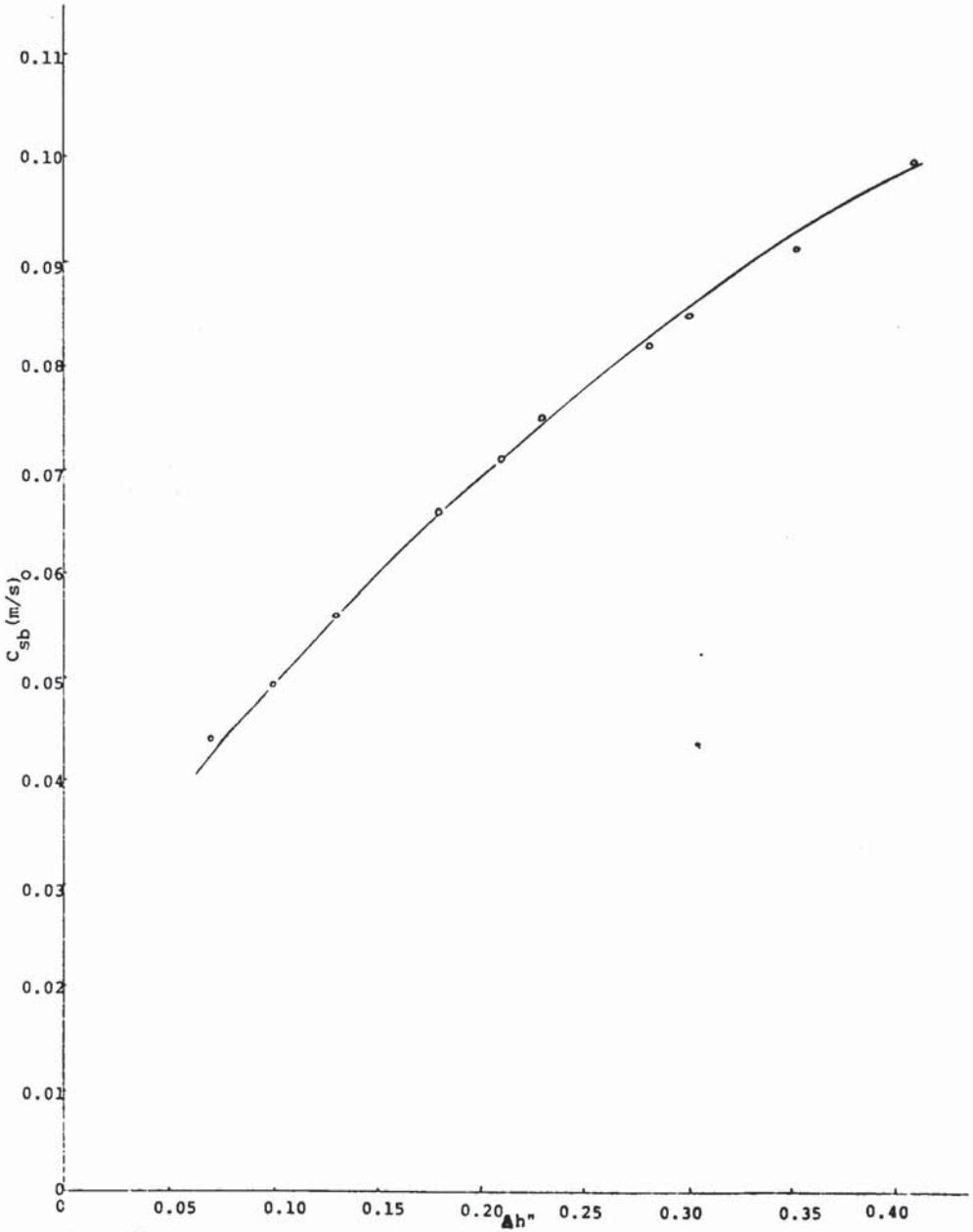

Fig.A:B2 Load factor against cal ibrated manometer readings

APPENDIX C

Program C1: Data Logging Computer Program DALOG

Computer: Commodore 4000 Series Micro-Computer

Programming Language: Basic

```
10   REM *** DATA COLLECTION ***
14   DEFFNA(A)=INT((A/6-INT(A/6))*6+0.5)
20   DIM W$(32),V(32),F(32)
22   DIM A(32),D(32),B$(26),C$(9)
24   GOSUB 100
26   OPEN 1,3
28   IF T3$="YES" THEN OPEN 2,4,1:OPEN3,4,2:OPEN4,4,0:PRINT#4," "
30   FOR C1=1 TO T1%
40   GOSUB 400
50   NEXT C1
60   IF T3$="YES" THEN GOSUB 4000
62   CLOSE 1
64   CLOSE 2
66   CLOSE 3
68   CLOSE 4
70   END
100  REM *** INITIAL CONTROL ***
110  GOSUB 200
120  GOSUB 278
125  GOSUB 360
130  RETURN
200  REM *** INITIALIZATION ***
210  PRINT "    "," DATA COLLECTION  "
220  INPUT " NUMBER OF TAKES",T1%
230  IF (T1%<1) OR (T1%>1000) THEN 220
240  PRINT "  "
250  INPUT " TIME PERIOD (IN MINS)";T2%
260  IF (T2%<1) OR (T2%>30) THEN 250
262  PRINT "  "
264  INPUT " PRINTED COPY";T3
266  IF (T3$<>"YES") AND (T3$<>"NO")THEN 264
268  PRINT " "
270  INPUT " ADJUSTMENTS";T4%
272  IF (T4$<>"YES") AND (T4$<>"NO") THEN 270
274  RETURN
278  REM *** SET VALUES ***
280  T1$="000000"
300  A1=2.4383248E-2
310  A2=9.7830251E-2
320  A3=3.6276965E-12
330  A4=-2.5756438E-16

332  S$=CHR$(29)
334  C$(1)=" ":C$(2)="r":C$(3)="s"
336  C$(4)="x":C$(5)="t":C$(6)="u"
338  C$(7)="v":C$(8)="w":C$(9)="z"
350  RETURN
```

```
360 REM *** DRAW CIRCLE ***
362 PRINT " ";TAB(17);"PLATES"
364 FOR C2=1 TO 180 STEP 4
366 RD = C2*PI/180
368 X1 = 20 + 15*COS(RD)
370 Y1 = 11 - 10*SIN(RD)
372 Y2 = 11 + 10*SIN(RD)
374 PRINT " "
376 FOR C3=0 TO Y1
378 PRINT
380 NEXT
382 FOR C3=Y1 TO Y2
384 PRINT SPO(X1);" "
386 NEXT
387 NEXT
388 RETURN

400 REM *** DATA COLLECTION CONTROL ***
420 GOSUB 600
430 GOSUB 1000
440 GOSUB 1600
450 IF T3$="YES" THEN GOSUB 3000
460 RETURN

600 REM ***WAIT UNTIL TIME TO TAKE ***
610 IF C1=1 THEN RETURN
620 IF VAL(T1$)/100<((C1-1)*T2%) THEN 620
630 RETURN

800 REM *** DATA COLLECTION ***
810 FOR BD=1 TO 2
830 OPEN 5,7,BD
840 PRINT#5,CHR$(16);
850 INPUT#5,W$(BD)
855 I1=(BD-1)*15+2
860 FOR C2=1 TO 15
870 PRINT#5,CHR$(C2+48);
880 INPUT#5,W$(I1+C2)
890 NEXT
900 CLOSE 5
910 NEXT
920 RETURN

1000 REM *** CONVERSION OF VALUES ***
1010 GOSUB 1200
1020 GOSUB 1400
1025 GOSUB 1520
1030 RETURN
```

```
1200 REM *** ASCII TO BINARY ***
1210 FOR C2=1 TO 32
1220 M1% = 1
1230 V(C2) = 0
1240 FOR C3=3 TO 1 STEP -1
1250 V(C2)=V(C2)+(ASC(MID$(W$(C2),C3,1))-64)*M1%
1260 M1%=M1%*16
1270 NEXT C3
1280 NEXT C2
1290 RETURN

1400 REM ** TEMPERATURE CONVERTION ***
1410 FOR BD=1 TO 2
1430 VOUT=(V(BD)-1024)/80000
1440 RX=100*(0.5+VOUT)/(0.5-VOUT)
1445 TREF=(RX-100)*2.5707
1450 VOFF=(3.9557007E1*TREF)+(1.7584397E-2*TREF)
1455 F(BD)=TREF
1457 IF T4$="YES"THEN DX=F(1)-F(BD):F(BD)=F(1)
1458 I1=(BD-1)*15+2
1460 FOR C2=1 TO 15
1470 VADC=(V(I1+C2)-1024)*2.511
1480 VZ=VOFF+VADC
1490 F(I1+C2)=(A1*VZ)+(A2*VZ*VZ)+(A3*VZ^3)+(A4*VZ^4)
1495 IF T4$="YES" THEN F(I1+C2)=F(I1+C2)+DX
1500 NEXT C2
1510 NEXT BD
1515 RETURN

1520 REM *** CALCULATION FOR MEAN AND STANDARD DEVIATION ***
1530 FOR C2=1 TO 32
1540 A(C2)=A(C2)+F(C2)
1550 D(C2)=D(C2)+(F(C2)*F(C2))
1560 NEXT C2
1570 RETURN

1600 REM *** OUTPUT TO SCREEN ***
1610 GOSUB 1700
1620 GOSUB 1800

1700 REM *** CALCULATION OF DISPLAY BLOCKS ***
1710 FOR C2=1 TO 26
1714 CH=INT(F(C2+2)-20)
1718 IF CH<1 THEN CH=1
1720 IF CH>9 THEN CH=9
1722 Z$=C$(CH)+C$(CH)+C$(CH)
1726 B$(C2)=" "+Z$+"    "+Z$
1740 NEXT C2
1750 RETURN
```

```
1800 REM *** DISPLAY BLOCKS ON SCREEN ***
1810 PRINT "    ";SPC(18);"INLET","     ";B$(1);"             "
1820 FOR C2=2 TO 25
1830 PRINT B$(C2);
1840 IF FNA(C2)=1 THEN PRINT "                        "
1850 NXET C2
1860 PRINT "          ";B$(26)
1870 RETURN

3000 REM *** PRINT RESULTS ***
3002 IF (FNA(C1)=1) OR (FNA(C1)=3) OR (FNA(C1)=5) THEN
     PRINT#4,"XX"
3003 PRINT#2
3004 PRINT#2
3005 PRINT#2
3005 PRINT#3,"                    AAAAAAAAAAA          AAAA   999"
3010 PRINT#2,"TEMPERATURES",S$,"PASS",S$,"TEMP"
3015 PRINT#2
3017 PRINT#3,"AAAAAAAAA      AAAAAA     AAAAAA      AAAAAAAAAA"
3020 PRINT#2,"COUPLE",S$,"TEMP",S$,"COUPLE",S$,"TEMP"
3030 PRINT#2,"      ",S$," BD1",S$,"      ",S$," BD2"
3035 PRINT#2
3036 PRINT#3,"AAAAAAAAAA     999.99                          999.99"
3037 PRINT#2,"REFERENCE",S$,F(1),F(2)
3038 PRINT#2
3039 PRINT#3,"99               999.99       99              999.99"
3040 FOR C2=3 TO 17
3050 PRINT#2,C2-2,F(C2),C2+15,F(C2+15)
3060 NEXT C2
3070 RETURN

4000 REM *** PRINT STATISTICS ***
4010 GOSUB 4200
4020 GOSUB 4400
4030 RETURN

4200 REM *** CALCULATION OF TOTALS AND STATISTICS ***
4210 FOR C2=1 TO 32
4220 A(C2)=A(C2)/T1%
4230 D(C2)=SQR(ABS((D(C2)/T1%)-(A(C2)*A(C2)))
4240 NEXT C2
4250 RETURN
```

```
1400 REM *** PRINT STATISTICS ***
1410 PRINT#4,"XX"
1412 PRINT#2
1415 PRINT#2,"TOTALS"
1417 PRINT#2
1418 PRINT#3,"AAAAAAAAA        AAAAAAAAA           AAAAAAAAAA"
1420 PRINT#2,"COUPLE",S$,"AVERAGE",S$,"SD"
1425 PRINT#2
1427 PRINT#3,"AAAAAAAAAA    999.99         999.99"
1430 FOR C2=1 TO 32
1432 IF C2<=2 THEN PRINT#2,"REFERENCE",
1432 IF C2>2 THEN PRINT#2,STR$(C2-2),
1440 PRINT#2,S$,A(C2),D(C2)
1450 NEXT C2
1460 PRINT#2
1470 PRINT#2,"TAKES:",S$,T1%,"TIME(MINS):",S$,T2%
1476 PRINT#4,"XX"
1480 RETURN
```

A Description of the Voltage Detection used in data logging.

The Equations used in the program above are presented

The thermocouple voltage detection is effected by the Tc-16 module linked to the isothermal box, see flow sheet in figure 4.9. It is equiped with a Platinum Resistance Temperature Detector (or RTD) which serves as a pseudo cold junction. The temperatures of the thermocouples on the tray are calibrated against the RTD, thus it is the reference thermocouple. Voltages are detected by balancing a Wheatstone Bridge arrangement for which the RTD is one arm.

A relationship for the RTD resistance against the measured or output voltage is derived from the equations of the bridge, giving:

$$R_x = 100 * (0.5 + V_{out})/(0.5 - V_{out}) \qquad a1$$

where R_x is the RTD resistance. An amplifier gain in the Tc - 16 IEEE bus is preset, say to G = 200. This must be considered in calculating V_{out}, such that if X_{adc} is the number of signals sent to the computer as data,

$$V_{out}=((X_{adc}- 1024) * 0.0025)/G \qquad a2$$

see reference [107J]

For the range of temperatures -20 C to 80 C a linear relationship between temperature and resistance may be assumed as;

$$T = (R_x- 100) * 2.5707 \qquad a3$$

This equation is used to calculate the temperature of the cold junction. Equation a4 is used to calculate the offset voltage of the cold junction. Add to the calculated voltage of the thermocouples the offset and from the result invoke the ploynomial equation a5 below to obtain the temperature.

Thermocouple Conversion Formulae

"K" type Thermocouples

Variable Reference Junction Correction 0 - 50 C

Equation: $V = a_1T + a_2T$ a4

where a_1= 3.9557007E01,

a_2= 1.7584397E-02,

V is in microvolts; T in C

Conversion To Temperature (Assuming 0 C Cold Junction)

Appendix C

Program C2: Water cooling Computer Program WALOG
Program Language: Standard Fortran 77

```
C     Program calculates temperatures from splines fitted to a
C     mesh. A regular rectangular grid is generated to include
C     extrapolated points at wall and weir boundaries. The finese
C     of the mesh allows a two dimensional plot of temperature
C     surface to be made using a graphics routine,GINOSURF. At the
C     same time calculations of average air enthalpies leading to
C     efficiencies are made with the grid temperatures generated

      COMMON /WAMDA/ W(60),WS(8600),DL(60),EU1(20),AMDA1(20)
      SPECIAL COMMON WAMDA
      COMMON /XYZ1/ X1(60),Y1(60),Z1(60),FF1(60),C1(60)
      SPECIAL COMMON XYZ1
      COMMON /SAX/ X(1200),Y(1200),FF(1200)
      SPECIAL COMMON SAX
      COMMON /CAT/ FI(1200),YNTR(1200)
      SPECIAL COMMON CAT
      COMMON /CAN/ W1(5000),AZ(32,30)
      SPECIAL COMMON CAN
      COMMON /FIX/ A(20),CT(20),E(20),CE(20),N7,M7
      SPECIAL COMMON FIX
      COMMON/THU/ T1(50),H1(50),U1(50),U2(4,30)
      SPECIAL COMMON THU
      COMMON /CONST/ DIA,XTE,XLEN,XWR,XBEL,XTS,XS,YS,YF,XL,YL,YM
     +,XM,YE,XX,XY
      SPECIAL COMMON CONST
      COMMON /NIAD/ NPOINT(100),IADRES(30)
      SPECIAL COMMON NIAD
      INTEGER MI,M2,R,NZ,N3,N7,M7,PY1,PX1,M1
      INTEGER IFAIL,NWS,MX,MY,QX1,QY1,NP1,NC1,RANK
      REAL EPS,SIGMA,X0,X2,Y0,Y2,TL,TU,HIN,EOG

C     Input total number of data points including extrapolates
C     from equations of the boundary cnditions as MI. Input data
C     points for saturated air versus water temperature curve,M1
      READ(11,-) M1,MI
      DO 5 I=1,M1
C     Input coordinates for data points on tray.
   5  READ(11,-) X1(I),Y1(I)
C     Input weir load, load factor and average inlet air enthalpy
      READ(13,-) Q1,V1,HIN
C     Input temperature measurements as dependent variable.
      READ(13,-) (Z1(I),I=1,M1)
C     Input data points corresponding to saturation air
C     temperature and enthalpy (from psychrometric tables).
  20  READ(11,-) (T1(I),H1(I),I=1,MI)
C     Set tolerance limit to a point where a number is regarded
C     as zero to enable determine the effective rank of matrix
      READ(11,-) EPS
```

```
C       Prescribe the number of internal knots
        READ(11,-) PX1,PY1,NZ,MZ
C       Number of intervals and lower and upper limits for X and Y
        READ(11,-) MX,X0,X2,MY,Y0,Y2
C       Set column radius,weir length,maximum distance between
C       column and column/weir intersect,and flow path length
        READ(11,-) RR,WL,CX,CY
        TIN=Z1(1)
C       Set work space
        NWS=8600
        M3=MZ+3
        M7=MZ+7
        N3=NZ+3
        N7=NZ+7
        IF(M3.LT.5) GO TO 150
C       Set internal knots on the Enthalpy/Temperature data
        READ(11,-) (E(J),J=5,M3)
 150    IF(N3.LT.5) GO TO 170
C       Set internal knots on the Enthalpy/Temperature data
        READ(11,-) (A(J),J=5,N3)
 170    IFAIL=1
C       Subruotine E02BAF forms a least squares cubic
C       approximation to the set of enthaply/temperature data
        CALL E02BAF(MI,N7,T1,H1,W,A,U1,U2,CT,SS,IFAIL)
        IF(IFAIL.EQ.0) GO TO 190
        WRITE(12,-) "IFAIL6"
        WRITE(12,-) IFAIL
        GO TO 390
 190    DO 99 R=1,MI
        IFAIL=1
C       Subroutine E02BBF evaluates a cubic spline from the
C       B-cubic representation in E02BAF above
        CALL E02BBF(N7,A,CT,T1(R),FIT,IFAIL)
        IF(IFAIL.EQ.0) GO TO 99
        WRITE(12,-) "IFAIL8"
        WRITE(12,-) IFAIL
        GO TO 390
  99    CONTINUE
        GO TO 400
 390    STOP


C       Define grid to include points at the edge of the
C       circular tray
 400    M=(MX+2)*MY
        DX=X2-X0
        DY=Y2-Y0
        RX1=MX-1
        RY1=MY-1
        DD=DX/RX1
        DE=DY/RY1
```

```
      K=1
      DO 80 J=1,MY
            JR=J-1
            YI=YO+(JR*DY)/RY1
            DO 60 I=1,MX
            IR=I-1
            X(K)=XO+(IR*DX)/RX1
            Y(K)=YI
            SET=SQRT(RR**2-(Y(K)-CY)**2)
            IF(X(K).LE.RR) THEN
            XZ=CX-SET
            GO TO 55
            END IF
            XZ=CX+SET
 55         IF(X(K).LT.XZ) THEN
            IF((X(K)+DD).GE.XZ) THEN
            K=K+1
            X(K)=XZ
            Y(K)=YI
            END IF
            END IF
            K=K+1
 60         CONTINUE
 80         CONTINUE
      QX1=PX1-4
      QY1=PY1-4
      NC1=QX1*QY1
      NP1=(PX1-7)*(PY1-7)
C     Specify internal knots
      IF(QX1.LT.5) GO TO 66
      READ(11,-) (AMDA1(J),J=5,QX1)
 66   IF(QY1.LT.5) GO TO 44
      READ(11,-) (EU1(J),J=5,QY1)
 44   IFAIL=1
C     Subroutine E02ZAF sorts two dimensional data into
C     rectangular panels for orderly and efficient computation
      CALL E02ZAF(PX1,PY1,AMDA1,EU1,M1,X1,Y1,NPOINT,M1+NP1,
     + IADRES,NP1,IFAIL)
      IF(IFAIL.EQ.0) GO TO 220
      WRITE(12,-) "IFAIL1"
      WRITE(12,-) IFAIL
      GO TO 180
 220  IFAIL=1
C     Subroutine E02DAF forms the minimal,weighted least squares
C     bicubic spline surface to the set of given data points
      CALL E02DAF(M1,PX1,PY1,X1,Y1,Z1,W,AMDA1,EU1,NPOINT,
     +M1+NP1,DL,C1,NC1,WS,NWS,EPS,SIGMA,RANK,IFAIL)
C     Output the sum of squares error
      WRITE(12,-) SIGMA
      IF(IFAIL.EQ.0) GO TO 230
      WRITE(12,-) "IFAIL2"
      WRITE(12,-) IFAIL
      GO TO 180
 230  IFAIL=1
```

```
:       Subroutine E02DBF calculates values of a bicubic spline
C       function from its B-spline representation at prescribed
C       points
        CALL E02DBF(M1,PX1,PY1,X1,Y1,FF1,AMDA1,EU1,NPOINT,M1+NP1
     +,C1,NC1,IFAIL)
        IF(IFAIL.EQ.0) GO TO 420
        WRITE(12,-) "IFAIL3"
        WRITE(12,-) IFAIL
        GO TO 180

 420    CALL SELM(PX1,PY1,AMDA1,EU1,M,NP1,NC1,C1)
        CALL INTEG(M,MX,MY,DX,DY,TL,TU,RR,WL,CX,CY,X0,
     +X0,X2,Y0,Y2,Q1,V1,TIN,HIN,EPS)
 180    READ(11,-) I
        IF(I-1) 200,20,420
 200    STOP
        END

C       Subroutine Selm calculates Splines at the Mesh (grid)
        points
        SUBROUTINE SELM(PX,PY,AMDA,EU,M,NP,NC,C)
        COMMON /SAX/ X(1200),Y(1200),FF(1200)
        SPECIAL COMMON SAX
        INTEGER I,J,K,M,PX,PY,NP,NC,IPOINT(2050)
        INTEGER IFAIL,ADRES(30)
        REAL EU(20),AMDA(20),C(60)

        IFAIL=1
        CALL E02ZAF(PX,PY,AMDA,EU,M,X,Y,IPOINT,M+NP,ADRES,NP,IFAIL)
        IF(IFAIL.EQ.0) GO TO 100
        WRITE(12,-) "IFAIL4"
        WRITE(12,-) IFAIL
        WRITE(12,-)
        GO TO 180
 100    IFAIL=1
        CALL E02DBF(M,PX,PY,X,Y,FF,AMDA,EU,IPOINT,M+NP,C,NC,IFAIL)
        IF(IFAIL.EQ.0) GO TO 120
        WRITE(12,-) "IFAIL5"
        WRITE(12,-) IFAIL
        GO TO 180
 120    RETURN
 180    STOP
        END
```

```
      SUBROUTINE INTEG(M,MX,MY,DX,DY,TL,TU,RR,WL,CX,CY,X0,X2
     +,Y0,Y2,Q1,V1,TIN,HIN,EPS)
C     INTEG integrates the temperatures over the tray area
C     Only a strip of width "DELY" is integrated at a time
C     The area of the strip "DELX*DELX" is set before
C     computation begins
      COMMON /SAX/ X(1200),Y(1200),FM(1200)
      SPECIAL COMMON SAX
      COMMON /CAT/ FI(1200),YNTR(1200)
      SPECIAL COMMON CAT
      COMMON /CAN/ W(5000),AZ(32,30)
      SPECIAL COMMON CAN
      COMMON /FIX/ A(20),CT(20),E(20),CE(20),N7,M7
      SPECIAL COMMON FIX
      REAL AREA,DELX,DELY,L,V,XX,XY,XZ,RR,CX,CY
      REAL HO(1200),XS(200),FS(200),TOU,TIN
      INTEGER MX,MY,M,IX,IY,N7,IW,DIM

C     State area of tray in centimeters squares
      AREA=8554.00
C     Set the average densities of water and air (kg/m3)
      PL=1000
      PV=1.22
      DIM=1800
C     Initialisation of variables for iteration
C     Set calculation limits for point efficiency
      EMAX=1.1
      EMIN=0.1
      EMI=EMIN
      EMX=EMAX
      EOG=EMI
      WL1=0.0
      XINT=0.0
      DINT=0.0
C     Calculation of flow rates from load factor and weir load
      L=Q1*(WL/100.0)*PL
      V=(V1/((PV/(PL-PV))**0.5))*(AREA/1.0E+4)*PV
C     Start of calculations
      XLA=1.5*V/L
      DELX=DX/(MX-1)
      DD=DELX/2
      DELY=DY/(MY-1)
      IW=WL/DELX
  999 CALL BNDRY(M,MX,MY,CX,CY,RR,TL,TU,XS,FS,EOG,HIN,DIM,HO)
      DINT=0.0
      DO 600 J=1,MY
      IF(J.EQ.1) THEN
      DO 500 I=1,IW
      DINT=DINT+FS(I)+FS(I+1)
  500 CONTINUE
      END IF
  600 CONTINUE
```

```
      TOU=DINT*DD/WL
      TOU=1.00*TOU
      HTV=(TIN-TOU)*(L/V)+HIN
      WRITE(12,-) HTV
              IFAIL=1
              CALL E02BBF(N7,A,CT,TOU,HE,IFAIL)
              IF(IFAIL.EQ.0) GO TO 90
              WRITE(12,-) "IFAIL0"
              WRITE(12,-) IFAIL
              GO TO 800
 90   K=1
      YINT=0.0
      DO 555 J=1,MY
      XINT=0.0
      DO 666 N=1,MX-1
      XINT=XINT+HO(K)+HO(K+1)
      K=K+1
 666  CONTINUE
      YNTR(J)=XINT*DELX/2
 555  CONTINUE
      CALL SIMPS(MY,YNTR,DELY,ZNTEG)
      TOTINT=ZNTEG
      AVERH=TOTINT/AREA
      WRITE(12,-) AVERH,HTV
      DIFF=HTV-AVERH
      EJS=EPS*900.0
      IF(ABS(DIFF).LE.EJS) GO TO 888
      EMV=(HTV-HIN)/(HE-HIN)
      WRITE(12,9001) EOG,EMV,TOU,DIFF
9001  FORMAT(///4F10.3)
      EOG=EOG+DIFF/HTV
      GO TO 900
      IF(EOG.NE.EMAX) GO TO 909
      EMM=(EMAX-EMIN)/2
      EOG=EMM
      GO TO 999
 909  IF(DIFF.GT.0.0) GO TO 808
      EMM=(EMX-EMI)/2
      EOG=EMM
      EMX=EMM
      GO TO 900
 808  EMM=(EMX-EMI)/2
      EOG=EMX
      EMI=EMM
 900  GO TO 999
C     Print the point efficiency, the product lamda by pt.eff.
C     tray efficiency,the ratio pt.eff. to tr.eff. and average
C     outlet temperature
 888  WRITE(12,9002) EOG,XLA*EOG,EMV,EMV/EOG,TOU
9002  FORMAT(5F10.4)
      CALL PRFILE(M,MX,MY,X0,X2,Y0,Y2,TL,TU,RR,WL,Q1,V1)
 800  RETURN
      END
```

```
C       Subroutine simps integrates the spline function
C       in the flow direction using Simpson's rule
        SUBROUTINE SIMPS(MY,YNTR,DELY,ZNTEG)
        DIMENSION YNTR(100)
        REAL ZNTEG

        INTV=MY-1
        IITV=INTV/2
        IEND=MY-2
        INTEG=0.0
        K=1
        IF((INTV-2*IITV).EQ.0) GO TO 400
        ZNTEG=3*DELY/8*(YNTR(1)+3*YNTR(2)+3*YNTR(3)+YNTR(4))
        K=4
 400    ZNTEG=ZNTEG+DELY/3*(YNTR(K)+4*YNTR(K+1)+YNTR(MY))
        K=K+2
        DO 500 I=K,IEND,2
        ZNTEG=ZNTEG+DELY/3*(2*YNTR(I)+4*YNTR(I+1))
 500    CONTINUE
        RETURN
        END

        SUBROUTINE BNDRY(M,MX,MY,CX,CY,RR,TL,TU,XS,FS
     +,EOG,HIN,DIM,HO)
C       Subroutine BNDRY allocates the value zero to
C       points lying outside the active area of the tray
C       This enables an integration of the tray to be confined
C       to the active space only.

        COMMON /SAX/ X(1200),Y(1200),FM(1200)
        SPECIAL COMMON SAX
        COMMON /CAT/ FI(1200),YNTR(1200)
        SPECIAL COMMON CAT
        COMMON /CAN/ W(5000),AZ(32,30)
        SPECIAL COMMON CAN
        COMMON /FIX/ A(20),CT(20),E(20),CE(20),N7,M7
        SPECIAL COMMON FIX
        REAL XZ,CX,CY,RR,V(100),XS(200),FS(200),HO(1200)
        INTEGER M,K,N7,M7
```

```
                L=1
                N=1
                IJ=1
                DO 22 J=1,MY
                DO 22 I=1,MX+2
                SET=SQRT(RR**2-((Y(N)-CY))**2)
                IF(X(N).LE.RR) THEN
                XZ=CX-SET
                IF(J.EQ.1.OR.J.EQ.MY) THEN
                IF(X(N).LT.XZ) GO TO 20
                XS(IJ)=X(N)
                FS(IJ)=FM(N)
                IJ=IJ+1
                END IF
                GO TO 19
                END IF
                XZ=CX+SET
                IF(J.EQ.1.OR.J.EQ.MY) THEN
                IF(X(N).GT.XZ) GO TO 20
                XS(IJ)=X(N)
                FS(IJ)=FM(N)
                IJ=IJ+1
                END IF
19              IF(X(N).EQ.XZ) THEN
                V(L)=FM(N)
                L=L+1
                END IF
20              N=N+1
22              CONTINUE
                J=1
                DO 100 K=1,M
                SET=SQRT(RR**2-((Y(K)-CY))**2)
                IF(X(K).LE.RR) THEN
                N=J
                XZ=CX-SET
                IF(X(K).LT.XZ) THEN
                FI(K)=0.0
                HO(K)=0.00
                GO TO 99
                END IF
                FI(K)=FM(K)
                GO TO 80
                END IF
                N=2*(J-1)+1
                XZ=CX+SET
                IF(X(K).GT.XZ) THEN
                FI(K)=0.0
                HO(K)=0.00
                GO TO 99
                END IF
                FI(K)=FM(K)
80              IFAIL=1
```

```
                TI=FI(K)
                CALL E02BBF(N7,A,CT,TI,HEQ,IFAIL)
C               WRITE(12,303) K,X(K),Y(K),FI(K)
                IF(IFAIL.EQ.0) GO TO 90
                WRITE(12,-) "IFAIL0"
                WRITE(12,-) IFAIL
                GO TO 500
 90             HO(K)=HIN+EOG*(HEQ-HIN)
 99             IF(K.EQ.(J*(MX+2))) THEN
                J=J+1
                END IF
 100            CONTINUE
                RETURN
 500            STOP
                END

        SUBROUTINE PRFILE(M,MX,MY,X0,X2,Y0,Y2,TL,TU,RR,WL,Q1,V1)
C       Prfile draws temperature profiles across the tray using
c       the package GINOSURF

        REAL X0,X2,Y0,Y2
        COMMON /CAT/ FI(1200),YNTR(1200)
        SPECIAL COMMON CAT
        COMMON /CAN/ W(5000),AZ(32,30)
        SPECIAL COMMON CAN
        COMMON /SAX/ X(1200),Y(1200),FM(1200)
        SPECIAL COMMON SAX
        COMMON /CONST/ DIA,XTE,XLEN,XWR,XBEL,XTS,XS,YS,YF,XL,YL,YM
     +,XM,YE,XX,XY
        SPECIAL COMMON CONST
        COMMON /PLOT/ YCL(40),ZI(40),XI(40),DX,MHF,IXX,IEND
        SPECIAL COMMON PLOT
        INTEGER M,MX,MY

        FRG=0.0
        RAF=(Q1/V1)-0.07
        TOL=0.05*0.07
        DIA=2*RR
        XX=RR-0.5*WL
        XY=DIA-XX
        DX=DIA/MX
        IXX=XX/DX
        MM=WL/DX-1
        MHF=MM/2
        DO 44 J=1,MY
        IJ=(J-1)*(MX+2)
        LL=(MY-J)*(MX+2)+MHF
        N=IXX+IJ
        K=N+MHF
        MST=N+MM+1
        IEND=MST-2
```

```
      IF((2*MHF-MM).EQ.0) GO TO 22
      FRG=3*DX/8*(FM(N)+3*FM(N+1)+3*FM(N+2)+3*FM(N+3))
      N=N+3
      YCL(J)=FM(K+1)
      XI(J)=Y(LL)
      GO TO 33
 22   YCL(J)=(FM(K+1)+FM(K+2))/2
      XI(J)=Y(LL)
 33   FRG=FRG+((DX/3)*(FM(N)+4*FM(N+1)+FM(MST)))
      N=N+2
      DO 66 II=N,IEND,2
      FRG=FRG+((DX/3)*(2*FM(II)+4*FM(II+1)))
 66   CONTINUE
      ZI(J)=FRG/(DX*MM)
      XI(J)=Y(LL)
      FRG=0.0
 44   CONTINUE
      IF(YCL(MY).GT.ZI(MY)) GO TO 777
      AZI=ZI(MY)
      GO TO 888
 777  AZI=YCL(MY)
 888  IF(YCL(1).LT.ZI(1)) GO TO 999
      WZI=ZI(1)
      GO TO 555
 999  WZI=YCL(1)
 555  L=1
      DO 88 J=1,MY
      DO 77 I=1,MX+2
      AZ(I,J)=FM(L)
      L=L+1
 77   CONTINUE
 88   CONTINUE
      CALL GINO
      CALL PICCLE
      CALL SHIFT2(0.00,50.00)
      CALL SCALE(0.5)
      CALL SETFRA(2)
      CALL LABCON(0,1,120.0,0)
      CALL DRACON(MX+2,X0,X2,MY,Y0,Y2,AZ,20,1,5000,W)
C     Convert GinoSurf Scale into ordinary GinoGraphics Scale
C     Values
      CALL CONSPA(X0,Y0,XZ,YA)
      CALL CONSPA(14.0,Y0,XA,YA)
      CALL CONSPA(108.0,Y0,XB,YA)
      CALL CONSPA(14.0,Y2,XA,YB)
      CALL CONSPA(108.0,Y2,XB,YB)
      CALL CONSPA(X2,Y2,XF,YB)
      CALL CONSPA(61.0,38.0,XR,YR)
```

```
      XF=XB-XA
      XS=XA+0.1*XF
      XCB=XS+0.16*XF
      YS=YA-0.06*YB
      YF=YS-0.05*YB
      YOUT=YF-0.04*YB
      YNW=YOUT-0.04*YB
      XL=XA+0.01*XF
      YZ=YB-YA
      YL=YF-0.005*YB
      YM=YA-0.035*YB
      YMLT=YM-0.016*YB
      XM=0.990*XR
      YE=YA-0.025*YB
      YLM=YA+0.8*YB
      YLM=YLM*0.86
      YTR=YM-0.02*YB
      XTE=XB+(16.91*XF/15.1)
      RXTE=XB+(7.28*XF/15.1)
      WXTE=XA-(7.28*XF/15.1)
      DXTE=RXTE-WXTE
      DOWY=YA-(5.7*YZ/12.3)
      HIGY=YB+(3.15*YZ/12.3)
      HEGT=HIGY-DOWY
      XBEL=XTE-0.085*XF
      XTS=XTE+0.10*XF
      XRTS=XTS+0.16*XF
      XK=YZ+XTE
      XWR=0.50*XF+XTE
      XV=XR-0.085*XF
      XOUT=XV-0.01*XF
C     Draw the Tray Shape to Scale using scale values above
      CALL MOVTO2(XA,YA)
      CALL LINTO2(XB,YA)
      CALL ARCTO2(XR,YR,XB,YB,1)
      CALL LINTO2(XA,YB)
      CALL ARCTO2(XR,YR,XA,YA,1)
      CALL MOVTO2(XS,YB*1.1)
      CALL CHAHOL(47HMeasured Temperature Profiles on a Sieve
     + Tray*.)
      CALL MOVTO2(XS,YB*1.08)
      CALL LINBY2(0.9*XF,0.00)
      CALL MOVTO2(XS,YB*1.05)
      CALL CHAHOL(18H(Temperature  C)*.)
      CALL MOVTO2(XV,YB)
      CALL CHAHOL(12Htray inlet*.)
      CALL MOVTO2(XS,YF)
      CALL CHAHOL(10HFIG:    *.)
      CALL MOVTO2(XS,YL)
      CALL LINBY2(0.12*XF,0.00)
```

```
      CALL MOVTO2(XCB,YOUT)
      CALL CHAHOL(6HCsb=*.)
      CALL CHAFIX(V1,6,4)
      CALL CHAHOL(5Hm/s*.)
      CALL CHAHOL(10H    q/b=*.)
      CALL CHAFIX(Q1,7,5)
      CALL CHAHOL(7Hm3/sm*.)
      CALL MOVTO2(XCB,YNW)
C     Specify tray type and label
C     CALL CHAHOL(15HSTANDARD TRAY*.)
C     CALL CHAHOL(31HMODIFIED TRAY:OUTLET WEIR GAP*.)
      CALL CHAHOL(21HSTEP-FLOW DOWNCOMER*.)
C     Draw separate plots of temperature profile along the flow
C     axis and in the rectangular section between the downcomers

      CALL MOVTO2(XTS,YF)
      CALL CHAHOL(10HFIG:    *.)
      CALL MOVTO2(XTS,YL)
      CALL LINBY2(0.12*XF,0.00)
      CALL MOVTO2(XRTS,YOUT)
      CALL CHAHOL(6HCsb=*.)
      CALL CHAFIX(V1,6,4)
      CALL CHAHOL(5Hm/s*.)
      CALL CHAHOL(10H    q/b=*.)
      CALL CHAFIX(Q1,7,5)
      CALL CHAHOL(7Hm3/sm*.)
      CALL MOVTO2(XRTS,YNW)
C     Specify and label tray type
C     CALL CHAHOL(15HSTANDARD TRAY*.)
C     CALL CHAHOL(31HMODIFIED TRAY:OUTLET WEIR GAP*.)
      CALL CHAHOL(21HSTEP-FLOW DOWNCOMER*.)
      CALL MOVTO2(XM,YE)
      CALL CHAHOL(3HC*.)
      CALL MOVTO2(XR,YM)
      CALL CHAHOL(3HL*.)
C     Determine if Operating Flow Conditions satisfy Spray,Mixed
C     or are at the Transition between Spray and Mixed
      IF(ABS(RAF).EQ.TOL) GO TO 333
      IF(RAF.GT.0.0) GO TO 444
      CALL MOVTO2(XCB,YF)
      CALL CHAHOL(14HSpray Regime*.)
      CALL MOVTO2(XRTS,YF)
      CALL CHAHOL(14HSpray Regime*.)
      GO TO 222
 444  CALL MOVTO2(XCB,YF)
      CALL CHAHOL(14HMixed Regime*.)
      CALL MOVTO2(XRTS,YF)
      CALL CHAHOL(14HMixed Regime*.)
      GO TO 222
 333  CALL MOVTO2(XCB,YF)
```

```
      CALL CHAHOL(16HTransition S/M*.)
      CALL MOVTO2(XRTS,YF)
      CALL CHAHOL(16HTransition S/M*.)
222   CALL MOVTO2(XOUT,YMLT)
      CALL CHAHOL(13Htray outlet*.)
      CALL MOVTO2(XM,YE)
      CALL CHAHOL(3HC*.)
      CALL MOVTO2(XR,YM)
      CALL CHAHOL(3HL*.)
      CALL MOVTO2(XTE,YA)
      CALL AXIPOS(1,XTE,YA,YZ,1)
      CALL AXIPOS(1,XTE,YA,YZ,2)
      CALL AXISCA(3,5,0.00,76.00,1)
      CALL AXISCA(3,10,WZI,AZI,2)
      CALL AXIDRA(2,1,1)
      CALL AXIDRA(-1,-1,2)
      CALL GRASYM(XI,ZI,MY,3,2)
      CALL GRACUR(XI,ZI,MY)
      CALL GRASYM(XI,YCL,MY,7,2)
      CALL GRACUR(XI,YCL,MY)
      CALL MOVTO2(XTE,YB*1.1)
      CALL CHAHOL(36HTemperature Change along Flow Axis*.)
      CALL MOVTO2(XTE,YB*1.08)
      CALL LINBY2(0.7*XF,0.00)
      CALL MOVTO2(XTS,1.00*YB)
      CALL CHAHOL(33H+ Rectangular Section (average)*.)
      CALL MOVTO2(XTS,0.95*YB)
      CALL CHAHOL(15Ho Centre Line*.)
      CALL MOVTO2(XTE,YS)
      CALL CHAHOL(4HIN*.)
      CALL MOVTO2(XTS,YS)
      CALL CHAHOL(22HFlow Path Length(cm)*.)
      CALL LINBY2(0.12*XF,0.00)
      CALL MOVTO2(XK,YS)
      CALL CHAHOL(5HOUT*.)
      CALL MOVTO2(XBEL,0.62*YB)
      CALL CHAHOL(5HT C*.)
      CALL DEVEND
      RETURN
      END
```

TO RUN: Open NAG10D and GINO-F Libraries.
Create data files and load information in order of program
Specify (and if necessary, change) internal knots till sum
of squares of weighted residuals is less than 2.0